Ice Transport in Great Lakes

by

Ralph R. Rumer
Randy Crissman
Akio Wake

September 1979

ICE TRANSPORT IN GREAT LAKES

by

Ralph R. Rumer, Jr.
Randy D. Crissman
Akio Wake

September 1979

TABLE OF CONTENTS

Preface

PREFACE

The authors have attempted to give fairly broad coverage to the available information on ice transport in large waterbodies. The intent has been to provide both an overview as well as in-depth treatment of selected topics, which, together, would form the basis for continued study and development of ice transport models applicable to the Great Lakes.

I.   INTRODUCTION

1.1   Description of the Physical System

Every winter season the waterbodies referred to as the Laurentian Great
Lakes (see Figure 1.1) release to the atmosphere the heat stored during the
preceding summer season. The rate at which this heat is released varies from
lake to lake, mainly because of regional differences in climatic conditions.
When the surface waters are chilled to zero degrees centigrade and the rate
of heat loss to the atmosphere exceeds the rate at which stored heat is
transported to the surface from within the lake, the condition for ice pro-
duction is present. This condition normally first occurs in sheltered areas
where water depths are shallow and migrates outward from the lake shore as
the winter cooling proceeds. Lake Erie is the waterbody most prone to complete
ice cover. Its shallow depth coupled with strong wind-driven vertical mixing
are important factors that contribute to the more rapid release of stored
heat: ultimately reducing the temperature to nearly $0^{o}C$ throughout the
waterbody (Stewart, 1973).

A comprehensive climatological analysis for the Great Lakes basin has
been prepared by Phillips and McCullough (1972). Their analysis is based
on climatic records from over 400 stations in the Great Lakes basin and, for
the most part, covers the period, 1931-1960. Their report includes seasonal
and regional averages and expected variability for air temperature, precipi-
tation (with snow fall separate), humidity, evaporation, radiation, sunshine,
sky cover, fog, ice, and wind. Also included is a comparison of mean surface
water temperatures and their standard deviations for the Great Lakes.

1

	Avg. Depth	Surface Area
Lake Superior	148 m	82621 km^2
Lake Michigan	84 m	58016 km^2
Lake Huron	59 m	59595 km^2
Lake Erie	18 m	25719 km^2
Lake Ontario	86 m	19476 km^2
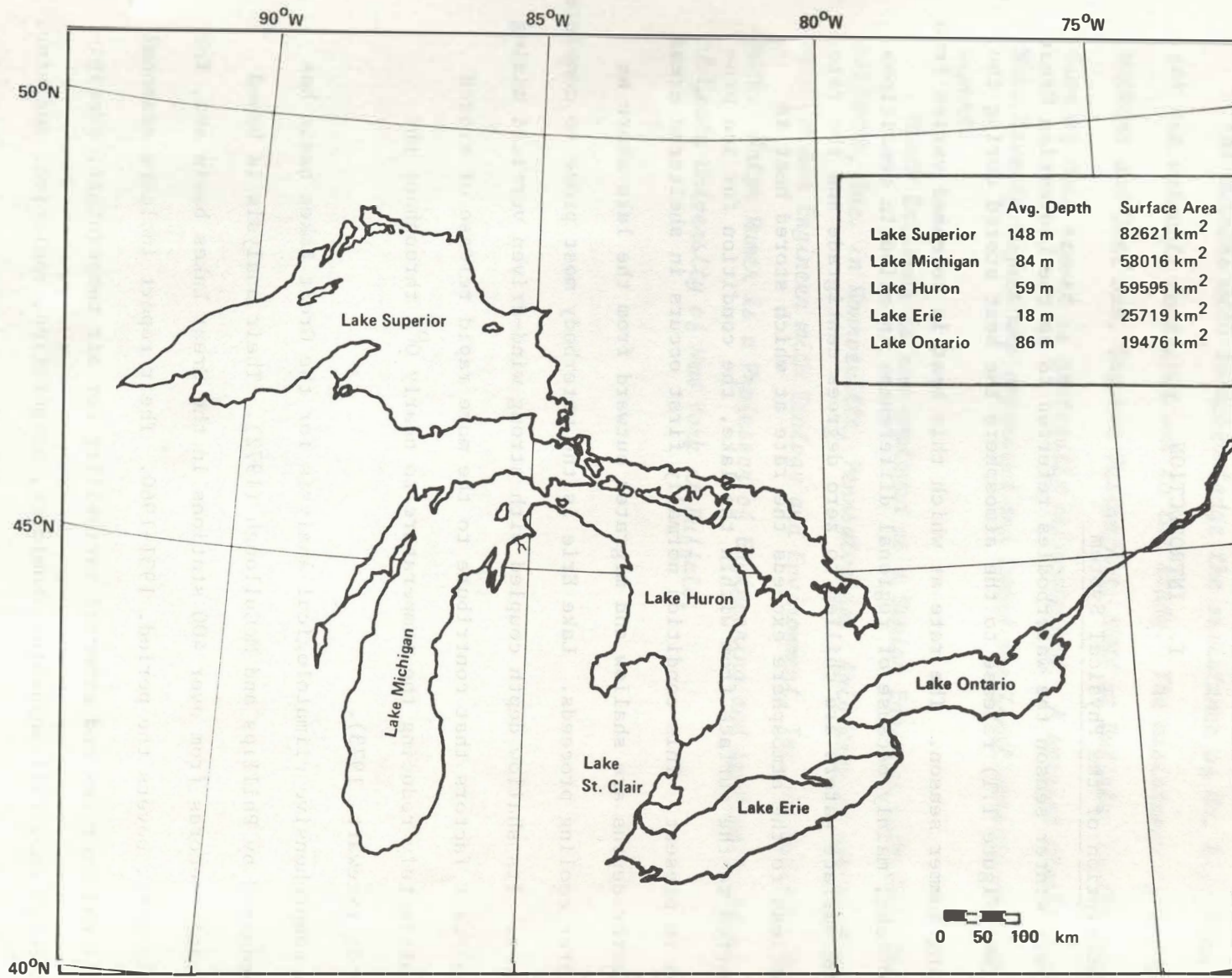
Figure 1.1 Location Map Showing North American Great Lakes

Snider (1974) presents a historical review of ice forecasting in the Great Lakes and discusses their thermal regimes, the physical processes affecting lake ice, and gives an account of the progress of a typical ice season. His manual includes the application of historical records and the degree day freezing concept to the forecasting of ice conditions. Among the appendices is a summary of the opening and closing dates for navigation at seven locations in the Great Lakes covering the years 1885 to 1973, except where data are missing.

Rondy (1971) has prepared an ice atlas for the Great Lakes in which he characterizes the nature and extent of the ice cover for each of the Great Lakes and Lake St. Clair. For normal winter seasons, Lake Erie and Lake St. Clair are the only lakes that can be expected to be almost 100 per cent ice covered. However, for winters classified as severe, all of the Great Lakes (with the exception of Lake Ontario) can be expected to be nearly 100 per cent ice covered. Rondy's classification of the severity of the winter season was based on the freezing degree-day concept. His report provides a good overview of the variability of the Great Lakes ice season. Marshall's (1966) pictorial essay of common ice features and patterns found in the Great Lakes along with his description and interpretation of these ice conditions provides a more detailed visual impression of the changing nature of the Great Lakes ice cover.

With the advent of satellites and their remote sensing capability, synoptic views of the Great Lakes have become possible. Radiation scanners carried by satellites provide photographic images in the visible and infrared portions of the electromagnetic wave spectrum. McMillan and Forsyth (1976) and Wartha (1977) have reported on the ice conditions of Lake Erie for

the winter seasons 1974-75 and 1975-76, respectively. McMillan and Forsyth included data from the Very High Resolution Radiometer (VHRR) carried by NOAA-4 environmental satellite. Wartha includes images obtained from NOAA-4 (VHRR), NOAA's Geostationary Operational Environmental Satellite (GOES), the NASA Landsat, and the U.S. Coast Guard aircraft Side Looking Airborne Radar (SLAR) systems. The meteorological and ice conditions that prevailed in the Great Lakes during the severe winter of 1976-77 have been compiled and summarized by Quinn et al (1978). The report by Quinn et al is well-illustrated with line drawings, graphs, and images from NOAA-5 and NOAA-GOES satellites. A more complete description of these satellite systems as well as other ice surveillance techniques, including those being developed for remote measurement of ice thickness, can be found in Chapter V of this report.

The large surface area of the Great Lakes system and the variability of meteorological conditions, both in time and space render it virtually impossible to give a complete and totally accurate description of the state of the ice cover. Climatic conditions bring about changes in the total ice mass through freezing and melting while wind, waves, and water currents cause deformation and movement of the ice cover. The thermodynamic and physical processes that alter the ice field are interdependent; however, the complexity of attempting to analyze them as coupled processes frequently leads to neglect of one or the other, depending on the specific needs or objectives of the observer.

1.2 Review of Ice Transport Modeling

Notwithstanding the limited capability to accurately simulate or model (i.e., utilizing a mathematical analog) ice dynamics and ice transport, there is a substantial body of literature on this topic. However, most investigators

4

have been concerned with the Arctic ice cover, its deformation and drift. The absence of work on ice transport modeling in lakes is evident in the recent bibliographic essay on ice in rivers and lakes compiled by Ficke and Ficke (1977) which cites no work dealing specifically with this topic. A technical report on hydrological forecasting practices prepared under the auspices of the World Meteorological Organization (1975), has a section on lake ice; but, again, no mention is made of the use of mathematical models for ice deformation and ice transport. Their report states that mechanical factors play a minor role in the break-up and disappearance of lake ice. In contrast, Michel (1971), in his monograph dealing with the winter regime of rivers and lakes, states that "...mechanical breaking of ice in rivers and lakes by wind and currents is sometimes more important than its melting..." and cites the work of Williams (1965) to illustrate this importance. Although Michel's monograph contains a mathematical analysis of ice jams, which do have importance in the connecting waterways between the Great Lakes and in their tributaries, no mathematical analogs for ice transport in lakes are presented. Bolsenga's (1968) comprehensive review of the literature dealing with ice jams in rivers has been up-dated by Ficke and Ficke (1977). Zubov (1944) provides a good summary of direct observations of ice drift in the Arctic Ocean distinguishing three characteristic cases from "...the great complexity of the wind movement of ice..." These cases are: (1) the wind drift of densely compacted (close) ice, (2) the wind drift of an isolated floe, and (3) the wind drift of loosely compacted (scattered) ice. His analysis of these three cases is largely based on his weighting of the relative importance of the wind and water currents.

The wind driven movement of close ice is assumed to cause a current in the sea beneath the ice. The resistance of the water on the ice

5

movement is dealt with by introducing a "wind factor" which is simply
the ratio of ice drift speed to wind velocity. Considerable attention
is devoted to developing estimates of the wind factor (concluded to be
0.02 for close ice fields) based on direct observations from drifting
vessels exploring the Arctic. His analysis leads to an explicit expression
showing the drift speed of the ice to be directly proportional to the at-
mospheric pressure gradient. The ice drift direction is concluded to be
parallel to the isobars of atmospheric pressure. Zubov considers these
rules to apply to so-called "pure wind drift" over the deep sea, far from
the influence of coastlines, and without the effect of "powerful steady
currents."

Zubov's study of the drift of isolated ice floes is based on a
balance of the wind pressure acting on the floe, the hydrodynamic resistance
to the ice floe drift when the "water is immobile," and the Corolis force.
His analysis leads to the conclusions that: the angle between the wind
direction and the ice drift direction increases with geographic latitude
and with thickness of the floe but decreases with increasing wind speed.
When wind-driven water currents and the Ekman spiral effect (1905) are
included, he deduces that the deeper the ice floe protrudes into the water,
the less will be the effect of the wind-driven water current since the water
current decreases very rapidly with depth as well as changing direction.
Thus he concludes, that the deeper the ice floe protrudes into the water and
the greater the size of the floe, the more it will be subject to prevailing
water currents (e.g., geostrophic flows). Correspondingly, for thin ice
floes, both direct wind pressure and wind-driven water currents, will have
the greatest influence. It is interesting to note that, based on direct
observation of isolated ice floes, wind factors as high as 0.15 were

reported. These high wind factors were not satisfactorily explained by Zubov's analysis, except that the surface form of the floe is recognized as playing a very distinct role. Although he did not explicitly account for it, the possible effect of water waves on ice drift is mentioned.

In his discussion of the wind drift of scattered ice, Zubov includes an added force which he states is due to the "...collision of individual ice floes moving differently." He cites the assumption in which the internal ice resistance is proportional to the ice drift and is oppositely directed. Based on some limited observations, Zubov indicates that scattered ice, with ice area concentrations of 0.1, drift four times faster than when the ice area concentration is 0.9. The form effect of ridges (or hummocks) in increasing ice drift speed is noted. He discusses the effect of compressive and dispersive winds on the movement of an ice field, particularly at the edge of the ice pack and near shorelines.

Zubov's work provides a valuable synthesis of observational data, physical reasoning, and simple theory which stands in interesting contrast to more recent treatments of ice dynamics that employ the continuum approximation and which utilize numerical methods and the computational capability of high speed electronic computers.

Field observations and empirical equations, relating ice drift speed and direction to measurable environmental factors such as wind speed and direction or atmospheric pressure gradients, can now be examined in light of results obtained from more complete mathematical analogs (i.e., differential equations). Mathematical analogs have been formulated to describe both the thermodynamics and mechanics of pack ice. However, as these mathematical representations of ice deformation and ice drift become more detailed, the quantity of field data needed for their calibration increases markedly.

The majority of Arctic ice dynamics models, developed since 1970, have attempted to simulate large scale movements and deformations. The primary effort has been to model these movements and deformations by treating the ice pack as a continuum. Some of the modeling efforts that have employed the continuum approximation have been briefly summarized here in order to establish a better appreciation of the present status of Arctic ice pack modeling. It is fair to say that most investigators have not provided much justification for their treatment of the pack ice medium as a continuum. In particular, the best representation for the internal ice resistance, which appears in the continuum formulations, has not been satisfactorily determined. Several different constitutive laws have been proposed and tested by various investigators. The two most prominent approaches view the ice pack as behaving either like an elastic-plastic solid or like a viscous-type fluid.

Campbell (1965) viewed the pack ice field as a viscous fluid in which each fluid element had a rigid upper and lower boundary with differing roughnesses. He obtained numerical solutions to the steady-state version of an ice drift equation which included air and water stress, the internal viscous-type stress, the Coriolis force, and the gravitational force due to a tilting of the sea surface. The computed steady-state ice drift exhibited two observed features of the Arctic pack ice, the anticyclonic gyre in the Beaufort Sea and the Transpolar Drift Stream that carries ice across the Polar region from Siberia to Greenland. (See Figure A.1 in Appendix A for a map of the Arctic region.) In calibrating his model, the sea ice viscosity coefficient was varied and a value of 3×10^{12} cm^2/sec was necessary in order to properly position the anticyclonic gyre on the Pacific side of the Arctic Basin.

Rothrock (1975b) obtained a mean annual Arctic ice drift similar to that of Campbell assuming the ice pack to be incompressible and inviscid. The governing equation for ice motion involved the air and water stresses, the

Coriolis force, the sea surface tilt, and the gradient of ice pressure. He utilized a 200 km x 200 km square grid for discretizing the equations.

Parkinson (1978) has recently reviewed the various efforts at modeling ice dynamics, categorizing each in terms of the number of forces included in the ice transport calculations. Only one new force has been included, the gravitational pull due to ice resting on a sloping water surface (called the force due to dynamic topography or sea surface tilt) in addition to the forces cited by Zubov; namely, wind stress, water stress, Coriolis force, and internal ice resistance. The contrasts between Zubov's early treatment and the later, more comprehensive, studies is vividly illustrated by Parkinson's numerical model of the growth and decay of sea ice in the Arctic and Anarctic including calculations of ice transport and specification of ice area concentrations. Although Parkinson's model is limited by many simplifications and assumptions, such as constant ice thickness within each 200 km x 200 km grid element, monthly atmospheric forcing, and the assumption of geostrophic ocean currents (i.e., a balance between dynamic topography and Coriolis force); the large scale features of the model output were found to correspond nicely with observations in the two hemispheres. Parkinson's modeling effort may likely serve as the forerunner to more sophisticated models which attempt to simulate ice growth and decay and ice transport with coupled atmospheric and oceanic flows and energy budgets. However, the size resolution and lack of observational data for calibration of these comprehensive synoptic models will create less than satisfactory results when dealing with site specific ice problems of engineering importance.

The Arctic Ice Dynamics Joint Experiment (AIDJEX) that has been active between 1970 and 1980, focuses on a smaller region of the Arctic, namely the Beaufort Sea area north of Canada and the State of Alaska. The AIDJEX work

9

which has been reported in 40 AIDJEX technical bulletins, various scientific journals, and book reviews, has been summarized in the Proceedings of a Symposium on Sea Ice Processes and Models held at the University of Washington, Seattle, Wash., Sept. 6-9, 1977. The AIDJEX effort included the establishment of manned camps and data buoys on the Beaufort Sea ice pack and the development and application of a numerical simulation model for ice dynamics. The scope and findings of the AIDJEX study have been summarized by Untersteiner (1977). The AIDJEX model employed the continuum assumption and a 100 km x 100 km grid size for numerical computations using difference approximations of the governing equations. The mathematical model is comprised of a momentum balance for the pack ice which includes air and water stresses, the Coriolis force, the gravitational force associated with sloping water surface, and the internal resistance of the ice; a constitutive law for the ice internal resistance based on elastic-plastic behavior of the pack ice for the space scale of the continuum; and an ice thickness distribution function incorporating both thermodynamic and mechanical deformation effects (Coon, 1977). It was found, in the application of the model, that internal ice stress played a minor role during summer periods but was important in spring and winter. The seasonal effect on the internal ice stress, particularly as related to the constitutive law employed for its representation, will be discussed in more detail in section 2.3.2. The most serious problem (Untersteiner, 1977) with the AIDJEX model appears to be in the adequacy of the assumed constitutive law for pack ice. The inadequacy of observed data on the ice thickness distribution also leads to unsatisfactory calibration of that model component. This, in turn, causes further uncertainty in the constitutive law which is dependent upon the ice thickness distribution.

Another significant study, called SEA ICE-75, involved field tests in the Bay of Bothnia between Sweden and Finland during the 1974-75 winter season (Blomquist et al, 1976). The field tests were designed to measure: ice motion at different times and places, the ice mass and its distribution, the winds over the ice and the water currents beneath the ice, and the sea level and its changes at different places. The collected data were used to evaluate and calibrate an ice dynamics model based on a momentum balance for the ice field including wind and water stress, Coriolis force, sea surface tilt, and internal ice stress (Udin and Omstedt, 1976). The main objectives of this effort were to provide a better understanding of ice dynamics in the Baltic Sea area and to aid in the development of a more reliable method for forecasting ice conditions for navigational purposes.

The conclusions drawn from the dynamical modeling effort of SEA ICE-75 are summarized in some detail because of the similarity of scales between the Bay of Bothnia and the Great Lakes. The conclusions are as follows:

(1) The neglect of the ice mass acceleration term in the momentum balance equation is justified if the time scale for atmospheric forcing is at least six hours, i.e., the time to achieve equilibrium ice drift for a specified set of driving forces was found to be 1 to 2 hours for ice thicknesses 20 to 40 cm. in thickness.

(2) Under equilibrium conditions, the sea ice was found to drift, on the average, at an angle of 30° to the right of the wind direction with a wind factor of 0.018.

(3) Temperature measurements showed neutral stability in the water layer beneath the ice and stable atmospheric stratification was found to be most common where the sea was ice covered.

(4)   Ice thickness variations due to mechanical deformation (ridging

and rafting) caused significant errors in estimating ice mass

when neglected and, consequently, significant errors in calcu-

lating the magnitude of the Coriolis force in the momentum balance.

(5)   In general, measurement of sea surface tilt revealed it to be

small and, therefore, this term was neglected in the momentum

balance except under unusual circumstances.

(6)   The two main forces in the momentum balance were the wind and

water stress. In computing the momentum balance for a specific

set of field observations, the rest term (an error residual term

which included the internal ice stress) in the momentum balance

was found to be larger when the ice field was breaking up,

smaller for a scattered freely floating ice field, and variable

in sign. The variation in the rest term suggested that the inter-

nal ice stress could be treated as a viscous-type force; i.e.,

momentum exchange between floes seemed physically plausible.

(7)   The field observations supported the use of a boundary layer

approach with an Ekman-type spiral in the air and water flows above

and beneath the ice cover. The velocity profiles were found to

be logarithmic near the ice surfaces.

(8)   Side looking aircraft radar was judged to be the primary sensor

to be used in future sea ice surveillance and mapping. None of

the remote sensing systems employed (radar altimeter, micro-wave

radiometer, or radiation scanner) gave reliable information on

ice surface roughness.

Hibler (1977) presents a dynamic-thermodynamic model for pack ice in

which the internal ice stress is treated as a nonlinear viscous continuum

characterized by both bulk and shear viscosities and a pressure term that is parameterized as a function of the ice compactness (ice area concentration) and ice thickness. The momentum balance equation is coupled to conservation equations for ice area and ice thickness with thermodynamic growth and decay of the ice accounted for. He applied the model to the Arctic Basin utilizing a 125 km x 125 km grid and integrated at one-day steps for up to eight years in order to obtain steady state results for ice drift and ice thickness. His model output includes a display of mean ice drift velocities at each grid point and ice thickness contours. The ice thickness changes due to freezing and melting are accounted for by assigning average ice thickness change rates that varied seasonally. Parkinson (1978) computed thermodynamic ice thickness changes utilizing various expressions for estimating the monthly heat exchange at the air-ice and ice-water interfaces due to radiation balances, latent heat exchanges and heat conduction.

Sodhi and Hibler (1977) present a finite element formulation for the drift of sea ice employing a viscous constitutive law without a pressure term. The model was applied to the Arctic Basin using 250 km x 250 km square elements. A unique feature of this modeling effort, besides the finite element formulation of the governing equations, is the analysis of pack ice movement due to tidal flow through the Strait of Belle Isle between Labrador and Newfoundland. The advantage of shaping elements to fit boundaries is apparent in the authors' descretization of the Strait of Belle Isle. The momentum balance equation was simplified for this latter application to include only specified time-dependent tidal currents as the driving force. The influence of winds and sea surface tilt were excluded. The viscous constitutive law

13

for ice internal resistance was utilized and the details of ice movement, especially near the shorelines of the Strait, were found to be sensitive to the magnitude of the assumed viscosity coefficients used in the computations. The steady-state ice drift in the Arctic Basin, was computed using the complete form of the governing momentum balance equation and the results were similar to those obtained by Campbell (1965), Rothrock (1975), Hibler (1977), and Parkinson (1978).

Recent attempts to model thermodynamic processes [Wake (1977), Rumer and Yu (1978), and Wake and Rumer (1979)] demonstrate that ice formation, growth, and dissipation can be simulated in Lake Erie. The two-dimensional convective-dispersion equation for the conservation of heat energy was utilized in conjunction with a one-dimensional vertical heat flux balance equation based on the heat exchange processes at the ice interfaces (in a manner similar to Parkinson (1979)). Limited observations for the Lake Erie 1975-76 winter season were used to calibrate the thermodynamic model [Wake and Rumer (1979)]. The model output produced the essential features of the Lake Erie regime. Probably the most significant limitation was the inability to account for the effects of wind and water currents. The transport and deformation of the ice cover can create open water areas, previously ice covered, in which new ice can form. It is not uncommon to observe layered ice on the order of 7 to 8 meters thick in Lake Erie during a winter season which could only produce 1 meter of "thermal-grown" ice. Thus, by not accounting for the mechanical redistribution of ice and new ice formation, the prediction of ice thicknesses and total ice mass in the lake could be subject to considerable error. The incorporation of the effects of wind and water currents on the dynamics of the ice cover would be a major improvement to the modeling effort of Wake and Rumer.

There are several incentives for developing the capability to predict ice conditions in the Great Lakes and their connecting waterways. There is, of course, the desire to better understand the natural process of ice formation, growth, transport, and dissipation. The potential for achieving such an understanding is greatly enhanced when observations and interpretations are based upon a sound theoretical formulation of the phenomenon being studied. There are, however, practical reasons for the study of ice dynamics in the Great Lakes. Were it not for ice, there would be year-round shipping in the Great Lakes-St. Lawrence Seaway system. ("Survey Study...," 1979). Extensions to the shipping season are possible if better forecasting of ice conditions can be achieved. The presence of ice poses a potential threat to man-made structures, whether a cargo vessel (see Figure 1.2), a municipal water intake, harbor facilities, or a shoreline

Figure 1.2 The lake ore carrier, Roger Blough, pinned between
           shore fast grounded ice and drift pack ice near
           Conneaut, Ohio (Feb. 8, 1979).

home. The ability to more accurately forecast ice forces and hazardous ice
conditions would reduce the hazards and level of uncertainty associated with
winter navigation and the potential for property damages and injury to per-
sons. The design of better and more cost-effective structures subjected to
ice loading would also be possible. Although man's capabilities to manage
or control ice for his own purposes in the Great Lakes are modest, they can
be extended through better knowledge and understanding of the behavior of
the Great Lakes ice cover.

1.3 Study Objectives and Method of Approach

The objective of this study has been to achieve a better understanding
of the effects of winds, waves, and water currents on the Great Lakes ice
cover through a selective combination of theory, experiment, and observation
in the field. Although the interdependence of thermodynamic processes and
and the mechanics of ice transport will be frequently cited and discussed,
the emphasis of this study has been on the elaboration of physical mechanisms
for ice deformation and ice transport. The report discusses the analytical
representation of these physical processes and how they can be incorporated
into the formulation of a mathematical model (governing field equations)
designed to simulate ice dynamics. The use of the continuum assumption and
the need for an equation that relates ice pressure to the ice cover state are
considered in some detail. The report deals with simplified versions of
the governing field equations in the analysis of single floe and multi-
floe ice fields, first in one-dimension and then in two-dimensions. The
report includes a discussion of the limitations in the understanding of ice
dynamics and suggests lines of inquiry towards the further development of
methodologies for forecasting ice movement and ice conditions in the Great
Lakes.

The capability to accurately forecast ice conditions in the Great Lakes is inherently limited by the capability to accurately forecast weather conditions. Even armed with simulation models that adequately describe the cause and effect relationships governing the ice growth, ice movement, and ice dissipation; environmental conditions such as wind speed and direction, air temperature, snow fall, etc. must be known in order to operate such models. It is, therefore, likely that such simulation models will be developed along the lines of providing limited duration forecasts with frequent updating required during the progression of a winter season. If such models are made operational, it will become important to coordinate field data collection programs and to centralize the storage of ice observational data for use in model calibration and, eventually, in model operation.

A particularly difficult aspect of forecasting ice conditions deals with the level of uncertainty regarding the deformational characteristics of an ice cover. Structural irregularities in an ice cover are dependent upon the evolution of the ice mass and this will vary widely over water-bodies as large as the Great Lakes. It is the irregularities that play an important role in the manner in which a given ice cover will deform. The mechanical deformation of an ice cover leads to changes in the frictional character of the ice surfaces, to changes in ice thickness, and to changes in ice surface albedo. These changes, in turn, operate to feedback and further influence the dynamic evolution of the ice field. Although progress in modeling ice dynamics will likely be made utilizing the assumption of uniformity of ice properties (at least within the representative elemental area used in the continuum approximation); ultimately, the ice condition may have to be viewed as non-deterministic in terms of deformational behavior. This will lead to efforts at stochastic modeling. The present study has dealt only with the development of deterministic models.

II. FORMULATION OF ICE TRANSPORT EQUATIONS

2.1 General Considerations

Thermodynamic processes at the air-water interface cause the release of stored heat and ultimately the formation of ice in the Great Lakes. However, these processes are significantly influenced by the transport and diffusion of heat within the atmospheric and hydrodynamic flows above and below this interface, respectively. The presence of ice at this interface further modifies the heat exchange processes by reflecting incoming solar radiation, and slowing the further release of heat from lake water to air. Circulation and mixing within the lake are also altered by ice shielding the lake surface from the direct action of the wind. Although thermodynamic processes are important to a thorough and full understanding of ice conditions, this report focuses on the mechanical response of the ice to the atmospheric and hydrodynamic flows.

Winds, waves, and currents fracture and fragment the Great Lakes ice cover, and rotate and translate the individual fragments called ice floes. Interaction of the floes can produce ridges of ice rubble or rafted (layered) areas of ice. New thin ice that forms between older and thicker ice floes is particularly susceptible to the ridging and rafting process. Thus, the deformation and shifting of the ice field under the action of these environmental forces redistributes the ice mass through thickening and compacting. Near the lake boundary, where the lake bottom and shoreline constrain ice field drift, these environmental forces can produce grounded mounds of ice rubble which are nearly impenetrable. (See Figure 2.1). Ideally, one would want to be able to forecast these hazardous ice conditions and the ice forces that accompany them.

Figure 2. 1 Shore Fast Grounded Ice at the Harbor Entrance to Conneaut, Ohio (Feb. 8, 1979). The Bow Imprint of the U.S. Coast Guard Icebreaker Westwind can be Discerned in the Foreground of the Upper Photograph. The Lower Photograph is Looking Lakeward.

Because of the large size of the Great Lakes, the behavior of their ice covers bears resemblance to the Arctic Ocean pack ice. Therefore, the studies of Arctic pack ice motion will likely provide important insights and suggest methods of approach that may be useful in the study of the dynamics of ice transport in the Great Lakes. However, the degree to which direct comparisons can be made is limited by significant differences between the two situations. First, and foremost, is the permanence of the Arctic pack ice in contrast to the impermanence of lake ice. Multi-year old ice forms a nucleus for the Arctic pack ice, whereas, in the Great Lakes, ice age is measured in months and disappears annually. Secondly, the thermodynamic processes, buoyancy-driven convective flows, and the strength characteristics of sea ice are all influenced by the presence of high concentrations of dissolved salts found in sea water. Obviously, this is not a factor in the Great Lakes. Finally, the proximity of the shoreline and shallow depths in the Great Lakes have a greater influence on ice movement than in the Arctic Ocean, where the depths are greater and the shorelines more distant.

2.2 Use of Continuum Approximation

As outlined in section 1.2, the primary effort in modeling Arctic ice motions has been to treat the ice pack as a continuum. This requires that the elemental length of the continuum be large compared to the typical floe size and small compared to the space scales of the driving forces. Since floe sizes in the Arctic rarely exceed 10 km and atmospheric pressure systems are typically 1000-2000 km across, a continuum elemental length scale on the order of 100 km has been adopted in most of the models. The ice mass, ice velocity and ice stress for these continuum models are then representative averages over a region large enough to contain many ice floes.

21

The other prominent feature of these modeling efforts is that they are two-dimensional in that the ice has velocity components only in the horizontal plane of the mean water surface. Variations in ice thickness, when considered, are accounted for in separate mass conservation equations that may or may not include both deformational and thermal changes in ice thickness. The justification for the use of the continuum approach in modeling ice movement in the Great Lakes will likely depend upon ice age, environmental factors, and geographical location. The formulation of the ice transport equations in two-dimensions is not as difficult to justify as the continuum assumption.

The parameters that describe the physical ice state are ice mass density, concentration of ice floes or compactness, ice thickness, ice pressure, and ice velocity. Obviously, averaging these parameters over some prescribed representative "macroscopic" area will "smooth out" many important details from a "microscopic" point of view. The extent to which these details can be sacrificed depends, to some extent, on the objectives of the modeler and the desired model output. More importantly, it depends on the nature of the ice field itself. Clearly, the treatment of a single rigid floe does not require the continuum approach; nor would it be required to describe the movement of several floes. The movement and interaction of thousands of floes, varying in size and shape, however, compels a serious consideration of the continuum approach.

As stated, the continuum approach requires that the typical floe size be much smaller than the size of the representative elemental area. Similarly, the representative elemental area should be much smaller than the size of the overall domain. There are several anologies between flow

through porous media and multi-floe ice transport. In order to apply the continuum approach to porous media flow, the size of a representative elemental volume is defined using porosity as a measure (porosity being defined as the volume of void space divided by the total volume which includes voids and the solid matrix of the medium) (Bear, 1972). In In a similar manner, the size of the representative elemental area for ice modeling could be, conceptually at least, related to the measurement of areal concentration of the ice mass (refer to Figure 2.2). For an area very much larger than a single ice floe (with $\underline{P}$ as the centroid of the area) the ice area concentration, N, can be defined as:

$$N = \frac{A_i}{A_T} \tag{2.1}$$

where A_i = ice area and A_T = the total area (ice area plus area of open water). As the total area, A_T, is gradually reduced in size the value of N would be expected to vary gradually or not at all, depending on whether the field of pack ice were nonhomogeneous or homogeneous. Below a certain value of A_T, N should be relatively insensitive to further reductions in A_T, until the value of $A_T = A_{T_o}$ were reached. Thereafter, N would begin to have large fluctuations. As $A_T \to 0$ (converging on the point, P), N would become either zero or one, depending upon whether P were located on open water or on an ice floe. It can be seen from this description that A_{T_o} defines the limiting size of the representative elemental area. For $A_T < A_{T_o}$, there is no single value of N that can represent the ice area concentration. For $A_T > A_{T_o}$, the value of N remains constant unless at larger and larger values of A_T, the nonhomogeneity of the ice floe-configuration has an influence.

This latter situation could happen, for instance, where a large region

of fragmented ice floes is adjacent to a very large unbroken ice sheet.

In this case, the continuum domain would be restricted to the region of

ice floes.

By introducing the concept of ice area concentration, N, and the defini-

tion of a representative elemental area, the actual medium of discrete ice

floes and open water areas has been replaced by a fictitious continuum to

which values of any property can be assigned to any point within it.
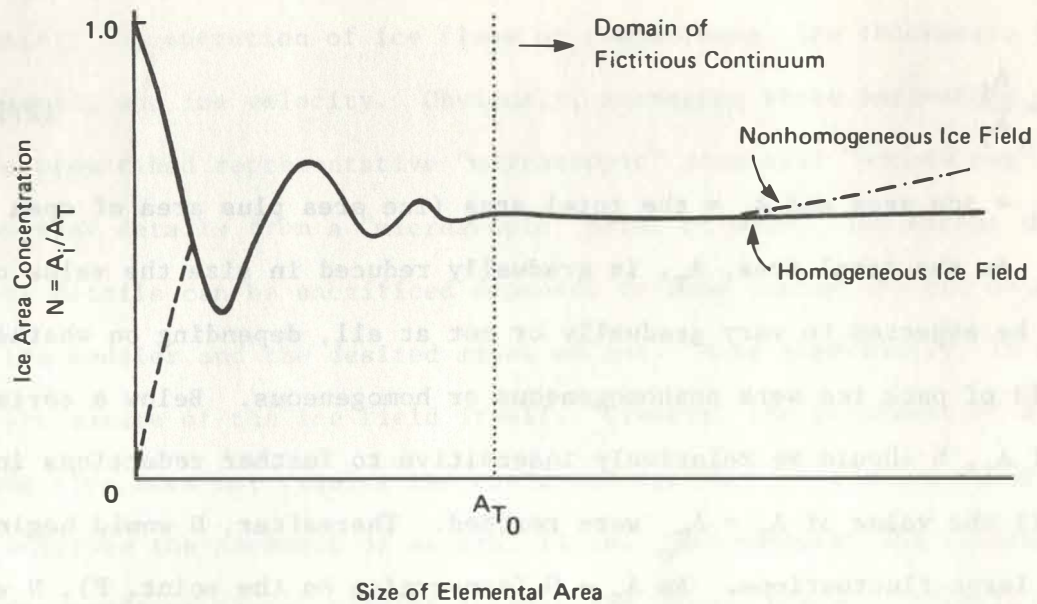
Figure 2.2 Definition of Representative Elemental Area (see Bear, 1972)

Typical mid-winter ice thicknesses (10-100 cm neglecting variations due

to ridging and rafting) in the Great Lakes are nearly ten times less than

those encountered in the Arctic (1 - 5 m). Combining these ice thicknesses

with the high temporal variability in weather patterns typical of the Great

Lakes basin creates considerable potential for ice deformation. This is

evident in the size distribution of ice floes as substantiated by inspec-

tion of side-looking radar images and their accompanying ice chart products.

Figure 2.3 is presented as an example of Lake Erie during mid-winter condi-

tions. The figure shows, excluding shallow harbors and bays, that areas

having little or no open water contain a high proportion of floes less than

0.5 km in diameter. No upper limit on floe size is specified, but a careful

study of the corresponding SLAR image could lead to the establishment of an ice

floe size distribution for the ice area present on that day. To do this manually

would be fairly tedious and time-consuming; however, it might be that a

light-sensitive computerized scanning technique could be designed for this

purpose which would facilitate the rapid analysis of ice floe dimensions and

floe size distribution.

The period of freezing temperatures in the Great Lakes basin is seldom

long enough to create lakewide stable ice sheets and, in fact, ice accretion

and ice dissipation can occur simultaneously in the same lake. Table 2.1

illustrates the probable percentage of ice cover for each of the Great Lakes

during mild, normal and severe winters.

Since stable ice covers are infrequent, large· expanses of open water

prevail, especially in early and late winter. However, because of the

weather variability, substantial movement and deformation of the ice cover

occurs during the ice season. This mechanical deformation and movement can

contribute greatly to the creation of open water areas; thereby enhancing

the rate of release of heat from the waterbody and the production of new ice.

The SLAR images portrayed in Figure 5.9 (p.197) illustrate this phenomenon.

A: Age
MED: 15-35 cm Thick
THN: 5-15 cm Thick
SS: Slush Ice

$\dfrac{A}{SS\text{-}THN} \dfrac{10}{10}$

$\dfrac{A}{MED} \dfrac{10}{253}$

$\dfrac{T}{14''}$
$\dfrac{T}{10\text{-}14''}$
$\dfrac{T}{12''}$
$\dfrac{T}{8\text{-}14''}$
$\dfrac{T}{6''}$

OPEN WATER

$\dfrac{10}{253}$ ⎰ 10: 100% Ice Cover
2: 20% of Floes Are Less Than 10 m in Diameter
5: 50% of Floes Are 10-500 m in Diameter
3: 30% of Floes Are Greater Than 500 m in Diameter
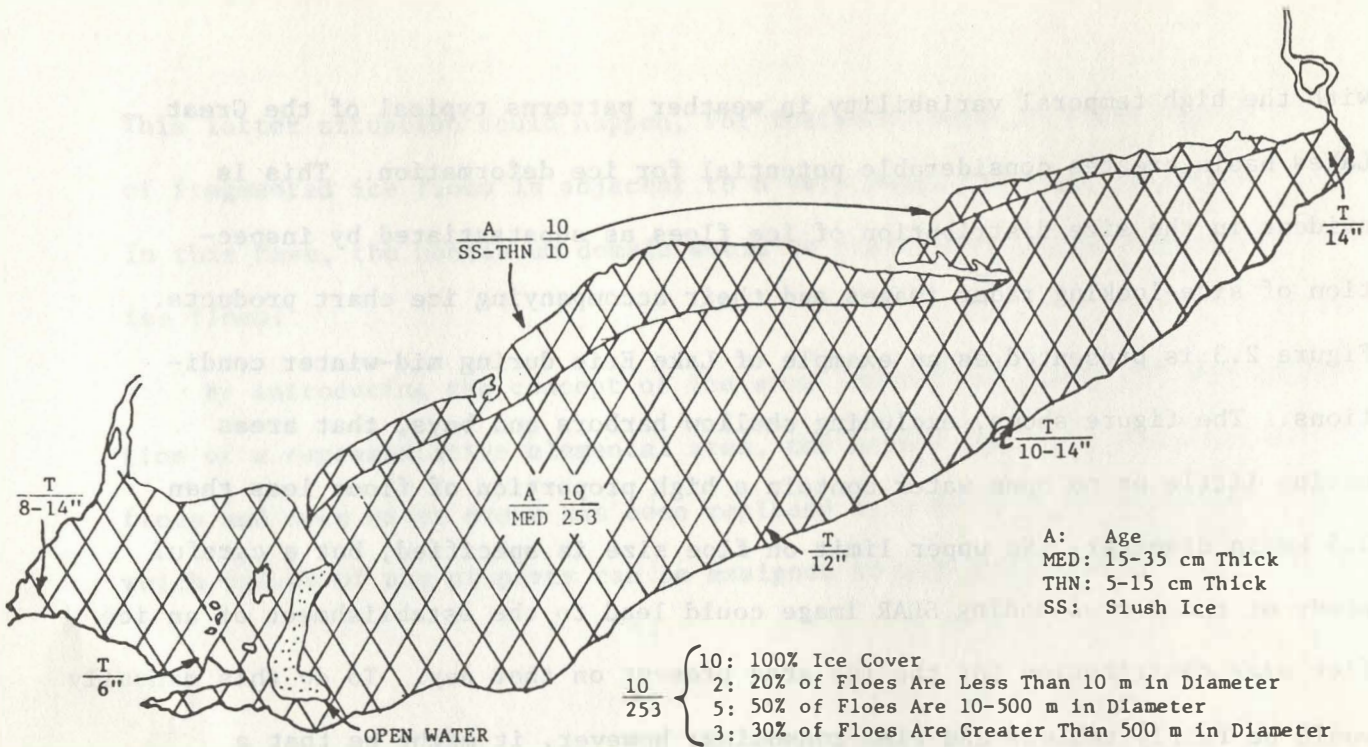
LAKE ERIE ICE COVER (FEBRUARY 4, 1976)

Figure 2.3   Ice Chart Product Prepared by U.S. Coast Guard Ice Navigation Center

Table 2.1

Maximum Percentage (%) of Lake Surface Covered During Mild, Normal
and Severe Winters for Each of the Great Lakes (After Rondy, 1971)

	Lake Superior	Lake Michigan	Lake Huron	Lake Erie	Lake Ontario
Mild Winter	40	10	40	50	8
Normal Winter	60	40	60	95	15
Severe Winter	95	80	80	100	25

During this period of the winter, a large expanse of open water was formed along the north shore of Lake Erie due to a combination of westerly and northwesterly winds and relatively warm temperatures. Cold weather brought about the formation of new ice where open water previously existed.

The simultaneous occurrence of open water, variable ice area concentration, and ridging (where the ice field is compacted) is illustrated in Figure 2.4. The areas of high radiation backscatter (light regions) in the SLAR image illustrate the highly fractured state of the ice cover. The darker areas are characteristic of open water or thin ice. In the ice chart product, which is an interpretation of the SLAR image combined with available direct observations from ship or shore, the spatial variation in concentration is distinctly shown, as are areas of open water. Where the ice area concentration is one, evidence of ridging is depicted.

In the following section, field equations will be developed for the ice field employing the continuum approximation. The limitations of this approach will be considered further in the application of the field equations to specific ice transport situations.

2.3 Development of Field Equations for Ice Transport

The governing equations for ice transport are derived in an Eulerian reference frame utilizing the concept of a representative elemental area. The ice cover is assumed to behave as a two-dimensional compressible continuum in which the continuum density is related to the ice area concentration. The governing equations include the equations of motion in the two coordinate directions, a conservation of ice mass equation, a conservation of ice area

27
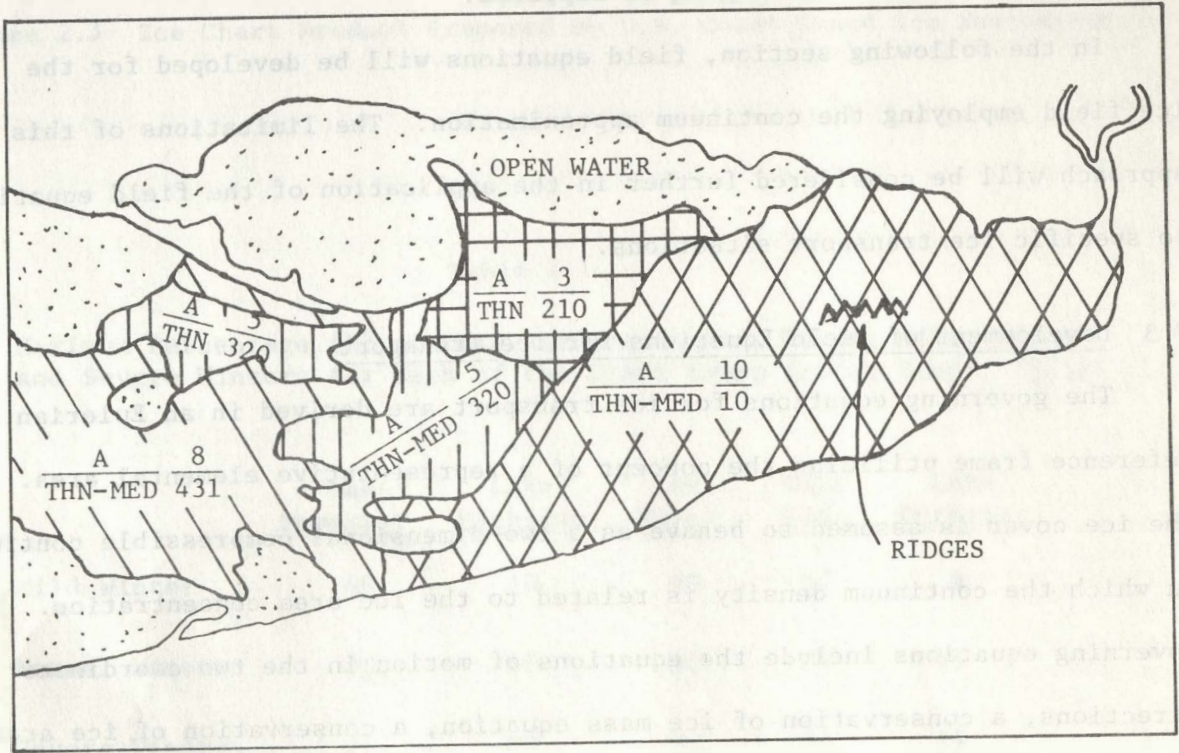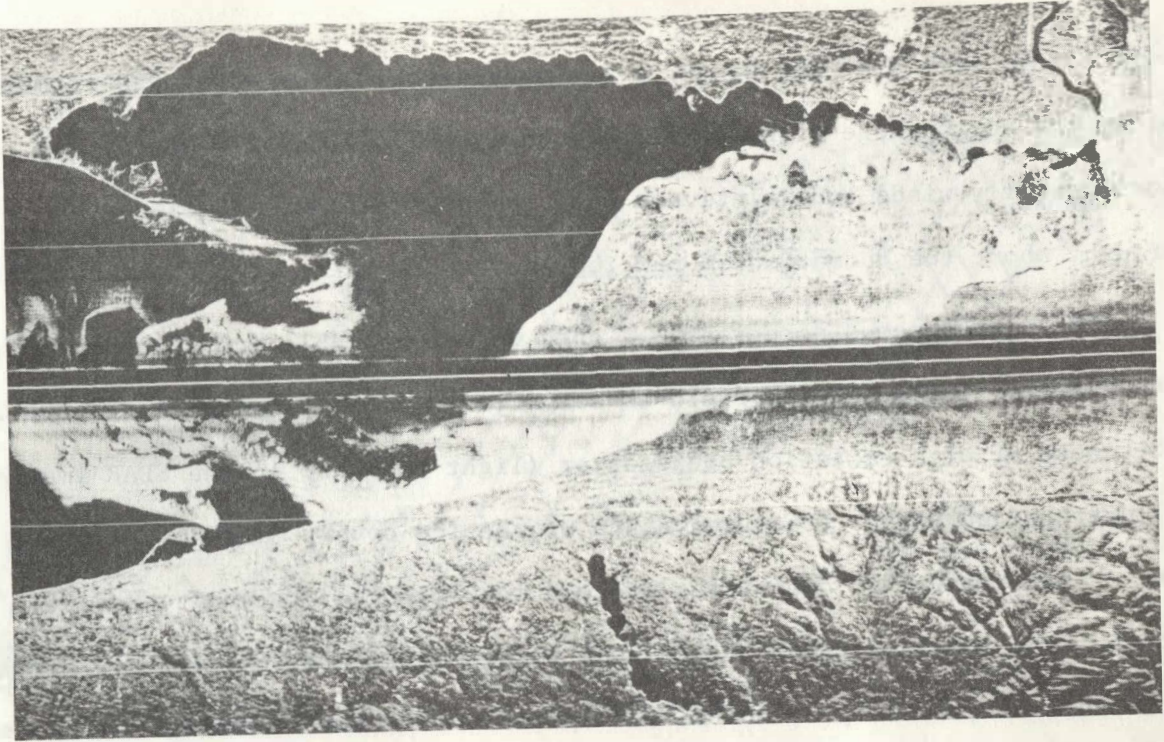
Figure 2.4   SLAR Image and Ice Chart Product of Lake Erie (March 8, 1976)

equation, and an equation of state that relates the internal ice pressure to the state of the ice field.

The state of the ice cover is treated in a macroscopic sense in this development. As previously indicated in the discussion of the variation of the ice area concentration in the macroscopic domain (section 2.2), the local microscopic pressures at specific points within the representative elemental area will vary considerably from the continuum internal ice pressure. At points of contact between ice floes the pressure could approach the crushing strength of ice. On the other hand, the pressure would be zero at points where no ice exists (open water).

Evans and Rothrock (1975) have dealt with the problem of relating the continuum ice pressure to local pressures which are of importance in engineering problems. They suggest the use of a probability distribution function for relating local pressure to the continuum ice pressure. This function is based on a maximization of the entropy within the respresentative elemental area in which the magnitude of local pressure is bounded by zero and the ultimate or crushing strength of the ice mass. They conclude that the continuum pressure will be much less than the crushing strength of ice with only a 0.68% chance of its ever being greater than one half of the crushing strength value. Intuitively, there would seem to be a good deal of randomness in the microscopic variables within the representative elemental area, and a stochastic analysis (similar to that of Evans and Rothrock) may very well be the best approach to relating macroscopic continuum variables to their local or microscopic counterparts within the elemental area. The topic of ice pressure is discussed later when considering the need for an equation relating ice pressure to the state of the ice cover.

2.3.1 Equations of Motion for Ice Field Continuum

The equations of motion are derived by considering the force balance on the representative elemental area of the physical system depicted in Figure 2.5.

$$\sigma_{xx} N t_i \, dy - \frac{1}{2} \frac{\partial}{\partial x} (\sigma_{xx} N t_i) \, dx \, dy$$

$$\sigma_{xy} N t_i \, dx + \frac{1}{2} \frac{\partial}{\partial y} (\sigma_{xy} N t_i) \, dy \, dx$$

$$\sigma_{xx} N t_i \, dy + \frac{1}{2} \frac{\partial}{\partial x} (\sigma_{xx} N t_i) \, dy \, dx$$

$$\sigma_{xy} N t_i \, dx - \frac{1}{2} \frac{\partial}{\partial y} (\sigma_{xy} N t_i) \, dx \, dy$$

t_i
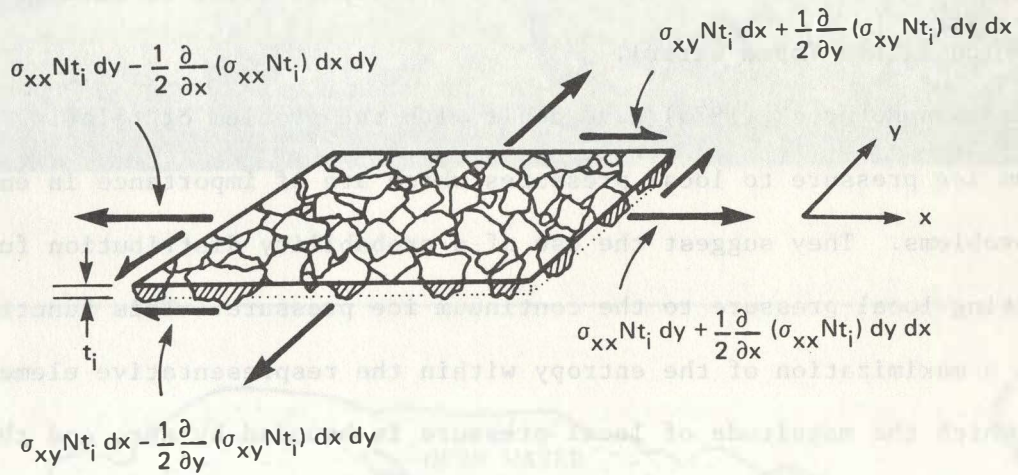
Figure 2.5   Schematic Sketch of Force Balance on the Representative
Elemental Area Containing Ice Floes and Open Water

The definition for the notation used is as follows:

t_i = average ice thickness within representative elemental area

N = ice area concentration [see Equation (2.2)]

u,v = average ice drift velocity components within the representative

elemental area

ρ_i = average ice mass density within the representative elemental area (assumed to be equal to 920 kg/m^3)

σ_{xx}, σ_{yy} = average normal ice stress in the x-y plane, acting over the average ice thickness at the boundaries of the representative elemental area.

σ_{xy}, σ_{yx} = average tangential ice stress in the x-y plane, acting over the average ice thickness at the boundaries of the representative elemental area.

τ_{a_x}, τ_{a_y} = wind stress components at the ice-air interface of the representative elemental area.

τ_{w_x}, τ_{w_y} = water stress components at the ice-water interface of the representative elemental area.

H = height of the water surface elevation measured from a mean water surface elevation

f = Coriolis parameter (= $2\Omega\sin\phi$)

Ω = angular velocity of earth's rotation (= 7.27 x 10^{-5} rad/sec)

ϕ = geographical latitude of ice field

$$(\rho_i Nt_i)\frac{du}{dt} = \frac{\partial}{\partial x}(\sigma_{xx} Nt_i) + \frac{\partial}{\partial y}(\sigma_{xy} Nt_i) + \tau_{a_x} N + \tau_{w_x} N$$

$$- (\rho_i Nt_i) g \frac{\partial H}{\partial x} + f(\rho_i Nt_i) v \qquad (2.2)$$

$$(\rho_i Nt_i)\frac{dv}{dt} = \frac{\partial}{\partial y}(\sigma_{yy} Nt_i) + \frac{\partial}{\partial x}(\sigma_{yx} Nt_i) + \tau_{a_y} N + \tau_{w_y} N$$

$$-(\rho_i Nt_i) g \frac{\partial H}{\partial y} - f(\rho_i Nt_i) u \qquad (2.3)$$

Equations (2.2) and (2.3) can be expressed symbolically in one vector

equation as

$$M_i \frac{d\vec{V}_i}{dt} = \vec{R} + \vec{F}_a + \vec{F}_w + \vec{G} + \vec{C} \tag{2.4}$$

where M_i is the ice mass per unit surface area of the continuum ($= \rho_i N t_i$),

$\vec{V}_i$ is the ice drift velocity ($= \vec{i}\, u + \vec{j}\, v$), $\frac{d\vec{V}_i}{dt}$ is the ice mass accelera-

tion expressed in material derivative form with a local and convective

term [$= \frac{\partial \vec{V}_i}{\partial t} + (\vec{V}_i \, \mathrm{grad}) \, \vec{V}_i$], $\vec{R}$ denotes the internal ice stress due to

interfloe forces and is given by $\vec{R} = \vec{i}\, R_X + \vec{j}\, R_y$ where $R_x = \frac{\partial}{\partial x}(\sigma_{xx} N t_i)$

$+ \frac{\partial}{\partial y}(\sigma_{xy} N t_i)$ and $R_y = \frac{\partial}{\partial y}(\sigma_{yy} N t_i) + \frac{\partial}{\partial x}(\sigma_{yx} N t_i)$, $\vec{F}_a$ is the stress at the air-ice

interface [$= \vec{i}(\tau_{a_X} N) + \vec{j}(\tau_{a_y} N)$], $\vec{F}_w$ represents the stress at the ice-water

interface [$= \vec{i}(\tau_{w_X} N) + \vec{j}(\tau_{w_y} N)$], $\vec{G}$ is the gravitational force arising from

the ice mass floating on a sloping water surface ($= - M_i g \vec{\nabla} H$), and $\vec{C}$ denotes

the Coriolis force that originates because the ice drift is viewed from a

rotating frame of reference [$= f M_i (\vec{k} \times \vec{V}_i)$].

The dependent variables in equations (2.2) and (2.3) are: the ice

area concentration, N; the ice thickness, t_i; the ice drift velocity com-

ponents, u and v; and the internal ice stress components, σ_{xx}, σ_{yy}, σ_{xy}, and

σ_{yx}. Invoking the requirement that there be a condition of equilibrium

of the representative elementary area with respect to the tangential stresses

[Yuan (1967), p. 83] gives $\sigma_{xy} = \sigma_{yx}$ and enables the state of stress at a

macroscopic point to be given by σ_{xx}, σ_{yy}, and σ_{xy}. The seven dependent

variables (N, t_i, u, v, σ_{xx}, σ_{yy}, σ_{xy}) can be further reduced if

a satisfactory constitutive law can be found to relate ice stress to

the velocity components or their space derivatives. A discussion of the

constitutive law for pack ice is presented in Section 2.3.2.

The usual picture of ice drift [Rothrock (1975b)] has the ice field

32

being dragged by the wind over a relatively motionless sea, with water

stress and internal ice stress being the principal resisting forces. The

steady-state version of equations (2.2) and (2.3) have been solved for

various combinations of the forces employing different constitutive laws

(see Section 1.2). Even though the steady-state form shows no explicit

dependence on time, temporal variability can be modeled by varying the

driving forces (the wind stress and sometimes the water stress) over a

period that is long compared to the transient response time for the ice

mass. The convective acceleration terms in the material derivative are

also usually neglected because of the slow movements of a drifting ice field.

The wind stress per unit surface area of ice is generally represented

by the following relation:

$$\tau_{a_k} = \rho_a C_a \left| V_{a_k} \right| V_{a_k} \tag{2.5}$$

where the subscript, k, is the index notation ($k = x,y$), ρ_a is the air mass

density, C_a is a stress coefficient, and V_{a_k} is the wind speed. The ab-

solute sign is used to retain the directional dependence of the wind stress.

Actually, the wind speed should be reduced by the ice speed, but since the

magnitude of $\vec{V}_i$ is almost always a small percentage of $\vec{V}_a$, it can usually

be neglected. The stress coefficient, C_a, is a function of the ice surface

roughness. Assuming C_a to be invariant with the wind speed seems justified

in view of the analysis of wind and water stress presented in Appendix A.

In the modeling of Arctic ice drift, the wind stress field is related to

the planetary boundary layer. This is accomplished by assuming a geostrophic

balance between the atmospheric pressure gradient force and the Coriolis

force in the free stream flow above the boundary layer and estimating

the momentum flux that is transported through the planetary boundary layer

[Brown (1977)]. The availability of wind speed and wind direction measurements
at many shore based stations will simplify the estimation of wind stresses
in the Great Lakes Basin. However, the problem of relating overland wind speeds
to over ice or over lake wind speeds remains [see Richards, et al (1966) or
Resio and Vincent (1976) for treatments of this problem in the Great Lakes
Basin].

The stress at the ice-water interface usually exerts a force counter
to the wind. The water stress per unit area of ice surface is given by:

$$\tau_{w_k} = \rho_w \ C_w \left| V_{i_k} - V_{w_k} \right| (V_{i_k} - V_{w_k}) \tag{2.6}$$

where ρ_w is the water density, C_w is a stress coefficient, and $V_{i_k} - V_{w_k}$ is
the relative velocity between the ice drift and water flow. The relative
velocity is used since V_{i_k} and V_{w_k} may be of the same magnitude. The stress
coefficient, C_w, as in the case of C_a, is also a function of the ice surfac
roughness at the ice-water interface and reflects a combination of both
skin friction and form drag. Usually, C_w is assumed to be independent of
the relative velocity. The stress has been shown (see Appendix A) to be
relatively constant for "medium rough" and "rough" ice surfaces, but seems
to increase with decreasing relative velocity for "smooth" ice. In the Arctic,
due to the lack of measured water currents, this stress field is also deter-
mined combining a boundary layer approach with the mean steady-state geo-
strophic ocean flow [McPhee (1975)].

In large lakes, the frictional influence of the lake bottom, the lateral
constraint of the lake shoreline, and the effect of tributary inflows and
outflows have been shown to be significant so that the assumption of a geo-
strophic flow is rarely valid. Three-dimensional time-dependent lake hydro-

34

dynamic models have been developed and applied during the last decade [Lick (1976), Simons (1976)]. Sheng and Lick (1973) have investigated the effect of a partial ice cover on the steady-state wind driven currents in Lake Erie. The ice was assumed stationary and a no-slip boundary condition was applied at the ice-water interface. Current velocities were computed numerically as a function of depth and horizontal location. Under-ice current velocities were demonstrated to be dependent on wind direction and location of ice cover and, in some cases, were comparable to velocities in open water (see Figure 2.6).

The stress coefficients for the ice-water interface in Arctic ice models (see Appendix A) are based on water current velocities one meter below the interface. A model similar to Sheng and Lick's could be used for estimating water currents for input to the ice transport equations (i.e., $\vec{V}_w(x, y)$). In general, however, spatial and temporal variations in $\vec{V}_w$ must be considered. Even in the presence of a constant applied wind stress, the changes in the size and location of open water areas that would result from ice drift, new ice formation, and ice dissipation can affect water currents. These variations could only be modeled by coupling the ice dynamics model with a time-dependent hydrodynamic model.

The gravitational force, $\vec{G}$, caused by spatial variations in the water surface elevation is generally a small contributing factor to the overall force balance. In the Arctic, the gradient of H can be evaluated from long-term averages of the sea surface topography. The availability of water level measurements at many shoreline points will simplify the estimation of the magnitude of $\vec{G}$ in the Great Lakes.
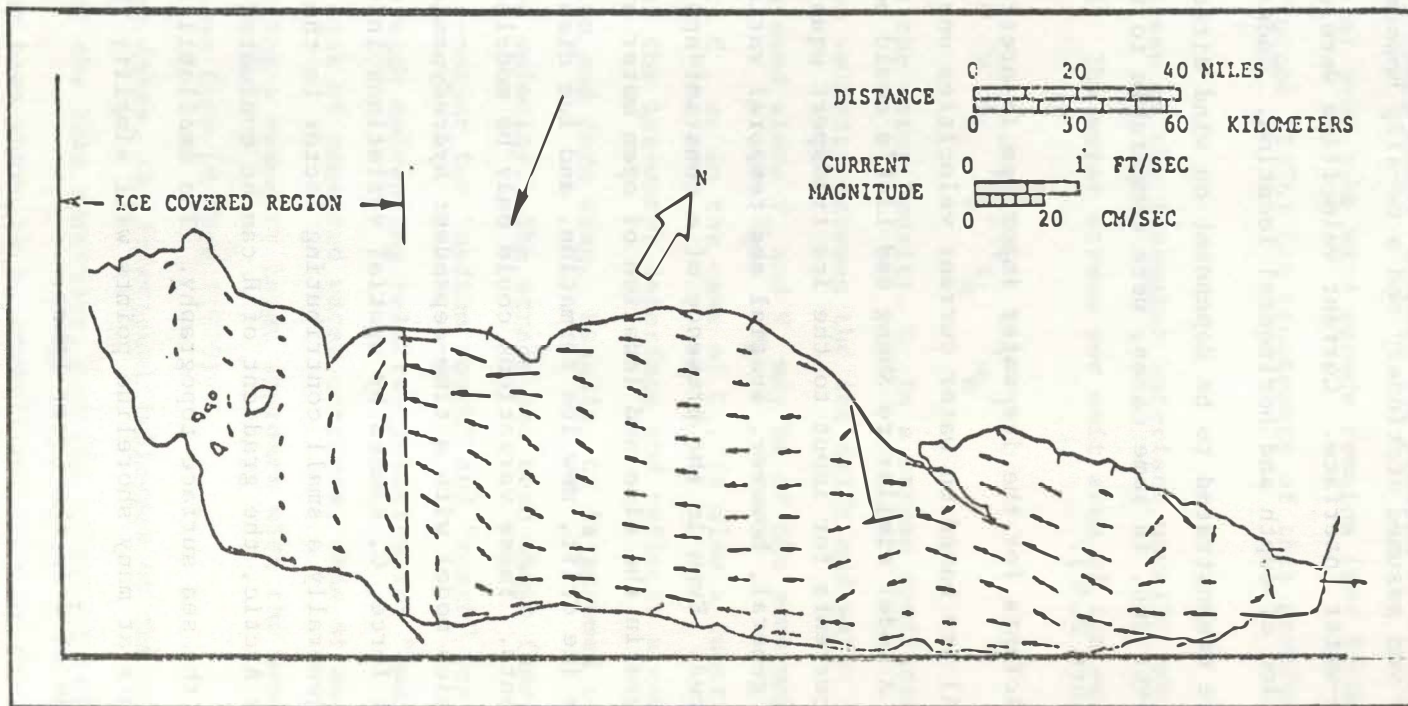
Figure 2.6   Circulation in a Partially Ice Covered Lake Erie
Horizontal Velocities at a Constant 3.6 Meters (12.0 ft) From Surface
Wind Velocity: 5.2 m/sec (18 fps), N7.5W
Frictional Depth: 18.2 m (60.0 ft)
Rivers: Detroit, Sandusky, Maumee, Niagara   (after Lick, 1976).

2.3.2 Constitutive Law for Pack Ice

Constitutive equations, which are also known as rheological equations of state, are essential to the complete mathematical formulation of the behavior of materials in response to external forces. The linear relationship between stress and strain (Hooke's Law) is the constitutive law for elastic solids. The linear relationship between stress and rate of strain is the basis for the constitutive law for Newtonian viscous fluids. The constitutive assumption for pack ice will be intimately related to the concept that pack ice exhibits continuum properties.

The development of a completely satisfactory constitutive law for pack ice in the macroscopic sense will depend, in large part, upon a good understanding of the microscopic processes. It is the microscopic processes that, together, produce the observed response in the fictitious continuum composed of ice floes and open water.

Thermodynamic and mechanical factors contribute to the evolution of an ice cover and its physical state at any given time during an ice season. It is unlikely that the continuum assumption is applicable either at all times or at all places. It is equally unlikely that one constitutive law will express the intrinsic behavior of an ice cover either at all times or at all places. Nevertheless, it is desirable to develop constitutive expressions for pack ice behavior, even if only applicable over short periods during the ice season or in selected regions of the ice field.

Reed and Campbell (1962), in their analysis of the unaccelerated drift of station Alpha (located on the Arctic pack ice) between April 1957 and November 1958, speculated on the role of internal ice resistance in the balance of forces. They conjectured that rubbing, bumping, and grinding of ice floes was not unlike the collision processes associated with fluid molecules. This analogy lead them to express the internal ice resistance with a term similar to the viscous term in the Navier-Stokes equations. Their findings, in applying this form of the internal ice resistance, were inconclusive. Campbell (1965) later applied this internal ice resistance concept to his calculations of wind-driven circulation of ice and water in the polar ocean (see Section 1.2).

Doronin (1970) modified Campbell's approach by using a variable ice viscosity that was linearly related to the ice area concentration, N. Neralla et al (1977) used this modified viscous approach to model the drift of pack ice in the Beaufort Sea with encouraging results. Glen (1970) assumed sea ice to be viscous, but with two ice viscosities; a shear ice viscosity relating the tangential ice stresses to rotational strain rates and a bulk ice viscosity relating the normal ice stresses to the linear strain rates (i.e., the compressibility of the ice pack).

Campbell and Rasmussen (1971) computed ice drift using three different versions of the viscous constitutive law, including the one proposed by Glen. They also introduced the concept that the magnitude of the ice viscosity might be different for converging and diverging ice fields. Hibler (1974) used Glen's constitutive law in his equlibrium drift model for the Arctic. In a later extension to this work, Hibler and Tucker (1976) developed an empirical linear relationship between ice viscosity and ice growth rate. This permitted seasonal variations in the viscosity coefficient.

Hibler and Tucker (1977) added a pressure term to the constitutive law proposed by Glen but assumed it to be a constant. The pressure term did not enter into their calculations of ice drift.

Plastic constitutive laws have also been proposed for sea ice. Proponents of the plastic laws [Coon (1974), Coon et al (1974), Pritchard, (1975), Rothrock (1975c)] contend that viscous laws do not produce results consistent with the behavior of an ice pack, i.e., the observed inability of an ice field to resist divergence and its rate-independent load-displacement response.

The plastic constitutive laws are based on notions that the ice pack is densely fractured, has a finite yield stress, and that the deformation processes such as ridging and rafting are rate independent and involve non-recoverable energy dissipation. The Arctic Ice Dynamics Joint Experiment model [Coon (1977)] utilizes such a plastic law. The internal ice stress is assumed to behave elastically until the yield strength is reached. The yield strength is dependent upon ice thickness. When the stress reaches the yield strength, no increase in ice stress can occur and the ice flows as a plastic material according to a prescribed flow law. Pritchard (1975) presents a detailed description of this constitutive law.

Hibler (1977a) relates the plastic and viscous laws for sea ice by considering the stochastic variations in sea ice deformation rates. These variations can cause an average stress-strain rate relationship that is viscous in nature, even though the non-averaged relationship exhibits plastic behavior. In an extension to this work, Hibler (1977b) used his averaged constitutive law to represent the internal ice stress with a non-constant ice pressure. By introducing the ice pressure term, the ice

field can remain stationary (i.e., where strain rates equal zero) and still have a balance between externally applied forces and internal ice stress. The viscosities used in this model were permitted to vary with the strain rates. This allowed Hibler to use time and space scales which were advantageous to his numerical scheme.

Rothrock (1975a) provides a good review of the formulation of continuum models of ice transport, including attempts to relate interfloe forces to kinematic variables. He states that a constitutive law for pack ice should not permit tensile stresses to exist (since ice is notoriously weak in tension, especially pack ice fields). Also, resistance to pure convergence or to shear should be of the same magnitude since both are due to the same processes of ridging and rafting. It is not apparent that this latter requirement necessarily be satisfied for scattered ice (or when ice area concentrations are significantly less than one). His request that explicit relationships be established between the internal ice stresses (σ_{xx}, σ_{yy}, σ_{xy}) and the kinematic variables (e.g., strain rates) before proceeding to write expressions for the internal ice resistance, $\vec{R}$, is well taken.

Both the viscous and the plastic constitutive approaches have their respective advantages and disadvantages. Numerical solutions of the ice drift equations, employing either approach, have produced the essential features of Arctic ice drift; but so has an inviscid solution (Rothrock (1975b).

The constitutive law outlined below employs the viscous analogy for the behavior of pack ice. Yuan (1967), in his text on the Foundations of Fluid Mechanics, gives the following equations for the internal stresses in a Newtonian viscous compressible fluid (in two dimensions).

$$\sigma_{xx} = 2\mu \frac{\partial u_f}{\partial x} + \frac{2}{3}(\mu_1 - \mu) \vec{\nabla} \cdot \vec{q} - p \qquad (2.7)$$

$$\sigma_{yy} = 2\mu \frac{\partial v_f}{\partial y} + \frac{2}{3}(\mu_1 - \mu) \vec{\nabla} \cdot \vec{q} - p \qquad (2.8)$$

$$\sigma_{xy} = \mu \left[\frac{\partial v_f}{\partial x} + \frac{\partial u_f}{\partial y} \right] \qquad (2.9)$$

In these equations, μ is the dynamic viscosity of the fluid, μ_1 is the so-called second viscosity coefficient or bulk viscosity, p is the hydrostatic pressure or reference pressure in the fluid, and $\vec{q} = \vec{i}u_f + \vec{j}v_f$, the velocity vector of the fluid. The assumptions used in the development of the above constitutive equations for a Newtonian viscous compressible fluid are: (1) that the stress components be linear functions of the strain rates, (2) that the equations relating stress to strain rates be invariant to coordinate transformations, and (3) that the stress components reduce to the static pressure, p, when all the velocity gradients (or strain rates) are zero. This last assumption will present difficulties when applied to the case of pack ice.

The constitutive equations for pack ice, using the viscous medium analogy, can be written in a manner similar to equations (2.7), (2.8) and (2.9) as:

41

$$\sigma_{xx} = 2k_1 \frac{\partial u}{\partial x} + (k_2 - k_1) \vec{\nabla} \cdot \vec{V}_i - p \qquad (2.10)$$

$$\sigma_{yy} = 2k_1 \frac{\partial v}{\partial y} + (k_2 - k_1) \vec{\nabla} \cdot \vec{V}_i - p \qquad (2.11)$$

$$\sigma_{xy} = k_1 \left(\frac{\partial v}{\partial x} + \frac{\partial u}{\partial y} \right) \qquad (2.12)$$

in which k_1 is the ice shear viscosity, k_2 denotes the ice bulk viscosity, and p is the ice pressure. Equations (2.10), (2.11), and (2.12) are directly analogous to the constitutive law proposed by Hibler (1977b).

As in fluid mechanics, the mean normal stress, $\bar{\sigma}$, is found by averaging σ_{xx} and σ_{yy} (in the two-dimensional ice continuum). This gives

$$\bar{\sigma} = -p + k_2 \vec{\nabla} \cdot \vec{V}_i \qquad (2.13)$$

which states that the ice pressure is constant in all directions at a macroscopic point within the continuum. If the ice field is incompressible or if it is stationary, $\vec{\nabla} \cdot \vec{V}_i = 0$, and the average normal stress at a "point" is equal to the internal ice pressure.

A common example of a static force balance is an ice field subjected to an onshore wind and constrained by a shoreline boundary. Considering the physical situation depicted in Figure 2.7, the basic force-momentum equations reduce to

$$0 = \frac{\partial(\sigma_{xx} N t_i)}{\partial x} + \tau_{a_x} N + \tau_{w_x} N - (\rho_i N t_i) g \frac{\partial H}{\partial x} \qquad (2.14)$$

$$0 = \frac{\partial(\sigma_{yy} N t_i)}{\partial y} + \tau_{a_y} N + \tau_{w_y} N - (\rho_i N t_i) g \frac{\partial H}{\partial y} \qquad (2.15)$$

All terms dependent upon the ice velocity or ice velocity gradients disappear since the ice field is stationary. The viscous constitutive law given by equations (2.10), (2.11), and (2.12) reduce to $\sigma_{xx} = \sigma_{yy} = -p$ and $\sigma_{xy} = 0$. Thus, for this special case of static equilibrium the ice pressure can be obtained from direct integration; i.e.,

$$p(x,y) = \frac{1}{Nt_i} \int \left[\tau_{a_x} N + \tau_{w_x} N - M_i g \frac{\partial H}{\partial x} \right] dx$$

$$+ \frac{1}{Nt_i} \int \left[\tau_{a_y} N + \tau_{w_y} N - M_i g \frac{\partial H}{\partial y} \right] dy + constant \qquad (2.16)$$
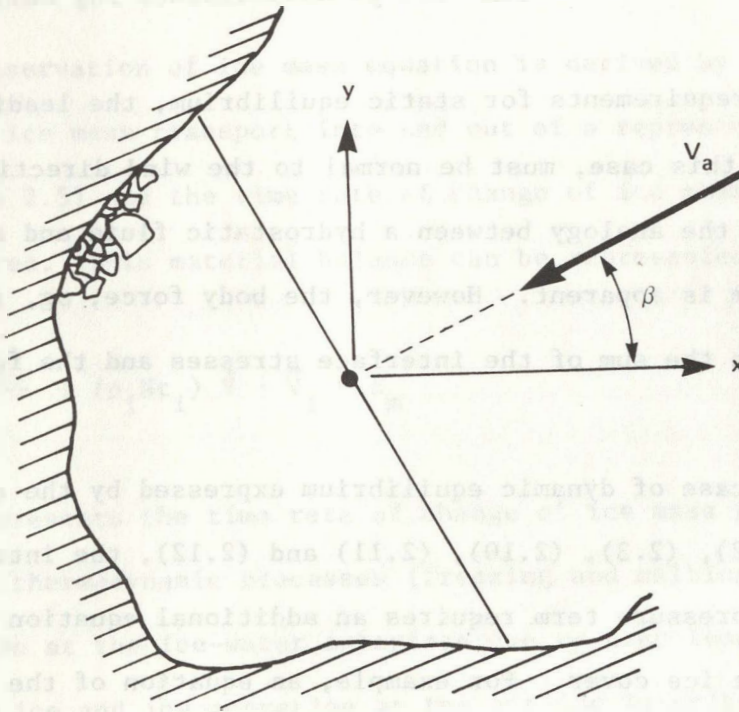
Figure 2.7   Schematic Sketch of Static Equilibrium of an Ice Field
with an Onshore Wind

In viewing the physical situation in Figure 2.6, it can be seen that rotating the coordinate axes counterclockwise through an angle, β, causes the y-component of wind stress to vanish. Furthermore, if τ_w and gradient of H are assumed zero, the expression for ice pressure becomes simply

$$p = \frac{1}{Nt_i} \int \tau_{a_x} N \, dx + \text{constant} \qquad (2.17)$$

If N = constant (probably N = 1) and τ_{a_x} = constant, equation (2.17) reduces to

$$p = \frac{\tau_{a_x}}{t_i} x \qquad (2.18)$$

To satisfy the requirements for static equilibrium, the leading edge of the ice field, in this case, must be normal to the wind direction for this special case. Thus, the analogy between a hydrostatic fluid and an ice field in static equilibrium is apparent. However, the body force, ρg, in the fluid case is replaced with the sum of the interface stresses and the force due to water surface tilt.

In the general case of dynamic equilibrium expressed by the complete set of equations (2.2), (2.3), (2.10), (2.11) and (2.12), the introduction of the internal ice pressure term requires an additional equation that relates p to the state of the ice cover. For example, an equation of the form

$$p = p(N, t_i, p_c, \ldots) \qquad (2.19)$$

44

where p_c = crushing strength of ice. Hibler (1977b) utilized the following equation

$$p = p^* \, t_i \, \exp[C(1 - N)] \qquad (2.20)$$

in which p^* and C were stated to be empirical strength constants. Rothrock (1975c) has discussed the dependence of p^* upon $g(t_i)$ (see equation 2.22). Equation (2.20) is considered to be highly tentative. The probe for a suitable equation of state for pack ice will involve laboratory testing, field studies, and the development of conceptual models that relate the important variables. Even so, it is likely that formulations of equations of state will only have application over limited ranges of these variables.

2.3.3 Equation for Conservation of Ice Mass

The conservation of ice mass equation is derived by considering the net flux of ice mass transport into and out of a representative elemental area (Figure 2.5) and the time rate of change of ice mass within the elemental area. This material balance can be represented as

$$\frac{d(\rho_i N t_i)}{dt} + (\rho_i N t_i) \, \vec{\nabla} \cdot \vec{V_i} = E_m \qquad (2.21)$$

where E_m represents the time rate of change of ice mass per unit surface area due to thermodynamic processes (freezing and melting). It includes ice accretion at the ice-water interface due to heat loss from the water through the ice and ice accretion at the air-ice interface due to freezing rain or snow. Ice melt could, of course, take place at either interface. It is noted that the ice thickness, t_i, is the average ice thickness of the

ice floes contained in the representative elemental area. Therefore, ice thickness changes due to mechanical deformation can not be specified in this form of the mass conservation equation.

Maykut and Thorndike (1973), Coon et al (1974), Thorndike et al (1975), and Rothrock (1975a) have described an ice thickness distribution equation which accounts for the ice thickness changes due to thermodynamic and mechanical processes separately. Conceptually, a thickness distribution $g(t_i)$ is defined which, when integrated between two specified thicknesses, gives the fraction of ice area covered by ice within that thickness band. This thickness distribution $g(t_i)$ is said to satisfy an ice thickness balance equation given by

$$\frac{dg(t_i)}{dt} = - g(t_i) \vec{\nabla} \cdot \vec{V}_i - \frac{\partial}{\partial t} \alpha g(t_i) + \psi \qquad (2.22)$$

in which α is the rate of ice thickness change due to thermodynamic processes and ψ is a redistribution function that represents mechanical changes in ice thickness due to rafting and ridging and the creation of open water due to lead formation. In application, the thermodynamic rate change, α, is considered to be specified. The estimation of the redistribution function, ψ, requires assumptions about the distribution of ice that fails in ridging, about the thickness of the ridged ice produced, and how ψ may depend on ice strain rates [Rothrock (1975a)]. Although knowledge of $g(t_i)$ would provide an estimate of the range of ice thicknesses that may be present within the representative elemental area and the proportion of that area that could be assigned to any specified thickness, the governing equation (2.22) appears too complicated for practical purposes.

2.3.4 Equation for Conservation of Ice Area

A second conservation equation is introduced since a solution to the equations of motion is dependent on both ice mass, M_i, and the ice area concentration, N. Redistributing the ice mass, M_i, does not, in itself, define the state of the ice cover in terms of the ice area concentration and the ice thickness. Therefore, to determine the contribution of each to the state of the ice cover, a conservation of ice area is employed which equates the net flux of ice area into and out of a representative elemental area to the time rate of change of ice area within the continuum element.

Changes in ice area occur due to new ice formation, ice dissipation, and mechanical redistribution. These changes can be accounted for, at least symbolically, by the addition of source and sink terms to the area balance equation.

The complete ice area balance equation is written as:

$$\frac{dN}{dt} + N \vec{\nabla} \cdot \vec{V}_i = E_a - R_a \tag{2.23}$$

where E_a represents the rate of ice area change due to thermodynamic processes and R_a denotes the rate of ice area changes due to mechanical redistribution. A similar equation, without the source/sink terms has been employed by Doronin (1970).

2.4 Summary of Governing Field Equations

The equations that govern the transport and conservation of ice utilizing the continuum approximation and the viscous constitutive law relating ice stress to ice strain rate are summarized here. Collectively, they form a set of four partial differential equations with an additional (and yet

unspecified) equation that relates the ice pressure to the state of the
ice cover. The equations of motion are formed by substituting equations
(2.5), (2.6), (2.10), (2.11), and (2.12) into equations (2.2) and (2.3).
The components of the equations of motion then become:

$$M_i \frac{du}{dt} = N\rho_a C_a |V_{a_x}| V_{a_x} - N\rho_w C_w |u - V_{w_x}| (u - V_{w_x})$$

$$- M_i g \frac{\partial H}{\partial x} + f M_i v$$

$$+ \frac{1}{\rho_i} \frac{\partial}{\partial x} \left\{ \left[k_1 \left(\frac{\partial u}{\partial x} - \frac{\partial v}{\partial y} \right) + k_2 \vec{\nabla} \cdot \vec{V}_i - p \right] M_i \right\}$$

$$+ \frac{1}{\rho_i} \frac{\partial}{\partial y} \left\{ \left[k_1 \left(\frac{\partial v}{\partial x} + \frac{\partial u}{\partial y} \right) \right] M_i \right\} \qquad (2.24)$$

$$M_i \frac{dv}{dt} = N\rho_a C_a |V_{a_y}| V_{a_y} - N\rho_w C_w |v - V_{w_y}| (v - V_{w_y})$$

$$- M_i g \frac{\partial H}{\partial y} - f M_i u$$

$$+ \frac{1}{\rho_i} \frac{\partial}{\partial y} \left\{ \left[k_1 \left(\frac{\partial v}{\partial y} - \frac{\partial u}{\partial x} \right) + k_2 \vec{\nabla} \cdot \vec{V}_i - p \right] M_i \right\}$$

$$+ \frac{1}{\rho_i} \frac{\partial}{\partial x} \left\{ \left[k_1 \left(\frac{\partial v}{\partial x} + \frac{\partial u}{\partial y} \right) \right] M_i \right\} \qquad (2.25)$$

The conservation equations are written again for completeness. The con-
servation of ice mass equation is

$$\frac{dM_i}{dt} + M_i \vec{\nabla} \cdot \vec{V}_i = E_m \qquad (2.26)$$

48

and the conservation of ice area equation is

$$\frac{dN}{dt} + N \vec{\nabla} \cdot \vec{V}_i = E_a - R_a \qquad (2.27)$$

where all terms are as previously defined.

The above four equations contain five dependent variables: u, v, N, M_i, and p. In general, therefore, a fifth equation is needed to relate p and the state of the ice cover. The form of this equation is not known. However, the general functional relationship between p and the state variables may be approximated by

$$p = p(N, \ t_i, \ p_c) \qquad (2.28)$$

in which p_c is the crushing strength of ice which is known to be dependent upon ice type and ice temperature [Michel (1978)].

The ice thickness, t_i, can be determined from knowledge of M_i and N since

$$t_i = \frac{M_i}{\rho_i N} \qquad (2.29)$$

Thus, in principle, the formulation of the governing field equations for ice transport has been accomplished. Various coefficients must be determined empirically. These are: the wind stress coefficient, C_a; the water stress coefficient, C_w; the ice shear viscosity, k_1; and the ice bulk viscosity, k_2. Of course, the complete mathematical formulation requires the specification of appropriate initial and boundary conditions. This aspect will be considered in the application of simplified

49

versions of these equations to specific physical situations.

The governing equations can be put into dimensionless form by introducing reference quantities as follows:

$$x' = \frac{x}{L} \ , \ y' = \frac{y}{L} \ , \ H' = \frac{H}{L} \ , \ M_i' = \frac{M_i}{\rho_i L}$$

$$u' = \frac{u}{\left|\vec{V}_a\right|} \ , \ v' = \frac{v}{\left|\vec{V}_a\right|} \ , \ t' = \frac{t\left|\vec{V}_a\right|}{L} \ , \ p' = \frac{p}{\rho_i V_a^2}$$

When these new dimensionless variables are substituted into the governing equations, the following dimensionless forms of those equations are obtained:

$$M_i' \frac{du'}{dt'} = C_1 N \left|\frac{V_{a_x}}{\vec{V}_a}\right| \frac{V_{a_x}}{\left|\vec{V}_a\right|} - C_2 N \left| u' - V_{w_x}' \right| (u' - V_{w_x}')$$

$$- \frac{1}{F_a^2} \frac{\partial H'}{\partial x'} + \frac{1}{R_o} v' + \frac{\partial}{\partial x'} \left\{ \left[R_1^{-1} \left(\frac{\partial u'}{\partial x'} - \frac{\partial v'}{\partial y'} \right) + R_2^{-1} \vec{\nabla}' \cdot \vec{V}_i' - p' \right] M_i' \right\}$$

$$+ \frac{\partial}{\partial y'} \left\{ \left[R_1^{-1} \left(\frac{\partial v'}{\partial x'} + \frac{\partial u'}{\partial y'} \right) \right] M_i' \right\} \tag{2.30}$$

$$M_i' \frac{dv'}{dt'} = C_1 N \left|\frac{V_{a_y}}{\vec{V}_a}\right| \frac{V_{a_y}}{\left|\vec{V}_a\right|} - C_2 N \left| v' - v_{w_y}' \right| (v' - V_{w_y}')$$

$$- \frac{1}{F_a^2} \frac{\partial H'}{\partial y'} - \frac{1}{R_o} u' + \frac{\partial}{\partial y'} \left\{ \left[R_1^{-1} \left(\frac{\partial v'}{\partial y'} - \frac{\partial u'}{\partial x'} \right) + R_2^{-1} \vec{\nabla}' \cdot \vec{V}_i' - p' \right] M_i' \right\}$$

$$+ \frac{\partial}{\partial x'} \left\{ \left[R_1^{-1} \left(\frac{\partial v'}{\partial x'} + \frac{\partial u'}{\partial y'} \right) \right] M_i' \right\} \tag{2.31}$$

$$\frac{dM_i'}{dt'} + M_i' \vec{\nabla}' \cdot \vec{v}_i' = E_m' \tag{2.32}$$

$$\frac{dN}{dt'} + N \vec{\nabla}' \cdot \vec{v}_i' = E_a' - R_a' \tag{2.33}$$

in which

$$C_1 = \frac{\rho_a}{\rho_i} C_a \quad, \quad C_2 = \frac{\rho_w}{\rho_i} C_w \quad, \quad R_o = \frac{|\vec{V}_a|}{fL}$$

$$F_a = \frac{|\vec{V}_a|}{\sqrt{gL}} \quad, \quad R_1 = \frac{|\vec{V}_a|\rho_i L}{k_1} \quad, \quad R_2 = \frac{|\vec{V}_a|\rho_i L}{k_2}$$

$$E_m' = \frac{E_m}{\rho_i |\vec{V}_a|} \quad, \quad E_a' = \frac{E_a L}{|\vec{V}_a|} \quad, \quad R_a' = \frac{R_a L}{|\vec{V}_a|}$$

$$V_{w_x}' = \frac{V_{w_x}}{|\vec{V}_a|} \quad, \quad V_{w_y}' = \frac{V_{w_y}}{|\vec{V}_a|}$$

The solution of the complete set of governing equations (which includes the unspecified relation between p and the state of the ice cover) for any waterbody requires careful consideration of initial and boundary conditions; a reasonably adequate set of input data for the environmental para-meters such as wind speed and direction; reliable estimates of the coefficients (C_a, C_w, k_1, k_2, etc.); and a significant commitment to analysis. This includes stability and sensitivity testing of the numerical scheme employed. The governing equations presented here are based on the viscous analogy for representation of the constitutive law for pack ice. They also are dependent on the applicability of the continuum concept. Many of the details related

51

to ridging, rafting, and lead formation are simply not dealt with. The mathematical model will probably not always adequately represent real world ice dynamics. Similar mathematical models have been found to satisfactorily reproduce the large scale features of ice drift in the Arctic Basin, which is a promising virtue. Undoubtedly, they will be further revised, modified, and improved as experience in application is buttressed with better physical understanding and a more adequate data base.

In subsequent sections, various simplified forms of these governing equations will be investigated; mainly to clarify the physics of ice transport processes and to provide a better understanding of ice transport in large lakes. As mentioned early in this report, thermodynamic processes will be neglected as well as the mechanical processes of ridging and rafting. This is not to minimize their importance. It is felt that these simplifications will not detract greatly in the development of ice transport models for large lakes, since there is much to be learned and understood about the behavior of their ice covers.

III. ANALYSIS OF THE DYNAMICS OF AN ISOLATED ICE FLOE

3.1 Introduction

Although the usual image of an iceberg has little validity in lakes, there are occasions when isolated floes or assemblages of floes can be analyzed as rigid bodies. Studying the behavior of isolated ice floes provides an opportunity to increase one's understanding of ice dynamics without the complexities of compactness and floe interaction effects.

The motion of a free floating, rigid body ice floe is discussed in this chapter. Numerical solutions to the governing equation for a single rigid body ice floe in one dimension and in two dimensions are presented. The effects of water waves on the transport of an ice floe are investigated and shown to have importance under certain conditions. The results of experiments conducted in a wind-wave tank with simulated model ice floes are presented. The interfacial stress coefficients, C_a and C_w, are estimated by comparison of the numerical solution to the governing equation with the experimental findings. In these experiments, the transient responses of the model ice floes are examined and used to evaluate the justification for neglecting the acceleration term in two-dimensional multi-floe ice dynamics models.

3.2 Uni-Directional Transport of an Isolated Ice Floe

3.2.1 Formulation of Equation of Motion

The physical situation being considered is illustrated in Figure 3.1. In this one-dimensional analysis, the Coriolis force can be excluded. In
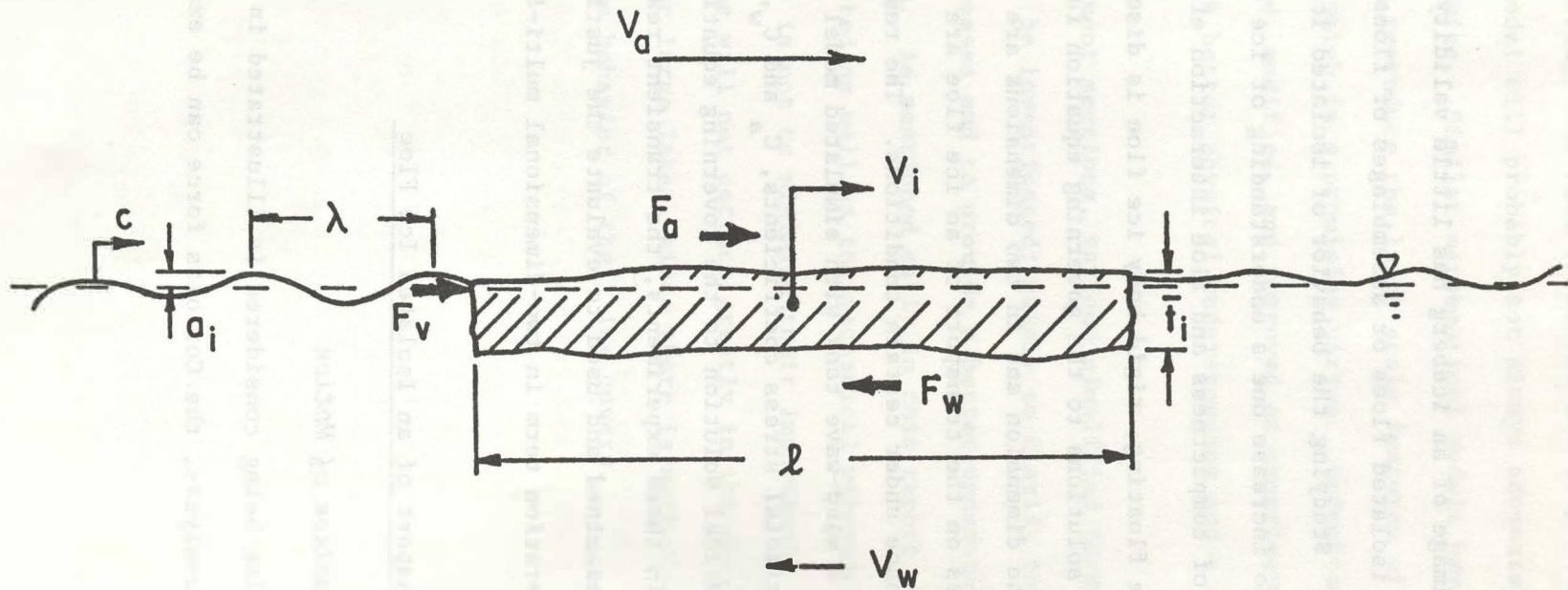
53

Figure 3.1 Schematic Representation of the One-Dimensional Force Balance on an Ice Floe
(C = Wave Celerity, λ = Wave Length, a_i = Incident Wave Amplitude, ℓ = Ice Floe Length,
t_i = Average Ice Floe Thickness, V_i = Ice Floe Velocity, V_w = Water Velocity, V_a = Wind
Velocity, F_V = Wave Force, F_a = Wind Drag, F_w = Water Drag)

addition, the gravitational force component due to a sloping water surface has been neglected. (This effect is treated separately later in this chapter.) With these simplifications, the one-dimensional equation of motion for the ice floe is given by:

$$m_i \frac{d\vec{V}_i}{dt} = \vec{F}_a + \vec{F}_w + \vec{F}_v + \vec{A}_r \qquad (3.1)$$

where m_i is the mass of the isolated ice floe, $\vec{V}_i$ is the ice floe velocity, $\vec{F}_a$ is the force exerted by the wind at the air-ice interface, $\vec{F}_w$ is the force exerted at the ice-water interface, $\vec{F}_v$ is the wave force, and $\vec{A}_r$ is an acceleration reaction.

Acceleration Reaction

The acceleration reaction, $\vec{A}_r$, is non-zero only when $\vec{V}_i$ is changing and is given by [Batchelor (1967)],

$$\vec{A}_r = - mC_m \frac{d\vec{V}_i}{dt} \qquad (3.2)$$

where m is the mass of fluid displaced by the ice and C_m is the virtual mass coefficient. The virtual mass, mC_m, is added to the ice mass itself to obtain the total mass affected. Since the ice is located at the interface of two fluids, the acceleration reaction becomes:

$$\vec{A}_r = - (C_{ma} \rho_a \Psi_a + C_{mw} \rho_w \Psi_w) \frac{d\vec{V}_i}{dt} \qquad (3.3)$$

where C_{ma} and C_{mw} are the virtual mass coefficients in air and water, and Ψ_a and Ψ_w are the displaced volumes of air and water, respectively.

The displaced volumes of air and water are given by $\Psi_a = \Psi_i(1 - S_i)$ and $\Psi_w = \Psi_i S_i$, where Ψ_i is the volume of the ice floe and S_i is the specific gravity of ice. The virtual mass effect caused by the air flow can be neglected relative to the virtual mass effect of the water flow (i.e., $C_{ma} \rho_a \Psi_a << C_{mw} \rho_w \Psi_w$. Additionally, $\rho_w S_i$ is equal to the ice density, ρ_i, and C_{mw} is replaced by C_m for simplicity. Therefore, equation (3.3) reduces to:

$$\vec{A}_r = - C_m m_i \frac{d\vec{V}_i}{dt} \tag{3.4}$$

Force at the Air-Ice Interface

The total wind drag is obtained by integrating the tangential stress and the normal pressure over the ice surface area. It is impractical to make this distinction, in general, and, therefore, C_a is represented as an average surface stress coefficient that incorporates both the frictional and form drag effects. The total wind drag is estimated by integrating τ_a over the surface area of the ice floe [see equation (2.5)]. Utilizing the concept of an "integrated average" stress coefficient, $\overline{C}_a$, the wind force is given by

$$\vec{F}_a = \vec{i} F_{a_x} + \vec{j} F_{a_y} = F_{a_k} = \rho_a \overline{C}_a A |V_{a_k}| (V_{a_k}) \tag{3.5}$$

In principal, one must consider the effect of the difference in the roughness of the water surface and ice floe surface and the modification of the atmospheric boundary layer flow in evaluating the wind drag. However, in practice, this will generally not be done because of the lack of

sufficient information on ice surface roughness and ice and water tempera-
tures. An analysis of data from several Arctic sea ice experiments (see
Appendix A) indicates that the wind stress coefficient, C_a, has little
dependence on the wind speed. Its magnitude is determined primarily by
the surface roughness characteristics of the ice floe.

Force at the Ice-Water Interface

Similar to the case of the wind stress coefficient, the local water
stress coefficient, C_w, may be treated as being independent of the relative
velocity between the ice floe and the water current. The ice underside
roughness has the greatest influence on the magnitude of C_w. Again utiliz-
ing the concept of an "integrated average" water stress coefficient, $\overline{C}_w$,
the total force at the ice-water interface can be estimated using [see
equation (2.6)].

$$\vec{F}_w = \vec{i} \, F_{w_x} + \vec{j} \, F_{w_y} = F_{w_k} = \rho_w \overline{C}_w A |V_{i_k} - V_{w_k}| (V_{i_k} - V_{w_k}) \tag{3.6}$$

A free-floating ice floe may be surrounded by a significant area of
open water. Horizontal momentum can, in this case, be transferred to the
water by the wind, creating water currents near the surface. Thus, an
indirect mechanism for transferring wind energy to the ice floe is estab-
lished. The complexities of the variation of water velocity with depth
below the surface and the interaction of the ice floe movement with water
currents preclude an accurate estimate of $\vec{V}_w$.

The characteristics of wind-generated water currents ve been studied
by several investigators, with most of the work being laboratory oriented
in one-dimensional wind-wave tanks. Determination of the magnitude of the

57

surface current at the air-water interface (the surface drift current) has received the most attention [Keulegan (1951); Plate et al (1971); Wu (1968), (1975)]. It has been shown that the wind drift surface current ranges between 3% and 3.5% of the wind speed. Below the surface, water velocities decay rapidly, with a logarithmic variation given by:

$$\frac{U_o - V_w}{U_{*_w}} = \frac{1}{\kappa} \ln(\frac{z}{z_{o_w}}) + 8.5 \qquad (3.7)$$

where U_o is the surface drift velocity, V_w is the water velocity at depth, z, below the surface, U_{*_w} is the friction velocity (= $\sqrt{\tau_a/\rho_w}$) where τ_a is the stress at the air-water interface, κ is the von Karman constant (≈ 0.4), and z_{o_w} is the roughness height of the air-water interface. In two-dimensional flows where the effect of the earth's rotation is important, the water velocity vector rotates (or turns) with depth in addition to decaying exponentially [Ekman (1905)].

Ordinarily the information available for predicting the motion of a single floe is the wind velocity and sometimes an estimate of the surface area of the floe. Estimating the wind-generated drift current characteristics using only a reported wind velocity is only a crude first approximation. Even if such an estimate were available, the selection of an appropriate water current, V_w, for use in estimating water drag depends upon the depth to which the ice floe penetrates beneath the water surface. Neglecting the existence of the water surface current has been a common approach for circumventing the difficulty of establishing the "correct" $\vec{V}_w$.

Wave Force

Water waves may contribute significantly to the transport of an ice floe. Of primary concern here are wind generated waves which accompany wind induced drift currents. The characteristics of these waves are determined primarily by the wind velocity and the fetch over which the wind acts. In very large waterbodies, waves propagating from distant storms may also affect the motion of the ice floe.

Karwowski (1962) reported the results of some experiments, in which, model ice floes made of paraffin moved according to the direction of wave propagation in a laboratory wave tank. His qualitative analysis of the wave force, when the floe was at the wave crest or at the wave trough, showed that a net force existed in the direction of the wave motion. He concluded that movements of icebergs and ice floes may sometimes be significantly influenced by water waves, as well as wind and water currents.

Hendrickson et al (1962) investigated the response of ice floes to water waves but dealt primarily with the deformation of the floe and the probability of floe fracture. They found, when the floe length was small compared to the water wave length, the probability of floe fracture was low because the transmitted energy was absorbed in rigid body motion. This case is examined in detail in a subsequent section of this report. Their analysis indicated that, for shorter incident wave lengths, the response of the floe was dependent upon floe thickness and the amount of incident wave energy transmitted beneath the floe. This is more comparable to the situation being analyzed in this section; however, the internal ice stresses and floe deformation are not considered. The floe is treated as a rigid body.

Rigby (1974) and Hunkins (1974) have examined the additional retarding force due to the generation of internal waves by ice keels drifting in a

stratified ocean. Arctic ice keels (which form the underside of a pressure

ridge) can protrude to significant depths. Although stratification is

virtually absent in Lake Erie during the winter season, the other Great

Lakes display typical winter-time stratification. The effect of stratifi-

cation on the drift of ice in the Great Lakes is not thought to be signi-

ficant (although it could be a factor under rare conditions).

Water waves transport horizontal momentum and a floating body will

absorb, transmit, or reflect this momentum. As a result, a mean horizontal

wave force on the ice floe can result. For small amplitude waves the force

can be calculated when the incident, reflected, and transmitted wave amplitudes

are known. Small amplitude waves possess an average horizontal momentum, M,

which is proportional to the square of the wave amplitude, a [Longuet-Higgins

(1977)].

$$\vec{M} = \vec{i} \, M_x + \vec{j} \, M_y = M_k = \frac{1}{2} \, \rho_w \, ga^2 \left(\frac{1}{C_k} \right) \qquad (3.8)$$

where C_k is the wave celerity. The momentum in a wave train travels with

the wave group velocity, $\vec{C}_g$. Therefore, the horizontal flux of momentum

per unit length perpendicular to the direction of wave travel is given by:

$$M_{F_k} = \frac{1}{2} \, \rho_w \, ga^2 \left(\frac{C_{g_k}}{C_k} \right) \qquad (3.9)$$

In general, a, C, and C_g can be functions of time and distance. Since the

ice motion is being viewed in one dimension, the water waves can only

travel in the same or opposite direction in which the ice travels. The

magnitude and direction of the wave momentum imparted to the ice floe will

depend on the wave amplitude and the magnitude and direction of $\vec{V}_i$ relative

to C and C_g. The horizontal flux of momentum, in this case, is given by

$$M_{F_k} = \frac{1}{2} \rho_w \, ga^2 \left[\frac{C_{g_k} - V_{i_k}}{C_k - V_{i_k}} \right] \qquad (3.10)$$

The momentum imparted to the ice floe is determined by the amount which is reflected and transmitted. In general, the wave force is given by:

$$\vec{F}_V = (\vec{M}_F)_{incident} + (\vec{M}_F)_{reflected} - (\vec{M}_F)_{transmitted} \qquad (3.11)$$

Substituting Equation (3.10), the wave force can be written as:

$$F_{V_k} = \frac{1}{2} \rho_w g \left[1 + \left(\frac{a_r}{a_i} \right)^2 - \left(\frac{a_t}{a_i} \right)^2 \right] a_i^2 \left[\frac{C_{g_k} - V_{i_k}}{C_k - V_{i_k}} \right] \qquad (3.12)$$

in which a_i, a_r, and a_t are the incident, reflected, and transmitted wave amplitudes, respectively, a_r/a_i is a reflection coefficient, and a_t/a_i is a transmission coefficient.

Accurate estimates of the wave force on an ice floe may be difficult. Seldom are incident, reflected, and transmitted wave characteristics known. The incident wave characteristics can be estimated based on wind-generated wave growth models [Kinsman (1965); Shore Protection Manual (1975)]. These models require as input the wind speed, fetch over which the wind acts, and the duration of the wind (water depth can sometimes be a factor also). The output includes wave celerity, wave height (amplitude), and wave length. With an estimate of the reflection properties of the ice floe being considered, the wave force could be estimated. Methodologies for estimating wave forces on ice floes could be improved with appropriately designed laboratory testing and careful field data collection programs.

Dimensionless Equation of Motion

The one dimensional equation of motion for a single ice floe can now be written after substitution of equations (3.4), (3.5), (3.6) and (3.12) in (3.1);

$$
\frac{dV_{i_k}}{dt} = \frac{\rho_a}{\rho_i} \left(\frac{\overline{C}_a}{1 + C_m} \right) \frac{1}{t_i} |V_{a_k}| (V_{a_k}) - \frac{\rho_w}{\rho_i} \left(\frac{\overline{C}_w}{1 + C_m} \right) \frac{1}{t_i} |V_{i_k} - V_{w_k}| (V_{i_k} - V_{w_k})
$$

$$
+ \frac{\rho_w/2\rho_i}{1 + C_m} \left[1 + \left(\frac{a_r}{a_i} \right)^2 - \left(\frac{a_t}{a_i} \right)^2 \right] g \frac{a_i^2}{\ell t_i} \left[\frac{C_{g_k} - v_{i_k}}{C_k - v_{i_k}} \right] \tag{3.13}
$$

In dimensionless form, equation (3.13) becomes,

$$
\frac{dV_{i_k}'}{dt'} = \frac{\ell}{t_i} \left[K_1 V_{a_k}' - K_2 |V_{i_k}' - V_{w_k}'| (V_{i_k}' - V_{w_k}') + k_3 \left(\frac{C_{g_k}' - v_{i_k}'}{C_k' - v_{i_k}'} \right) \frac{1}{F_a^2} \right]
$$

$$
\tag{3.14}
$$

in which dimensionless variables are given by

$$
V_{i_k}' = \frac{V_{i_k}}{|\vec{V}_a|} , \quad V_{w_k}' = \frac{V_{w_k}}{|\vec{V}_a|} , \quad C_{g_k}' = \frac{C_{g_k}}{|\vec{V}_a|} , \quad C_k' = \frac{C_k}{|\vec{V}_a|} , \quad t' = \frac{t|\vec{V}_a|}{\ell}
$$

and the Coefficients are given by

$$
K_1 = \frac{\rho_a}{\rho_i} \frac{\overline{C}_a}{(1 + C_m)}
$$

$$K_2 = \frac{\rho_w}{\rho_i} \frac{\overline{C}_w}{(1 + C_m)}$$

$$K_3 = \frac{\rho_w/2\rho_i}{(1 + C_m)} \left(\frac{a_i}{\ell}\right) \left[1 + \left(\frac{a_r}{a_i}\right)^2 - \left(\frac{a_t}{a_i}\right)^2\right]$$

$$F_a = \frac{|\vec{V}_a|}{\sqrt{g\ell}}$$

$V'_{a_k} = \pm 1$ (depending on wind direction)

An alternate dimensionless form of the basic equation (3.13) is obtained if the dimensionless quantities are defined using the steady-state (or terminal) ice velocity, $|\vec{V}_{i_T}|$, as the reference velocity instead of $|\vec{V}_a|$. The coefficients, K_1, K_2 and K_3 do not change if this is done; however, the Froude-like parameter, F_a, becomes $F_T = |\vec{V}_{i_T}| / \sqrt{g\ell}$.

3.2.2 Sensitivity Analysis

Predicting the motion of an arbitrary ice floe with Equation (3.14) is difficult because of the number of unknowns. The primary unknowns are the water drag, wind drag, virtual mass, reflection, and transmission coefficients. Therefore, this analysis is concerned with the sensitivity of the solution to variations in these coefficients. Due to the complexity of Equation (3.14), the solution is approximated numerically.

For this analysis, the air-ice-water system is assumed to be at 0°C which gives $\rho_a \simeq 1.29$ kg/m^3, $\rho_w = 1000$ kg/m^3, and assuming pure ice, $\rho_i = 916.8$ kg/m^3 (Pounder, 1965). Values for the other dimensionless

63

parameters in Equation (3.14) are based on the dimensions of a typical ice floe and a reasonable wind velocity. Deep water waves with small amplitude, compared to the wavelength, are assumed to travel in the same direction as the wind. Table 3.1 lists the values used in the analysis.

TABLE 3.1

VALUES FOR THE PARAMETERS OF EQUATION (3.14)

USED IN THE SENSITIVITY ANALYSIS

PARAMETER	SYMBOL	VALUE
Froude Number	F_a	1.43
Ratio of Wave Amplitude to Ice Floe Length	a_i/ℓ	0.01
Ratio of Ice Floe Length to Thickness	ℓ/t_i	25.0
Water Current	V_w'	0
Incident Wave Celerity	c'	0.15
Incident Wave Group Velocity	c_g'	0.075

To test the solution sensitivity to variations in one of the coefficients, the remaining coefficients are held constant. The values are given in Table 3.2. The initial condition for the solution to each variation is $V_k' = 0$ at $t' = 0$.

64

TABLE 3.2

VALUES FOR THE COEFFICIENTS USED IN EACH SENSITIVITY
TEST

SENSITIVITY TEST ON	$\bar{C}_a$	$\bar{C}_w$	C_m	a_r/a_i	a_t/a_i
$\bar{C}_a$	Variable	0.01	0.0	0.0,1.0	0.0,1.0
$\bar{C}_w$	0.01	Variable	0.0	0.0,1.0	0.0,1.0
C_m	0.01	0.01	Variable	0.0,1.0	0.0,1.0
a_r/a_i	0.01	0.01	0.0	Variable	0.0
a_t/a_i	0.01	0.01	0.0	0.0	Variable

The two characteristics of the solution examined most closely are the steady state ice velocity and the time required to attain steady state. Although the distance over which the floe travels is also important, it can be evaluated by integrating the solutions to Equation (3.14) with respect to time. The time required to attain steady state is needed to evaluate the justification for neglecting the acceleration term in two-dimensional ice transport models.

Figures 3.2 and 3.3 illustrate the sensitivity of the solution to changes in the wind drag coefficient, $\bar{C}_a$. There is a significant variation in both the terminal velocity and response time for the range of values examined. There can be as much as a 25% increase in the terminal velocity and a 25% reduction in the response time when the coefficient is doubled. From Figure 3.3 it can be seen that even when the wind exerts no force
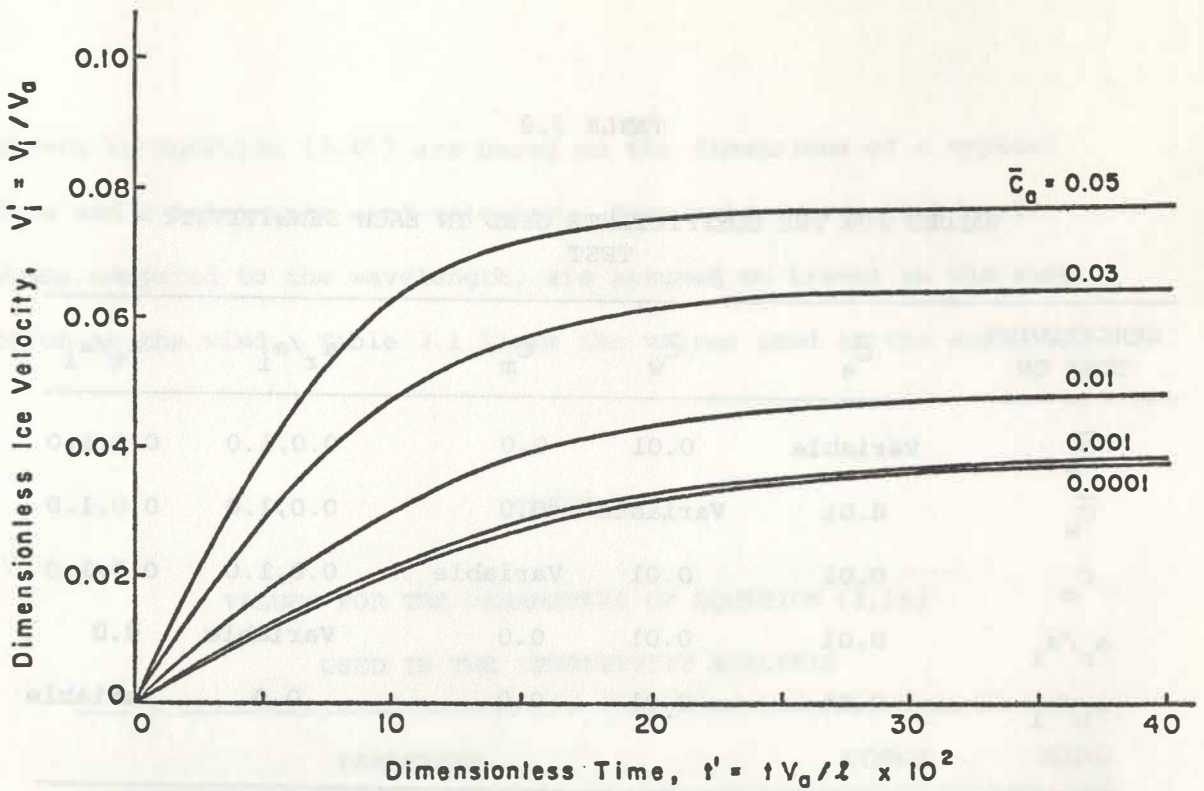
65

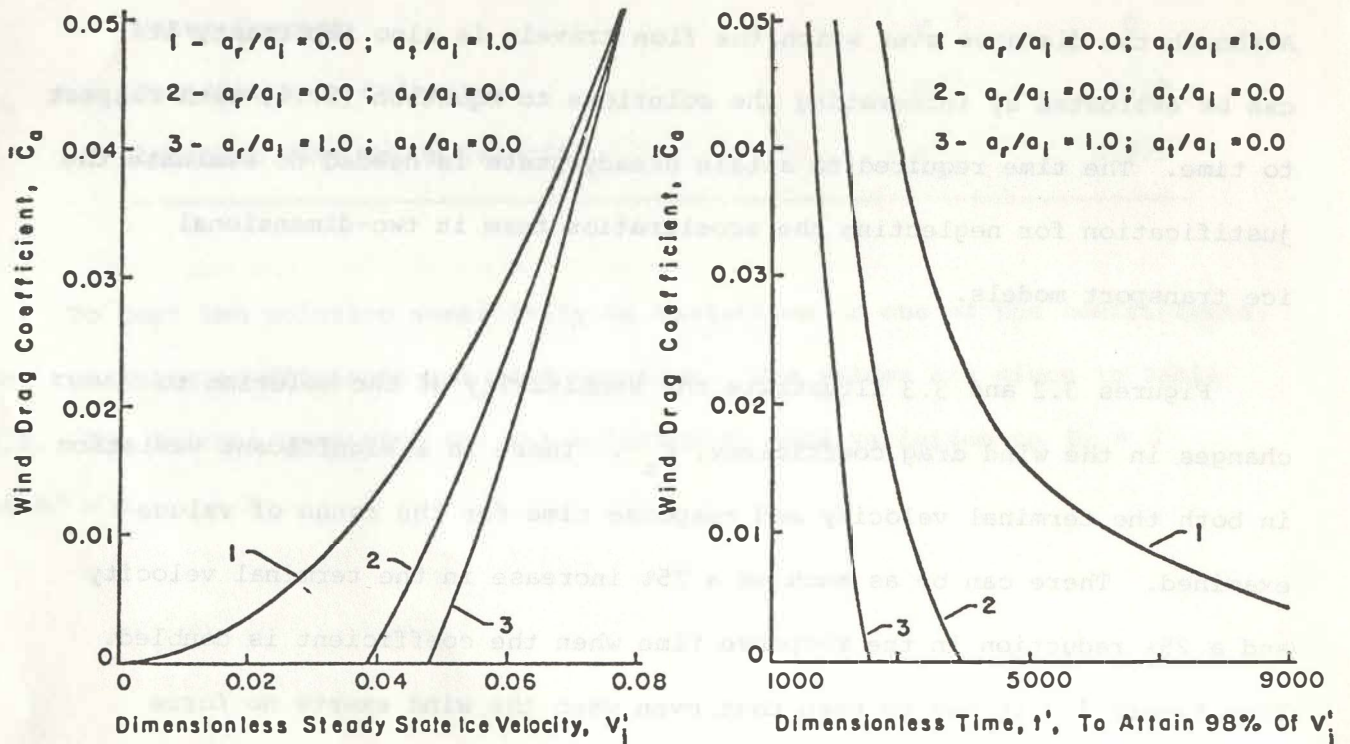Figure 3.2 Sensitivity of Ice Floe Velocity to Variation in the Wind Drag Coefficient

Figure 3.3 Sensitivity of Ice Floe Velocity and Response Time to Variation in the Wind Drag Coefficient

66

on the ice surface ($\overline{C}_a = 0$), the ice is still transported by the momentum imparted by the waves. For the case when $\overline{C}_a = 0$ and there is total transmission of wave momentum, V_i' remains zero and the time to achieve terminal velocity becomes infinite.

Figure 3.4 and 3.5 illustrate the sensitivity of the solution to changes in the water drag coefficient, $\overline{C}_w$. Again there is a significant variation in both the terminal ice velocity and the response time. Since the water drag acts as the retarding force, both of these parameters approach infinity as $\overline{C}_w$ approaches zero. In this case, the ice velocity can exceed the group velocity of the water waves, when $\overline{C}_w$ becomes small enough. This situation will rarely, if ever, occur, since $\overline{C}_w$ is expected to be the same order of magnitude or greater than $\overline{C}_a$.

Figures 3.6 and 3.7 illustrate the solution's sensitivity to variations in the virtual mass coefficient, C_m. Over the range of values tested, the steady state velocity increases by only 20%, while the response time increases by 60%. For a typical ice floe, one in which the length is much greater than the thickness, the virtual mass coefficient is small and can be neglected. When this is not the case, (say for massive icebergs) experimental or computational (Garrison, 1974) determination of C_m may be warranted.
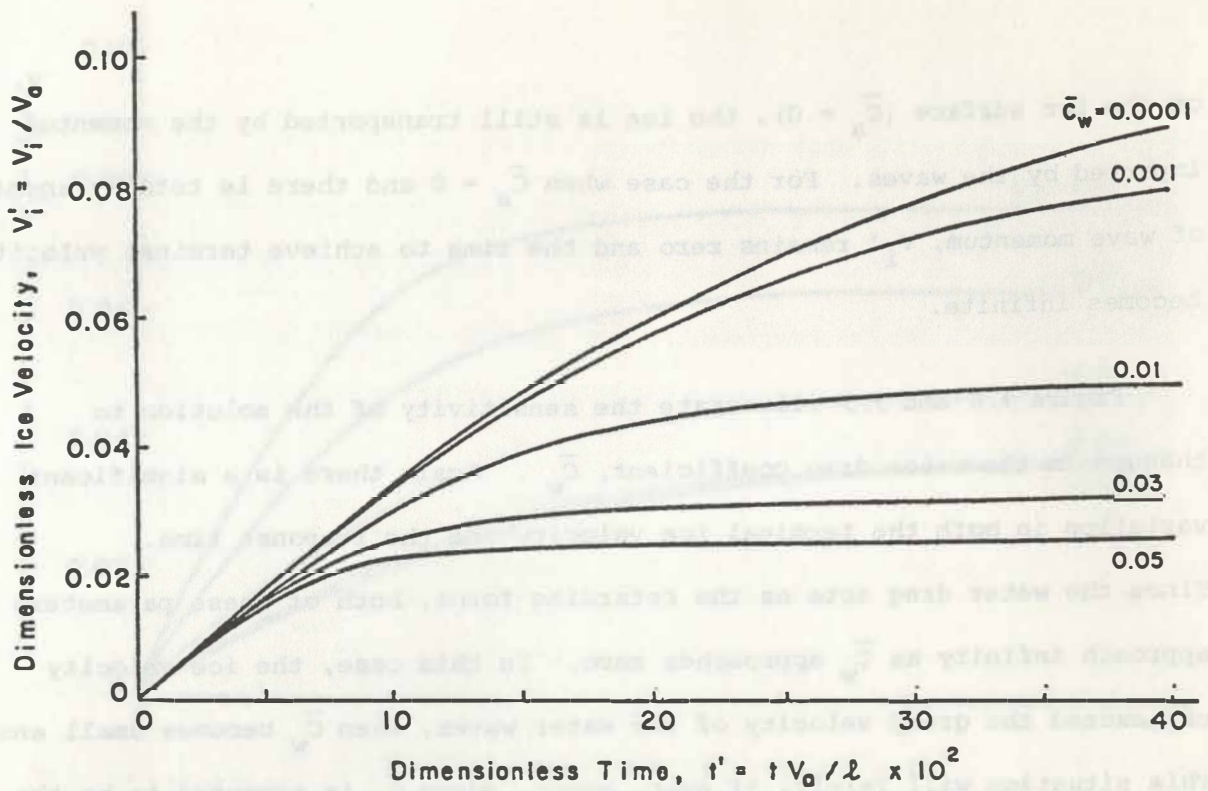
67

Figure 3.4   Sensitivity of Ice Floe Velocity to Variation in the Water Drag
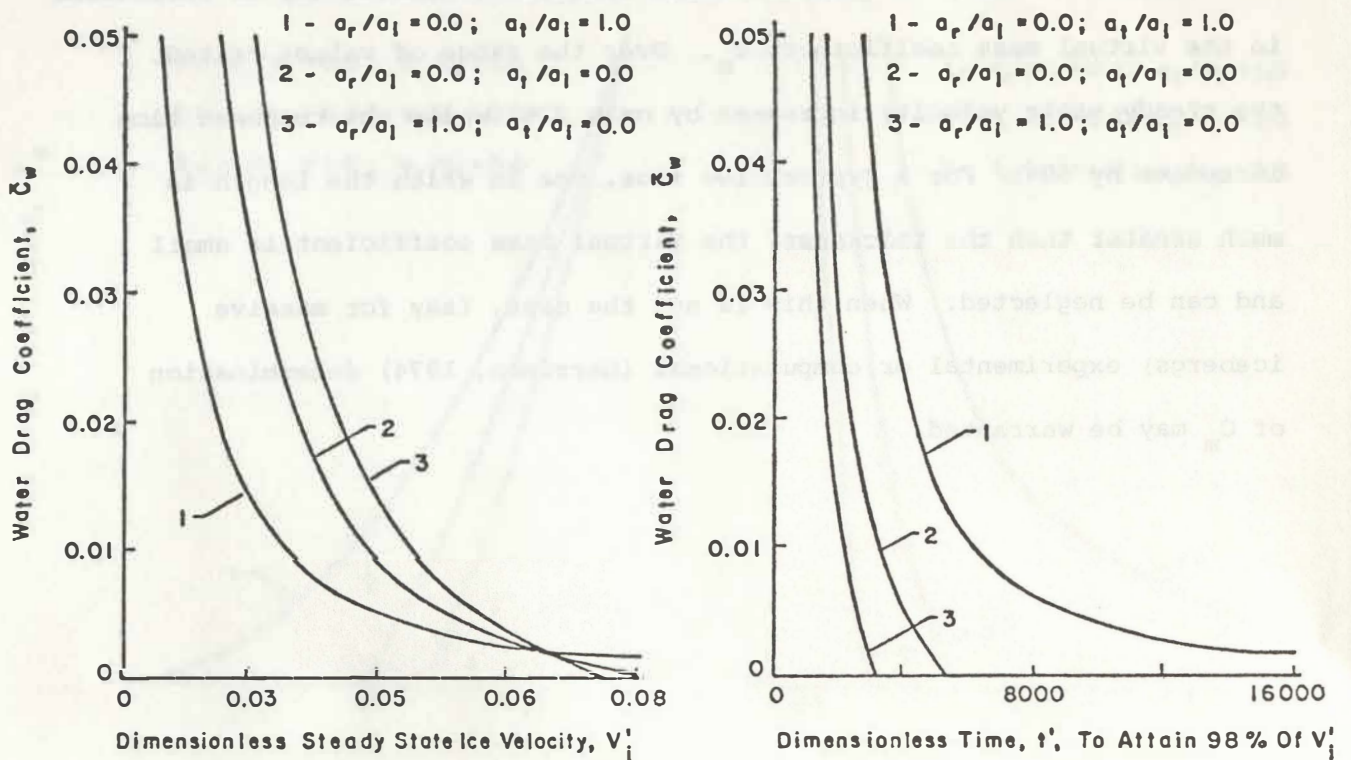Coefficient

Figure 3.5   Sensitivity of Ice Floe Velocity and Response Time to Variation
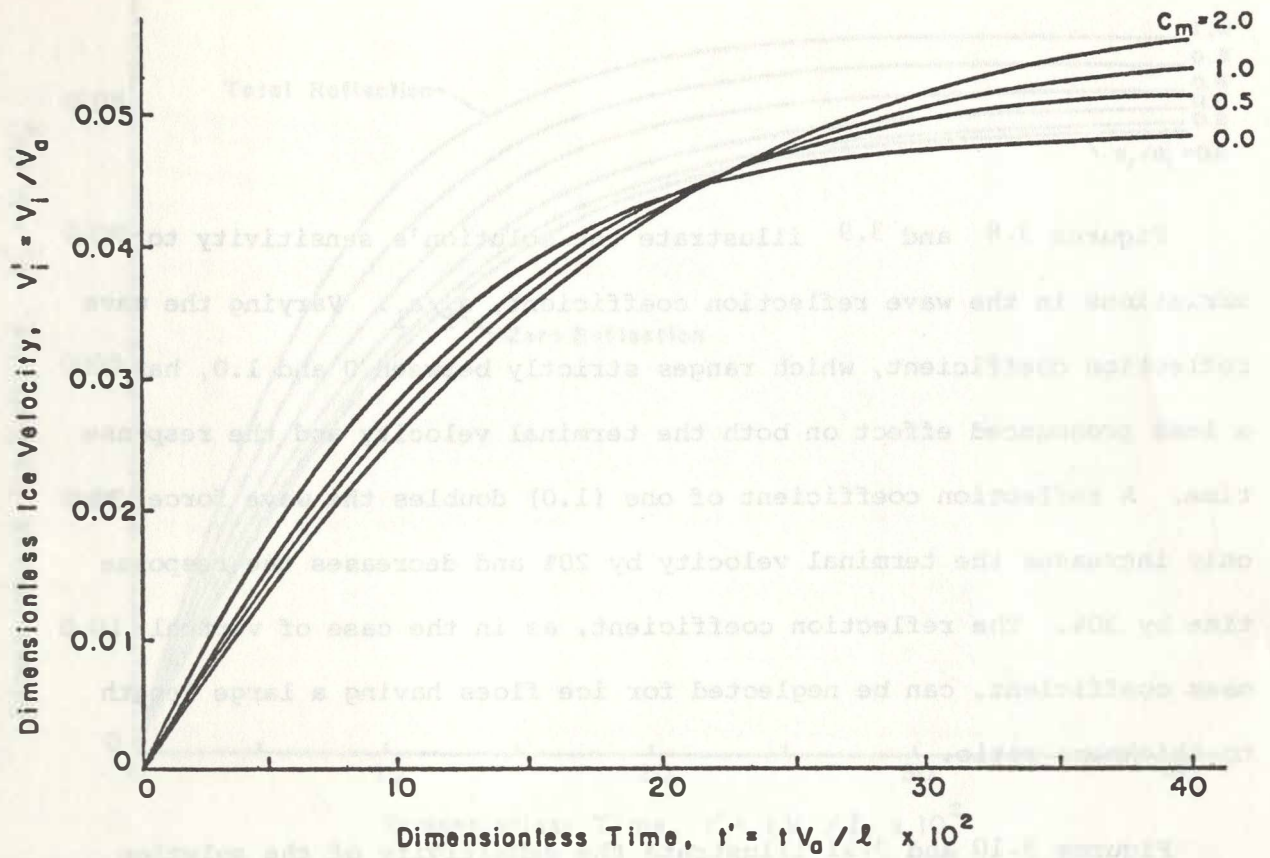in the Water Drag Coefficient

Figure 3.6 Sensitivity of Ice Floe to Variations in the Virtual Mass
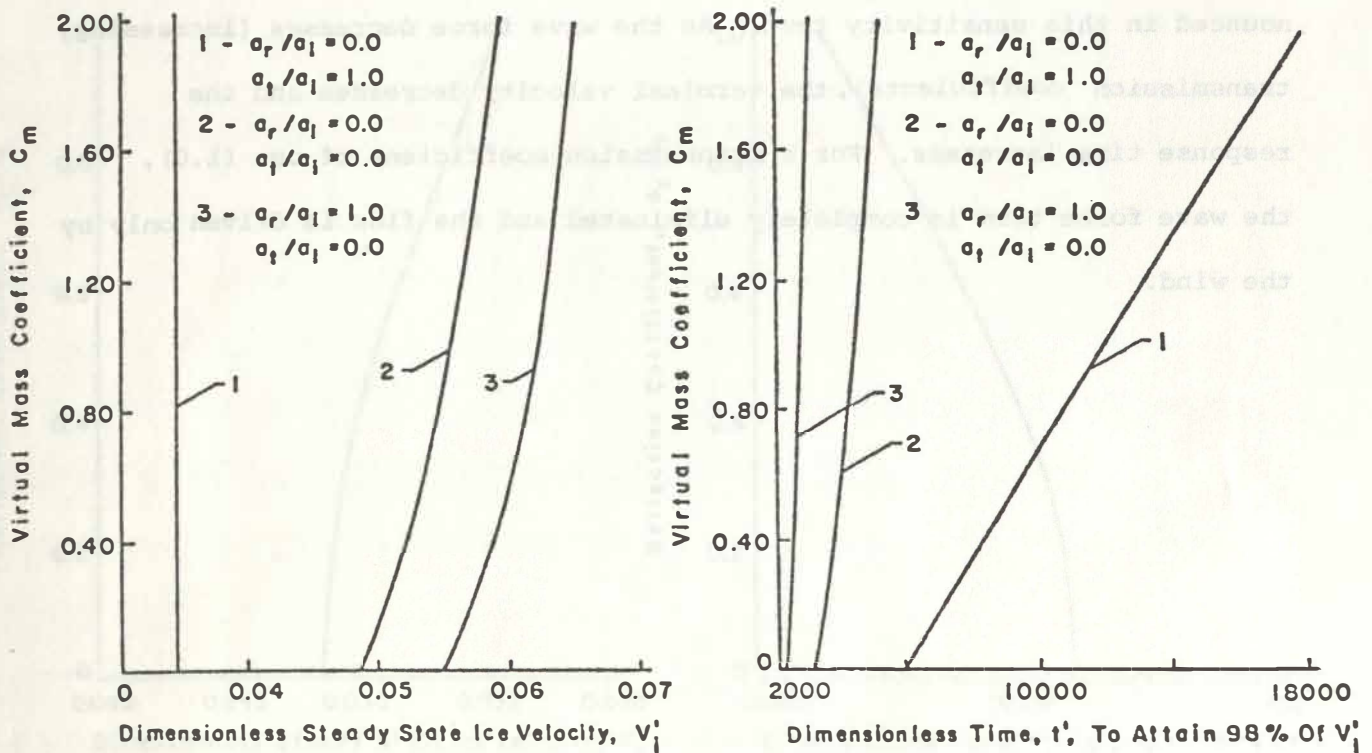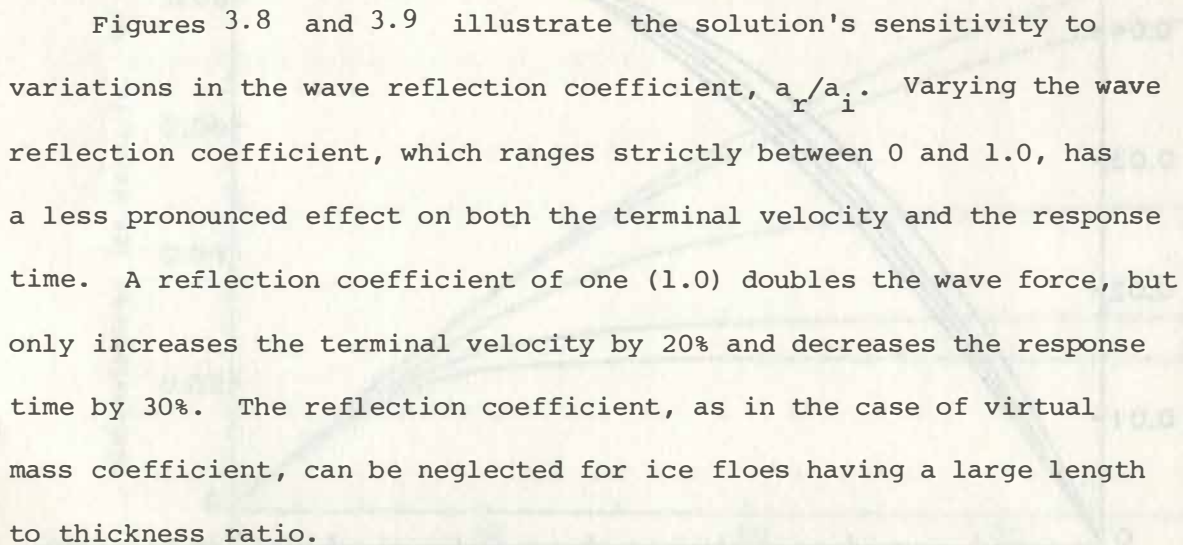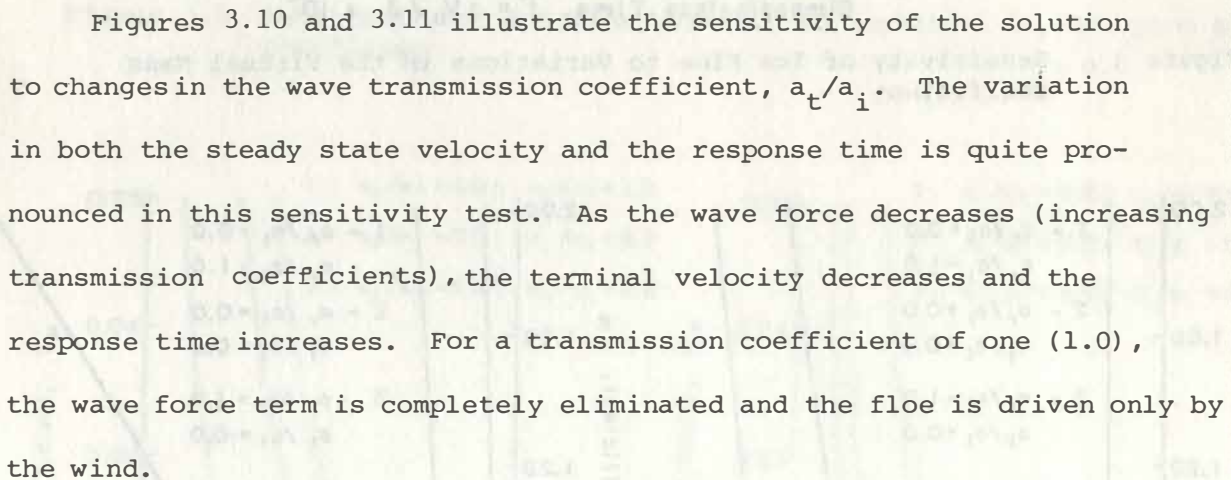Coefficient

Figure 3.7 Sensitivity of Ice Floe Velocity and Response Time to Variations
in the Virtual Mass Coefficient

69

Figures 3.8 and 3.9 illustrate the solution's sensitivity to variations in the wave reflection coefficient, a_r/a_i. Varying the wave reflection coefficient, which ranges strictly between 0 and 1.0, has a less pronounced effect on both the terminal velocity and the response time. A reflection coefficient of one (1.0) doubles the wave force, but only increases the terminal velocity by 20% and decreases the response time by 30%. The reflection coefficient, as in the case of virtual mass coefficient, can be neglected for ice floes having a large length to thickness ratio.

Figures 3.10 and 3.11 illustrate the sensitivity of the solution to changes in the wave transmission coefficient, a_t/a_i. The variation in both the steady state velocity and the response time is quite pronounced in this sensitivity test. As the wave force decreases (increasing transmission coefficients), the terminal velocity decreases and the response time increases. For a transmission coefficient of one (1.0), the wave force term is completely eliminated and the floe is driven only by the wind.

Figure 3.8   Sensitivity of Ice Floe Velocity to Variations in the Wave
              Reflection Coefficient

Figure 3.9   Sensitivity of Ice Floe Velocity and Response Time to Variations
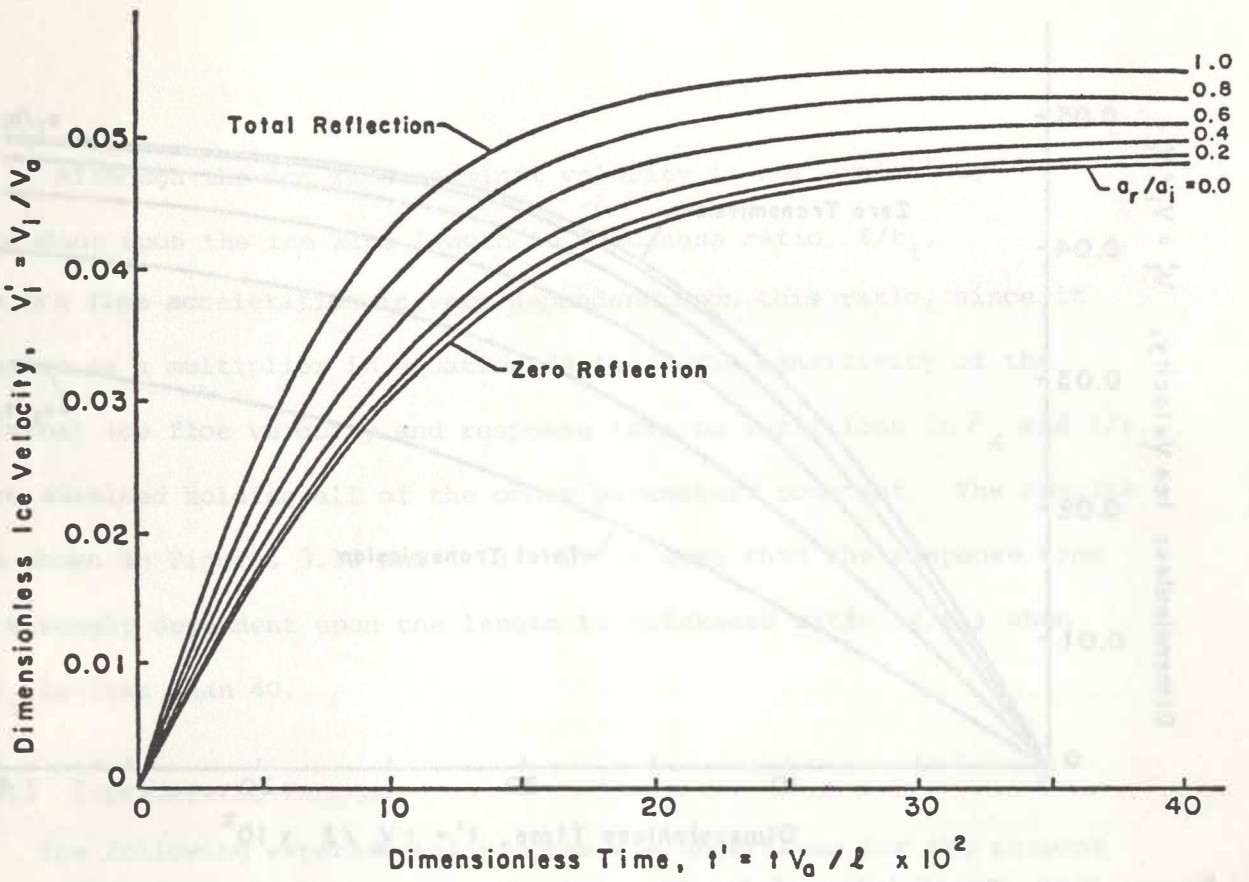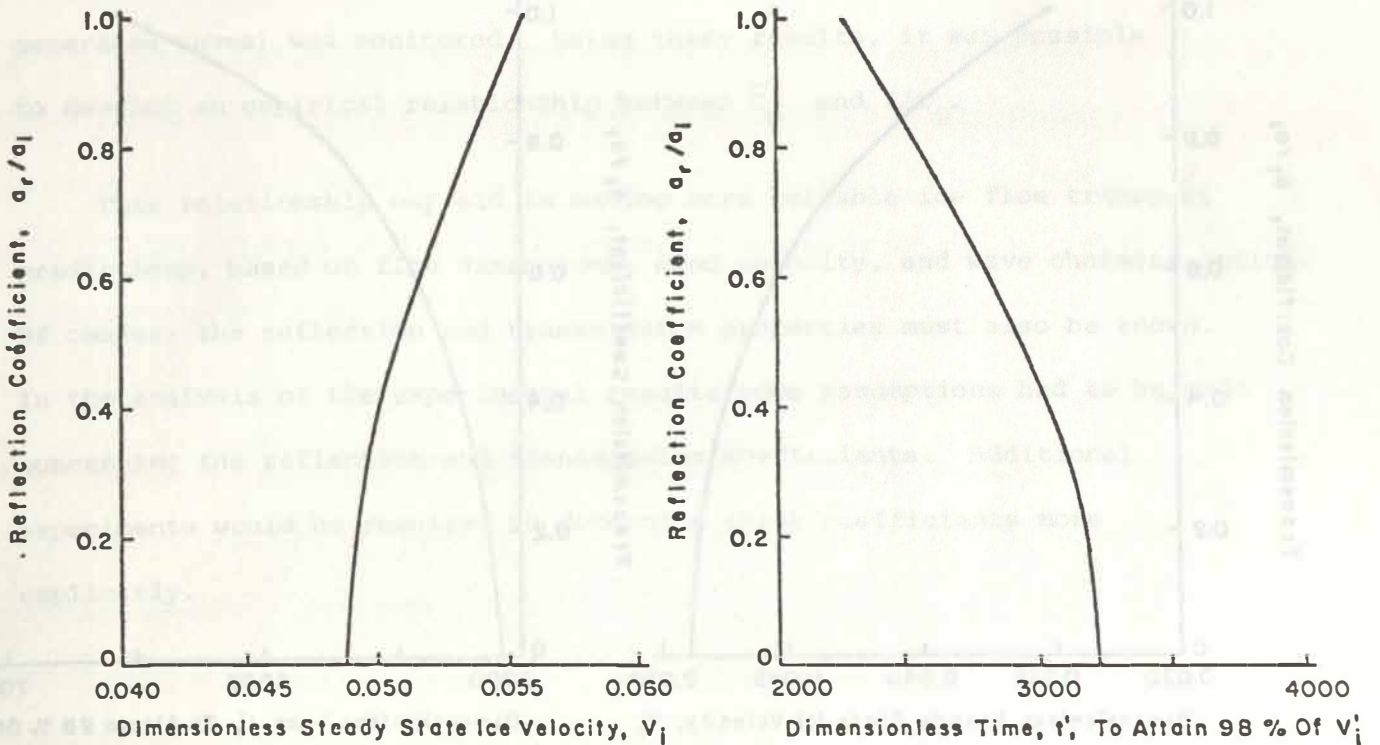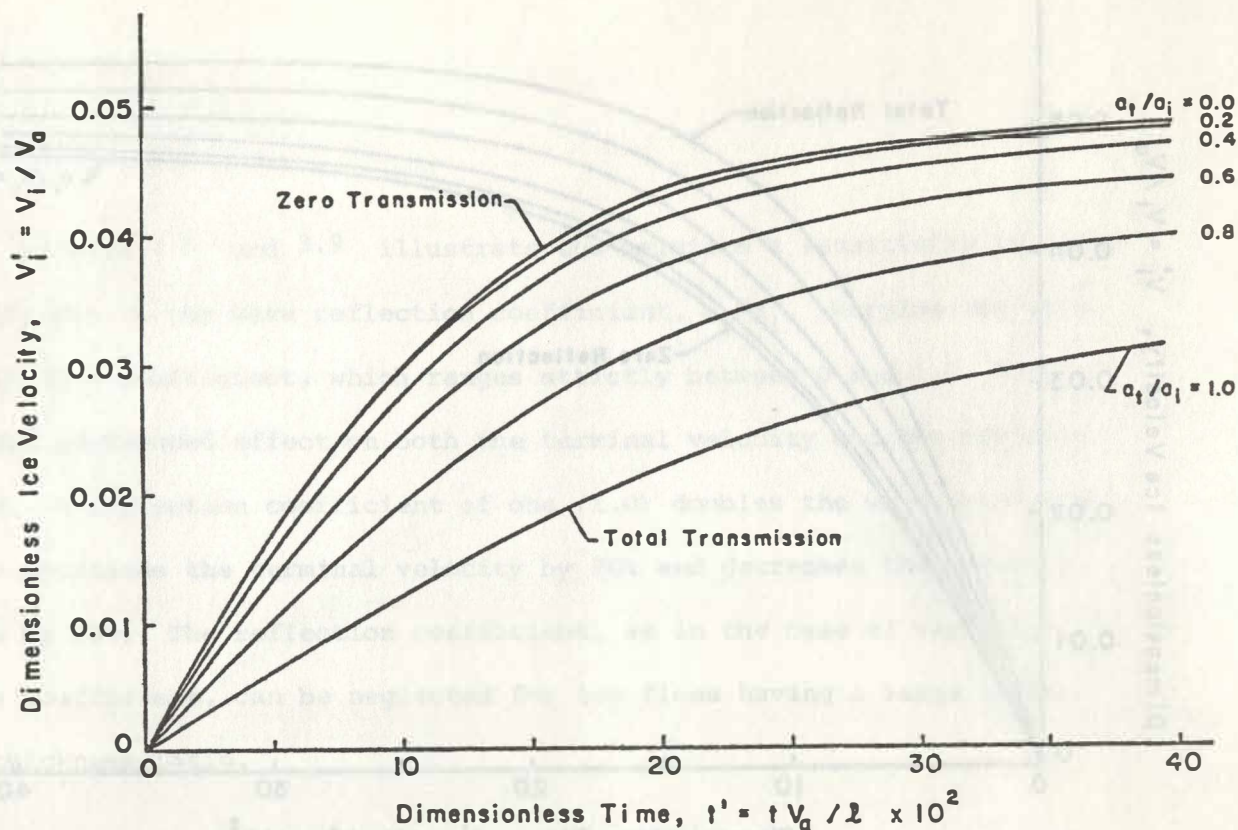   in the Wave Reflection Coefficient

Figure 3.10 Sensitivity of Ice Floe Velocity to Variations in the Wave Transmission Coefficient
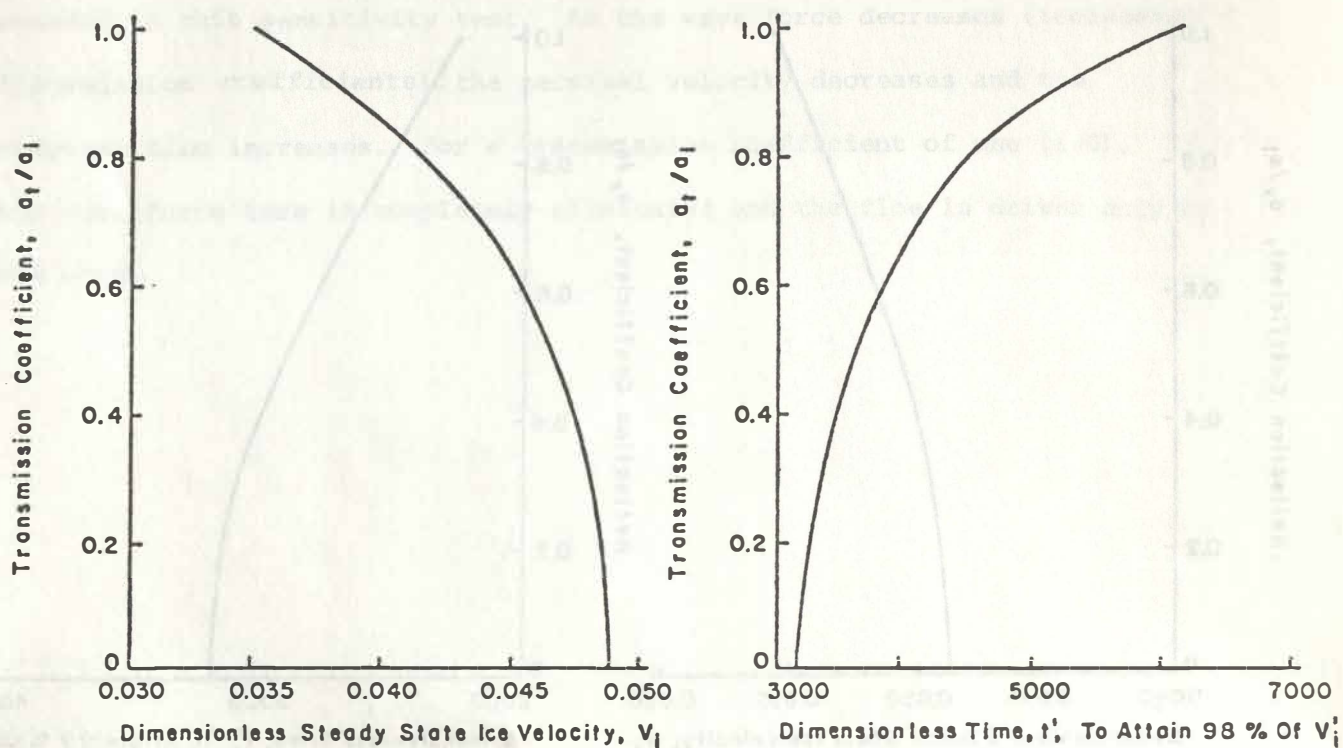
Figure 3.11 Sensitivity of Ice Floe Velocity and Response Time to Variations in the Wave Transmission Coefficient

Although the ice floe terminal velocity is not explicitly dependent upon the ice floe length to thickness ratio, ℓ/t_i, the ice floe acceleration is very dependent upon this ratio, since it appears as a multiplier in equation (3.14). The sensitivity of the terminal ice floe velocity and response time to variations in $\bar{F}_a$ and ℓ/t_i were examined holding all of the other parameters constant. The results are shown in Figures 3.12 and 3.13. It is seen that the response time is strongly dependent upon the length to thickness ratio (ℓ/t_i) when ℓ/t_i is less than 40.

3.2.3 Experimental Program

The following experimental program was undertaken for the purpose of obtaining a better understanding of the transient motion of an ice floe and as a means to calibrate some of the model parameters. Basically, the transient motion of a simulated ice floe driven by wind (and wind-generated waves) was monitored. Using these results, it was possible to develop an empirical relationship between $\bar{C}_w$ and ℓ/t_i.

This relationship may aid in making more reliable ice floe transport predictions, based on floe dimensions, wind velocity, and wave characteristics. Of course, the reflection and transmission properties must also be known. In the analysis of the experimental results some assumptions had to be made concerning the reflection and transmission coefficients. Additional experiments would be required to determine these coefficients more explicitly.
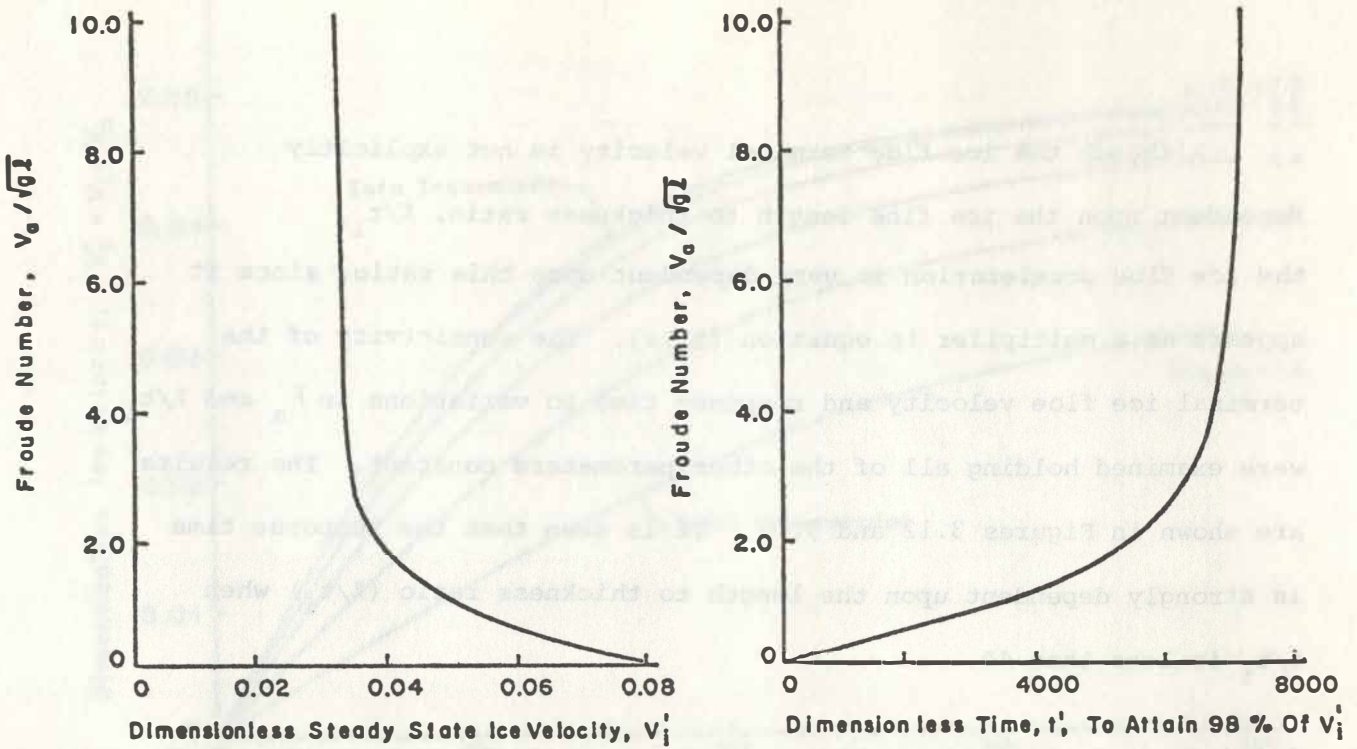
Figure 3.12 Sensitivity of Ice Floe Velocity and Response Time to Variations in the Froude Number, F_a
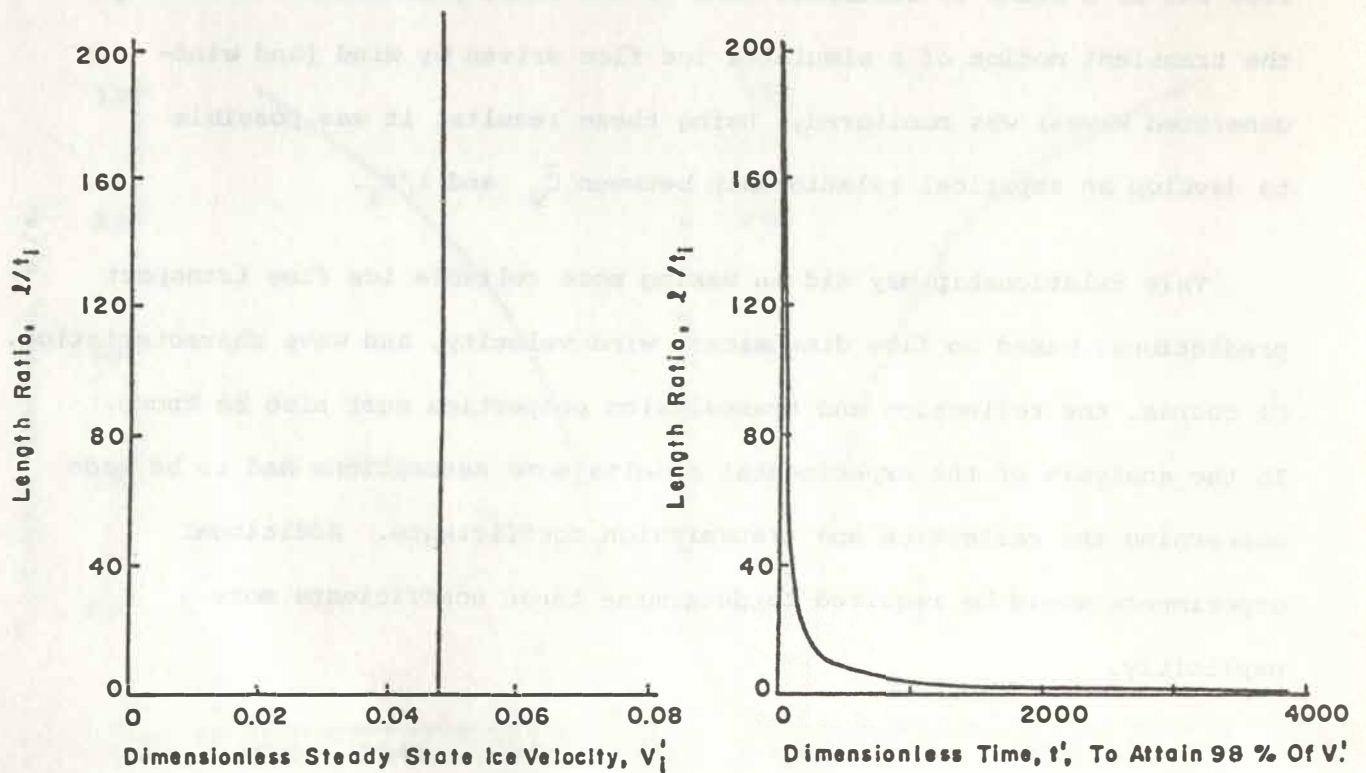
Figure 3.13 Sensitivity of Ice Floe Velocity and Response Time to Variations in the Length to Thickness Ratio, ℓ/t_i

Experimental Apparatus

The experiments were conducted in the University of Delaware's wind-wave tank located in the Department of Civil Engineering. The wind-wave tank specifications are:

> Length (exposed to wind) : 18.29 m
>
> Width : 0.62 m
>
> Maximum Blower Discharge : 194.24 m^3/min

Since the blower output is positioned in the upper 30.48 cm of the tank, the water depth used during the experiments was 96.5 cm. Maintaining this water level ensured reliable wind-ice interaction as well as optimal utility of the available length. At this depth, the maximum attainable wind speed was 14.5 m/sec.

Low density polyethylene was used to simulate an ice floe. The average specific gravity of the polyethylene was 0.92, which is comparable with that of fresh water ice (0.91). A rectangular floe (0.31m x 0.81m, surface area dimensions) was used to achieve optimal utilization of a polyethylene sheet (1.22m x 2.44m x .025m). This allowed the thickness to be varied by assembling pieces in layers.

To prevent the floe from colliding with the tank walls, the floe was guided along the center of the tank with a strand of high tensile strength wire. Wind setup in the tank was not an important factor at the wind speeds investigated, and the wire was stretched, with no sag, parallel to and 5 cm above the water surface. The floe itself was equipped with guides as illustrated in Figure 3.14. The wind drag on these guides was taken into account in the analysis.

75
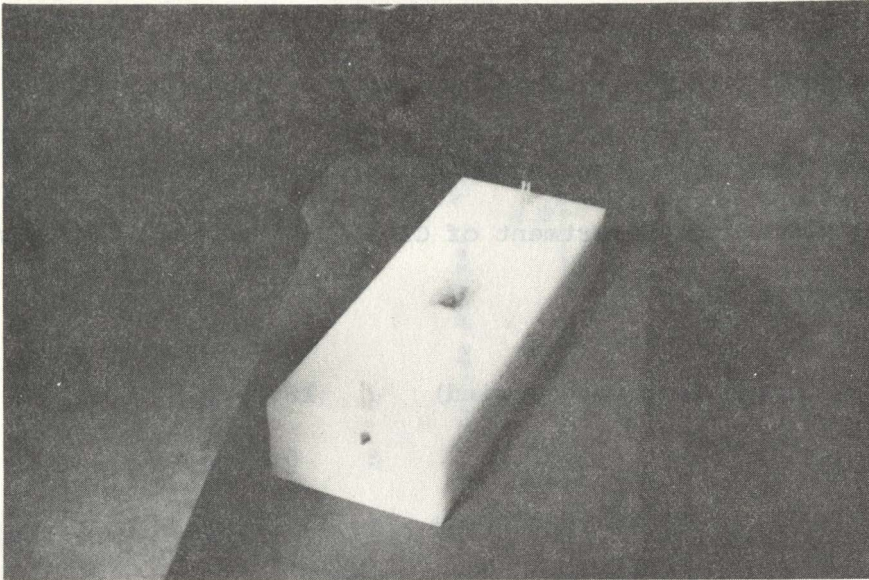
Figure 3.14   Photograph of Simulated Ice Floe Showing
Location of Light Source and Guides

The apparatus for monitoring the position of the ice floe as a function
of time is illustrated in Figure 3.15. Fifteen photoconductive cells were
mounted above the guide wire at predetermined intervals along the tank.
Velocity changes were expected to be the greatest near the initiation of
the motion (from rest). Accordingly, the photocell spacings were initially
close and then gradually lengthened as the fetch increased. The photocells,
which act as variable resistors, were connected in parallel to a resistance
recorder. It was, therefore, possible to record the time required for the ice
floe (which contained a light source consisting of a prefocused pilot light
and two penlight batteries) to pass between two consecutive photocells.
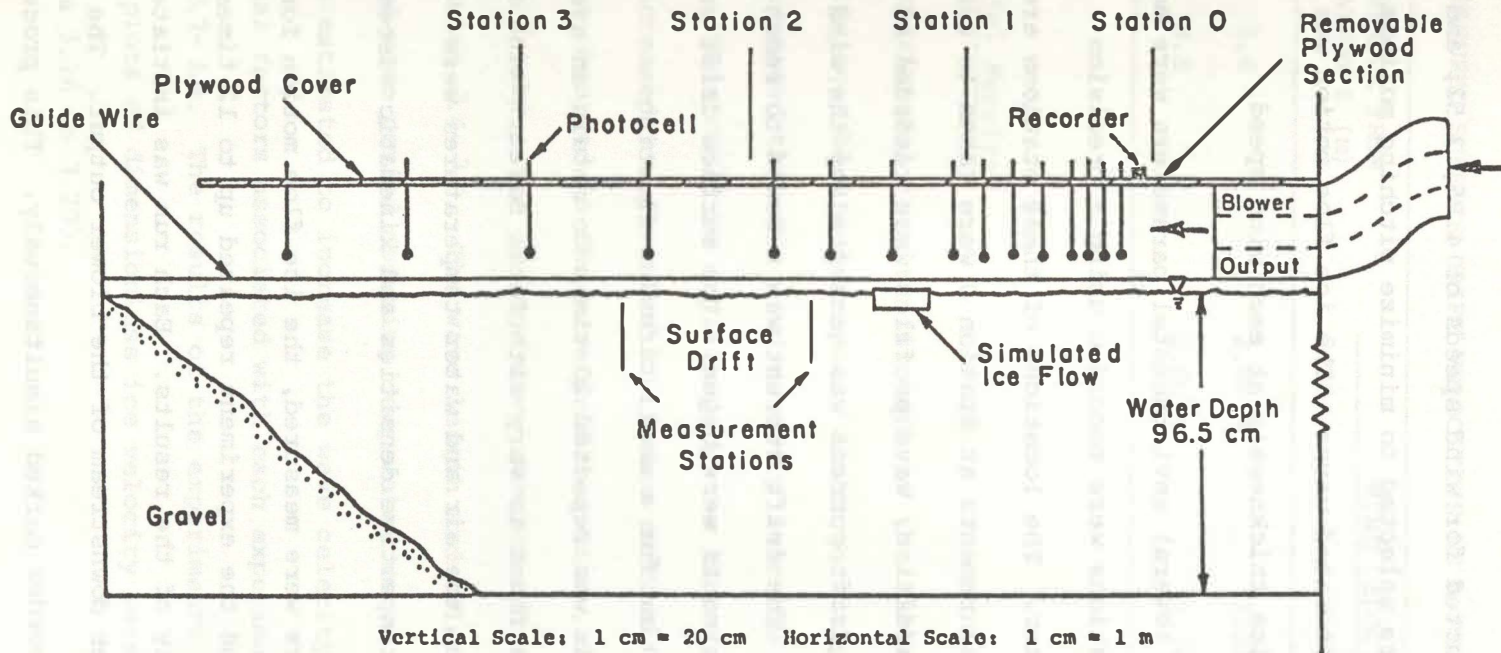
CROSS SECTIONAL SCHEMATIC OF EXPERIMENTAL SETUP SHOWING LOCATION OF PHOTOCELLS AND MEASUREMENT STATIONS FOR THE WIND AND WAVE PROFILES AND SURFACE DRIFT CURRENT

Figure 3.15

Experimental Procedure

The experiment was conducted for wind speeds of 4.85, 3.52, and 2.50 m/sec. These wind speeds were selected to minimize pitching motions of the floe caused by wind-generated waves. The ice floe motion was recorded for five different ice thicknesses at each wind speed.

Before each experiment, several environmental parameters were measured. The wind profiles at four stations were recorded using a precision differential pressure manometer. The locations of these stations are shown in Figure 3.15. The wind measurements at Station 0 were taken to ensure a uniform wind profile. In addition, wave profiles were recorded at Stations 1-3. A significant drift current was generated by the wind stress on the water surface. The drift current was allowed to reach steady-state before the experiments were begun. The surface drift was determined by measuring the time for a small circular floating disk to traverse 1.44 m. This was repeated 20 times to obtain an average value. The surface drift was found to vary with fetch for each wind speed (Table 3.3). Before each run, the air and water temperatures were recorded to ascertain their respective densities and kinematic viscosities.

Once the above parameters were measured, the ice floe motion for each ice thickness was recorded and the experiment repeated up to 12 times to illustrate the reproducibility of the results. Each run was initiated by placing the ice floe one meter downstream of the blower output. The ice floe was released and the recorder marked simultaneously. This procedure required a removable cover section at Station 0, which was replaced before the ice floe was released.

TABLE 3.3

MEASURED SURFACE DRIFT VELOCITIES AS A PERCENTAGE OF WIND SPEED

DISTANCE FROM STATION 0 (m)	WIND VELOCITY (m/sec)		
	2.50	3.52	4.85
5.6	2.88 %	3.33 %	2.93 %
8.8	2.60 %	2.74 %	2.63 %

Experimental Results

The experimental results for each of the three wind speeds are presented in the following tables and graphs. Although not presented here, the wind profiles indicated that the wind velocity near the water surface increased with fetch. This could be explained by the increased air turbulence associated with the increased roughness of the water surface. This surface roughness increase was observed in the wave profiles (i.e., the increase in wave height with fetch). The average wave characteristics at each wind speed are given in Tables 3.4-3.6. The wave length and celerity were determined from the measured wave period assuming deep water waves. The effect of surface tension was estimated to increase the wave celerity by no more than 2%. The environmental factors associated with each experimental run are reported in Tables 3.7-3.9. The results of the experiments are presented in the subsequent plots of dimensionless ice velocity versus dimensionless time. (See Figures 3.16 to 3.20).

TABLE 3.4

AVERAGE WAVE CHARACTERISTICS AT EACH MEASUREMENT STATION
FOR THE 2.50 M/SEC REFERENCE WIND SPEED

LENGTH OF WAVE RECORD: 93 SEC

STATION	NO. OF WAVES	WAVE HEIGHT (MM)	WAVE PERIOD (SEC)	WAVE LENGTH (M)	WAVE CELERITY (M/SEC)
1	406	0.64	0.23	0.08	0.35
2	397	1.47	0.23	0.08	0.35
3	352	1.51	0.28	0.12	0.44

TABLE 3.5

AVERAGE WAVE CHARACTERISTICS AT EACH MEASUREMENT STATION
FOR THE 3.52 M/SEC REFERENCE WIND SPEED

LENGTH OF WAVE RECORD: 100 SEC

STATION	NO. OF WAVES	WAVE HEIGHT (MM)	WAVE PERIOD (SEC)	WAVE LENGTH (M)	WAVE CELERITY (M/SEC)
1	378	3.17	0.26	0.11	0.41
2	341	4.04	0.29	0.13	0.45
3	294	6.87	0.34	0.18	0.53

TABLE 3.6

AVERAGE WAVE CHARACTERISTICS AT EACH MEASUREMENT STATION
FOR THE 4.85 M/SEC REFERENCE WIND SPEED

LENGTH OF WAVE RECORD: 107 SEC

STATION	NO. OF WAVES	WAVE HEIGHT (MM)	WAVE PERIOD (SEC)	WAVE LENGTH (M)	WAVE CELERITY (M/SEC)
1	365	8.69	0.29	0.13	0.45
2	306	8.48	0.35	0.19	0.54
3	265	15.69	0.40	0.25	0.63

TABLE 3.7

Environmental Factors for Experiments Conducted

at a Wind Velocity of 2.50 m/sec

$\frac{\ell}{t_i}$	Run	Air Temp. (°C)	Water Temp. (°C)	Density of Air (kg/m^3)	Density of Water (kg/m^3)	Viscosity of Air (m^2/sec)	Viscosity of Water (m^2/sec)
15.3	A-F	25.0	19.4	1.18	998	1.55×10^{-5}	1.02×10^{-6}
7.6	A-F	25.6	20.0	1.18	998	1.55×10^{-5}	1.00×10^{-6}
5.1	A-F	26.1	20.0	1.18	999	1.55×10^{-5}	0.95×10^{-6}
3.8	A-F	26.1	23.3	1.18	997	1.55×10^{-5}	0.97×10^{-6}
3.1	A-D	26.7	22.2	1.17	997	1.56×10^{-5}	0.97×10^{-6}
3.1	E-H	26.7	23.3	1.17	997	1.56×10^{-5}	0.97×10^{-6}

TABLE 3.8

Environmental Factors For Experiments Conducted

at a Wind Velocity of 3.52 m/sec

$\dfrac{\ell}{t_i}$	Run	Air Temp. (°C)	Water Temp. (°C)	Density of Air (kg/m^3)	Density of Water (kg/m^3)	Viscosity of Air (m^2/sec)	Viscosity of Water (m^2/sec)
15.3	G-N	20.0	16.9	1.20	999	1.49×10^{-5}	1.09×10^{-6}
7.6	G-L	28.9	21.1	1.16	998	1.58×10^{-5}	0.98×10^{-6}
5.1	G-L	28.9	21.1	1.16	998	1.58×10^{-5}	0.98×10^{-6}
3.8	G-L	28.9	21.1	1.16	998	1.58×10^{-5}	0.98×10^{-6}
3.1	I-N	26.7	20.0	1.17	998	1.56×10^{-5}	1.00×10^{-6}

TABLE 3.9

TABLE 3.9

Environmental Factors for Experiments Conducted

at a Wind Velocity of 4.85 m/sec

$\dfrac{\ell}{t_i}$	Run	Air Temp. (°C)	Water Temp. (°C)	Density of Air (kg/m^3)	Density of Water (kg/m^3)	Viscosity of Air (m^2/sec)	Viscosity of Water (m^2/sec)
15.3	O-S	20.6	17.5	1.20	999	1.50×10^{-5}	1.07×10^{-6}
15.3	T-V	21.1	17.5	1.20	999	1.50×10^{-5}	1.07×10^{-6}
7.6	M-P	21.9	17.8	1.19	998	1.51×10^{-5}	1.07×10^{-6}
7.6	Q-U	21.1	16.7	1.20	999	1.50×10^{-5}	1.10×10^{-6}
7.6	V-X	21.1	17.5	1.20	999	1.50×10^{-5}	1.07×10^{-6}
5.1	M-T	21.1	16.7	1.20	999	1.50×10^{-5}	1.10×10^{-6}
3.8	M-T	21.1	16.7	1.20	999	1.50×10^{-5}	1.07×10^{-6}
3.1	O-X	21.1	17.5	1.20	999	1.50×10^{-5}	1.07×10^{-6}

DIMENSIØNLESS ICE VELØCITY, VI=VI/VA *10⁻¹

DIMENSIØNLESS TIME, T=T*VA/TI *10²

V_a (m/s)	Run
2.50	A-F
3.52	G-N
4.85	O-V

$$\frac{\ell}{t_i} = 15.3$$

Figure 3.16   Experimental Results for an Ice Floe Length to Thickness Ratio of 15.3

Figure 3.17 Experimental Results for an Ice Floe Length to Thickness Ratio of 7.6

Figure 3.18 Experimental Results for an Ice Length to Thickness Ratio of 5.1
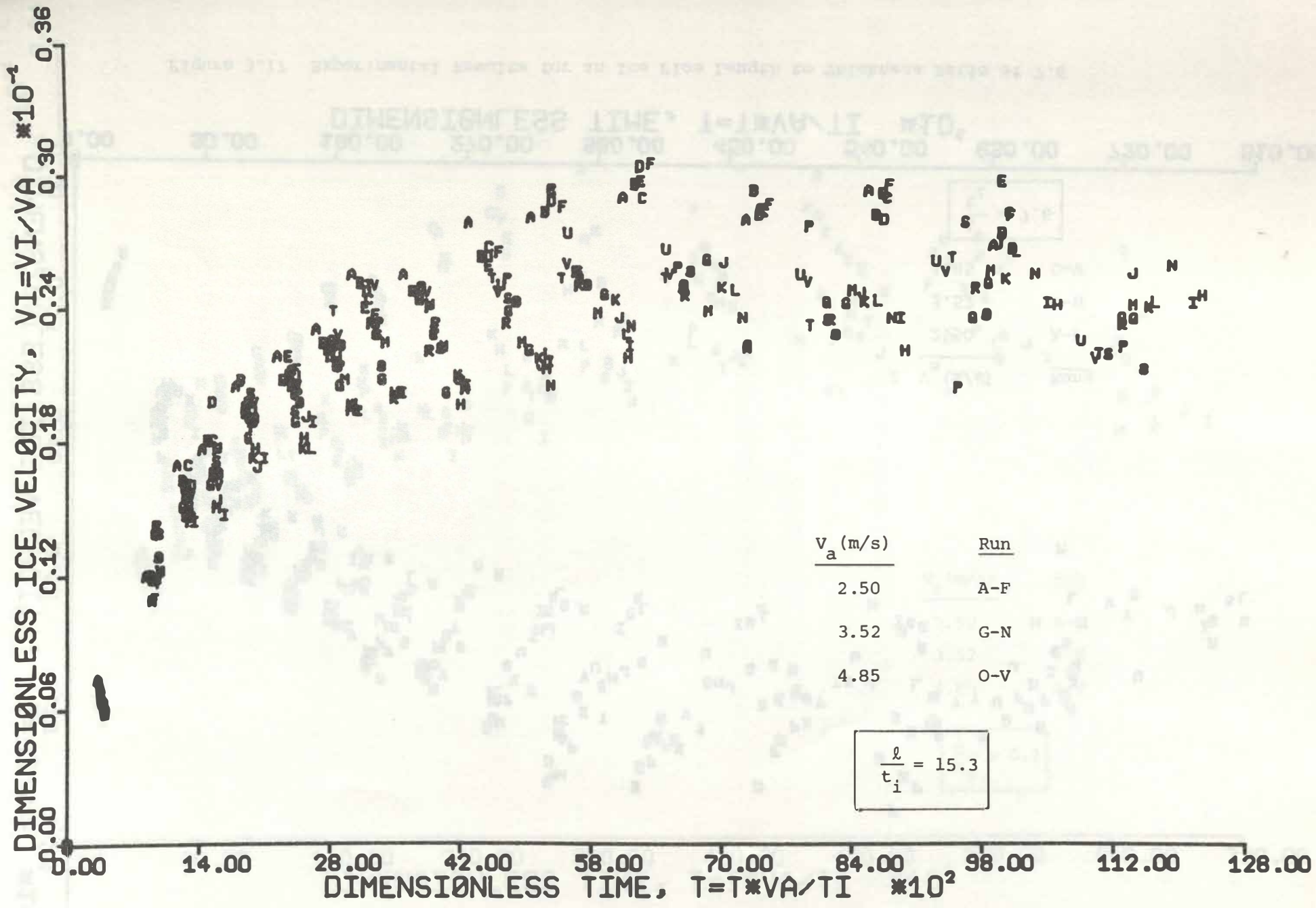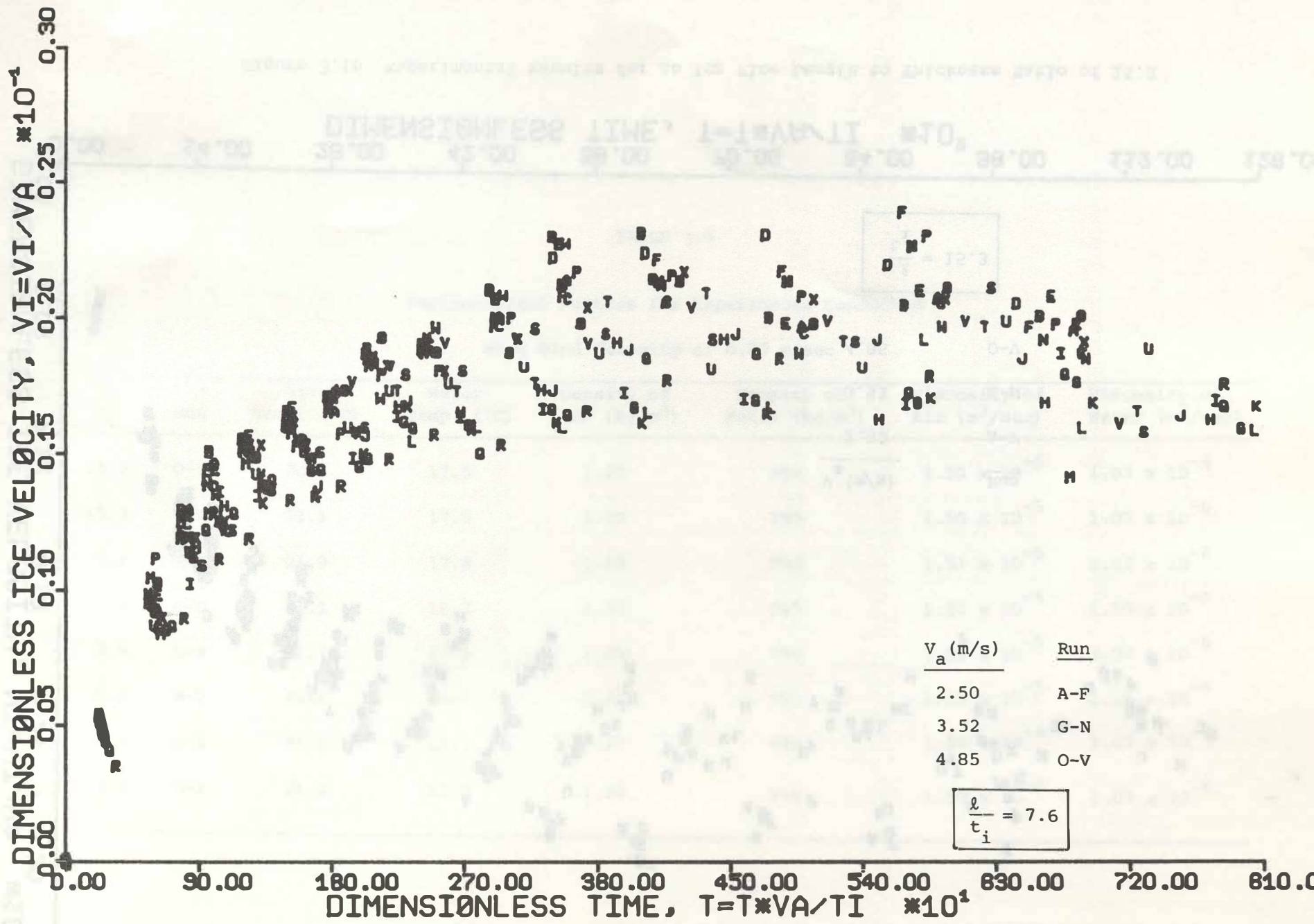
Figure 3.19   Experimental Results for an Ice Floe Length to Thickness Ratio of 3.8

Figure 3.20 Experimental Results for an Ice Floe Length to Thickness Ratio of 3.1
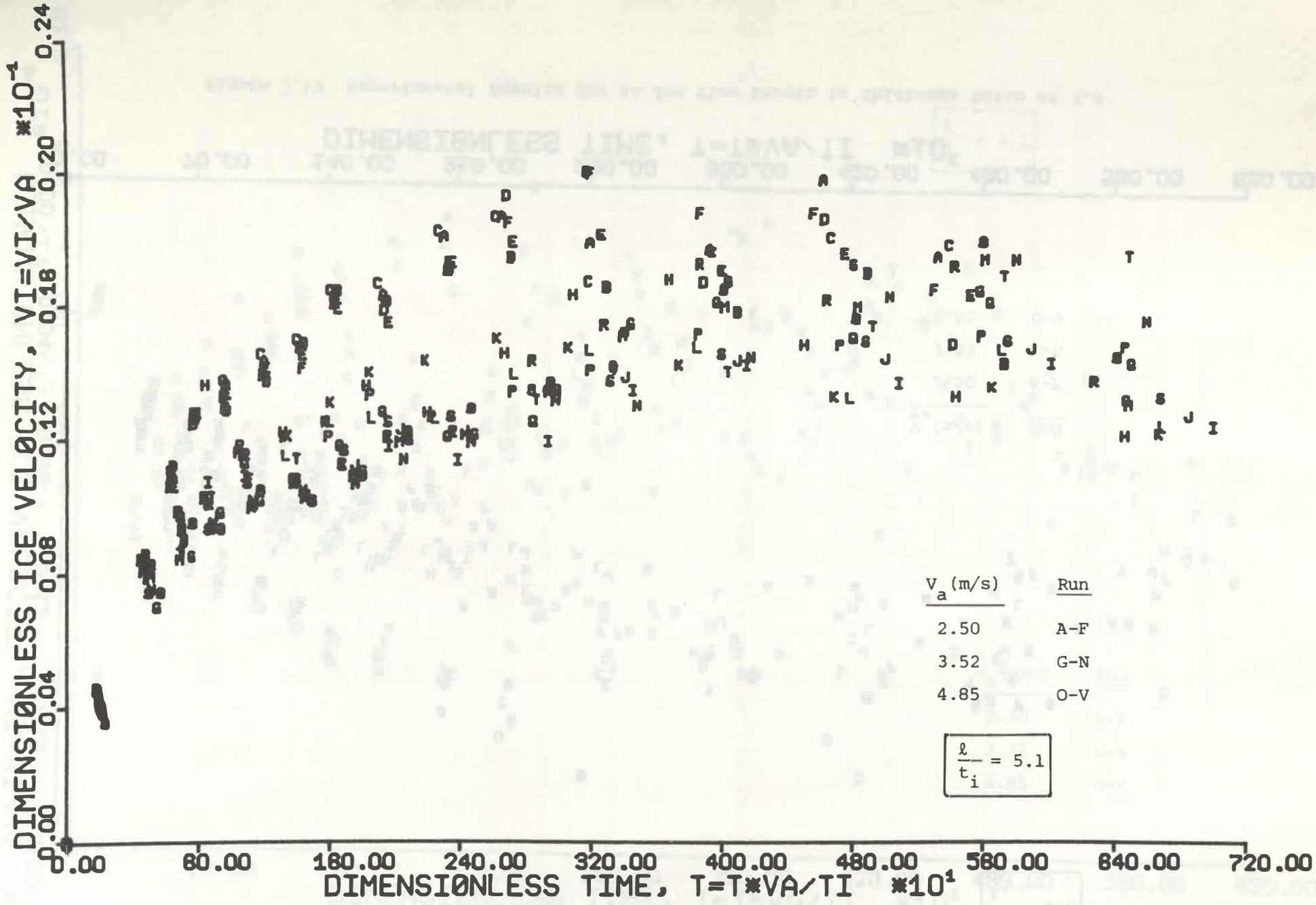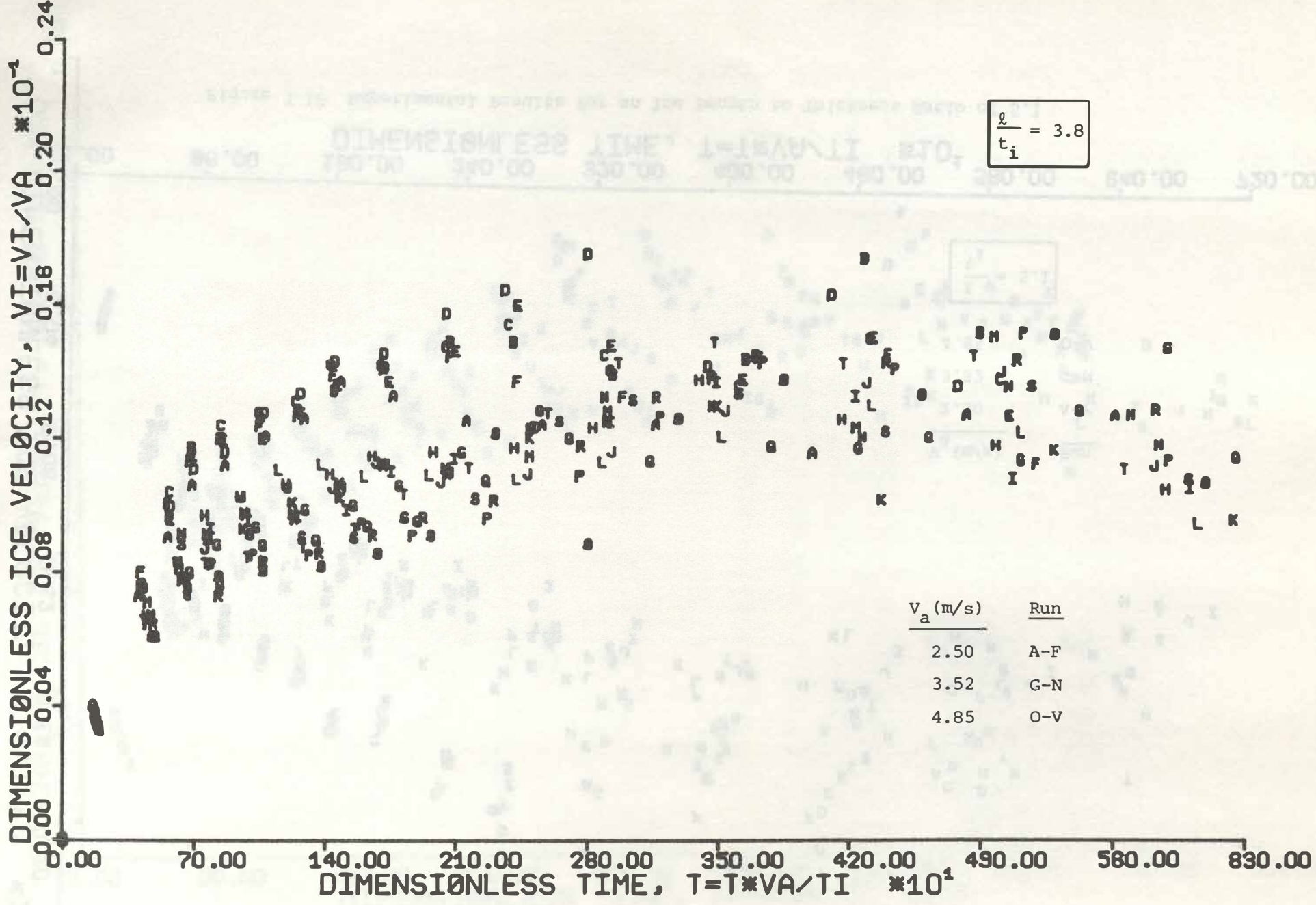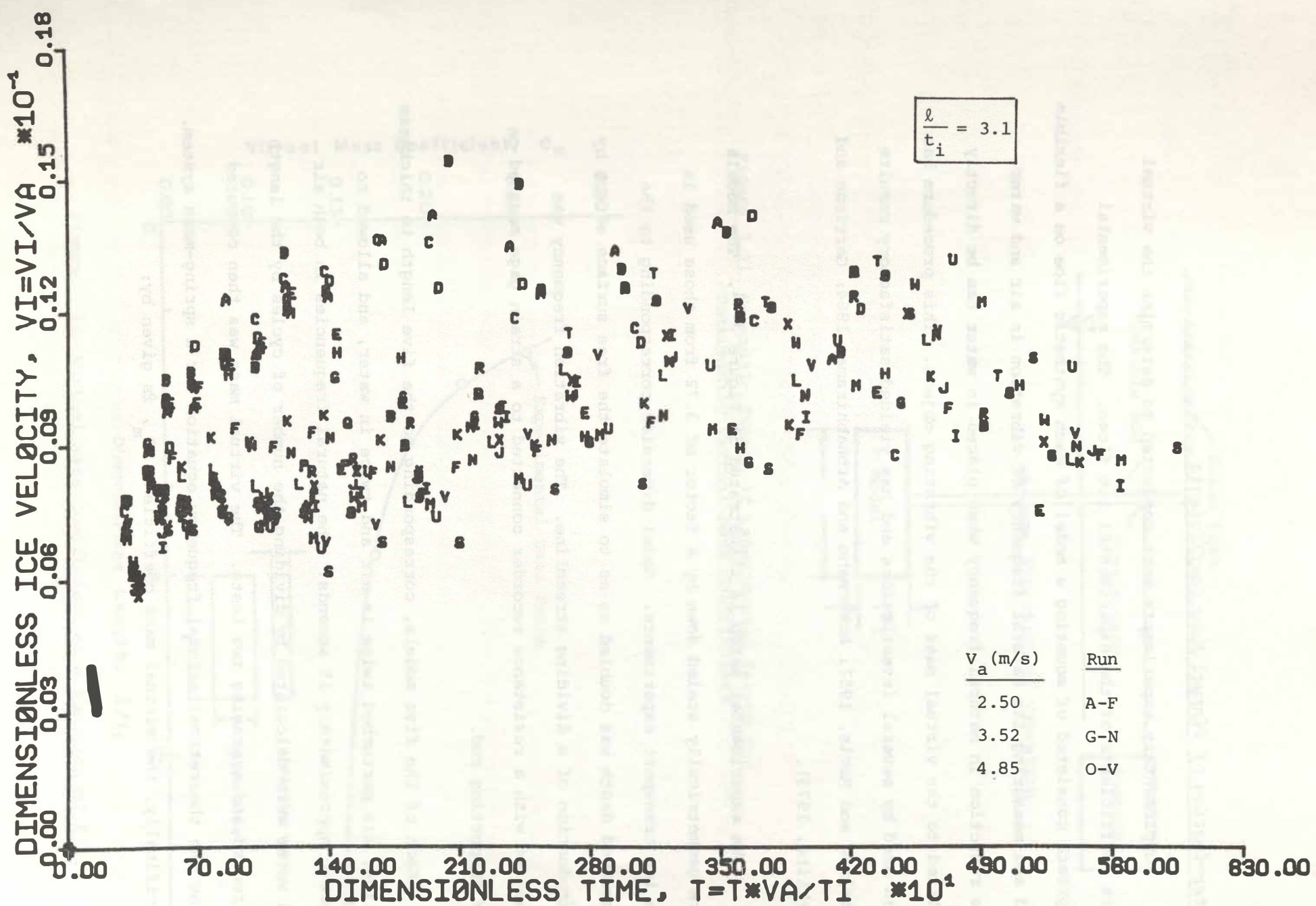
The chart axes and legend:

DIMENSIONLESS ICE VELOCITY, $VI=VI/VA$ $*10^{-1}$

DIMENSIONLESS TIME, $T=T*VA/TI$ $*10^1$

$\frac{\ell}{t_i} = 3.1$

V_a (m/s)	Run
2.50	A-F
3.52	G-N
4.85	O-V

68

Determination of Virtual Mass Coefficients

Supplementary experiments were conducted to determine the virtual mass coefficients of the experimental ice floes. The experimental approach consisted of mounting a model of each synthetic floe on a flexible rod and measuring its natural frequency of vibration in air and water. The reduction in natural frequency when placed in water can be directly related to the virtual mass of the vibrating object. This procedure has been used by several investigators and has yielded satisfactory results (Stelson and Mavis, 1957; Ackermann and Arbhabhirama, 1964; Garrison and Berklite, 1973).

The experimental setup is illustrated in Figure 3.21. The models were geometrically scaled down by a factor of 3.72 from those used in the ice transport experiments. Model dimension corresponding to the submerged depth was doubled so as to simulate the free surface effect by introduction of a dividing streamline. The vibration frequency was measured with a resistance recorder connected to a strain gage mounted on the supporting rod.

Each of the five models, corresponding to the five length to thickness ratios, was perturbed twice in air and twice in water, and allowed to vibrate approximately 15 seconds. The natural frequencies in both air and water were calculated by dividing the number of cycles by the length of record and averaging two tests. The virtual mass was then computed using the theoretical natural frequency equation for a spring-mass system. Specifically, the virtual mass coefficient, C_m, is given by:
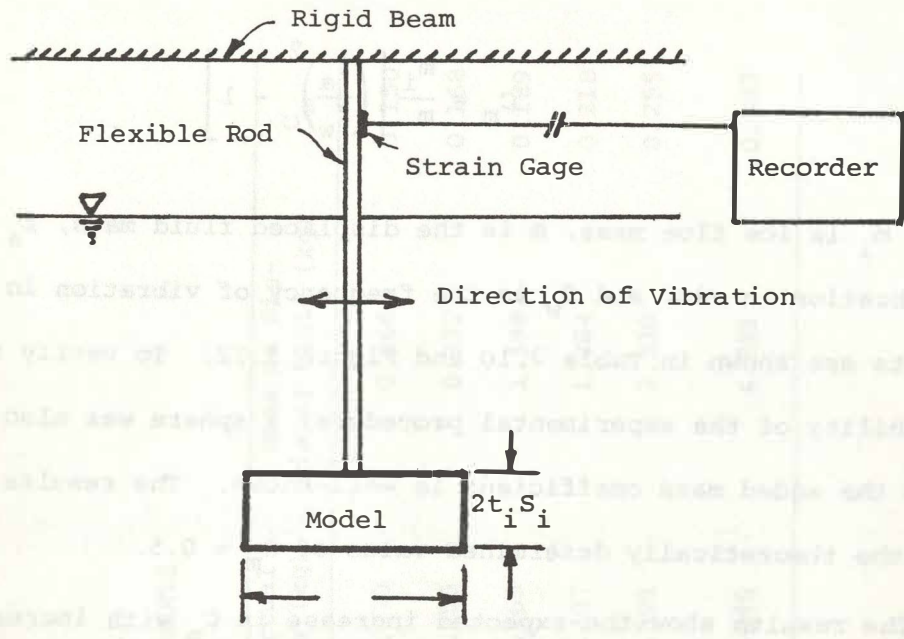
90

Figure 3.21   Schematic Sketch of Experimental Set-Up for
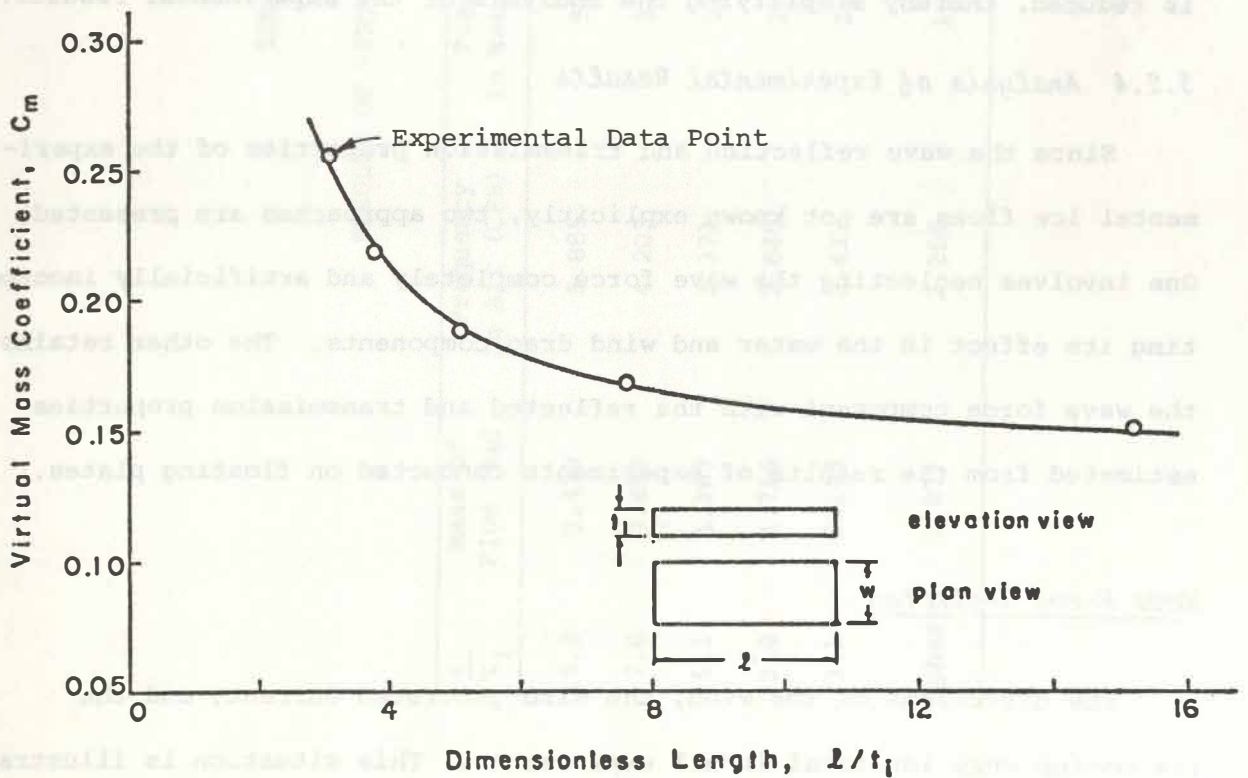Determining Virtual Mass Coefficients

Figure 3.22   Virtual Mass Coefficient as a Function of ℓ/t_i

$$C_m = \frac{m_i}{m}\left[\left(\frac{f_a}{f_w}\right)^2 - 1\right]$$

(3.15)

where m_i is ice floe mass, m is the displaced fluid mass, f_a is the frequency of vibration in air, and f_w is the frequency of vibration in water. The results are shown in Table 3.10 and Figure 3.22. To verify the reliability of the experimental procedure, a sphere was also tested for which the added mass coefficient is well-known. The results agreed well with the theoretically determined value of $C_m = 0.5$.

The results show the expected increase in C_m with increasing thickness. Increasing the length to thickness ratio effectively streamlines the flow around the object, thus reducing C_m. With these values for the virtual mass coefficient, the number of unknowns in Equation (3.14) is reduced, thereby simplifying the analysis of the experimental results.

3.2.4 Analysis of Experimental Results

Since the wave reflection and transmission properties of the experimental ice floes are not known explicitly, two approaches are presented. One involves neglecting the wave force completely and artificially incorporating its effect in the water and wind drag components. The other retains the wave force component with the reflected and transmission properties estimated from the results of experiments conducted on floating plates.

Wave Force Neglected

The directions of the wind, the wind generated current, and the ice motion were identical in all experiments. This situation is illustrated schematically in Figure 3.23. Neglecting the wave force component in

92

TABLE 3.10

RESULTS OF VIRTUAL MASS EXPERIMENTS

$\dfrac{\ell}{t_i}$	Mass of Floe (kg)	Frequency in Air (CPS)	Frequency in Water (CPS)	Virtual Mass (kg)	Mass of Dis-Placed Fluid (kg)	C_m
15.3	0.429	5.885	5.455	0.070	0.466	0.150
7.6	0.858	4.203	3.864	0.156	0.932	0.168
5.1	1.287	3.371	3.070	0.265	1.398	0.189
3.8	1.716	2.840	2.553	0.407	1.864	0.218
3.1	2.145	2.439	2.206	0.594	2.330	0.255
Sphere	1.877	2.266	1.493	2.440	4.821	0.507
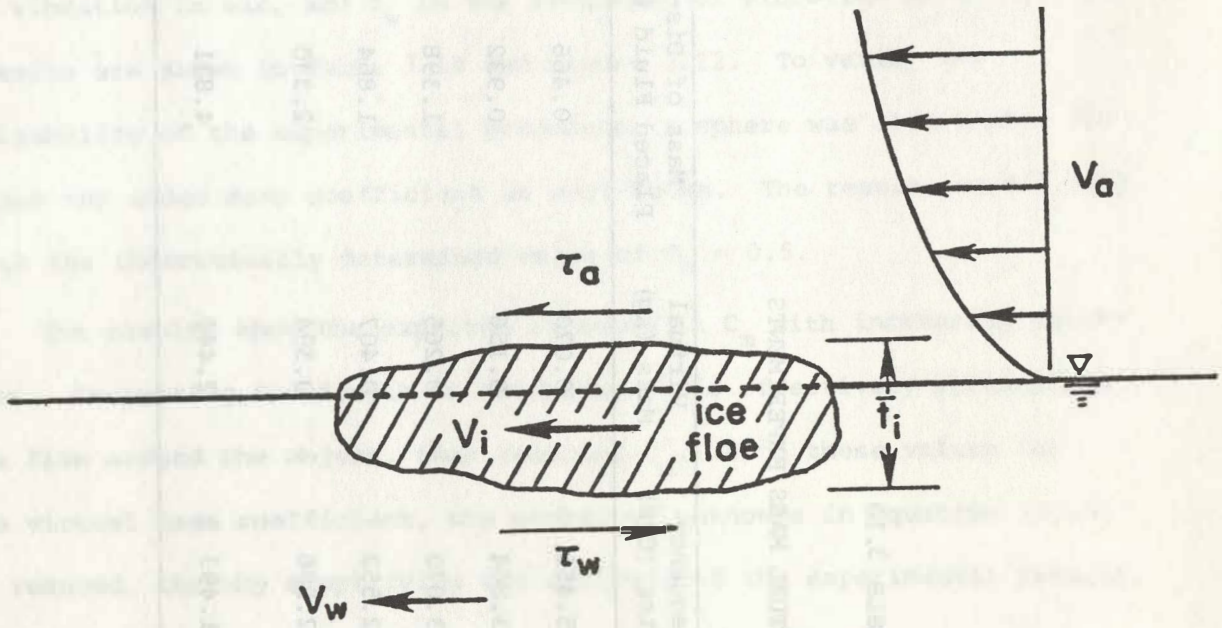
Figure 3.23   Schematic Sketch of Physical Situation With Wave Force Neglected

Equation (3.14) and eliminating the absolute value signs, the following

conditions apply ($V_a' = 1$):

$$\frac{dV_i'}{dt} = A + B (V_i' - V_w')^2 \quad ; \quad V_i' \leq V_w' \qquad (3.16)$$

$$\frac{dV_i'}{dt'} = A - B (V_i' - V_w')^2 \quad ; \quad V_i' \geq V_w' \qquad (3.17)$$

The problem is separated into two parts so that an analytical solution can

be presented. This is advantageous since both $\overline{C}_a$ and $\overline{C}_w$ can be

determined explicitly based on the experimental results.

The constant, A, is modified to account for the drag contributed by

the guides (Figure 3.12). This drag contribution is approximated by:

$$D_g = C_D \rho_a A_g V_a^2 \qquad (3.18)$$

where D_g is the drag on the guides, C_D is a drag coefficient ($\simeq 0.15$),

ang A_g is the projected cross-sectional area of the guides normal to the

air flow. The constants A and B then become:

$$A = \frac{\rho_a \overline{C}_a'}{\rho_i (1 + C_m)} \quad ; \quad B = \frac{\rho_w \overline{C}_w}{\rho_i (1 + C_m)} = K_2$$

$$\text{where} \quad \overline{C}_a' = \overline{C}_a + \overline{C}_D \quad ; \quad \overline{C}_D = \frac{C_D A_g}{\ell \cdot w} = 0.0026$$

95

Since the experimental ice floes were initially at rest, the
solutions to both Equations (3.16) and (3.17) are required to describe
the motion. The solution to Equation (3.16) with the initial condition
$V_i' = 0$ at $t' = 0$ is:

$$V_i' = A^* \left[\frac{\tan B^* t' - \frac{1}{A^*}}{1 + \frac{1}{A^*} \tan B^* t'} \right] + V_w' \qquad (3.19)$$

where $A^* = \sqrt{\dfrac{\rho_a \overline{C_a}'}{\rho_w \overline{C_w}}}$

$$B^* = \frac{\sqrt{\overline{C_a}' \; \overline{C_w} \; \rho_a \rho_w}}{(1 + C_m) \rho_i}$$

The initial velocity for the solution to Equation (3.17) is $V_i' = V_w$. The
initial time is calculated from Equation (3.19) by substituting $V_w' = V_i'$.

$$t_o' = \frac{1}{B^*} \tan^{-1} \left(\frac{V_w'}{A^*} \right) \qquad (3.20)$$

The solution to Equation (3.17) then becomes:

$$V_i' = A^* \tanh B^* (t' - t_o') + V_w' \qquad (3.21)$$

The dimensionless terminal velocity and the time required to attain
98% of this velocity are the two parameters used to estimate $\overline{C_a}$ and $\overline{C_w}$.
The dimensionless terminal velocity is given by:

$$V_{i_T}' = A^* + V_w' \qquad (3.22)$$

Therefore,

$$\frac{\overline{C_a}'}{\overline{C_w}} = \frac{\rho_w}{\rho_a} (V_{i_T}' - V_w')^2 \qquad (3.23)$$

Similarly the dimensionless time to attain 98% of the dimensionless terminal velocity is given by:

$$t_{.98}' = \frac{1}{B^*} [\tanh^{-1} C^* + \tan^{-1} D^*] \qquad (3.24)$$

where

$$C^* = .98 + .02 \frac{\rho_w}{\rho_a} V_w' (V_{i_T}' - V_w')$$

$$D^* = \frac{\rho_w}{\rho_a} V_w' (V_i' - V_w')$$

Therefore,

$$\overline{C_a}' \, \overline{C_w} = \frac{[(1+C_m) \rho_i \{\tanh^{-1} C^* + \tan^{-1} D^*\}]^2}{(t_{.98}')^2 \rho_a \rho_w} \qquad (3.25)$$

Solving Equation (3.23) for $\overline{C_a}'$ and substituting into Equation (3.25) gives an explicit expression for $\overline{C_w}$.

$$\overline{C_w} = \frac{(1+C_m) \rho_i \{\tanh^{-1} C^* + \tan^{-1} D^*\}}{t_{.98}' \rho_w (V_{i_T}' - V_w')} \qquad (3.26)$$

The drag coefficients for the experimental ice floes are obtained by estimating the terminal velocity and the time required to attain 98% of the terminal velocity for each length to thickness ratio ($\frac{\ell}{t_i}$). These relationships are illustrated in Figures 3.24 and 3.25   The data plotted in these figures represent averages for each wind velocity at the corresponding value of $\frac{\ell}{t_i}$. The terminal velocity is shown approaching the surface drift velocity asymptotically as the length to thickness ratio increases. The following empirical equation is used to represent this relationship:

$$V_{i_T}' = 0.03(1 - e^{-0.145 \frac{\ell}{t_i}})$$

(3.27)

The plot of ℓ/t_i versus $t'.98$ is consistent with the sensitivity findings shown in Fig. 3.13. However, when the data are plotted as shown in Fig. 3.13, the same general trend is found between ℓ/t_i and $t'.98$. The following empirical equation approximates the relationship suggested by the data in Fig. 3.25.

$$t_{.98}' = 0.25 \frac{\ell}{t_i} + 1850$$

(3.28)

A relationship between $\overline{C}_w$ and $\frac{\ell}{t_i}$ is obtained by substituting Equations (3.27) and (3.28) into Equation (3.26). As discussed earlier, the appropriate value of V_w to use in estimating $\overline{C}_w$ is not obvious. Therefore, Equation (3.26) is evaluated for different values of V_w' and plotted in Figure 3.26. The virtual mass coefficient for each value of $\frac{\ell}{t_i}$ is taken from Figure 3.22.
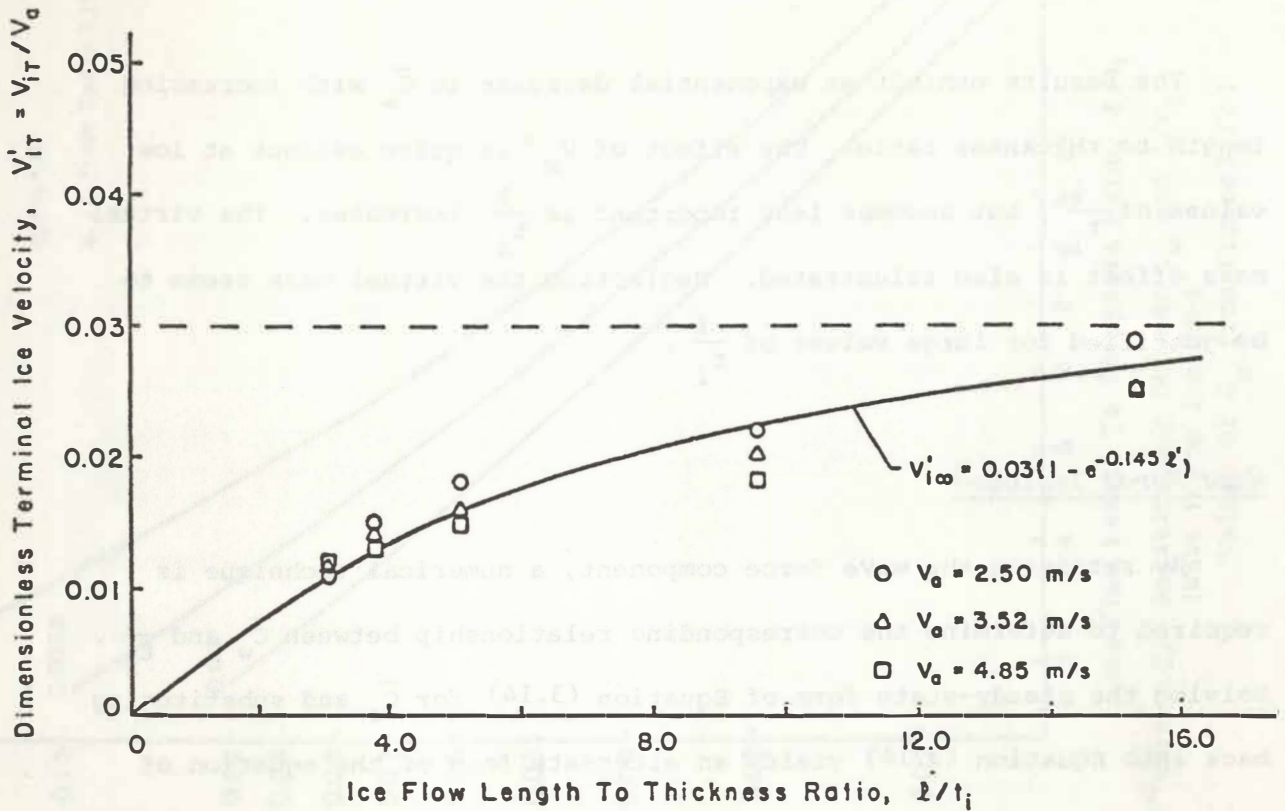
Figure 3.24 Experimental Results: Terminal Ice Floe Velocity as a Function of ℓ/t_i
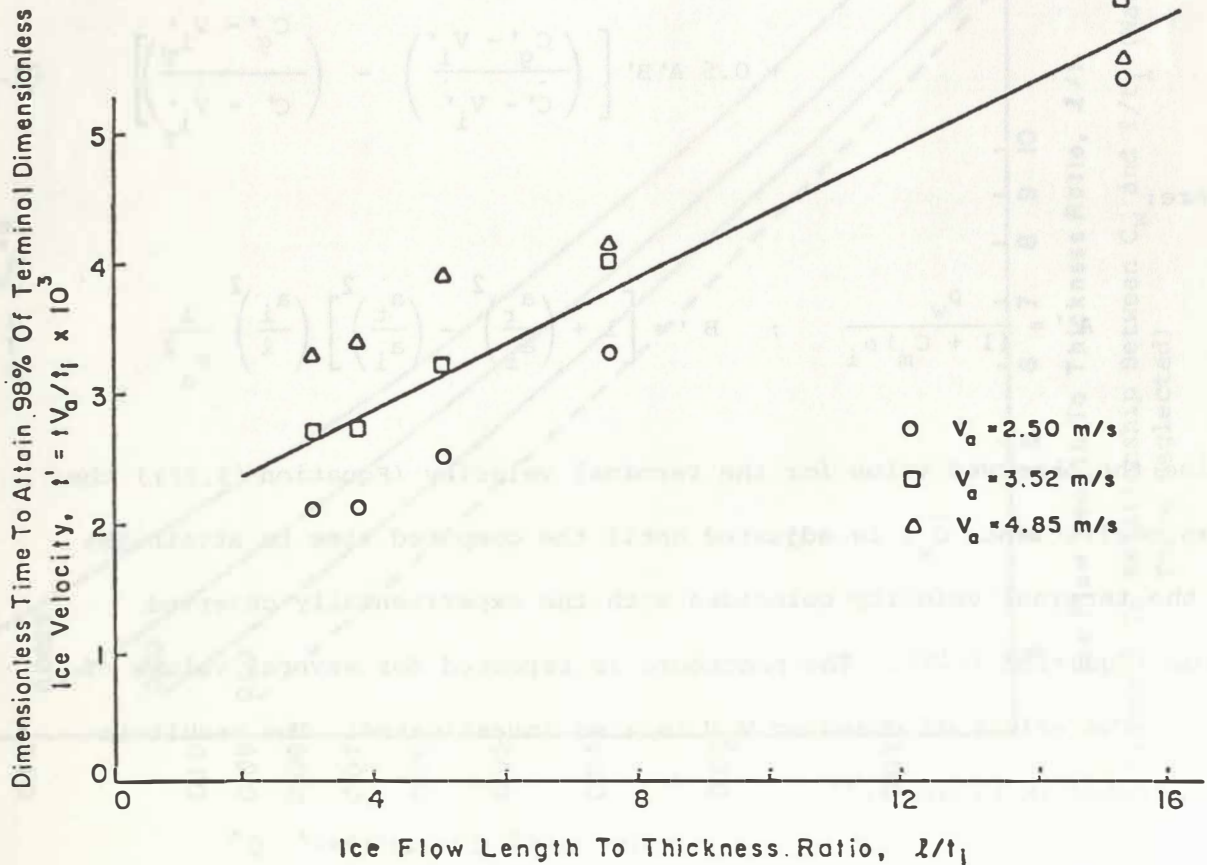

Figure 3.25 Experimental Results: Ice Floe Response Time as a Function of ℓ/t_i

99

The results exhibit an exponential decrease in $\overline{C}_w$ with increasing length to thickness ratio. The effect of V_w' is quite evident at low values of $\frac{\ell}{t_i}$, but becomes less important as $\frac{\ell}{t_i}$ increases. The virtual mass effect is also illustrated. Neglecting the virtual mass seems to be justified for large values of $\frac{\ell}{t_i}$.

Wave Force Included

By retaining the wave force component, a numerical technique is required to determine the corresponding relationship between $\overline{C}_w$ and $\frac{\ell}{t_i}$. Solving the steady-state form of Equation (3.14) for $\overline{C}_a$ and substituting back into Equation (3.14) yields an alternate form of the equation of motion:

$$\frac{dV_i'}{dt'} = C_w A' \left[\left| V_{i_T}' - V_w' \right| \left(V_{i_T}' - V_w^r \right) - \left| V_i' - V_w' \right| \left(V_i' - V_w' \right) \right]$$
$$+ 0.5 A'B' \left[\left(\frac{C_g' - V_i'}{C' - V_i'} \right) - \left(\frac{C_g' - V_{i_T}'}{C' - V_{i_T}'} \right) \right] \tag{3.29}$$

where:

$$A' = \frac{\rho_w}{(1 + C_m)\rho_i} \quad ; \quad B' = \left[1 + \left(\frac{a_r}{a_i} \right)^2 - \left(\frac{a_t}{a_i} \right)^2 \right] \left(\frac{a_i}{\ell} \right)^2 \frac{1}{F_a^2}$$

Using the observed value for the terminal velocity (Equation (3.27)) the drag coefficient, $\overline{C}_w$, is adjusted until the computed time to attain 98% of the terminal velocity coincides with the experimentally observed value (Equation 3.28). The procedure is repeated for several values of $\frac{\ell}{t_i}$. The effect of changing V_w' is also investigated. The result is illustrated in Figure 3.27.
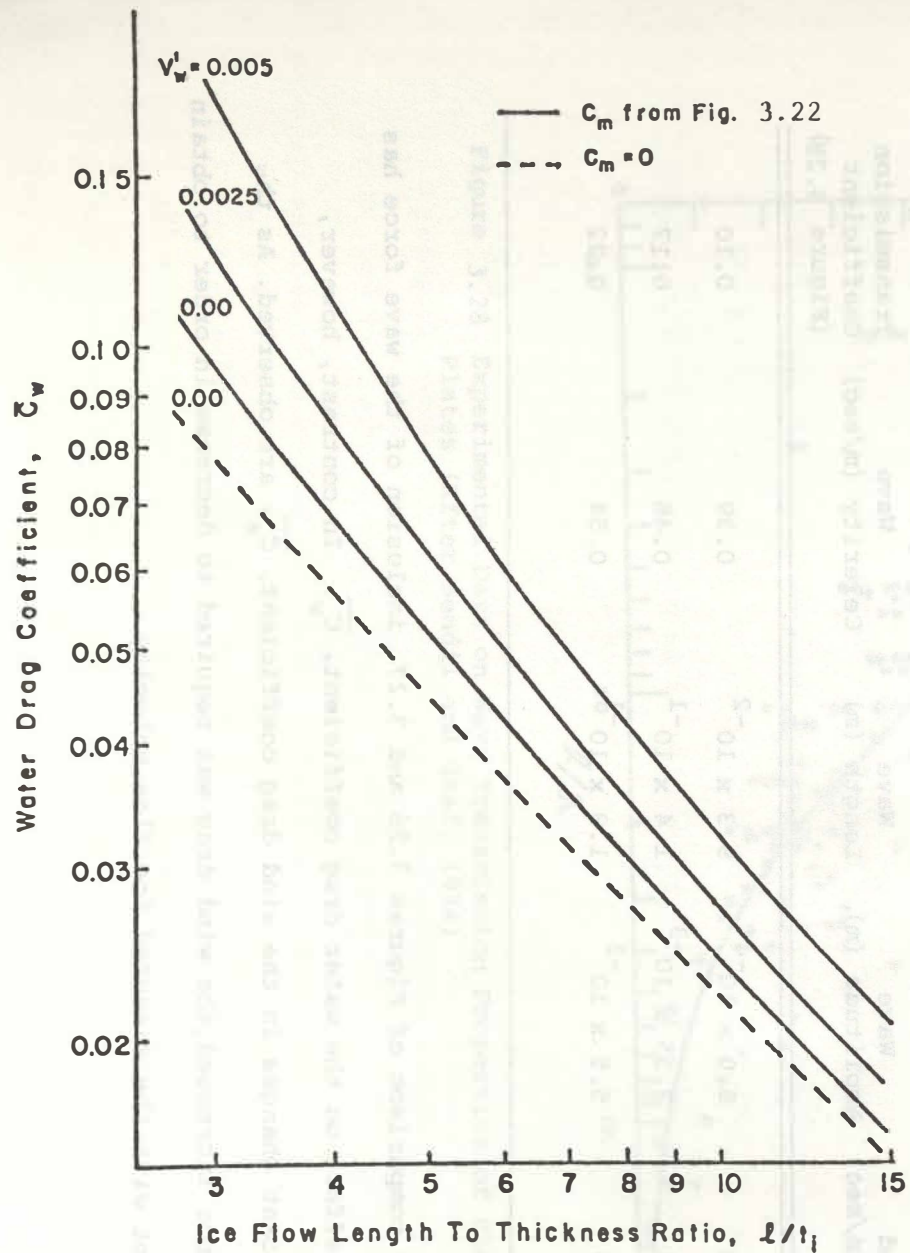
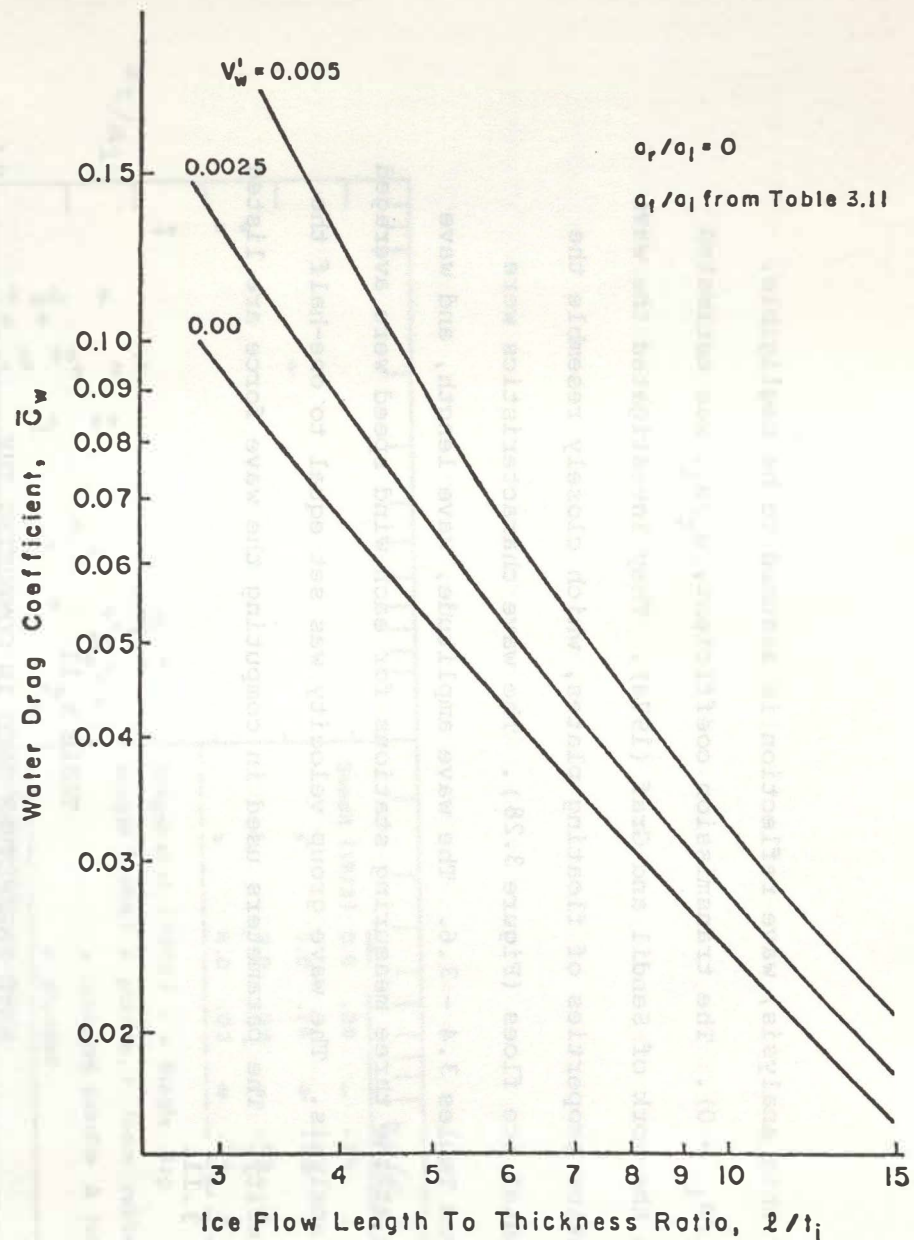Figure 3.26 Relationship Between C_w and ℓ/t_i (Wave Force Neglected)

Figure 3.27 Relationship Between C_w and ℓ/t_i (Wave Force Included Values of C_m from Figure 3.72)

For this analysis, wave reflection is assumed to be negligible, (i.e., $a_r/a_i = 0$). The transmission coefficient, a_t/a_i, was estimated based on the work of Sendil and Graf (1974). They investigated the wave transmission properties of floating plates, which closely resemble the experimental ice floes (Figure 3.28). The wave characteristics were taken from Tables 3.4 - 3.6. The wave amplitude, wave length, and wave celerity at the three measuring stations for each wind speed were averaged for the analysis. The wave group velocity was set equal to one-half the wave celerity. The parameters used in computing the wave force are listed in Table 3.11.

TABLE 3.11

WAVE PARAMETERS USED IN COMPUTING THE
WAVE FORCE ON THE EXPERIMENTAL ICE FLOES

Wind Speed (m/sec)	Wave Amplitude (m)	Wave Length (m)	Wave Celerity (m/sec)	Transmission Coefficient (Figure 3.28)
2.50	6.0×10^{-4}	9.3×10^{-2}	0.39	0.10
3.52	2.35×10^{-3}	1.4×10^{-1}	0.46	0.17
4.85	5.5×10^{-3}	1.9×10^{-1}	0.54	0.22

By comparison of Figures 3.26 and 3.27 inclusion of the wave force has little effect on the water drag coefficient, $\overline{C}_w$. In contrast, however, significant changes in the wind drag coefficient, $\overline{C}_a$, are observed. As the wave force increased, the wind drag was required to decrease in order to obtain agreement with the measured ice floe velocity.
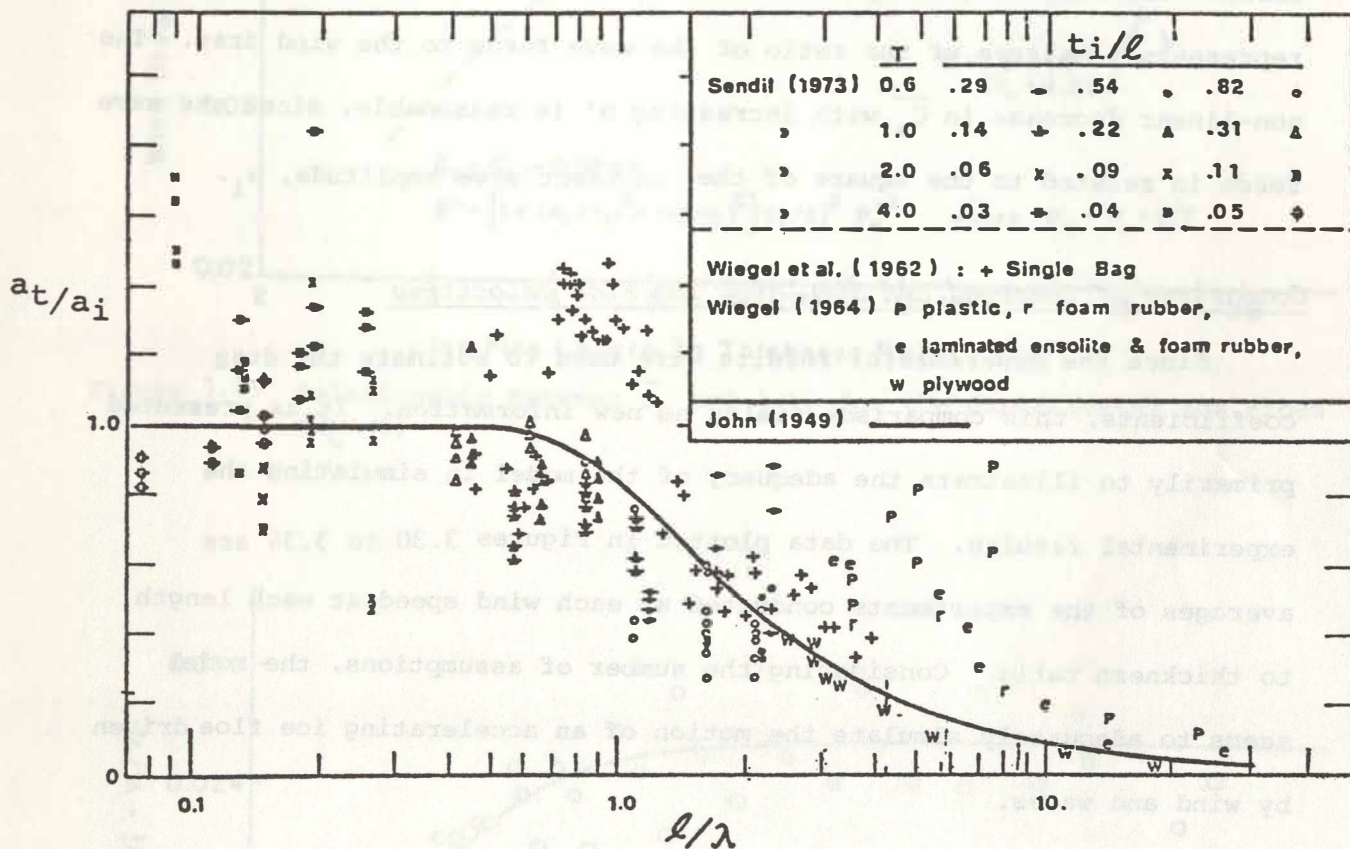
Figure 3.28 Experimental Data on Wave Transmission Properties of Floating
Plates (After Sendil and Graf, 1974)

In Figure 3.29, $\overline{C_a}$ is plotted against ℓ/t_i for one value of $V_w{}'(=0)$. The effect of increasing $V_w{}'$, although it decreases $\overline{C_a}$ for any value of ℓ/t_i, is not illustrated since the curve shapes are similar. The solid curve in Figure 3.29 represents the results obtained when the wave force is neglected in the analysis. The dashed curves represent the effect of retaining the wave force. The dimensionless parameter, B', from Equation (3.29) essentially represents a measure of the ratio of the wave force to the wind drag. The non-linear decrease in $\overline{C_a}$ with increasing B' is reasonable, since the wave force is related to the square of the incident wave amplitude, a_i.

Comparison of Observed and Simulated Ice Floe Velocities

Since the experimental results were used to estimate the drag coefficients, this comparison yields no new information. It is presented primarily to illustrate the adequacy of the model in simulating the experimental results. The data plotted in Figures 3.30 to 3.34 are averages of the experiments conducted at each wind speed at each length to thickness ratio. Considering the number of assumptions, the model seems to adequately simulate the motion of an accelerating ice floe driven by wind and waves.

3.2.5 *Discussion*

In the previous sections, the results of the experimental program to measure the velocity of wind-driven simulated ice floes were presented. These results were used, along with the equation of motion presented in Section 3.2.1 to determine relationships between the water and wind drag coefficients, $\overline{C_w}$ and $\overline{C_a}$, and the length to thickness ratio of the ice floe, ℓ/t_i. In this section the scaling of the physical processes in the experiments and the assumptions used in the analysis are discussed.
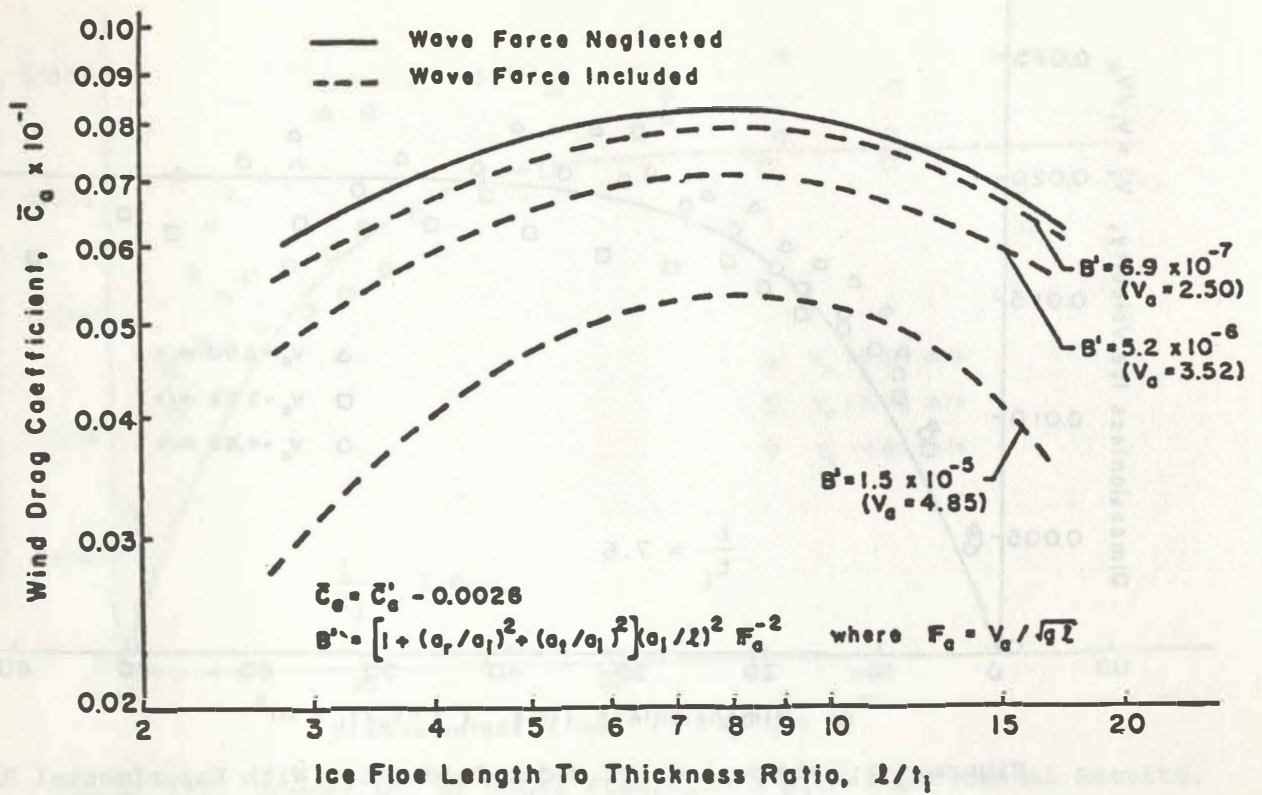
Figure 3.29 Relationship Between $\bar{C}_a$ and ℓ/t_i for the Experimental Ice Floes $(V_w'=0)$
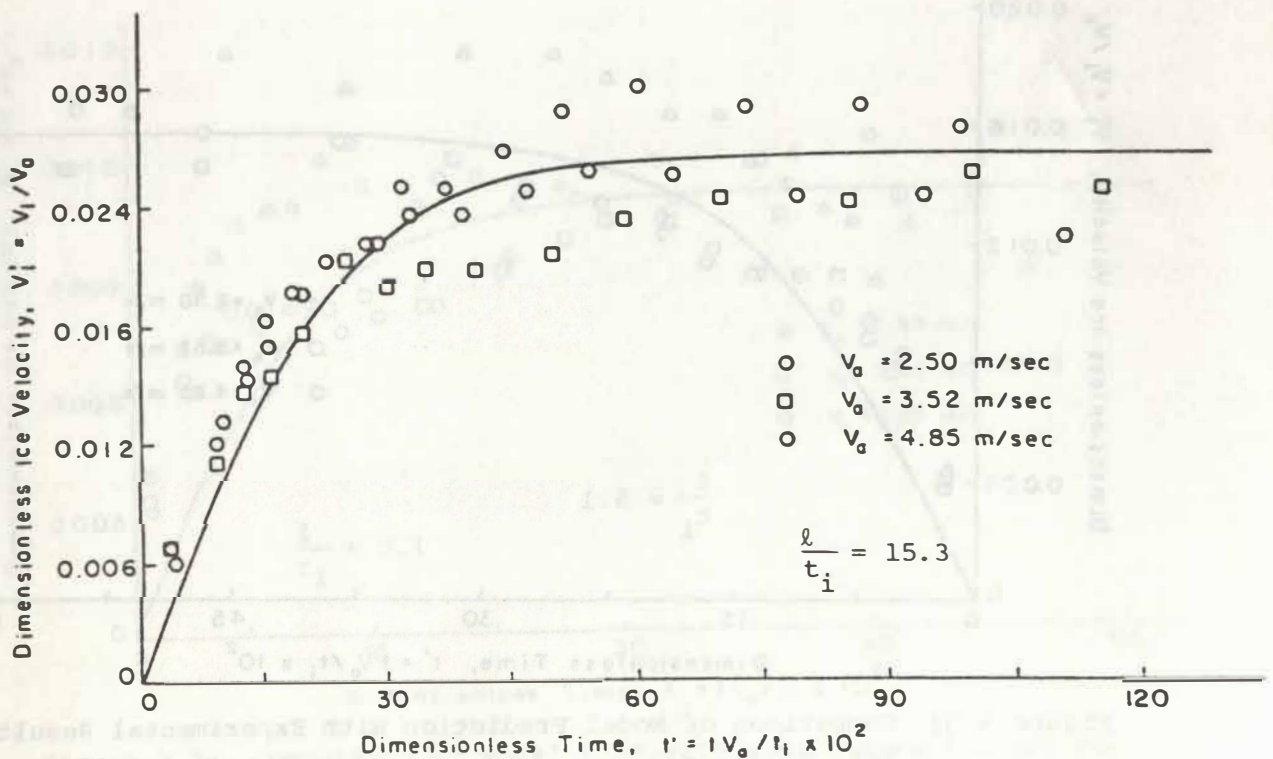
Figure 3.30 Comparison of Model Prediction With Experimental Results, $\ell/t_i = 15.3$
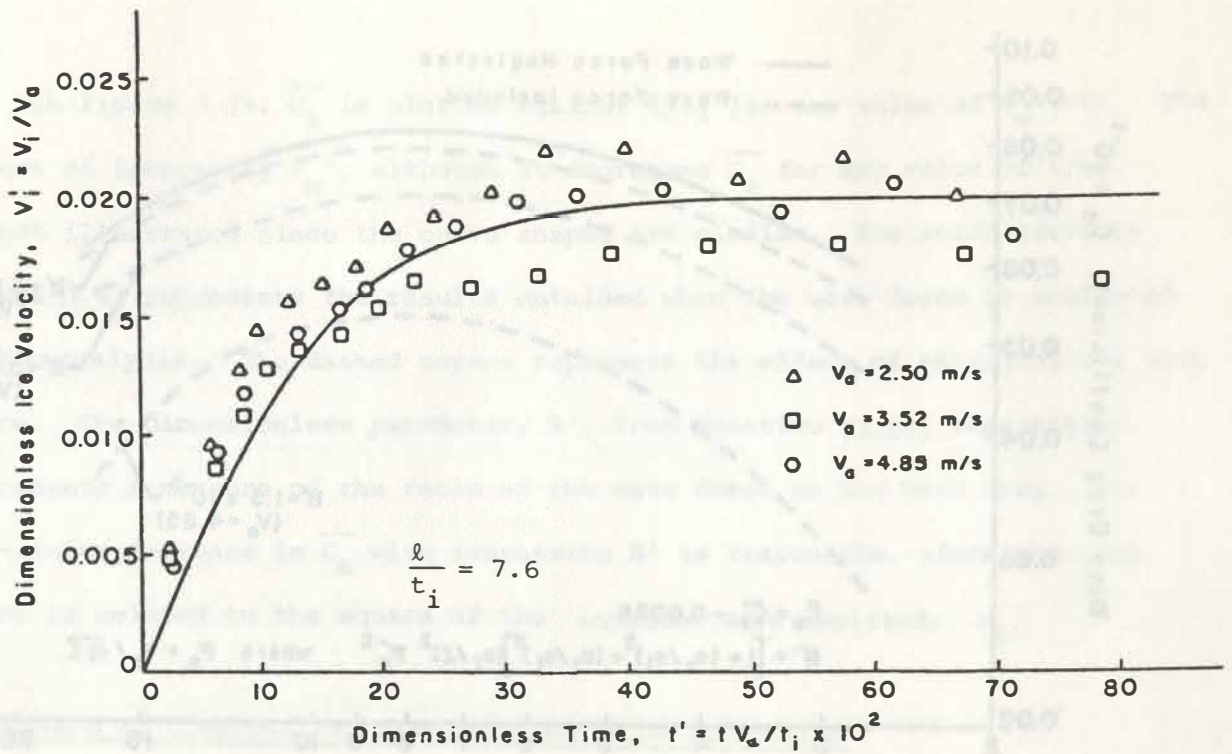
Figure 3.31 Comparison of Model Prediction With Experimental Results, $\ell/t_i = 7.6$
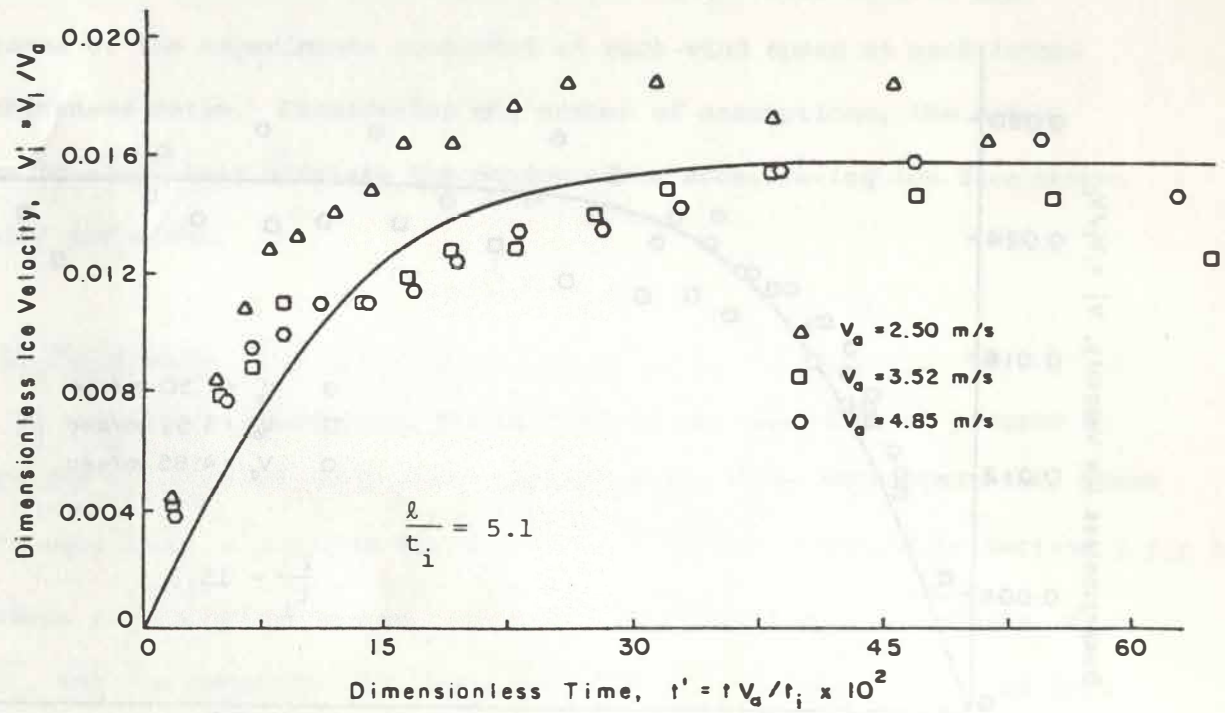
Figure 3.32 Comparison of Model Prediction With Experimental Results, $\ell/t_i = 5.1$

106
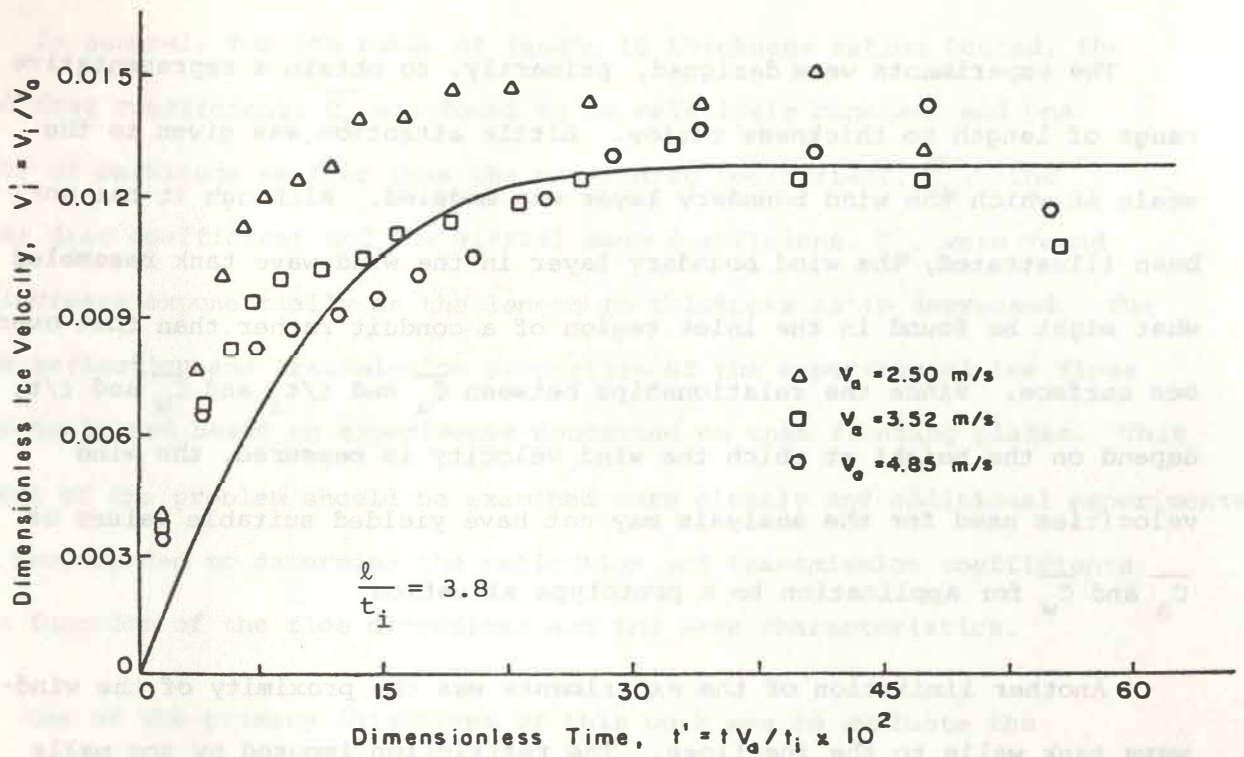
Figure 3.33   Comparison of Model Predictions With Experimental Results, $\ell/t_i = 3.8$
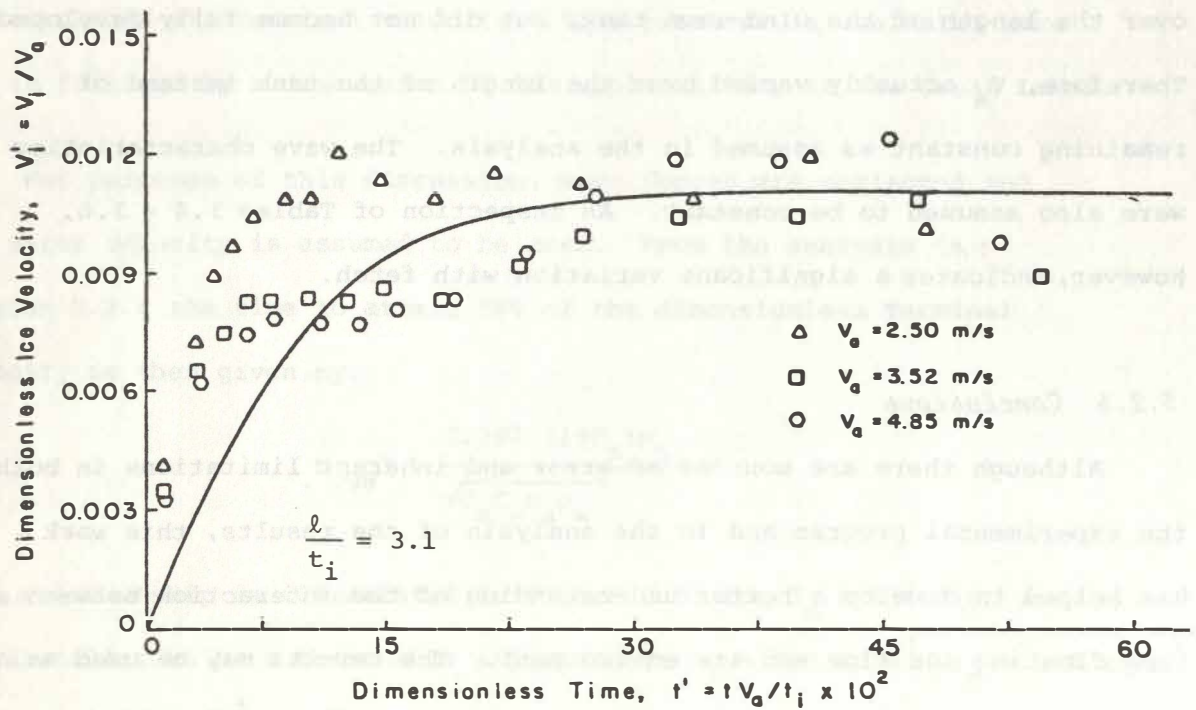
Figure 3.34   Comparison of Model Predictions With Experimental Results, $\ell/t_i = 3.1$

The experiments were designed, primarily, to obtain a representative range of length to thickness ratios. Little attention was given to the scale at which the wind boundary layer was modeled. Although it has not been illustrated, the wind boundary layer in the wind-wave tank resembled what might be found in the inlet region of a conduit rather than that over a sea surface. Since the relationships between $\overline{C_a}$ and ℓ/t_i and $\overline{C_w}$ and ℓ/t_i depend on the height at which the wind velocity is measured, the wind velocities used for the analysis may not have yielded suitable values of $\overline{C_a}$ and $\overline{C_w}$ for application to a prototype situation.

Another limitation of the experiments was the proximity of the wind-wave tank walls to the ice floes. The restriction imposed by the walls may have increased the water drag above that in an unrestricted case.

As already mentioned, the wind boundary layer in the experiments resembled that in the inlet portion of a conduit. The boundary layer grew over the length of the wind-wave tank, but did not become fully developed. Therefore, V_a actually varied over the length of the tank instead of remaining constant as assumed in the analysis. The wave characteristics were also assumed to be constant. An inspection of Tables 3.4 - 3.6, however, indicates a significant variation with fetch.

3.2.6 Conclusions

Although there are sources of error and inherent limitations in both the experimental program and in the analysis of the results, this work has helped to develop a better understanding of the interaction between a free floating ice floe and its environment. The results may be used as a guide in estimating the motion of a floating ice floe. The most useful findings relate to the water and wind drag coefficients.

In general, for the range of length to thickness ratios tested, the wind drag coefficient, $\overline{C}_a$ was found to be relatively constant and one order of magnitude smaller than the water drag coefficient, $\overline{C}_w$. The water drag coefficient and the virtual mass coefficient, C_m, were found to increase exponentially as the length to thickness ratio decreased. The wave reflection and transmission properties of the experimental ice floes were estimated based on experiments conducted on thin floating plates. This aspect of the problem should be examined more closely and additional experiments are recommended to determine the reflection and transmission coefficients as a function of the floe dimensions and the wave characteristics.

One of the primary objectives of this work was to evaluate the practice of neglecting the acceleration term in the equation of motion for two dimensional ice dynamics models. The justification for this is based on the wind-ice interaction time, and thus the time step in the numerical model being much longer than the time needed for the ice to attain its terminal velocity. This practice is evaluated here and is followed by a discussion of its applicability to the Great Lakes.

For purposes of this discussion, wave forces are neglected and the water velocity is assumed to be zero. From the analysis in Section 3.2.4 the time to attain 98% of the dimensionless terminal velocity is then given by:

$$t_{.98}' = \frac{2.297\ (1+C_m)\rho_i}{\sqrt{C_a C_w \rho_a \rho_w}}$$

This relationship is illustrated in Figure 3.35 for $C_m = 0$ (which was shown earlier to be a reasonable assumption), $\rho_i = 910\ Kg/m^3$ $\rho_a = 1.2\ Kg/m^3$ and $\rho_w = 1000\ Kg/m^3$. The time to attain terminal velocity is seen to be related to three variables; the wind speed, the ice thickness and the

109
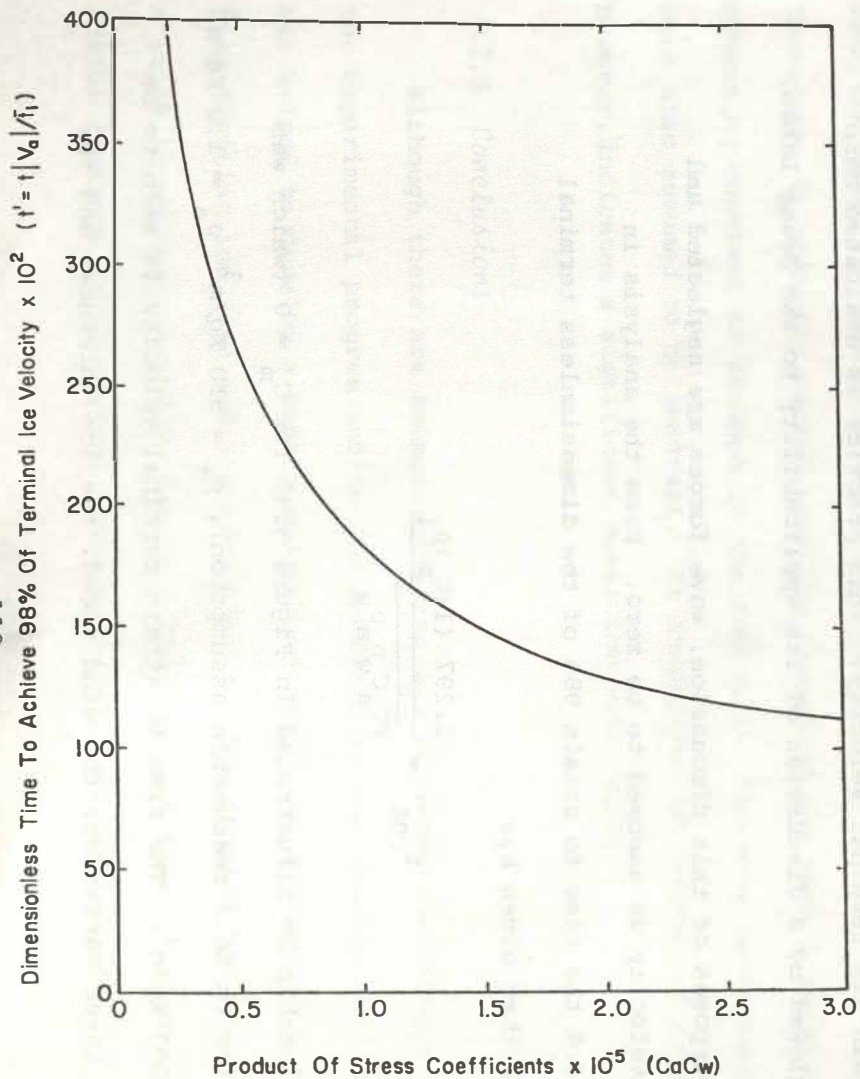
Figure 3.35   Relationship Between $C_a C_w$ and
the Response Time ($V_w' = 0$,
$C_m = 0$)
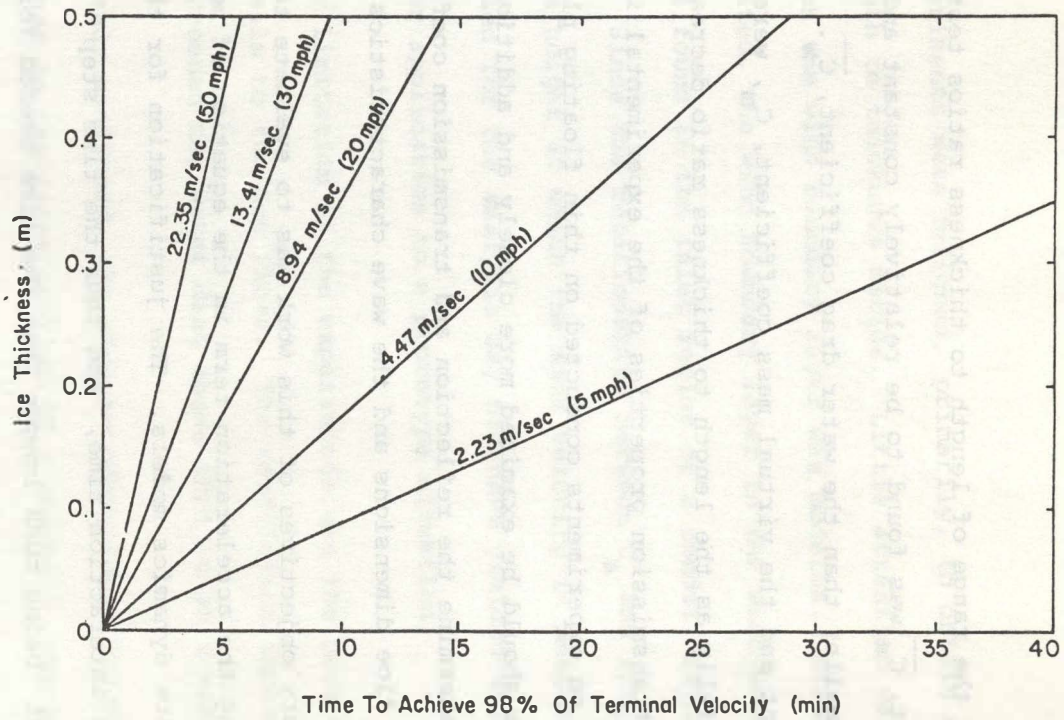
Figure 3.36   Relationship Between Ice Thickness
and Response Time for Varying Wind
Velocities ($V_w' = 0$)

product of the stress coefficients. To gain further insight into the implications of this result, Figure 3.36 is presented. It illustrates the time to attain 98% of the terminal velocity for a constant stress coefficient product ($C_a C_w = 1.44 \times 10^{-5}$, where $C_a = 1.55 \times 10^{-3}$ and $C_w = 9.27 \times 10^{-3}$) versus ice thickness and wind speed. The ranges of ice thickness and wind speed are representative of those encountered in the Great Lakes.

From Figure 3.36 the time to attain steady state is variable depending on the combination of ice thickness, wind speed, and product of the stress coefficients selected. Therefore, the criteria for neglecting the acceleration term must be dependent on the specific situation being modeled. A reasonable criteria for neglecting the acceleration term may be based on a time step being at least 10 times greater than the time to attain 98% of steady state. On the other hand, were the acceleration term to be retained, the time step would need to be substantially smaller than the time to attain 98% of the steady state velocity in order to accurately model the transient response. In this case, the smallest time step corresponding to the range. of wind speed-ice thickness-stress coefficient combinations for any particular. situation would have to be used. This would probably lead to time steps much too small for economical prediction of ice transport in the Great Lakes. Based on this analysis, each situation should be evaluated separately. The appropriate modeling procedure would depend on user requirements, accuracy of the prediction, and the availability of computer time and funds.

3.3 Transport by Long Waves

The motion of a single floating ice floe due to wind-induced momentum transfer has been treated in the earlier section in some detail. The effect of short water waves (wavelength $<<$ ice floe length) on ice floe transport due

111

to wave reflection, absorption and transmission has also been discussed
briefly. In addition to the forces discussed earlier, the effect of long
progressive waves (wavelength >> ice floe length) on the motion of an ice
floe may also be significant in large waterbodies such as the Great Lakes
To study this effect, the minor forces due to wave reflection, adsorption
and transmission will be neglected. Therefore, for long waves, the
horizontal force exerted on an ice floe consists of three components:
the gravitational force component due to the water surface tilt, the
drag force due to water wave particle velocity, and the force due to
the pressure gradient $(\partial p/\partial x)$. In a long wave, the pressure gradient
is considered to be small compared to other forces and can be neglected.
In this section, only the gravitational force and the water drag force
are considered.

3.3.1 Analysis

The situation being considered is depicted in Figure 3.37.
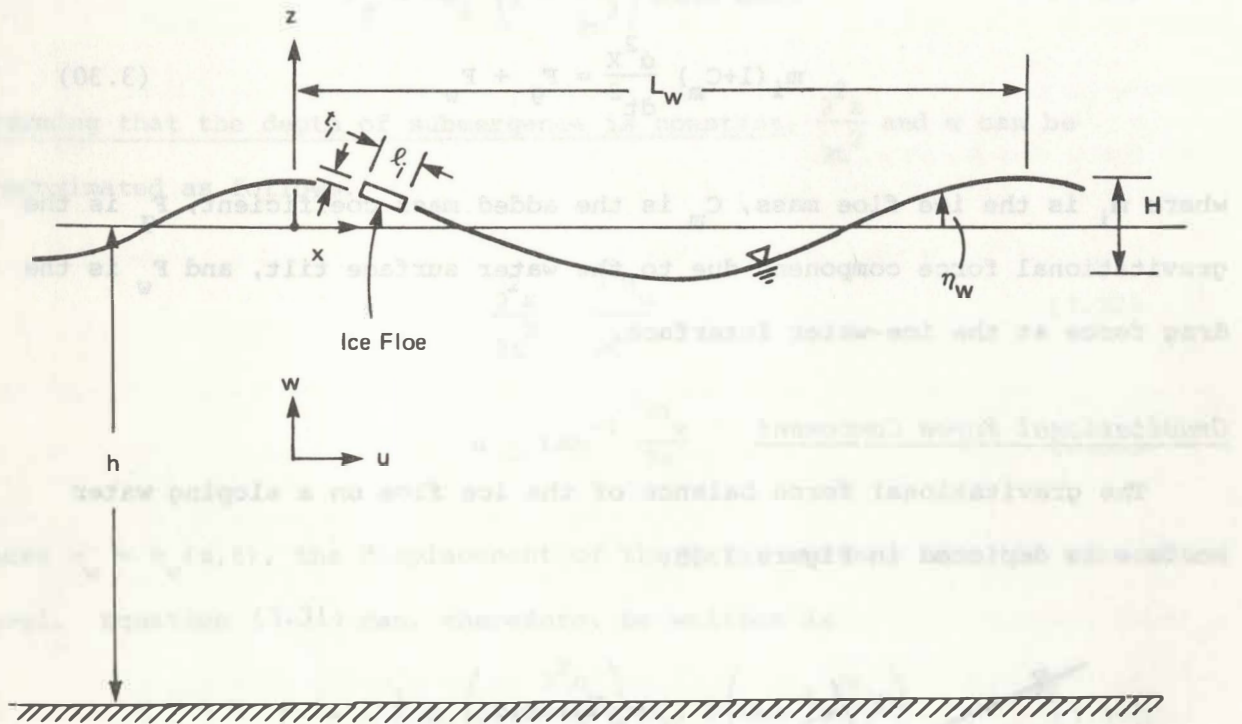
Figure 3.37 Schematic Sketch of Ice Floe in a Long Wave

In Figure 3.37, H is the wave height, h is the water depth, L_w is the wave length, η_w is the surface displacement from the mean water level, α is the water surface slope, ℓ_i is the ice floe length and t_i is the ice thickness.

113

Neglecting the pressure gradient term, the one-dimensional equation of motion in the x direction for the ice floe in a long wave can be expressed in a general form as:

$$m_i(1+C_m) \frac{d^2x}{dt^2} = F_g + F_w \qquad (3.30)$$

where m_i is the ice floe mass, C_m is the added mass coefficient, F_g is the gravitational force component due to the water surface tilt, and F_w is the drag force at the ice-water interface.

Gravitational Force Component

The gravitational force balance of the ice floe on a sloping water surface is depicted in Figure 3.38.
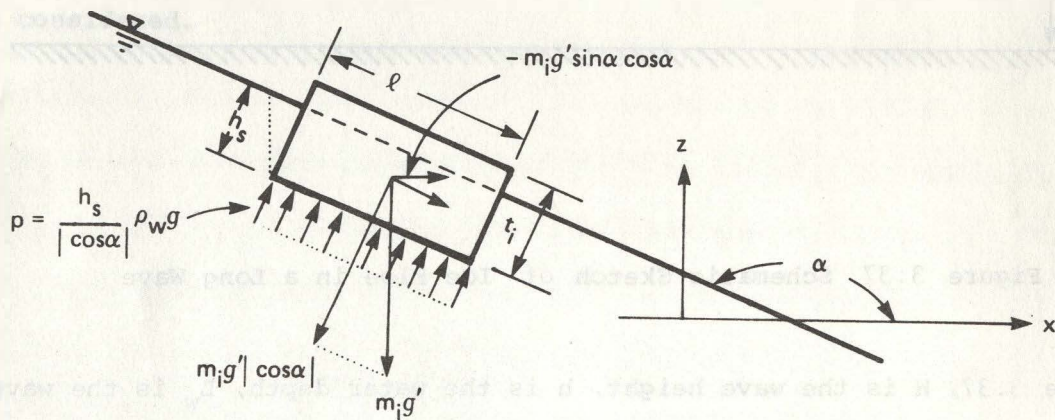
Figure 3.38 Ice Floe Force Balance on a Sloping Water Surface

In Figure 3.38, g' is the vertical acceleration consisting of the gravitational acceleration, g, and the vertical acceleration of ice floe

itself, $\frac{\partial^2 z}{\partial t^2}$. Thus, the gravitational force component in the x direction can be written as

$$F_g = -m_i \left(g + \frac{\partial^2 z}{\partial t^2} \right) \sin\alpha \cos\alpha \qquad (3.31)$$

Assuming that the depth of submergence is constant, $\frac{\partial^2 z}{\partial t^2}$ and α can be approximated as follows.

$$\frac{\partial^2 z}{\partial t^2} \simeq \frac{\partial^2 \eta_w}{\partial t^2} \qquad (3.32)$$

$$\alpha \simeq \tan^{-1} \frac{\partial \eta_w}{\partial x} \qquad (3.33)$$

where $\eta_w = \eta_w(x,t)$, the displacement of the water surface from the mean water level. Equation (3.31) can, therefore, be written as

$$F_g = -\frac{1}{2} m_i \left(g + \frac{\partial^2 \eta_w}{\partial t^2} \right) \sin 2 \left(\tan^{-1} \frac{\partial \eta_w}{\partial x} \right) \qquad (3.34)$$

The evaluation of Equation (3.34), however, requires knowledge of the surface profile, $\eta_w(x,t)$ and will be discussed in a later subsection.

Drag Force Component

The drag force, F_{w_k}, exerted at the ice-water interface is given in a general form by:

$$F_{w_k} = \rho_w \overline{C}_w A \left| V_{w_k} - V_{i_k} \right| (V_{w_k} - V_{i_k}) \qquad (3.35)$$

where ρ_w is the water density assumed to be constant at $10^3 Kg/m^3$, $\overline{C}_w$ is the integrated average drag coefficient, A ,is the surface area of the ice floe at the ice-water interface, and $(V_{w_k} - V_{i_k})$ is the velocity

115

of the ice relative to the water. Since the depth of submergence is small

compared to water depth, V_{w_k} can be approximated by the water particle

velocity at the surface, $V_{w_{sk}}$, rather than the vertically integrated

average water velocity over the ice draft. In the x direction, the

drag force can be expressed as

$$F_{D_x} = \rho_w \overline{C}_w A \left| V_{w_{sx}} - V_i \right| (V_{w_{sx}} - V_i). \qquad (3.36)$$

Expressions for $\eta_w(x,t)$ and $V_{w_{sx}}(x,t)$

As discussed earlier, evaluation of the equation of motion [Equation

(3.30)] requires functional representation of the water surface displacement,

$\eta_w(x,t)$ and the horizontal surface water particle velocity component,

$V_{w_{sx}}(x,t)$ due to wave motion. All of the existing water wave theories

are approximate solutions to the basic Laplace equation [Equations (3.36)

and (3.37)] with a variety of simplified boundary conditions.

$$\nabla^2 \phi_w = 0 \qquad (3.36)$$

or

$$\nabla^2 \psi_w = 0 \qquad (3.37)$$

where ϕ_w is the velocity potential and ψ_w is the stream function. The

simplest of all is the "small amplitude theory" based on the assumption

that motions are sufficiently small to allow the free surface boundary

conditions to be linearized; terms involving the wave amplitude to the

second and higher orders are considered negligible. Although this

approach is simple, when the wave amplitude is large, the small amplitude

116

considerations are not valid and it is necessary to retain higher order

terms to obtain an accurate representation of the wave motion. In many

cases, actual heights are within the nonlinear range requiring that the

representation of wave motion be based on a more accurate finite amplitude

theory. Moreover, due to the linearized free surface boundary condition,

the water particle velocity above the mean water level cannot be defined

by the small amplitude theory. Among the existing higher order

theories, Stokes second order theory is adopted for the present study

for its relative simplicity, although it is possible to extend the Stokes

theory to any order accuracy (Ippen, 1966).

The wave profile $\eta_w(x,t)$, correct to the second order approximation

is given by

$$\eta_w(x,t) = \frac{H}{2} \cos(kx-\sigma t) + \frac{\pi}{8} \frac{H^2}{L_w} \frac{\cosh kh(2+\cosh 2kh)}{(\sinh kh)^3} \cos 2(kx-\sigma t) \qquad (3.38)$$

where H = wave height

   k = wave number = $2\pi/L_w$

   σ = wave angular frequency = $2\pi/T$

   L_w = wave length

   T = wave period

   h = mean water depth

and the water particle velocity in the x direction, V_{w_x} for the second

order theory is given by

$$V_{w_x}(x,t) = \frac{\pi H}{L_w} C \frac{\cosh k(h+z)}{\sinh kh} \cos(kx-\sigma t)$$

$$+ \frac{3}{4} (\frac{\pi H}{L_w})^2 C \frac{\cosh 2k(h+z)}{(\sinh kh)^4} \cos 2(kx-\sigma t) \qquad (3.39)$$

where C is the wave celerity to a second order approximation given by

$$C^2 = \frac{g}{k} \tanh kh \qquad (3.40)$$

Thus, the vertical acceleration of the ice floe [$\frac{\partial^2 z}{\partial t^2}$ in Equation (3.31)]

can be approximated as

$$\frac{\partial^2 z}{\partial t^2} \simeq \frac{\partial^2 \eta_w}{\partial t^2} = -\frac{H}{2} \sigma^2 \cos(kx-\sigma t) - \frac{\pi}{2} \frac{H^2}{L_w} \sigma^2 \frac{\cosh kh(2+\cosh 2kh)}{\sinh^3 kh} \cos 2(kx-\sigma t)$$

$$(3.41)$$

The surface slope, α, is

$$\alpha = \tan^{-1} \frac{\partial \eta_w}{\partial x} = \tan^{-1} [-\frac{H}{2} k \sin(kx-\sigma t) - \frac{\pi}{8} \frac{H^2}{L_w} 2k \frac{\cosh kh(2+\cosh 2kh)}{\sinh^3 kh} \sin 2(kx-\sigma t)]$$

$$(3.42)$$

Equation (3.30) can now be solved for x or u with the proper initial

conditions (i.e., x and u at time t=0), an estimate of the added mass

coefficient, C_m, and the integrated average drag coefficients, $\overline{C}_w$.

Numerical Solution to the Equation of Motion

The equation of motion for a single ice floe in a long progressive

wave [Equation (3.30)] was evaluated numerically using a fourth order

Kutta-Simpson method. The length scale and the time scale were

nondimensionalized with reference to wave length and wave period.

Figure 3.39 is a sample solution for the ice floe trajectory for an ice floe aspect ratio, $\ell_i/t_i = 15$, ice mass, $m_i = 3.7$ Kg, $\frac{H}{L} = 0.02$, and $\frac{h}{L} = 0.18$ with initial conditions of $x_i(t=0)=0$ (at wave crest) and u (t=0)=0. The corresponding drag and added mass coefficients were determined from the experimental analysis in a previous section. (See Figures 3.26 and 3.22). As seen in Figure 3.39, the ice floe motion reaches a quasi-steady state after an initial transient response. For the range of parameters examined, it was found that only the transient portion of the trajectory is affected by the aspect ratio (thus the drag and added mass coefficients), ice mass, and initial condition. If the ice is initially introduced at the wave trough the transient motion shifts to the positive x direction. The decrease in ice aspect ratio and ice mass results in shorter transient response. The quasi-steady portion of the trajectory, which is the primary concern here, is affected only by the parameters $\frac{H}{L}$ and $\frac{h}{L}$. The effects of these parameters on the horizontal ice transport are shown in Figures 3.40 and 3.41. In the figures, all the cases were examined with constant ice mass and aspect ratio: 3.7 Kg and 15, respectively. The initial conditions of $x_i(t=0)=0$ and u (t=0)=0 were applied for all the cases. Disregarding the transient responses, it is seen that the transport velocity is quasi-linear for all cases. The nonlinear dependence of transport velocity on $\frac{H}{L}$ and $\frac{h}{L}$ is quite reasonable from the expression for the surface water particle velocity [Equation (3.39)].

$$m_i \quad = \quad 3.7 \text{ Kg}$$
$$\ell_i/t_i \quad = \quad 15$$
$$H/L_w \quad = \quad 0.02$$
$$h/L_w \quad = \quad 0.18$$

Initial Position, $\vec{v}_i(t=0)=0$

Z/H

0.50

0.00

-0.50

-0.05   -0.03   0.00   0.03   0.05   0.08   0.10

DIMENSIØNLESS DISTANCE X'=X/L$_w$
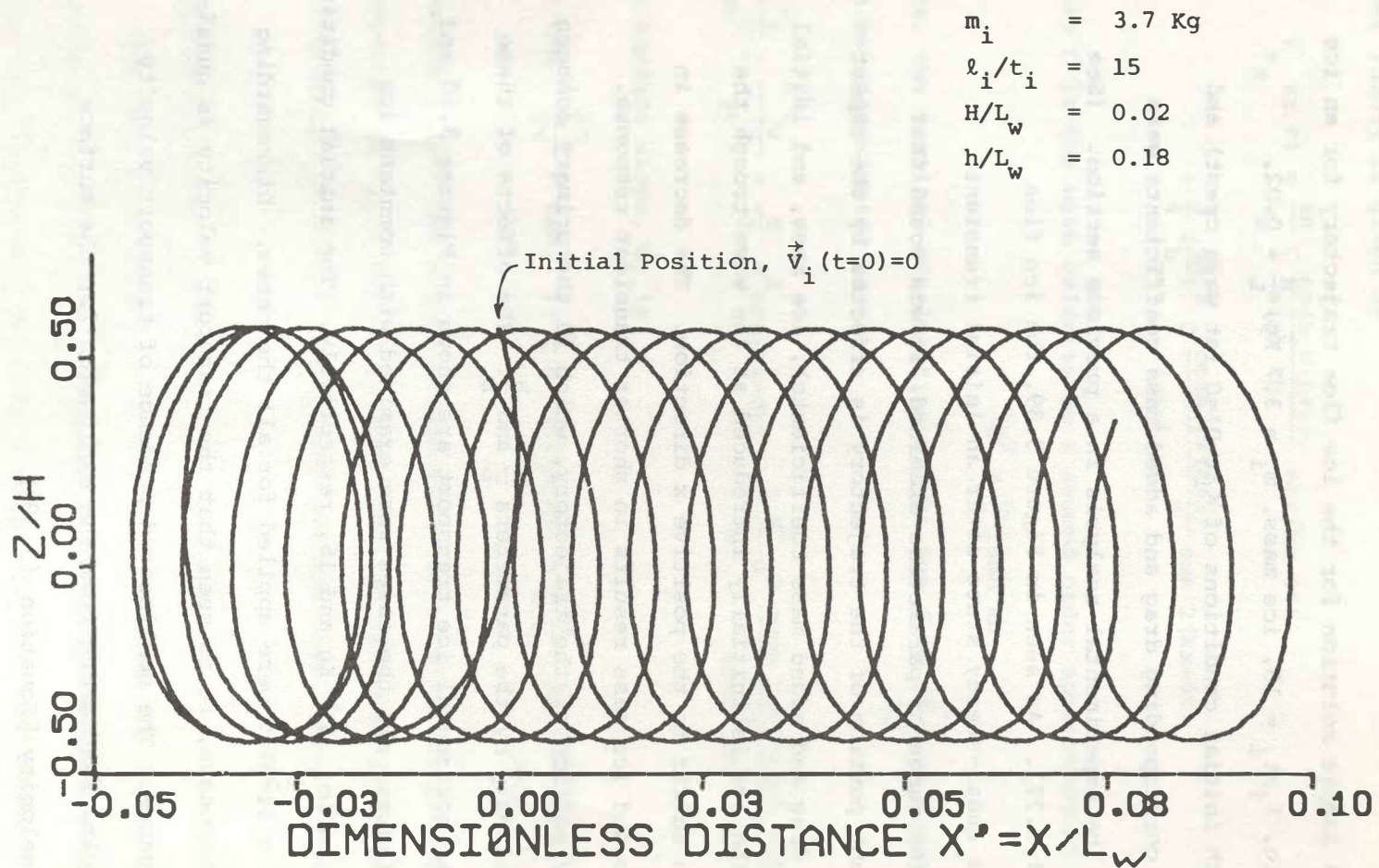
Figure 3.39   Ice Floe Trajectory in a Long Progressive Wave
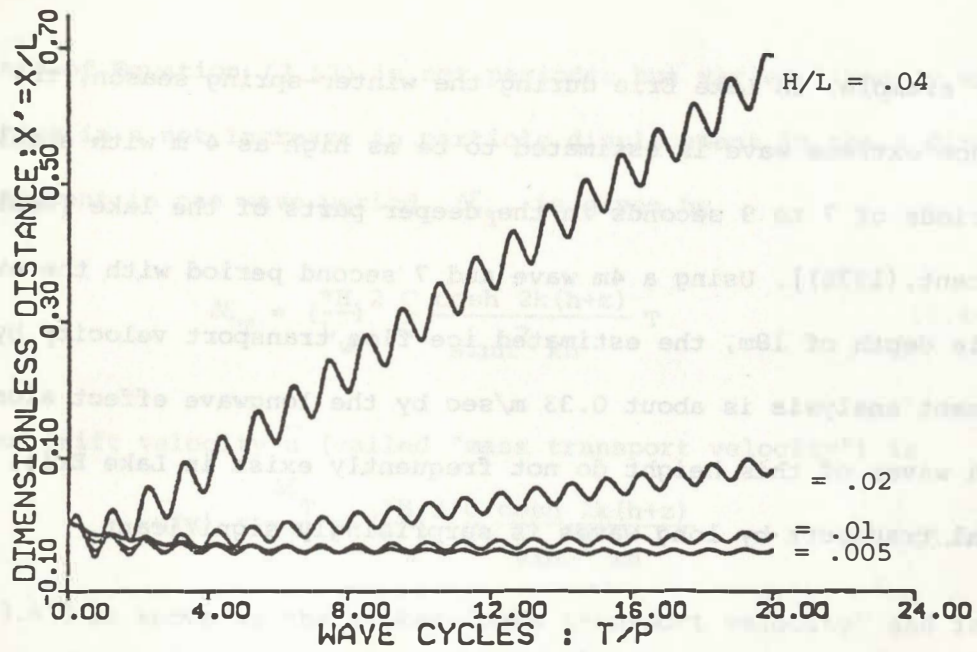
Figure 3.40   Dependence of Ice Floe Velocity on Wave Steepness
(h/L_w = .12, m_i = 3.7 kg, ℓ_i/t_i = 15)
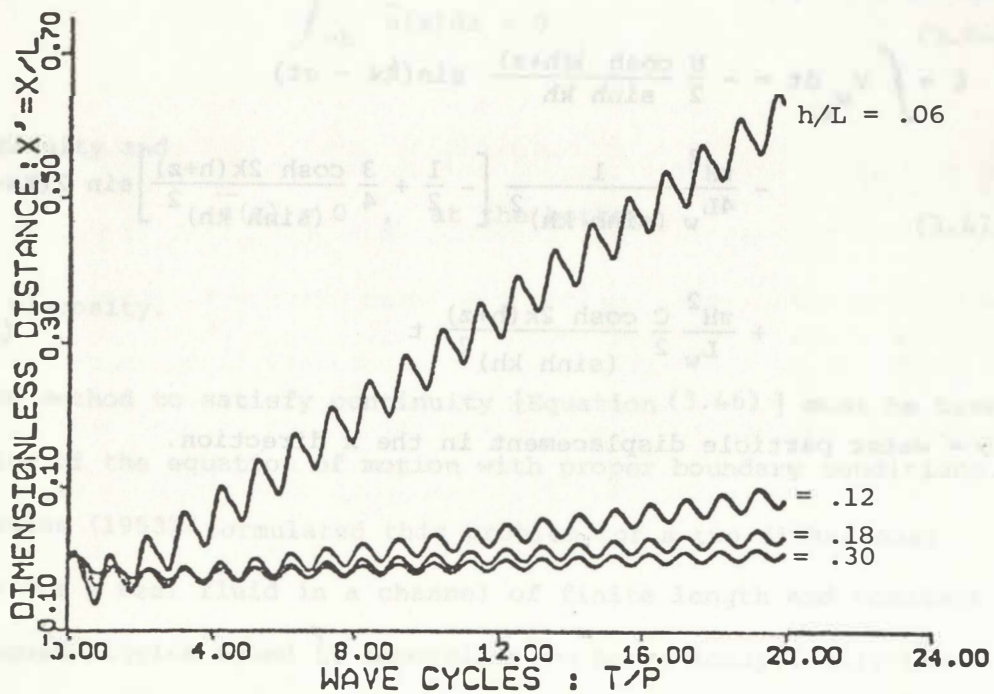
Figure 3.41   Dependence of Ice Floe Velocity on Water Depth.
(H = 2m; L_w = 73.6m, 100m, 116.8m, 137.3m; m_i = 3.7 kg;
ℓ_i/t_i = 15)

For example, in Lake Erie during the winter-spring season, the 5-year recurrence extreme wave is estimated to be as high as 4 m with significant wave periods of 7 to 9 seconds in the deeper parts of the lake [Resio and Vincent, (1976)]. Using a 4m wave and 7 second period with the average Lake Erie depth of 18m, the estimated ice floe transport velocity by the present analysis is about 0.33 m/sec by the longwave effect alone. Although waves of this height do not frequently exist in Lake Erie, the potential transport by long waves is surprisingly significant.

Mass Transport Velocity Approach

As early as 1847, Stokes predicted the existence of a net drift current in the direction of wave propagation. The second order equation for the water particle trajectory in the x direction beneath a finite amplitude wave is given by

$$\xi = \int V_{w_x} dt = -\frac{H}{2}\frac{\cosh\ k(h+z)}{\sinh\ kh}\ \sin(kx - \sigma t)$$

$$-\frac{\pi H^2}{4L_w}\frac{1}{(\sinh\ kh)^2}\left[-\frac{1}{2} + \frac{3}{4}\frac{\cosh\ 2k(h+z)}{(\sinh\ kh)^2}\right]\sin\ 2(kx-\sigma t)$$

$$+\frac{\pi H^2}{L_w}\frac{C}{2}\frac{\cosh\ 2k(h+z)}{(\sinh\ kh)^2}\ t \qquad\qquad (3.43)$$

where ξ = water particle displacement in the x direction.

The last term of Equation (3.43) is not periodic but varies linearly with time resulting in a net increase in particle displacement in the x direction. This displacement in one wave period, $\Delta \xi_T$, is given by

$$\Delta \xi_T = (\frac{\pi H}{L_w})^2 \frac{C}{2} \frac{\cosh 2k(h+z)}{\sinh^2 kh} T \qquad (3.44)$$

and the mean drift velocity $\bar{u}$ (called "mass transport velocity") is

$$\bar{u}(z) = \frac{\Delta \xi_T}{T} = (\frac{\pi H}{L_w})^2 \frac{C}{2} \frac{\cosh 2k(h+z)}{\sinh^2 kh} \qquad (3.45)$$

Equation (3.45) is known as the Stokes "mass transport velocity" and is assumed valid for a channel of infinite length and constant depth, neglecting the viscosity effect. In any realistic water wave system the following two conditions must be met which are not satisfied by Equation (3.45).

$$\int_{-h}^{0} \bar{u}(z) dz = 0 \qquad (3.46)$$

due to continuity and

$$\bar{u}(z) = 0 \quad , \quad \text{at the bottom} \qquad (3.47)$$

due to the viscosity.

The solution method to satisfy continuity [Equation (3.46)] must be based on a solution of the equation of motion with proper boundary conditions. Longuet-Higgins (1953) formulated this problem for a two-dimensional wave system for a real fluid in a channel of finite length and constant depth. Longuet-Higgins found it impossible to solve analytically the Navier-Stokes equation retaining both the convective acceleration term and the viscosity terms, thus he obtained a solution known as the conduction

123

solution by omitting the convective acceleration but retaining the viscosity terms. The equation he solved had the form

$$\left[\frac{\partial}{\partial t} - \nu\nabla^2\right]\nabla^2 \psi_w = 0 \tag{3.48}$$

where ν = kinematic viscosity of fluid.

Longuet-Higgins showed that his solution to Equation (3.48) is valid only if

$$\frac{H}{2(\nu T/\pi)^{1/2}} << 1 \tag{3.49}$$

For realistic waves this parameter is almost always much greater than unity. However, the solution is generally assumed to be valid for the interior of the fluid where it is given, in a modified form, by:

$$\bar{u}(z) = \left(\frac{\pi H}{2L_w}\right)^2 \frac{C}{\sinh^2 kh} \left\{2\cosh 2k(h+z) + 3 + kh\left[3\left(\frac{z}{h}\right)^2 + 4\left(\frac{z}{h}\right) + 1\right]\sin 2kh\right.$$

$$\left. + 3\left[\frac{\sinh 2kh}{2kh} + \frac{3}{2}\right]\left[\left(\frac{z}{h}\right)^2 - 1\right]\right\} \tag{3.50}$$

The experimental studies by Russel and Osorio (1959) and by Mei, et al. (1972) have shown that, provided that sufficient time is allowed for the motion to attain equilibrium, the "mass transport velocity" for waves whose amplitude is large compared to the boundary layer thickness is generally significantly different from that given by the Longuet-Higgins' conduction solution. Sleath (1973) has shown that there is no a priori reason why $\frac{H}{2(\nu T/\pi)^{1/2}} << 1$ even for very small waves. Sleath obtained the solution to the vorticity equation retaining the convective acceleration terms, neglecting only terms of the order of $H^2\sigma k_i h/\nu$, where k_i is the damping coefficient for general cases (Hunt, 1952). Using a systematic

iteration for the convergence of a power series form of solution and
retaining the first 400 terms of the series, Sleath found the solution
for the "mass transport velocity":

$$\bar{u}(z) = u_o + \frac{H^2 \sigma k}{8} \frac{\cosh 2k(z+h)}{\sinh^2 kh} \qquad (3.51)$$

where u_o = Eulerian component of velocity in the x-direction

The time averaged Eulerian component of velocity, $\bar{u}_o$, is effectively zero
at the surface (Sleath, 1973). It is of interest here to compare the "mass
transport velocities" at the water surface evaluated by these three
expressions, [Equations (3.45), (3.50) and (3.51)].

Using a wave height of 4m, a wave period of 7 sec, and a water depth of
18 m, the "mass transport velocities" at the water surface evaluated by
these three expressions are given as,

Stokes: $\bar{u}(z)$ = 34 cm/sec

Longuet-Higgins: $\bar{u}(z)$ = 43 cm/sec
(conduction solution)

Sleath: $\bar{u}(z)$ = 34 cm/sec

Both Stokes' and Sleath's expressions give good agreement with the value of
33 cm/sec evaluted from the numerical solution of the equation of ice floe
motion [Equation (3.30)] for the same case.

3.3.2 Experiments

A preliminary experiment was carried out in a concrete wave tank 36.5 m
long and 2.44 m wide. Waves were generated at one end by a recipro-
cating paddle and partially absorbed at the other end by a sand beach.
The profile was measured at about 5 wave lengths away from the generator.

125

Possibly due to the inadequate wave absorbing capacity of the sand beach
and the higher harmonics generated by the wavemaker, the observed wave
profile showed irregular variation with time. The horizontal origin, x = 0
was set at the wave gage. A simulated ice floe of 6.35 cm x 6.35 cm and
2.54 cm thick made of low density polyethylene (sp.gr. 0.92) was introduced
at the origin at time t = 0 and its horizontal movement was recorded with
time. Measurements were made when the wave generator had been running
about one hour. The following wave parameters were used for the experiment.

> Water Depth: 85.0 cm
>
> Wave Height: 6.60 cm
>
> Wave Period: 1.125 sec
>
> Wave Length: 195.9 cm

Figure 3.42 shows the measurements of ice floe distance versus time. The
figure indicates that the experimental results in the vicinity of the origin
(where the wave gage is located) seem to agree very well with both the
numerical evaluation of the equation of motion [Equation (3.30)] and the
mass transport velocity computed according to Stokes and Sleath.
The comparison, as depicted in Figure 3.42, is only valid for the particular
wave parameters used in the experiments. The possible reasons for the in-
creasing downward deviation of the measurements from the analytical predic-
tions with increased distance are thought to be: (a) increasing wave reflec-
tion from the sand beach, (b) effects of higher harmonics, (c) three dimen-
sionally in the wave characteristics, (d) secondary currents in the wave
tank, and (e) cumulative errors in measurements.

126
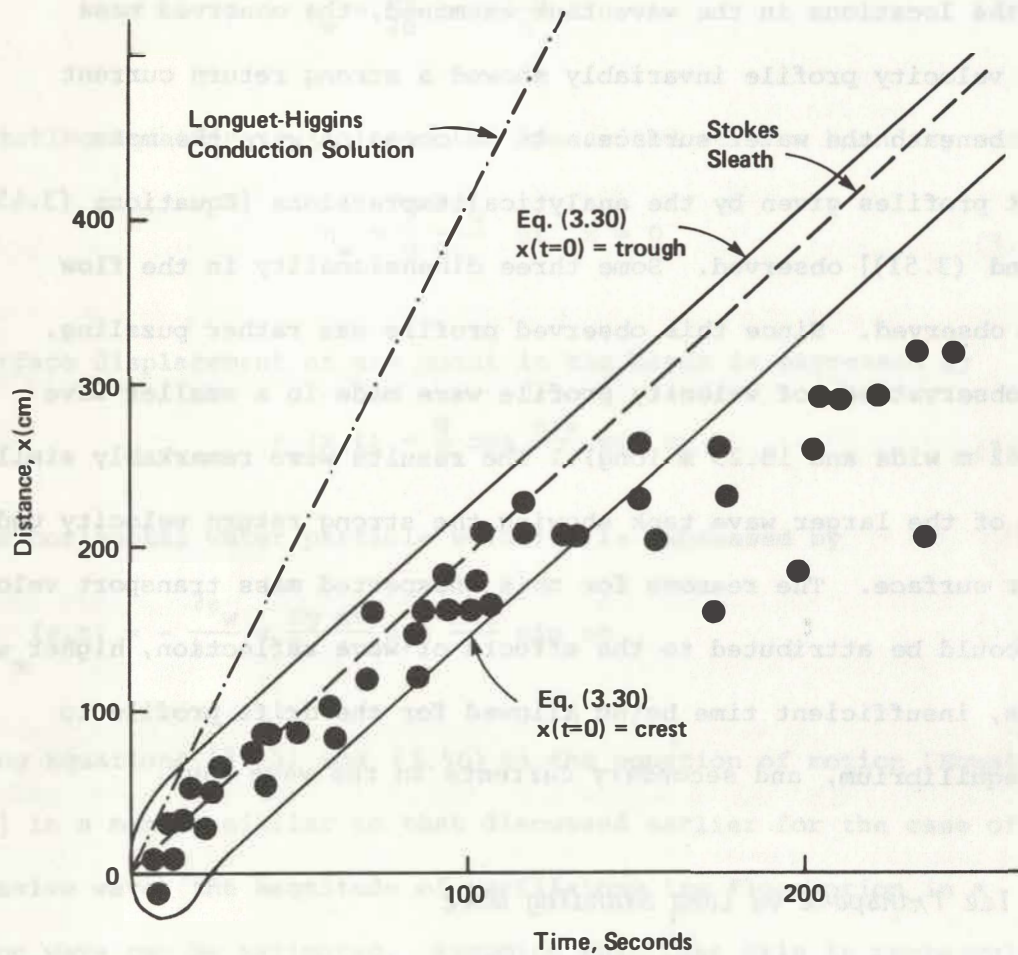
Figure 3.42 Comparison of Experimental Results with Analytical
Predictions for Ice Floe Transport due to a Train
of Progressive Long Waves

During the experiments, the mass transport velocity profile was also examined in the interior of the fluid. Observations were made by dropping dye crystals through the water surface and then following the deformation of the trace through the side wall glass of the wave tank. For all the locations in the wave tank examined, the observed mass transfer velocity profile invariably showed a strong return current directly beneath the water surface. On no occasion were the mass transport profiles given by the analytical expressions [Equations (3.45), (3.50) and (3.51)] observed. Some three dimensionality in the flow was also observed. Since this observed profile was rather puzzling, similar observations of velocity profile were made in a smaller wave tank (0.62 m wide and 18.29 m long). The results were remarkably similar to those of the larger wave tank showing the strong return velocity under the water surface. The reasons for this unexpected mass transport velocity profile could be attributed to the effects of wave reflection, higher harmonics, insufficient time being allowed for the drift profile to achieve equilibrium, and secondary currents in the wave tank.

3.3.3 Ice Transport by Long Standing Wave

It may be of interest to estimate the magnitude of oscillatory ice move-ment due to a standing wave in large waterbodies (the seiche). Considering a rectangular closed basin and applying the small amplitude wave theory, the velocity potential for a standing wave in two dimensions is given by

$$\phi_w = \frac{Hg}{2\sigma} \frac{\cosh k(h+z)}{\cosh kh} \cos \frac{n\pi x}{\ell} \sin \sigma t \qquad (3.52)$$

where ℓ = basin length and n = integer (0,1,2,3...).

Using the shallow water wave approximation, Equation (3.52) reduces to

$$\phi_w = \frac{Hg}{2\sigma} \cos \frac{n\pi x}{\ell} \sin \sigma t \qquad (3.53)$$

Substituting Equation (3.53) into the linearized surface boundary condition:

$$\eta_w = \frac{1}{g} \frac{\partial \phi_w}{\partial t} \quad \text{at} \quad z = 0 \qquad (3.54)$$

The surface displacement at any point in the basin is expressed by

$$\eta_w(x,t) = \frac{H}{2} \cos \frac{n\pi x}{\ell} \cos \sigma t \qquad (3.55)$$

and the horizontal water particle velocity is expressed by

$$V_{w_x}(x,t) = -\frac{\partial \phi_w}{\partial x} = \frac{Hg}{2\sigma} \frac{n\pi}{\ell} \sin \frac{n\pi x}{\ell} \sin \sigma t \qquad (3.56)$$

Applying Equations (3.55) and (3.56) to the equation of motion [Equation (3.30)] in a manner similar to that discussed earlier for the case of a progressive wave, the magnitude of oscillatory ice floe motion in a standing wave can be estimated. Assuming that Lake Erie is rectangular, with uninodal (n=1) seiche period of 14.6 hours, basin length of 388 km, the approximate horizontal ice floe displacements were computed as shown in Table 3.12. For an amplitude of 1 m the effect of a seiche on ice floe motion can be considerable. In the western basin of Lake Erie, because of the shallowness and the narrowness; the water velocity due to the seiche motion is expected to be greater than predicted by Equation (3.56).

Table 3.12   Ice Floe Displacement in Idealized Lake Erie Basin Due
to Seiche Motion (Amplitude of 1 m)

Location	Horizontal Ice Floe Displacement
Lake Center (nodal position)	1110 m
Western Basin (5 km from western end)	410 m
Western Basin (1 km from western end)	95 m

The irregular geometry of the basin has not been considered in these sample
calculations. The net ice floe movement is, of course, zero in the standing
wave but in the presence of wind the seiche-induced current may contribute to
the drift and deformation of an ice field.

3.3.4 Summary and Conclusions

The equation of motion for a single floating ice floe in a long pro-
gressive wave has been formulated and evaluated. The equation was also
applied to the standing wave in a simplified form. The preliminary labora-
tory experiments conducted in a wave tank, although not conclusive, give
results in general agreement with the analytical prediction. The findings
are summarized as follows:

(a)   progressive long waves (ice floe length << wave length) can
   contribute significantly to the net transport of ice floes.

(b)   except for the transient response, ice mass and ice floe aspect
   ratio (thus drag and added mass coefficients) do not affect the
   net transport velocity.

(c)   the net ice floe transport velocity evaluated by the equation of
   motion is in close agreement with the "mass transport velocities"
   given by Stokes (1847) or Sleath (1973).

(d)   the results of laboratory experiments seem to agree with the

analytical prediction, but are not conclusive.

The analysis presented here is based on a hypothetical situation where waves are uniform with idealized surface profile. In real waterbodies, waves are always a complex combination of an infinite variety of waves propagating in various directions. The present analysis, therefore, in general is not directly applicable to real situations and should be taken only as rough estimates. It is possible to extend the present analysis to higher order accuracies but the associated complexities would appear to call for a stochastic analysis using random wave characteristics. It is suggested, however, that the integrated average water velocity over the ice draft be used when the ice thickness cannot be assumed small compared to water depth. The use of surface water velocity may result in an overestimate of ice transport in those cases.

3.4   Two Dimensional Transport by Winds and Currents

In large lakes, the two dimensional transport of an isolated ice floe by wind and current will be subject to the effect of the earth's rotation. The simplified form of the general ice transport equation applicable to this situation is:

$$(m_i + m') \frac{d\vec{v}_i}{dt} = \vec{F}_a + \vec{F}_w + \vec{C} \qquad (3.57)$$

In this equation, m' is the added mass (= $C_m m_i$) and $\vec{C}$ represents the Coriolis force which was not included in the one-dimensional analysis of the single ice floe. The other terms are as previously defined. This simplification [equation (3.57)] is useful in considering the trajectory

131

(or path line) and time of travel of an ice floe (or an assemblage of floes) when the internal inter-floe forces can reasonably be neglected. If the transient motion, or ice floe acceleration, can also be neglected, the equation is further simplified to,

$$\vec{F}_a + \vec{F}_w + \vec{C} = 0 \qquad\qquad (3.58)$$

Weeks and Mellor (1978) considered a simplified form of equation (3.57) in their analysis of the feasibility of towing an iceberg from the Antarctic northward towards the equator; however their equation contained an additional force representing the towing force of the tugboats. They included the ice acceleration but neglected the added mass effect.

Neralla et al (1977) analyzed the trajectory of an ice floe using equation (3.58) but neglected water currents. The water stress, $\vec{F}_w$, for this case is dependent only upon the ice velocity, not the relative velocity between ice floe and water current. They computed ice floe velocities for two cases in which the wind stress coefficient and ice thickness were varied. Their results were in general agreement with other early observations and simple theories (Zubov, 1943). They tested the model by comparison with two cases of sea ice drift, both of which were estimated to be water current driven rather than wind driven. The water currents were estimated using Ekman's (1905) expression in which the surface water current moves at 45° to the right of the wind direction. Their analysis of the relative magnitude of $\vec{F}_a$ and $\vec{F}_w$ gave the following criteria: water currents can be neglected when $V_a/V_w \geq 500$, wind stress can be neglected when $V_a/V_w \leq 5$.

Such simplifications can be a useful guide; but in general, the trajectory of an ice floe will be governed by both wind and water currents.

The wind can be inferred from atmospheric pressure gradients or from direct observations; however, the water currents are generally unknown and the use of the Ekman drift approximation neglects the existence of major currents and shoreline and lake bottom effects. Even in large lakes, the wind driven circulation is very much affected by boundary constraints, bottom friction, and the vertical momentum transport rate in the surface waters. The development of three-dimensional hydrodynamic models for large lakes has enabled the approximation of surface drift velocities taking these additional factors into consideration (Gedney and Lick, 1970; Simons, 1976; and Lick, 1976). The computed surface currents obtained from these models generally agree with the Ekman-type drift current over the lake surface interior (away from shorelines), although the deflection angle is usually less than 45°. Significant differences appear in the nearshore areas where the effects of lateral boundaries and shallow depths are most pronounced.

When the ice floe surface area is significantly large, it would be expected that $\vec{V}_w$ would be modified by its presence. Sheng and Lick (1973) have considered this case but the ice cover was considered as stationary. In principle, the hydrodynamic equations and the equation of motion for the ice floe are coupled and require simultaneous solution. In practice, it is useful and informative when considering the transport of a relatively small ice floe to assume the surface drift field, $\vec{V}_w$, to be specified and not influenced by the presence of the floe.

In order to compute the position and velocity of an ice floe, the additional equations $u = \dfrac{dx_i}{dt}$ and $v = \dfrac{dy_i}{dt}$ are utilized in which x_i and y_i are the ice floe position coordinates. The governing equations for this two dimensional analysis of a discrete ice floe are:

133

$$m_i(1 + C_m) \frac{du}{dt} = AC_a\rho_a|V_{a_x}|V_{a_x} - AC_w\rho_w|u - V_{w_x}|(u - V_{w_x})$$

$$+ m_i fv \qquad (3.59)$$

$$m_i(1 + C_m) \frac{dv}{dt} = AC_a\rho_a|V_{a_y}|V_{a_y} - AC_w\rho_w|v - V_{w_y}|(v - V_{w_y})$$

$$- m_i fu \qquad (3.60)$$

$$u = \frac{dx_i}{dt} \qquad (3.61)$$

$$v = \frac{dy_i}{dt} \qquad (3.62)$$

In order to solve this set of equations, the wind velocity field $\vec{V}_a(x,y,t)$ and the water current field $\vec{V}_w(x,y,t)$ must be known or estimated. The ice floe surface area, A; ice mass, m_i; stress coefficients, C_a and C_w; and the added mass coefficient, C_m, must also be known or estimated. Finally, the initial position and initial velocity of the ice floe must be known.

Solutions of these equations show that, in general, the Coriolis force must be included. Its effect is most pronounced when the wind speed is small or the tracking time is expected to be long. As mentioned previously, the estimation of $\vec{V}_w(x,y,t)$ will frequently be the most difficult and, therefore, the most uncertain quantity in model input.

IV. NUMERICAL ANALYSIS OF MULTI-FLOE ICE DYNAMICS

4.1 Introduction

In Chapter II the equations describing the dynamics of a multi-floe
ice field in response to external forces such as wind and water currents
were formulated in two spatial dimensions. The equations were formulated
on the basis that a representative elemental area could be defined which
permitted the ice field to be viewed as a continuum. The dependent
variables in the equations [Equations (2.24) to (2.27) and an expression
relating the internal ice pressure to the state of the ice cover] are the
ice velocity components, u and v ; the areal ice concentration, N; the
ice mass per unit area, $M_i = \rho_i t_i N$; and the internal ice pressure, p. The
ice mass, M_i, introduces an additional dependent variable, i.e., the ice
thickness, t_i, which is a function of the thermodynamic processes and
mechanical deformation processes.

In this chapter, simplified versions of these governing equations will
be investigated using numerical analysis techniques. In doing this, some
of the essential characteristics of multi-floe ice behavior can be examined
without the rather imposing complexities associated with the general problem.
It must be remembered that such an investigation is based on the continuum
approximation.

At the present stage of model development, the variation of ice thick-
ness (in time and space) will be neglected (without serious loss to model
generality). Now, only the ice area conservation equation is needed [Equation
(2.27)]. In equation (2.27), the thermodynamic and mechanical processes
causing changes in ice area concentration will be neglected (i.e., E_a

and $R_a = 0$). Thus, ice area concentration changes will be due to only convergence and divergence of the ice field. A further simplification can be obtained by neglecting the gravitational force due to water surface tilt; i.e., $\frac{\partial H}{\partial x} = \frac{\partial H}{\partial y} = 0$. This term is frequently much smaller than other terms in the general equations.

Even with these simplifications, the model system can not be readily evaluated because of the coupled nature of the set of governing equations. Therefore, multi-floe ice transport will be examined first as a one-dimensional problem (i.e., $v = 0$). This significantly reduces the remaining complexities of the multi-floe ice transport problem. However, the one-dimensional model provides a convenient tool for evaluating the basic model behavior. Despite the loss of the Coriolis term and the tangential internal ice stress, σ_{xy}; the model retains the essential features of multi-floe ice dynamics (i.e., variable ice area concentration and internal stress due to floe interaction). Both of these features, not present in the single floe model, will affect the response of the simulated ice pack behavior to wind and water stress.

This chapter deals mainly with the results of the model behavior analysis in one dimension. A special case of the general two-dimensional problem is presented as a preliminary feasibility study for future modeling efforts applied to large lakes.

4.2 General Consideration for Numerical Methods

4.2.1 Selection of Numerical Method

As with most fluid flow equations, the present ice transport model equations [Equations (2.24), (2.25), (2.26), and (2.27)] are non-linear and their solution must rely on numerical methods. A practical method

of numerical integration is either the explicit or the implicit finite difference procedure of which a variety of techniques exist (Roache, 1972A). For the standard forward time-centered space (FTCS) finite difference scheme, both the explicit and the implicit methods retain the same accuracies of first order in time and second order in space.

The fully explicit method, in which the forward time solutions depend on solutions at a present time level, permits solutions to each variable in a time-staggered manner allowing each equation of the coupled system to be treated individually. This is particularly advantageous for a multi-dimensional system of complex equations, such as the present two-dimensional ice transport equations, since the tedious computations for matrix coefficients can be eliminated. However, the conditions for numerical stability imposed on the explicit finite difference analog of hyperbolic equations restricts the time step to a small value, sometimes to an impractical extent.

The fully implicit method, in which the forward time solution is determined by solutions at an advanced time level, requires simultaneous solutions of equations at the advanced time level. Although this requirement imposes a penalty on programming complexities, the fully implicit method is unconditionally stable (dynamically) and permits an arbitrarily large time step. Despite this great advantage, the fully implicit method does not find frequent use in multi-dimensional non-linear problems since there is usually no reduction in computation time over simply using the explicit method many times.

Thus, the explicit method appears to be the first choice for the two-dimensional multi-floe ice transport case. For the one-dimensional case, however, the advantage of being able to use an arbitrarily large time step permitted by the implicit method may offset the programming complexity.

Therefore, for the one-dimensional simplification of the present model equations, both methods are applied and compared. For the two-dimensional case, only the explicit scheme has been used.

4.2.2 *Computational Stability of Numerical Methods*

The mathematical foundation for the analysis of convergence and stability of numerical schemes used in the solution of linear systems can be used as guidelines for dealing with non-linear problems with justification depending on practical applications. While a convergent finite difference scheme is defined as one in which all values of the solution approach the continuum solution as the discretization steps approach zero; stability is rather vaguely defined as a necessary and sufficient condition for convergence for a linear system of equations (Lax and Richtmyer, 1956), or in terms of the growth or decay of truncation errors (Eddy, 1949; O'Brien et al, 1950). Experience (Lilly, 1965; Thommen, 1966; Philips, 1959, etc.) has shown that, for non-linear systems, neither the linearized analysis nor the stability conditions are satisfactory and that linear and constant coefficient analysis may fail to predict instabilities. Also, none of the existing analyses account for the effect of boundary conditions. The destabilizing effect of boundary conditions is very often of practical importance (Roache, 1972A).

Therefore, analysis and definition of numerical stability for the present model equations should not be treated as an end in themselves, but rather as guidelines and as rational support for the numerical experiments. The following is a brief summary of stability conditions based on a linear constant-coefficient model equation. Details of the mathematical treatment can be found for example in Richtmyer and Morton (1967).

A linear one-dimensional analog for the present equation of motion [Equations (2.24) and (2.25)] can be written as,

$$\frac{\partial u}{\partial t} = - \hat{u} \frac{\partial u}{\partial x} + \alpha \frac{\partial^2 u}{\partial x^2} \qquad (4.1)$$

where u represents the ice velocity, $\hat{u}$ corresponds to the linearized advection velocity (a representative constant ice velocity) and α corresponds to the ice momentum transfer coefficient (the ice viscosity). Despite the absence of the other terms contained in the general equations, analysis of this simplified equation can be expected to provide inferences about the stability of the real system.

Applying the standard FTCS scheme in the explicit form at the ith node, the analogous finite difference equation (FDE) for Equation (4.1) is,

$$\frac{u_i^+ - u_i^n}{\Delta t} = - \hat{u} \frac{u_+^n - u_-^n}{2\Delta x} + \alpha \frac{u_+^n - 2u_i^n + u_-^n}{(\Delta x)^2} \qquad (4.2)$$

where Δt is the computational time step, Δx is the node spacing, the subscript represents the spatial index with (+), (i), (−) indicating node locations $i + 1$, i, $i - 1$ respectively; and the superscript is the temporal index with (+) and (n) indicating (n + 1) and n time level. A discrete perturbation analysis [Thoman and Szewczyk (1966)] gives the following necessary stability conditions for this model equation [Equation (4.2)] as:

$$\Delta t \le \frac{1}{2} \frac{\Delta x^2}{\alpha} \qquad (4.3)$$

$$\frac{\hat{u}\Delta t}{\Delta x} = c \le 1 \qquad (4.4)$$

$$\Delta t \le \frac{2}{\dfrac{2\alpha}{\Delta x^2} + \dfrac{\hat{u}}{\Delta x}} \qquad (4.5)$$

139

where c is called the Courant number.

Utilizing equations (4.3) to (4.5) [Thoman and Szewczyk (1966)] an additional requirement for zero overshoot (i.e., static stability) is,

$$\frac{\hat{u}\Delta x}{\alpha} = R_c \leq 2 \tag{4.6}$$

where R_c is called the "cell Reynolds number", based on the ice velocity and a characteristic length equal to the node spacing.

The von Neuman analysis gives identical stability conditions with additional information on dispersion errors (Roache,1972B). Hirt's method (Hirt, 1968) also leads to the Courant condition (i.e., $c \leq 1$ which includes $\Delta t \leq \Delta x^2/2\alpha$) but fails to disclose the cell Reynolds number limitation [Equation (4.6)]. The conditions that $\Delta t \leq \frac{\Delta x^2}{2\alpha}$ and $R_c \leq 2$ (which includes $c \leq 1$) are necessary and sufficient conditions only for the linear (constant u) one-dimensional finite-difference equation expressed in the explicit form for an infinite domain. The effects of varying $\hat{u}$ and the enforcement of particular boundary conditions cannot be ascertained by these analyses.

For the linear, constant-coefficient, two-dimensional problem, the von Neuman analysis can be extended to give the following conditions (when a square grid ($\Delta x = \Delta y$) is used in the discretization):

$$\Delta t \leq \frac{\Delta x^2}{4\alpha} \tag{4.7}$$

$$c \leq \frac{1}{2} \tag{4.8a}$$

140

and

$$\overline{R}_c \leq 4 \qquad (4.8b)$$

where $c = c_x = c_y$, $\overline{R}_c = (|\hat{u}| + |\hat{v}|) \, \Delta x/\alpha$. Thus, it is seen that for the two-dimensional case, the conditions for dynamic stability [Equations (4.7) and (4.8)] are more restrictive than the corresponding one-dimensional conditions, while the cell Reynolds number limitation (see above) is less restrictive.

The stability criteria for the fully implicit scheme are much less restrictive, although the error is still of order $O(\Delta t, \Delta x^2)$. The von Neuman analysis for the implicit scheme indicates (e.g. Richtmyer and Morton, 1969) that dynamic stability is satisfied regardless of the Courant number, thus permitting an arbitrarily large time step. However, the cell Reynolds number limitation is still imposed for static stability.

Thus, for the present equations of motion [Equation (2.24) and (2.25)], the following stability guidelines are obtained.

For the one-dimensional explicit formulation,

$$\Delta t < \frac{\Delta x}{\hat{u}} \qquad (4.9)$$

$$\Delta t < \frac{1}{2} \frac{\Delta x^2}{k_3} \rho i \qquad (4.10)$$

$$\Delta t < \frac{2}{\frac{2k_3}{\rho_i \Delta x^2} + \frac{\hat{u}}{\Delta x}} \qquad (4.11)$$

and

$$k_3 > \frac{\hat{u} \, \Delta x}{2} \rho_i \qquad (4.12)$$

141

where $k_3 = k_2 + k_1$ as discussed in Chapter 2. For the physical situations considered in the present study, $\hat{u}$ is typically $O(10^{-1}$ m/sec) and k_3 is thought to range from 10^3 to 10^{10} Ns/m^2. For the range of $\Delta x = 500$ m to 5 km, Equations (4.9) and (4.12) do not impose severe restrictions on Δt. Since $u/\Delta x$ is a negligible quantity in the present case, Equation (4.10) is the controlling condition. Thus, for example, when $k_3 = 10^5$ Ns/m^2 and $\Delta x = 500$ m, Equation (4.10) gives, $\Delta t < 1150$ sec.

For the implicit one-dimensional case, all the dynamic stability conditions are removed. The only restriction is Equation (4.12) which is not al all serious. For the two-dimensional explicit formulation, assuming the shear term and the Coriolis term do not have an effect, the dynamic stability guideline suggested by Equation (4.7) is

$$\Delt t < \frac{\Delta x^2}{4 k_1} \rho_i \tag{4.13}$$

where k_1 is the ice shear viscosity as discussed in Chapter 2. Thus, for example, when $\Delta x = 500$ m and $k_1 = 10^5$ Ns/m^2,

$$\Delta t < 575 \text{ sec} \tag{4.14}$$

which may be impractical. Therefore, if the explicit method is to be used, the selection of Δx, Δt and k_1 are extremely limited. From this point of view, a better approach may be to use an explicit method for the convective term and an implicit method for the viscous term.

The ice area conservation equation [Equation (2.26)] can be represented by the following one-dimensional linear equation:

$$\frac{\partial N}{\partial t} = - \hat{u} \frac{\partial N}{\partial x} \qquad (4.15)$$

which can be considered a special case of Equation (4.1) with $\alpha = 0$. From the previous discussion, it is seen that the FTCS finite difference representation of pure convection [Equation (4.15)] is unstable for all Δt. This instability can be removed by introducing a damping factor. One approach is to insert an artificial diffusion term,

$$\frac{\partial N}{\partial t} = - \hat{u} \frac{\partial N}{\partial x} + \alpha_a \frac{\partial^2 N}{\partial x^2} \qquad (4.16)$$

where α_a represents an artificial diffusion coefficient or damping coefficient. Another approach is the use of the "upwind differencing" (e.g. Lilly, 1965). The upwind differencing for the convective term involves the use of one-sided, rather than space-centered differencing. Backward difference for positive $\hat{u}$ and forward difference for negative $\hat{u}$ are used as,

$$\frac{\xi_i^+ - \xi_i^n}{\Delta t} = - \hat{u} \frac{\xi_i^n - \xi_-^n}{\Delta x} \qquad \text{for } \hat{u} > 0$$

$$= - \hat{u} \frac{\xi_+^n - \xi_i^n}{\Delta x} \qquad \text{for } \hat{u} < 0 \qquad (4.17)$$

where ξ is any convected quantity. Thus, the one-sided difference is always "upwind" of the node at which $\dfrac{\xi_i^+ - \xi_i^n}{\Delta t}$ is evaluated. The stabilizing effect of this difference method has been used under various names ("upstream", "weather", "skewed" differencing etc.). However, a Taylor series expansion

143

shows (Roache, 1972A) that Equation (4.17) is equivalent to

$$\frac{\partial \xi}{\partial t} = -\hat{u}\frac{\partial \xi}{\partial x} + \alpha_e \frac{\partial^2 \xi}{\partial x^2}$$ (4.18)

with the order of error of $O(\Delta t, \Delta x)$. In equation (4.18), α_e denotes an artificial (or numerical) diffusion of the upwind differencing method (Noh and Protter, 1963). The magnitude of α_e indicated by a Taylor series expansion is,

$$\alpha_e = \frac{1}{2}\hat{u}\Delta x(1 - c)$$ (4.19)

where c is the Courant number. Similarly for the two-dimensional case, a Taylor series expansion gives,

$$\alpha_{e_x} = \frac{1}{2}\hat{u}\Delta x(1 - c)$$ (4.20)

$$\alpha_{e_y} = \frac{1}{2}\hat{v}\Delta y(1 - c)$$ (4.21)

The use of non-physical or artificial damping is not unique to the upwind differencing. For example, the fully implicit FTCS formulation for the transient convective-dispersion equation has an artificial diffusion of $\alpha_e = u^2\Delta t/2$. A detailed discussion of artificial diffusion can be found in Roache (1972B).

Since both methods, the explicit artificial damping [Equation (4.16)] and the upwind differencing [Equation (4.17)], necessarily introduce non-physical diffusion terms to stabilize the solution, they are equivalent in terms of diffusion errors. For programming convenience, the method of explicit

144

artificial damping [Equation (4.16)] is used in the present study. The magnitude of α_a is kept very small, only large enough to satisfy the cell Reynolds number limitation [Equation (4.5)].

Thus, for the equation of ice area conservation [Equation (2.26)] the following stability guidelines are obtained.

For the explicit scheme,

$$\Delta t < \frac{\Delta x}{\hat{u}} \tag{4.22}$$

$$\Delta t < \frac{1}{2} \frac{\Delta x^2}{\alpha_a} \tag{4.23}$$

$$\Delta t < \frac{2}{(\frac{2\alpha_a}{\Delta x^2}) + \frac{\hat{u}}{\Delta x}} \tag{4.24}$$

and

$$\alpha_a > \frac{\hat{u}\,\Delta x}{2} \tag{4.25}$$

Since all of the above dynamic stability guidelines are less restrictive than for the equation of motion, the ice area conservation equation does not impose any additional limitation on the selection of the time step. Also, since $\hat{u}$ is typically 10^{-1} m/sec, and Δx is $0(10^2)$ to $0(10^3)$ m, the suggested magnitude of α_a is $0(10^1)$ to $0(10^2)$ m^2/sec, which is expected to have only minor effects on numerical results.

In summary, since the primary concern here is obtaining computational solutions, rather than the analysis of numerical methods, the need for numerical experimentation is unavoidable. All of the above linear analyses provide only guidelines.

4.3 Boundary Conditions

For relatively simple physical phenomena which can be described in terms of scalar or vector equations, the determination of the appropriate boundary conditions does not usually require elaborate mathematical analysis. In many cases, boundary conditions are physically evident and often deduced by intuition. However, when a system of equations involves second or higher order tensors, such as the present system of model equations, the set of necessary and sufficient boundary conditions may not be so obvious.

One of the methods for deducing boundary conditions for such a system of equations is the use of variational analysis. The concepts of virtual work and virtual displacement used in solid mechanics can be analogously applied to the present ice transport problem.

Considering a hypothetical infinitesimal variation in the ice velocity field, δU_k, in two spatial dimensions, the force balance can be expressed using the divergence theorem and Cauchy's formula (Dym and Shames, 1973) for a constant ice thickness, $\bar{t}_i$, as;

$$\bar{t}_i \iint_A \beta_k \, \delta U_k \, dA + \bar{t}_i \int_S T_k^{(\nu)} \, \delta U_k \, dS = \bar{t}_i \iint_A \sigma_{k\ell} \, \delta \dot{\varepsilon}_{k\ell} \, dA \qquad (4.26)$$

where subscripts are the standard tensor index notations, $\sigma_{k\ell}$ is the stress field, and $\delta\dot{\varepsilon}_{k\ell}$ is the variation in the strain rate field, corresponding to the variation in the velocity field, δU_k. β_k represents the sum of body forces: i.e., $\beta_k = F_{a_k} + F_{w_k} + C_k + G_k - M_i \frac{dVi_k}{dt}$ [see Equation (2.4)]. Since the present system does not include the vertical dimension, the wind stress, τ_a, and the water stress, τ_w, are treated as body forces. $T_k^{(\nu)}$ denotes the sum of all forces acting on the two-dimensional boundary and has the dimensions of force per unit area. The right-hand side of Equation (4.26) can be alternatively expressed using integration by parts as,

146

$$\iint_A \sigma_{k\ell} \, \delta\dot{\varepsilon}_{k\ell} \, dA = \int_S \sigma_{k\ell} \, \nu_\ell \, \delta U_k \, dS - \iint_A \sigma_{k\ell,\ell} \, \delta U_k \, dA \qquad (4.27)$$

where ν_ℓ denotes the direction cosines of the unit normal at the boundary interface where the boundary forces are applied and $\sigma_{k\ell,\ell}$ is the abbreviation of:

$$\sigma_{k\ell,\ell} = \frac{\partial \sigma_{xx}}{\partial x} + \frac{\partial \sigma_{xy}}{\partial y} \qquad \text{for } k = x$$

$$= \frac{\partial \sigma_{yx}}{\partial x} + \frac{\partial \sigma_{yy}}{\partial y} \qquad \text{for } k = y \qquad (4.28)$$

Substituting Equation (4.27) into (4.26) gives,

$$\iint_A (\beta_k + \sigma_{k\ell,\ell}) \, \delta U_k \, dA + \int_S (T_k^{(\nu)} - \sigma_{k\ell} \, \nu_\ell) \, \delta U_k \, ds = 0 \qquad (4.29)$$

The first term in Equation (4.29) must always be zero regardless of δU_k since the quantity $(\beta_k + \sigma_{k\ell,\ell})$ is zero by definition of the equation of motion [see Equation (2.4)]. Therefore, the line integral must be zero at any location along the boundary: i.e.,

$$(T_k^{(\nu)} - \sigma_{k\ell} \, \nu_\ell) \, \delta U_k = 0 \qquad (4.30)$$

which states that along the two-dimensional boundary, either the boundary force or the ice velocity must be specified.

Similarly, considering a hypothetical infinitesimal variation in ice area concentration, δN, the ice area balance can be expressed analogous to Equation (4.29) as,

147

$$\iint_A \left(\frac{\partial N}{\partial t} + \frac{\partial \psi_k}{\partial x_k} \right) \delta N \, dA + \int_S (\Phi_k - \psi_k \nu_k) \, \delta N \, ds = 0 \qquad (4.31)$$

where $\frac{\partial \psi_k}{\partial x_k}$ is the flux divergence within the boundary and Φ, is the ice area flux across the boundary. Since the first term in Equation (4.31) represents the ice conservation [see Equation (2.27)] without thermodynamic or mechanical changes in ice area , it must be zero, regardless of δN. Thus, we obtain the boundary condition for the ice area conservation equation,

$$(\Phi_k - \psi_k \nu_k) \, \delta N = 0 \qquad (4.32)$$

which indicates that at the boundary either the ice area flux or ice area concentration must be specified.

At a portion of the lake boundary from which ice mass flows lakeward with an offshore component of wind velocity (i.e., a no-flux upwind boundary), the external boundary force, $T_k^{(\nu)}$, is zero, and the ice pressure, p, must approach zero. However, the ice velocity, U_k, directed normal to the boundary and lakeward, cannot be zero; thus, from Equation (4.30), the normal velocity gradient must be zero. At the same boundary, there cannot be any ice area flux; therefore, from Equation (4.32), N must be zero. A similar boundary condition has been used by Doronin (1970) for Arctic sea ice.

At a downwind lake boundary without ice area flux, the normal ice velocity component must be zero which also satisfies the no flux condition for ice area conservation. Although the boundary conditions in reduced form do change depending on wind direction, the basic conditions given by Equations (4.30) and (4.32) are always independent of wind condition.

148

The tangential component of ice velocity at solid boundaries can be specified as zero to give the no-slip condition or the boundary force, $T_k^{(\nu)}$ (boundary friction), can be specified to give the slip condition.

At open boundaries (river mouths, embayments, etc.), the ice velocity is not necessarily zero. In the absence of external boundary forces, either the internal ice stress must be zero or the ice area flux must be specified.

All of the above boundary conditions are derivable from the two basic equations [Equations (4.30) and (4.32)] utilizing the variational principle. It is possible that in the application of these boundary conditions to specific ice transport situations, the numerical results to the discretized form of the governing equations may appear to violate intuition and even, perhaps, direct observation in the field. One explanation for this possible occurrence is that the representation of the ice field as a continuum naturally leads to the application of mathematical principles commonly employed in continuum mechanics. This is by way of saying that some sacrifices may have to be made in terms of the accuracy that can be achieved in the simulation of the real world by employing the continuum approximation. It is logical that these sacrifices may be greatest in regions adjacent to lake boundaries and where ice area concentrations are very small.

4.4 One-Dimensional Multi-Floe Analysis

4.4.1 *Simplified Equations*

With the assumptions of constant ice thickness and zero water surface tilt as discussed in Section 4.1, the dimensionless equation of motion [Equation (2.30)] reduces to the following in one spatial dimension.

$$\frac{du'}{dt'} = \frac{L}{t_i} \left[C_1 |V_{a_x}'| (V_{a_x}') - C_2 |u' - V_{w_x}'| (u' - V_{w_x}') \right]$$

$$+ \frac{1}{R_3} \left[\frac{1}{N} \frac{\partial}{\partial x'} \left(N \frac{\partial u'}{\partial x'} \right) \right] - \frac{1}{N} \frac{\partial}{\partial x'} (Np') \tag{4.33}$$

Similarly, the ice area conservation equation [Equation (2.33)] becomes (neglecting the source/sink terms);

$$\frac{dN}{dt'} + N \frac{\partial u'}{\partial x'} = 0. \tag{4.34}$$

In equation (4.33), the Reynolds number, R_3, is defined with a combined shear and bulk viscosity, i.e., $k_3 = k_1 + k_2$; therefore $R_3 = |\vec{V}_a| L \rho_i / k_3$. The other terms are as defined in section 2.3.

The boundary conditions for this one-dimensional equation of motion are given as [see section 4.3]:

at the upwind boundary: $x' = 0$

$$\left. \frac{\partial u'}{\partial x'} \right|_{x'=0} = 0, \text{ without mass flux} \tag{4.38}$$

$$\left. (T_x^{(x)} - \sigma_{xx}) \right|_{x'=0} = 0 \text{ or } \left. u' \right|_{x'=0} = \text{prescribed, with mass flux} \tag{4.39}$$

at the downwind boundary: $x' = 1$

$$\left. u' \right|_{x'=1} = 0, \text{ without mass flux} \tag{4.40}$$

$$\left. (T_x^{(x)} - \sigma_{xx}) \right|_{x'=1} = 0 \text{ or } \left. u' \right|_{x'=1} = \text{prescribed, with mass flux} \tag{4.41}$$

150

Similarly, for the ice area conservation equation (including the artificial damping term), the boundary conditions are,

at $x' = 0$

$$N\Big|_{x'=0} = 0, \text{ without mass flux} \qquad (4.42)$$

$$N\Big|_{x'=0} = \text{prescribed or flux specified, with mass flux} \qquad (4.43)$$

at $x' = 1$

$$\text{flux} = 0, \text{ without flux} \qquad (4.44)$$

$$\text{flux} = \text{prescribed, with flux} \qquad (4.45)$$

With the artificial damping term, $\alpha_a \, \partial^2 N/\partial x'^2$, the expression for mass flux is given by

$$\text{mass flux} = Nu' - \alpha_a \frac{\partial N}{\partial x'} \qquad (4.46)$$

Finally, considering that the ice field is initially at rest with a prescribed ice area concentration, the initial conditions are,

$$u'(x',0) = 0 \qquad (4.47)$$

$$N(x',0) = f(x') \qquad (4.48)$$

The system of equations [Equations (4.35) and (4.36)], with a proper combination of the boundary conditions and the initial conditions, comprises the mathematical representation of the one-dimensional multi-floe ice field transport problem. The physical situation under consideration is shown in Figure (4.1).
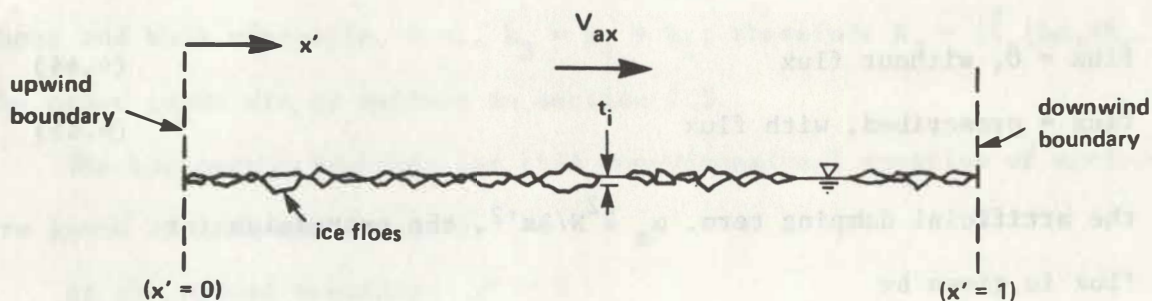

Figure 4.1 Schematic Sketch of one-Dimensional Multi-Floe Ice Field

4.4.2 Results and Discussion of One-Dimensional Analyses

Effect of Ice Pressure

As briefly discussed in Chapter 2, solution of the ice transport equations requires an appropriate mathematical expression for the internal ice pressure, p. For the characteristic dimensions of lake ice problems, the ice pressure term is essential in the model system to balance the externally applied stresses, particularly at downwind boundaries (see Figure 2.9). However, since it has not been possible to express a general equation of state for pack ice deterministically, pressure expressions must be developed on the basis of rational deduction and empiricism. In the present one-dimensional study, the following two types of expressions were examined.

$$p = \frac{1}{t_i} \int_0^x f(N) \, \tau_{ax} \, dx \qquad (4.49)$$

$$p = \frac{1}{t_i} \int_0^x f(N)(\tau_{ax} - \tau_{wx}) \, dx \qquad (4.50)$$

in which τ_{ax} is the wind stress, τ_{wx} is the water stress, and $f(N)$ is an empirical pressure modifier which is a function of areal ice concentration, N. Because of $f(N)$, the pressure is substantially reduced whenever the ice area concentration is less than one. For a static equilibrium at downwind boundaries, Equations (4.49) and (4.50) are identical since τ_{wx} is zero without ice motion or water current. However, as long as an ice field has motion relative to water, τ_{wx} must be present regardless of the specified water current, V_{w_x}. In this respect, Equation (4.50) is favored over

(4.49) since it retains both the static and some of the dynamic aspects of the force balance.

The pressure modifier, f(N), which is entirely empirical, can be changed in the numerical experiments. Initially, the following two types of expressions have been considered:

$$f(N) = e^{C(1-N)} \tag{4.51}$$

$$f(N) = N^k \tag{4.52}$$

both of which are designed to have a maximum value of one when the ice area concentration is one, and both can be made essentially equivalent by proper adjustment of C and k. The form of equation (4.51) was examined with a fixed value of $C = -20$ (Hibler, 1977b).

The sensitivity of the model response to various combinations of the pressure expressions were examined for the case of $\Delta t' = 0.1$ (for implicit scheme), $R_3 = 10^6$, $\Delta x' = 0.025$, $N(x', t' = 0) = 0.5$, $u'(x', t' = 0) = 0.0$, and with the no-flux boundary conditions at both the upwind and downwind boundaries. The results are shown in Figures 4.2 to 4.6. The figures are numbered consecutively in terms of expressions for pressure ranging from those that give lowest pressure (Fig. 4.2) to those that give highest pressure (Fig. 4.6). It is seen in the figures that increasing the ice pressure at lower ice concentrations (i.e. by decreasing k), has a significant smoothing effect on both the ice area concentration and velocity profiles. Since the present model equations are not valid for N exceeding 1.0, the pressure modifier $f(N) = N^{1.25}$ appears to give the most reasonable results in the region of the maximum ice area concentrations. The values

Figure 4.2 One-Dimensional Ice Area Concentration and Ice
Velocity Profiles with Ice Pressure given by

$$p = \frac{1}{t_i} \int_0^x e^{c(1-N)} (\tau_{a_x} - \tau_{w_x}) dx, \quad c = -20.$$

155
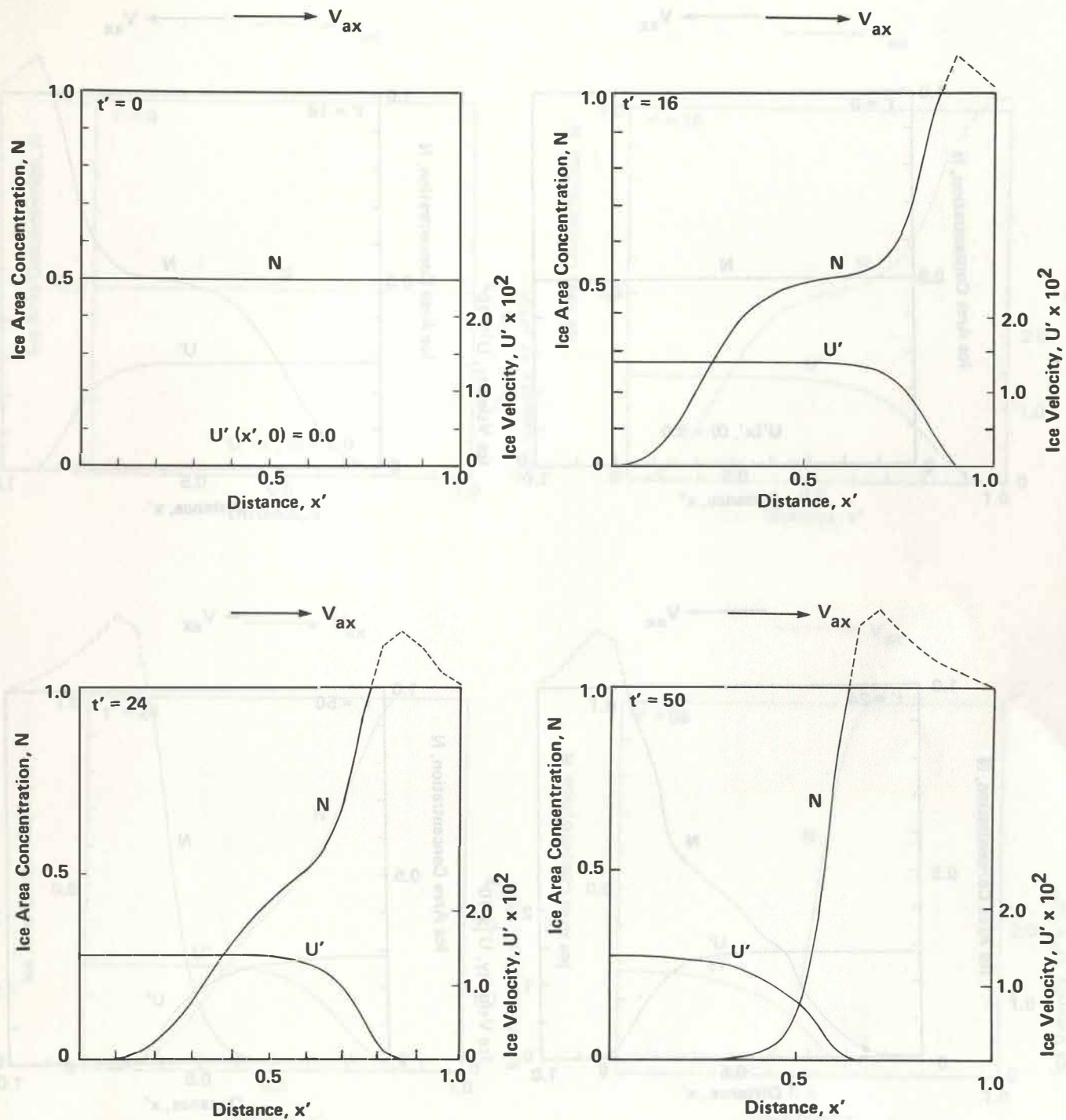
Figure 4.3 One-Dimensional Ice Area Concentration and Ice Velocity Profiles with Ice Pressure given by

$$p = \frac{1}{t_i} \int_0^x e^{c(1-N)} \tau_{a_x} dx, \quad c = -20.$$

156

Figure 4.4   One-Dimensional Ice Area Concentration and Ice
Velocity Profiles with Ice Pressure given by

$$p = \frac{1}{t_i} \int_0^x N^2 (\tau_{a_x} - \tau_{w_x}) dx.$$

157

Figure 4.5   One-Dimensional Ice Area Concentration and Ice
Velocity Profiles with Ice Pressure given by

$$p = \frac{1}{t_i} \int_0^x N^{1.25}(\tau_{a_x} - \tau_{w_x})dx.$$

158

$\xrightarrow{\quad} V_{ax}$ $\xrightarrow{\quad} V_{ax}$

t' = 0

Ice Area Concentration, N

1.0

0.5

0

N

U' (x', 0) = 0.0

Ice Velocity, U' × 10²

2.0

1.0

0

0.5   1.0
Distance, x'

t' = 10

1.0

0.5

0

N

U'

2.0

1.0

0

0.5   1.0
Distance, x'

$\xrightarrow{\quad} V_{ax}$ $\xrightarrow{\quad} V_{ax}$

t' = 24

Ice Area Concentration, N

1.0

0.5

0

N

U'

Ice Velocity, U' × 10²

2.0

1.0

0

0.5   1.0
Distance, x'

t' = 46

1.0

0.5

0

N

U'

Ice Velocity, U' × 10²

2.0

1.0

0

0.5   1.0
Distance, x'

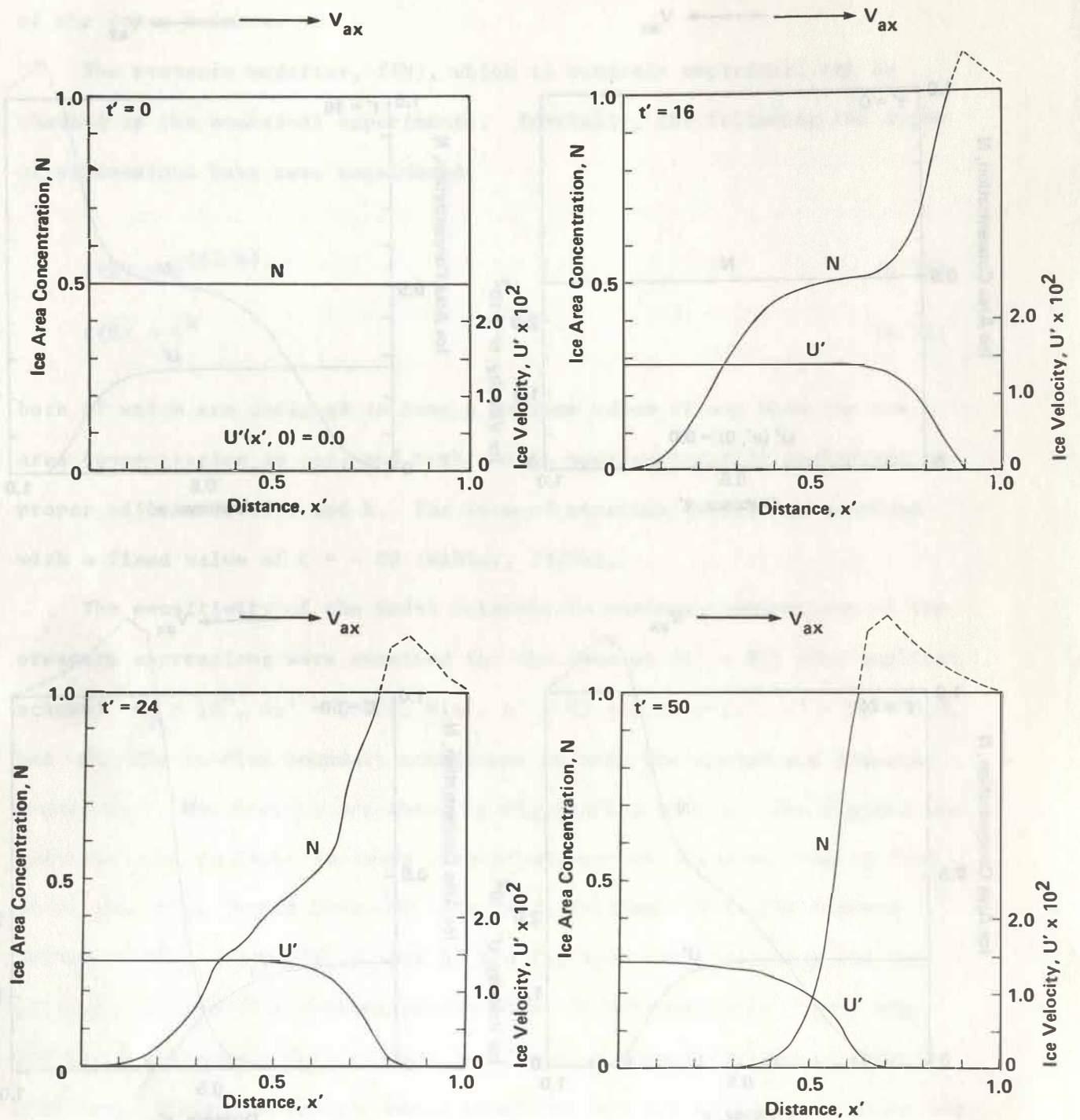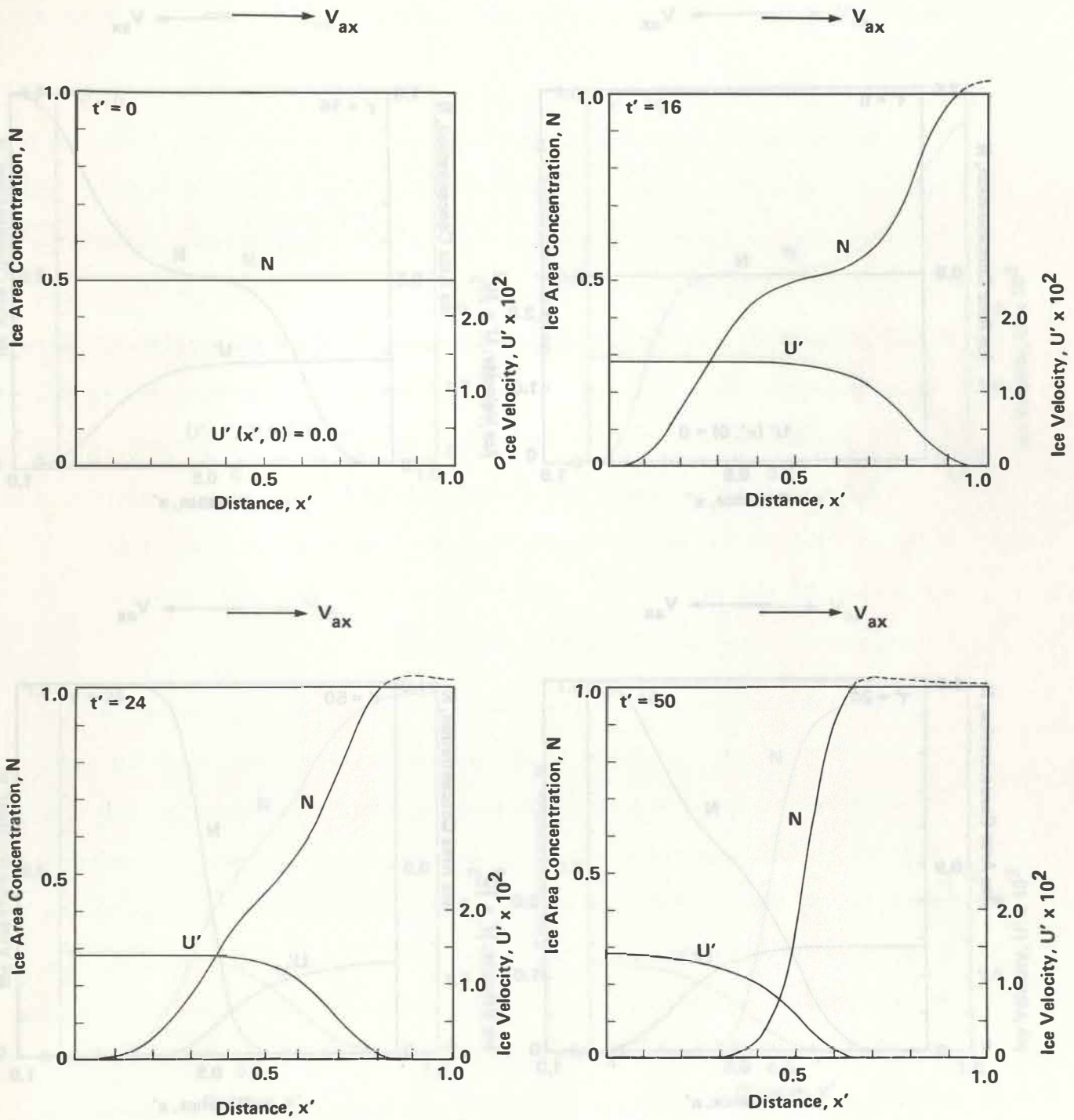Figure 4.6   One-Dimensional Ice Area Concentration and Ice Velocity Profiles with Ice Pressure given by

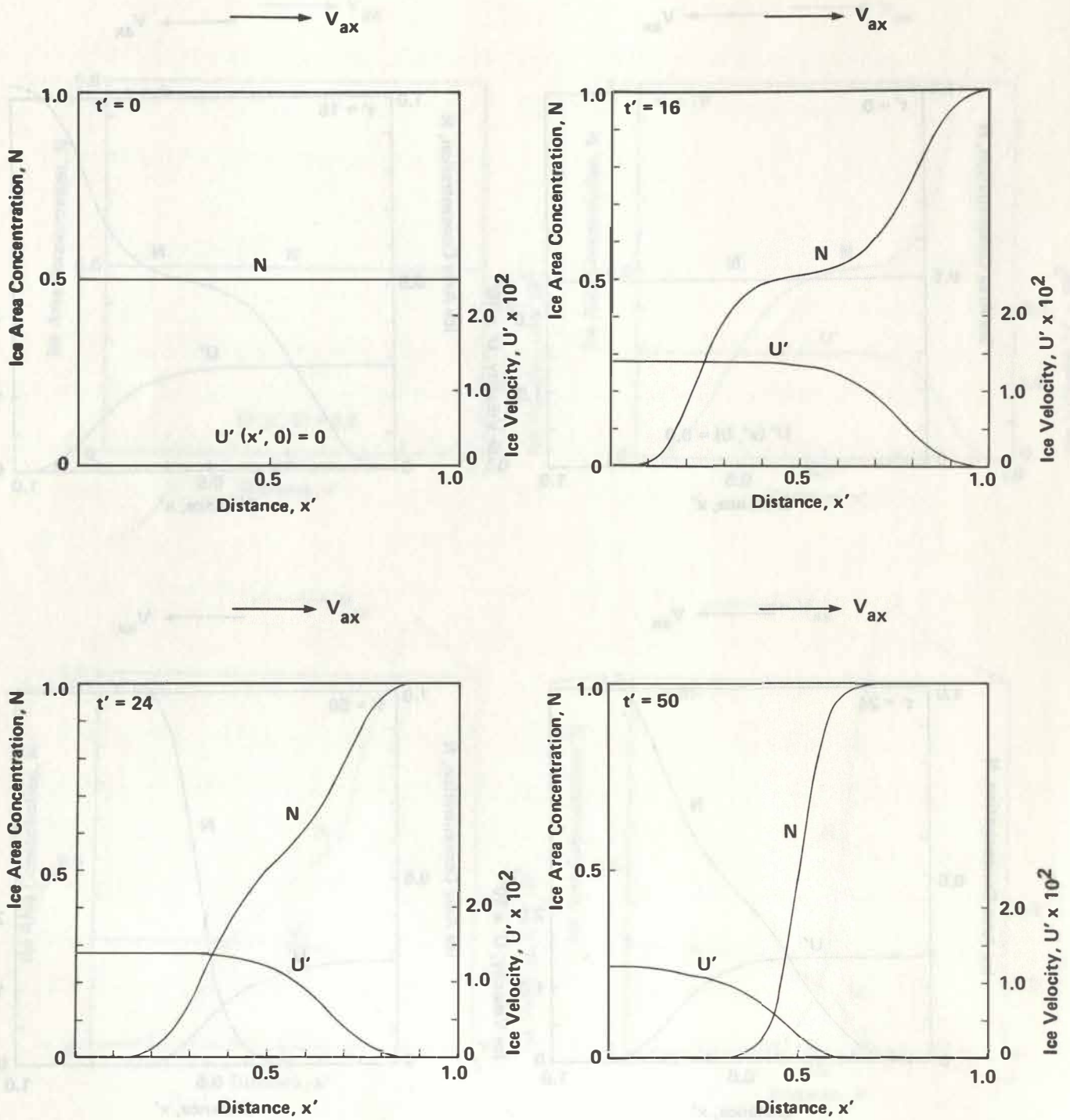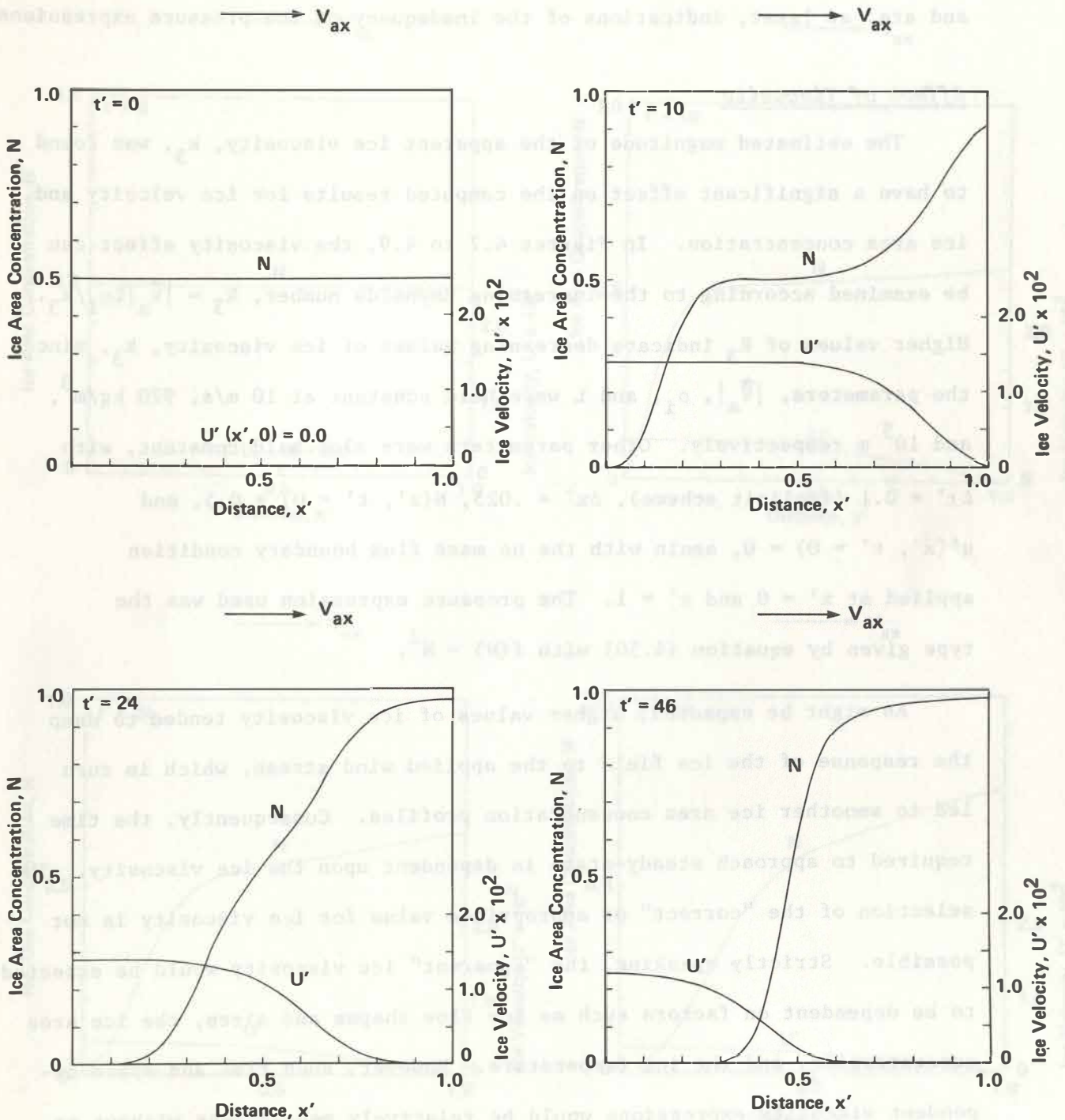$$p = \frac{1}{t_i} \int_0^x N(\tau_{a_x} - \tau_{w_x})dx.$$

of N in excess of 1.0 can not be interpreted physically in these cases, and are, at least, indications of the inadequacy of the pressure expressions.

Effect of Viscosity

The estimated magnitude of the apparent ice viscosity, k_3, was found to have a significant effect on the computed results for ice velocity and ice area concentration. In Figures 4.7 to 4.9, the viscosity effect can be examined according to the increasing Reynolds number, $R_3 = |\vec{V}_a| L \rho_i / k_3$. Higher values of R_3 indicate decreasing values of ice viscosity, k_3, since the parameters, $|\vec{V}_a|$, ρ_i, and L were held constant at 10 m/s, 920 kg/m^3, and 10^5 m respectively. Other parameters were also held constant, with $\Delta t' = 0.1$ (implicit scheme), $\Delta x' = .025$, $N(x', t' = 0) = 0.5$, and $u'(x', t' = 0) = 0$, again with the no mass flux boundary condition applied at $x' = 0$ and $x' = 1$. The pressure expression used was the type given by equation (4.50) with $f(N) = N^2$.

As might be expected, higher values of ice viscosity tended to damp the response of the ice field to the applied wind stress, which in turn led to smoother ice area concentration profiles. Consequently, the time required to approach steady-state is dependent upon the ice viscosity. The selection of the "correct" or appropriate value for ice viscosity is not possible. Strictly speaking, the "apparent" ice viscosity would be expected to be dependent on factors such as ice floe shapes and sizes, the ice area concentration, and the ice temperature. However, such time and space de-pendent viscosity expressions would be relatively meaningless without an extensive collection of laboratory and field data for use in model calibration.

Figure 4.7   One-Dimensional Ice Area Concentration and Ice
              Velocity Profiles with Ice Viscosity,
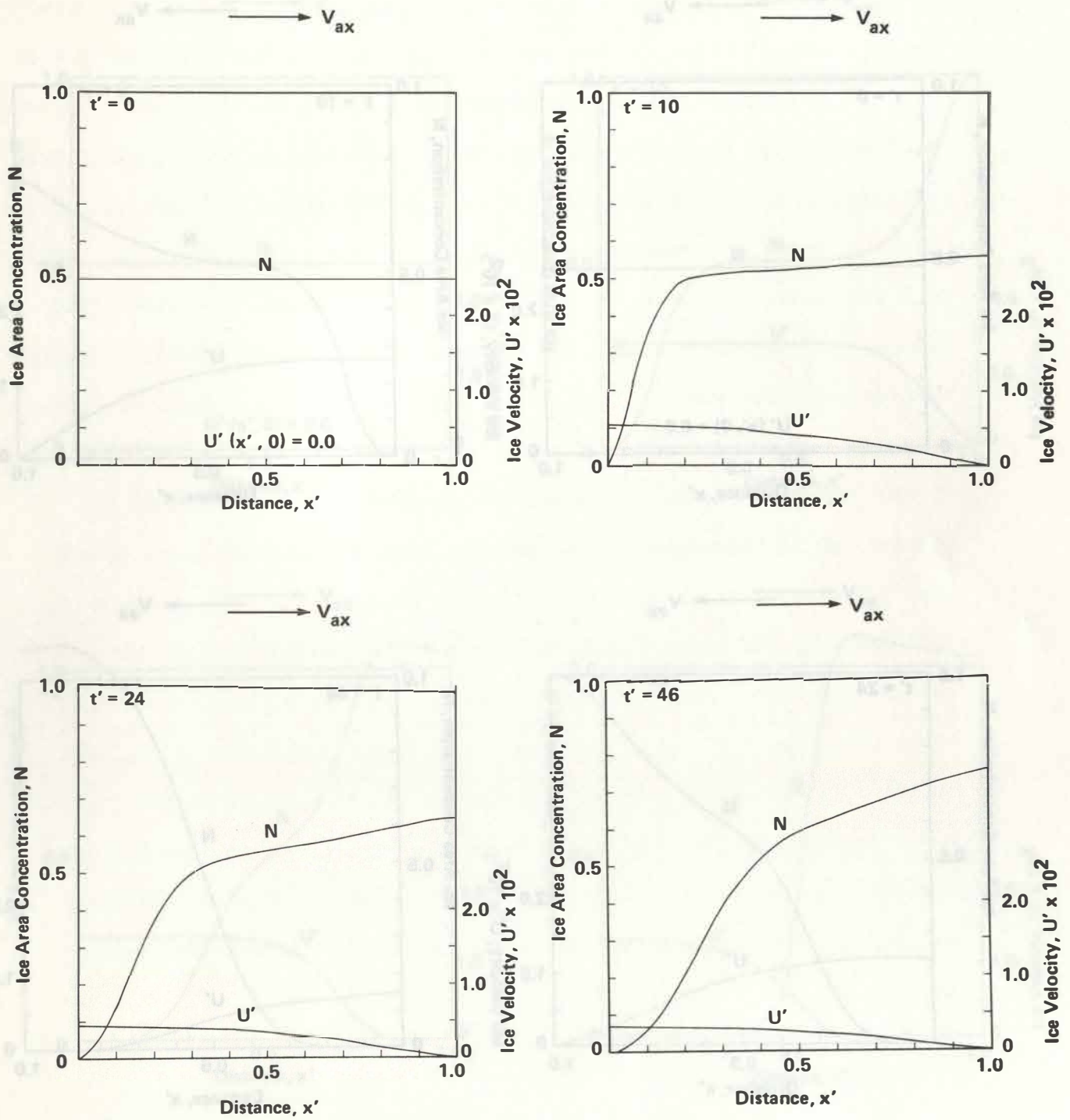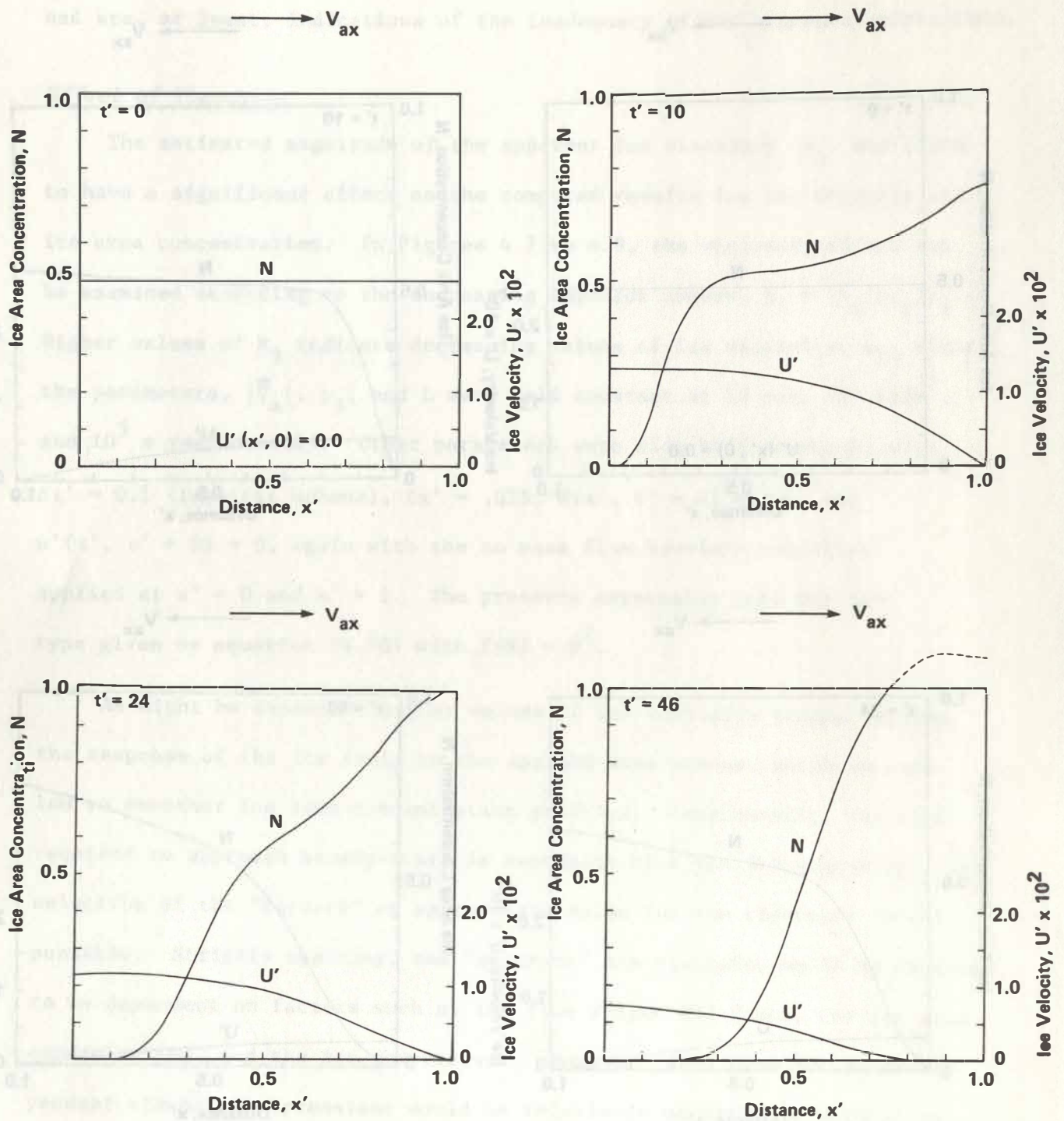 $k_3 = 9.2 \times 10^4$ Ns/m^2.

161

Figure 4.8   One-Dimensional Ice-Area Concentration and Ice
            Velocity Profiles with Ice Viscosity,
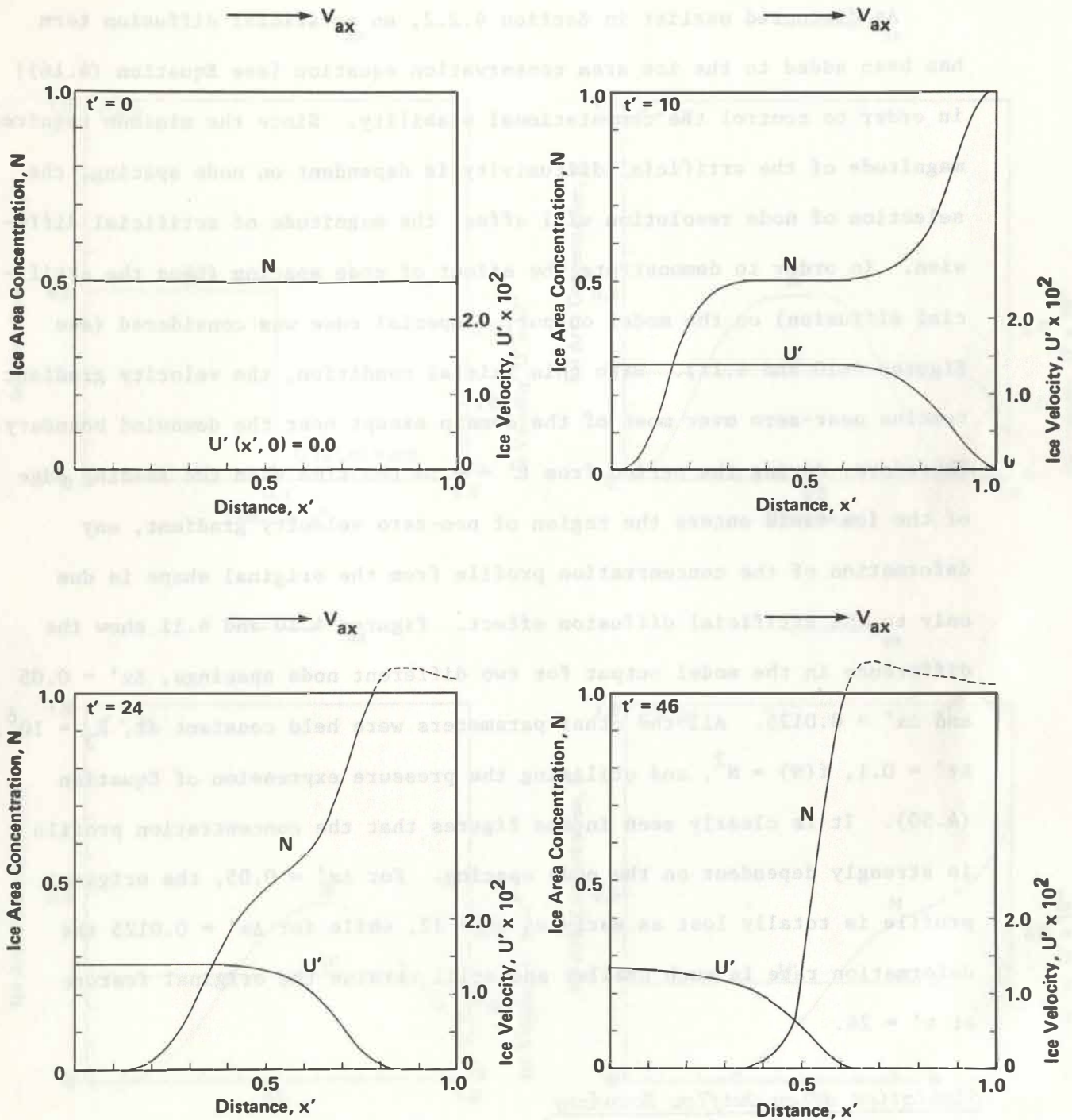 $k_3 = 9.2 \times 10^3$ Ns/m^2.

Figure 4.9   One-Dimensional Ice Area Concentration and Ice
Velocity Profiles with Ice Viscosity,

$$k_3 = 9.2 \times 10^2 \ Ns/m^2.$$

Effect of Artificial Diffusion

As discussed earlier in Section 4.2.2, an artificial diffusion term has been added to the ice area conservation equation [see Equation (4.16)] in order to control the computational stability. Since the minimum required magnitude of the artificial diffusivity is dependent on node spacing, the selection of node resolution will affect the magnitude of artificial diffusion. In order to demonstrate the effect of node spacing (thus the artificial diffusion) on the model output, a special case was considered (see Figures 4-10 and 4.11). With this initial condition, the velocity gradient remains near-zero over most of the domain except near the downwind boundary. Therefore, during the period from $t' = 0$ to the time when the leading edge of the ice field enters the region of non-zero velocity gradient, any deformation of the concentration profile from the original shape is due only to the artificial diffusion effect. Figures 4.10 and 4.11 show the difference in the model output for two different node spacings, $\Delta x' = 0.05$ and $\Delta x' = 0.0125$. All the other parameters were held constant at, $R_3 = 10^6$, $\Delta t' = 0.1$, $f(N) = N^2$, and utilizing the pressure expression of Equation (4.50). It is clearly seen in the figures that the concentration profile is strongly dependent on the node spacing. For $\Delta x' = 0.05$, the original profile is totally lost as early as $t' = 12$, while for $\Delta x' = 0.0125$ the deformation rate is much smaller and still retains the original feature at $t' = 24$.

Simulation of an Outflow Boundary

To simulate the outflow boundary condition (see Section 4.3), an abrupt change in the downwind boundary condition was tested. The case

Figure 4.10 One-Dimensional Ice Area Concentration and Ice
Velocity Profiles with Node Spacing, $\Delta x' = .05$.

165

$$N \xrightarrow{\hspace{1cm}} V_{ax} \qquad\qquad N \xrightarrow{\hspace{1cm}} V_{ax}$$

t′ = 0

Ice Area Concentration, N

N

U′ (x′, 0) = 0.0

Ice Velocity, U′ × 10²

1.0 — 0.5 — 0

Distance, x′: 0.5, 1.0

2.0 — 1.0 — 0

t′ = 12

Ice Area Concentration, N

N

U′

Ice Velocity, U′ × 10²

1.0 — 0.5 — 0

Distance, x′: 0.5, 1.0

2.0 — 1.0 — 0

$$N \xrightarrow{\hspace{1cm}} V_{ax} \qquad\qquad N \xrightarrow{\hspace{1cm}} V_{ax}$$

t′ = 24

Ice Area Concentration, N

N

U′

Ice Velocity, U′ × 10²

1.0 — 0.5 — 0

Distance, x′: 0.5, 1.0

2.0 — 1.0 — 0

t′ = 36

Ice Area Concentration, N

N

U′

Ice Velocity, U′ × 10²

1.0 — 0.5 — 0

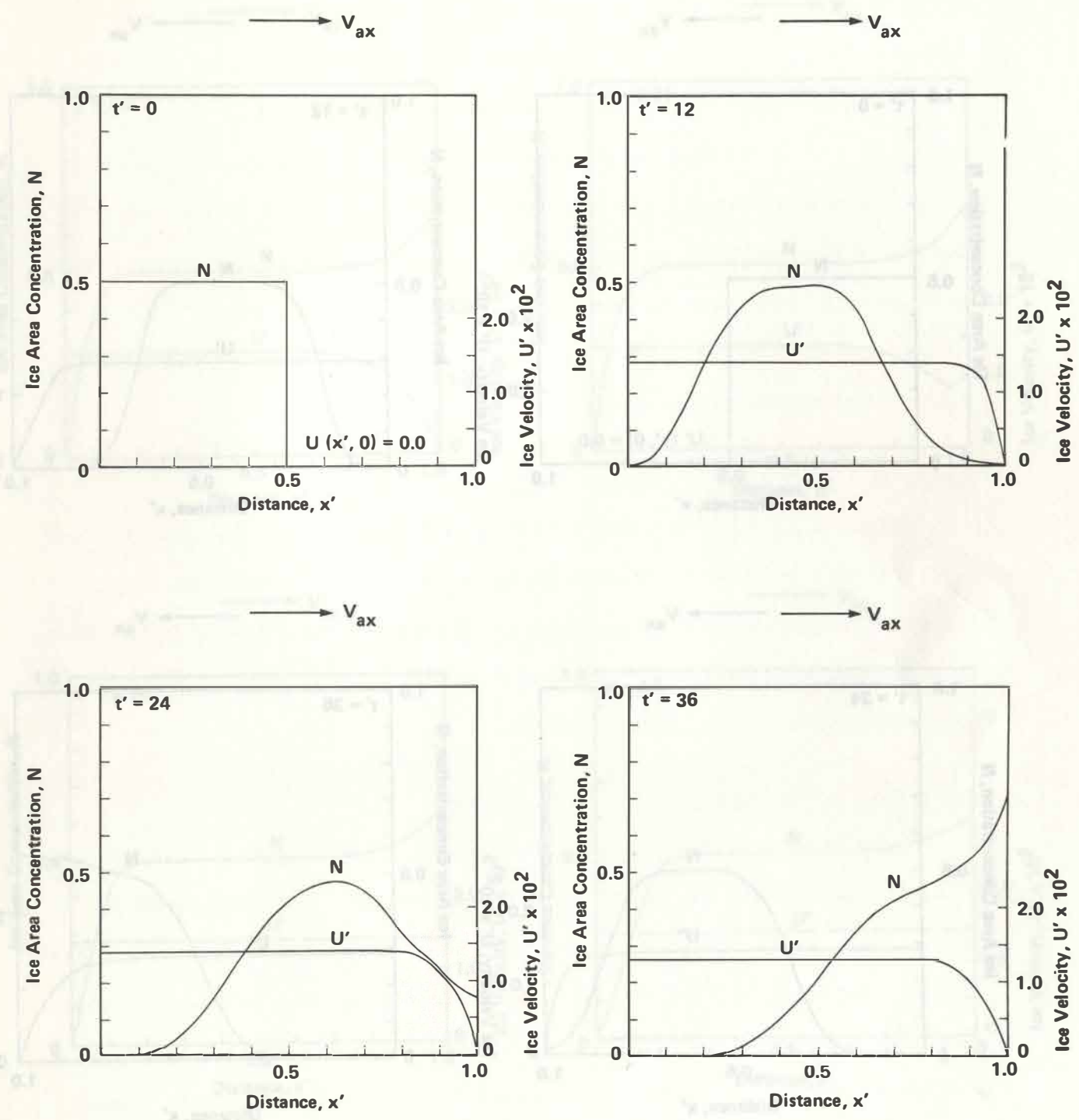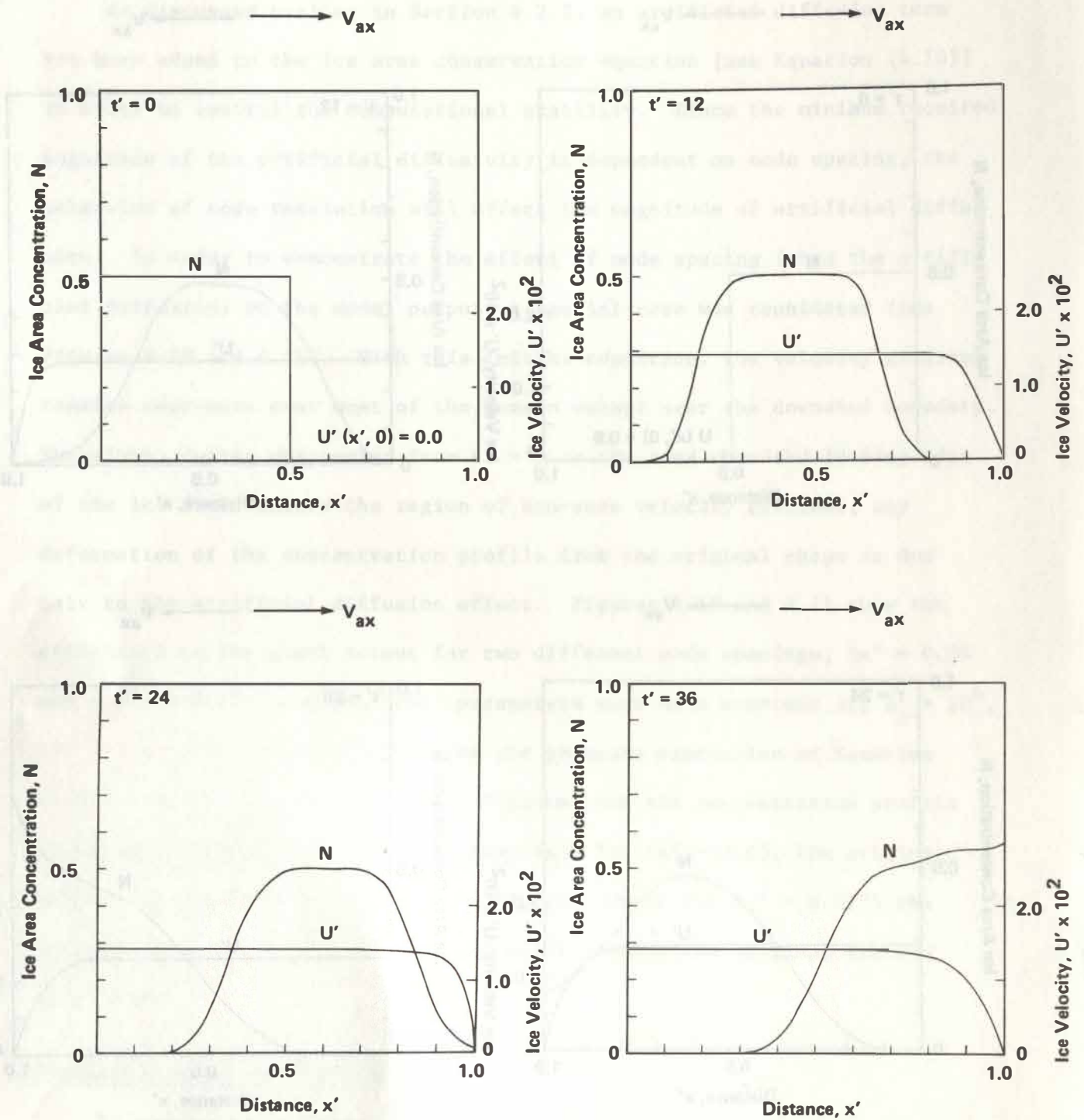Distance, x′: 0.5, 1.0

2.0 — 1.0 — 0

Figure 4.11   One-Dimensional Ice Area Concentration and Ice Velocity Profiles with Node Spacing, $\Delta x' = .0125$.
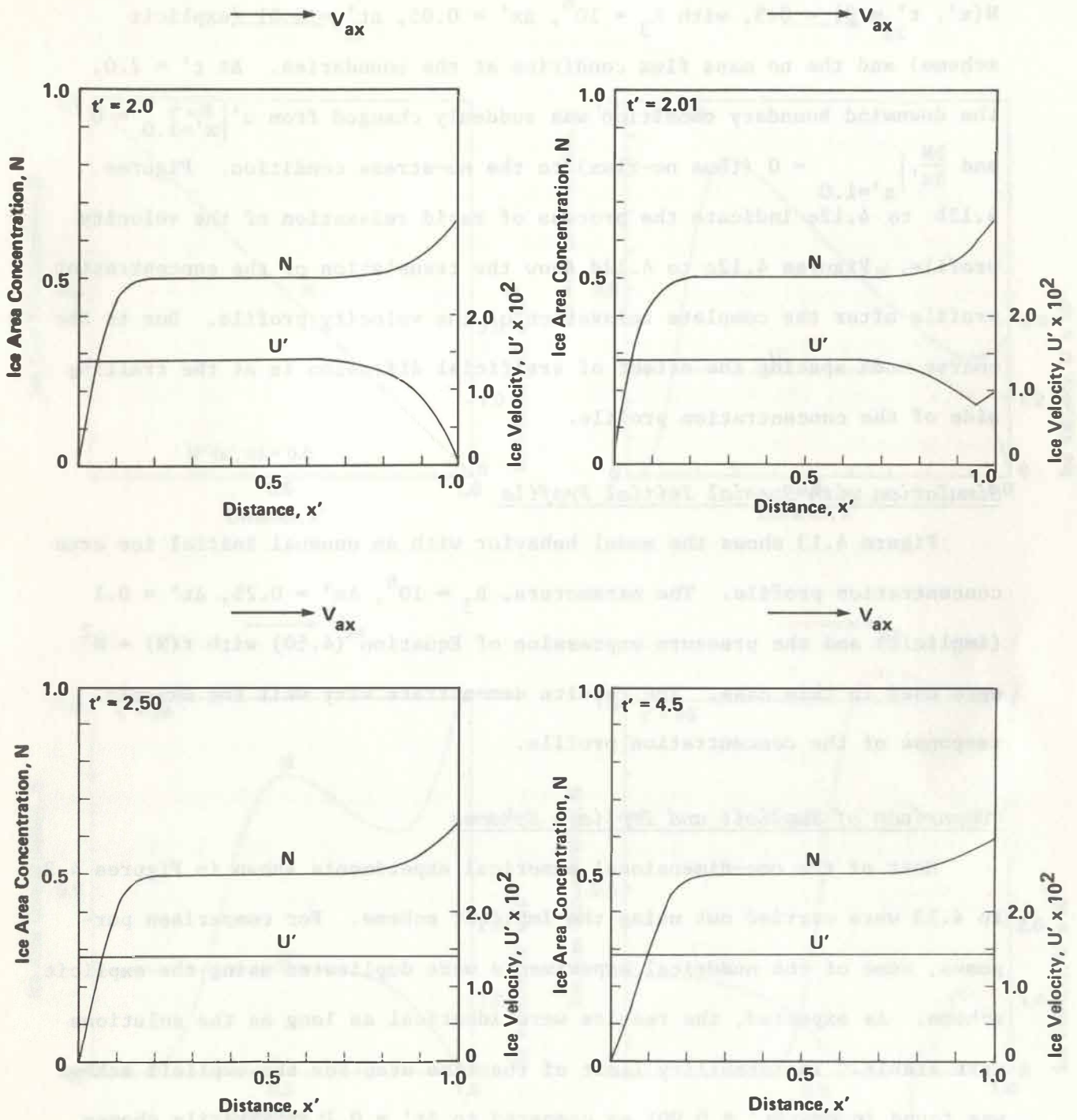
Figure 4.12   One-Dimensional Ice Area Concentration and Ice
Velocity Profiles: Case of Removing Downstream
Boundary at t' = 2.

shown in Figure 4.12 had the initial conditions, $u'(x', t' = 0) = 0.0$, $N(x', t' = 0) = 0.5$, with $R_3 = 10^6$, $\Delta x' = 0.05$, $\Delta t' = 0.01$ (explicit scheme) and the no mass flux condition at the boundaries. At $t' = 2.0$, the downwind boundary condition was suddenly changed from $u'|_{x'=1.0} = 0$ and $\frac{\partial N}{\partial x'}\Big|_{x'=1.0} = 0$ (thus no-flux) to the no-stress condition. Figures 4.12b to 4.12c indicate the process of rapid relaxation of the velocity profile. Figures 4.12c to 4.12d show the translation of the concentration profile after the complete relaxation of the velocity profile. Due to the coarse node spacing the effect of artificial diffusion is at the trailing side of the concentration profile.

Simulation with Special Initial Profile

Figure 4.13 shows the model behavior with an unusual initial ice area concentration profile. The parameters, $R_3 = 10^6$, $\Delta x' = 0.25$, $\Delta t' = 0.1$ (implicit) and the pressure expression of Equation (4.50) with $f(N) = N^2$ were used in this case. The results demonstrate very well the dynamic response of the concentration profile.

Comparison of Explicit and Implicit Schemes

Most of the one-dimensional numerical experiments shown in Figures 4.2 to 4.13 were carried out using the implicit scheme. For comparison purposes, some of the numerical experiments were duplicated using the explicit scheme. As expected, the results were identical as long as the solutions were stable. The stability limit of the time step for the explicit scheme was found to be, $\Delta t' \cong 0.001$ as compared to $\Delta t' = 0.1$ arbitrarily chosen for the implicit scheme. However, the explicit scheme required only about ten times as much computational time as the implicit scheme, even though the time step was less by a factor of 100.
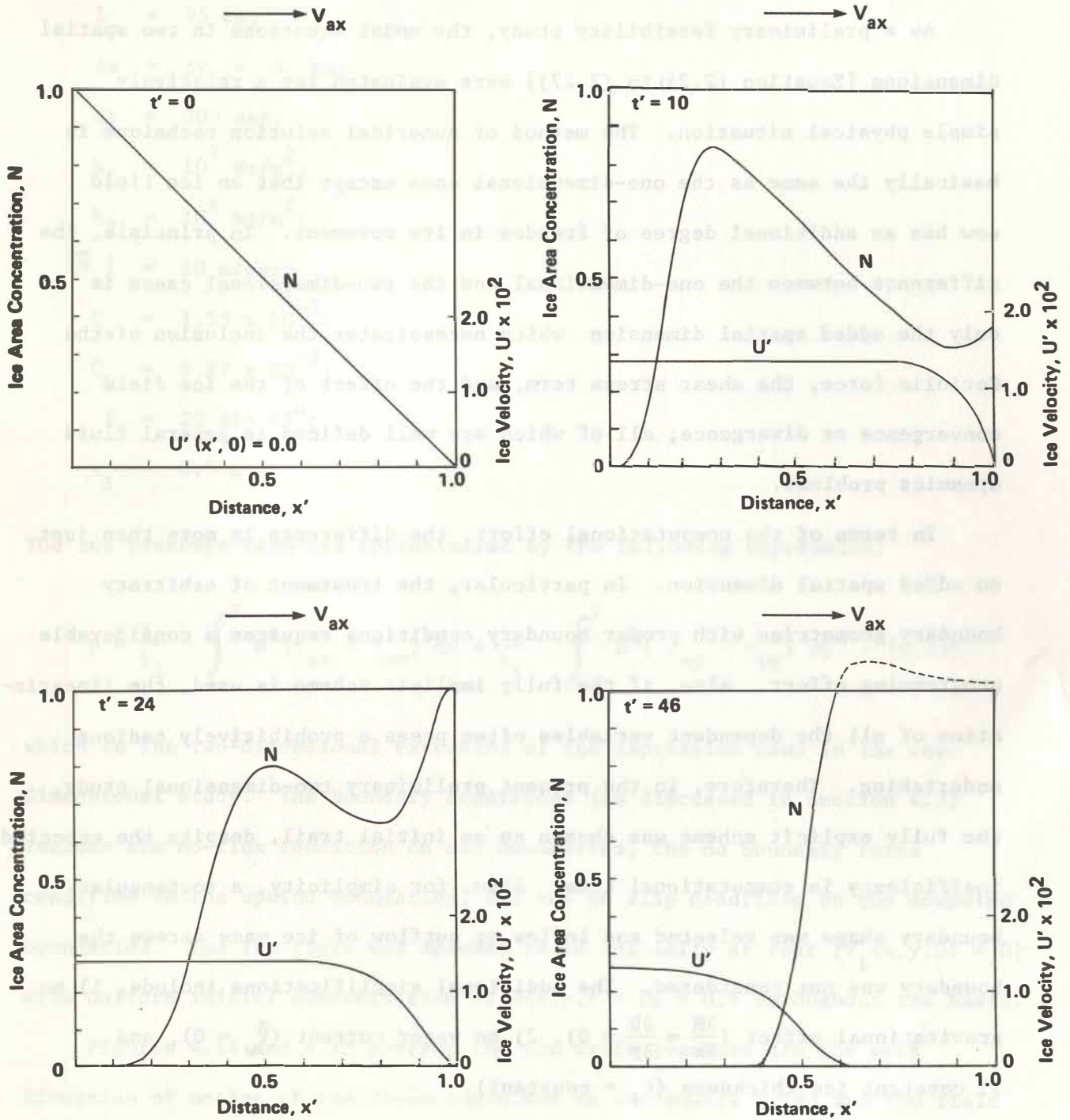
168

Figure 4.13   One-Dimensional Ice Area Concentration and Ice
Velocity Profiles with Non-Uniform Initial
Distribution of Ice Area Concentration.

169

4.5 Two Dimensional Analysis

As a preliminary feasibility study, the model equations in two spatial
dimensions [Equation (2.24) to (2.27)] were evaluated for a relatively
simple physical situation. The method of numerical solution technique is
basically the same as the one-dimensional case except that an ice field
now has an additional degree of freedom in its movement. In principle, the
difference between the one-dimensional and the two-dimensional cases is
only the added spatial dimension which necessitates the inclusion of the
Coriolis force, the shear stress term, and the effect of the ice field
convergence or divergence; all of which are well defined in general fluid
dynamics problems.

In terms of the computational effort, the difference is more than just
an added spatial dimension. In particular, the treatment of arbitrary
boundary geometries with proper boundary conditions requires a considerable
programming effort. Also, if the fully implicit scheme is used, the lineariz-
ation of all the dependent variables often poses a prohibitively tedious
undertaking. Therefore, in the present preliminary two-dimensional study,
the fully explicit scheme was chosen as an initial trail, despite the expected
inefficiency in computational time. Also, for simplicity, a rectangular
boundary shape was selected and inflow or outflow of ice mass across the
boundary was not considered. The additional simplifications include, 1) no
gravitational effect $(\frac{\partial H}{\partial x} = \frac{\partial H}{\partial y} = 0)$, 2) no water current $(\vec{V}_w = 0)$, and
3) constant ice thickness $(t_i = \text{constant})$.

With these simplifications, the two-dimensional model behavior was
examined based on Equations (2.24), (2.25), and (2.27). Figures 4.14 to
4.18 show the results of ice transport and ice field compaction in response
to a constant wind stress. The following dimensional parameters were used for
all the cases in the figures.

170

$$L_x = 75 \text{ km};$$

$$L_y = 95 \text{ km};$$

$$\Delta x = \Delta y = 5 \text{ km};$$

$$\Delta t = 200 \text{ sec};$$

$$k_1 = 10^7 \text{ Ns/m}^2;$$

$$k_2 = 10^6 \text{ Ns/m}^2;$$

$$|\vec{V}_a| = 10 \text{ m/sec};$$

$$C_a = 1.55 \times 10^{-3};$$

$$C_w = 9.27 \times 10^{-3};$$

$$f = 2\Omega \sin 42^\circ;$$

$$t_i = 0.5 \text{ m}$$

The ice pressure term was approximated by the following expression:

$$p = \frac{1}{t_i} \int_o^x N^k (\tau_{ax} - \tau_{wx}) \, dx + \frac{1}{t_i} \int_o^y N^k (\tau_{ay} - \tau_{wy}) \, dy \quad (4.53)$$

which is the two-dimensional extension of the expression used in the one-dimensional study. The boundary conditions (as discussed in Section 4.3) include the no-flux condition on all boundaries, the no boundary force condition on the upwind boundaries, and the no slip condition on the downwind boundaries. The ice field was assumed to be initially at rest $[\vec{V}_i(x,y,0) = 0]$ with uniform initial concentration of $N(x,y,t = 0) = 0.5$ throughout the basin.

Figures 4.14 and 4.15 portray the ice drift (vectors are the mean direction of motion of the floes contained in the square grid) and the field of ice area concentration at t = 24 hrs and t = 100 hrs, with k = 3 in the pressure expression [Equation (4.53)]. Figures 4.16 and 4.17 are the same but with k = 5 in the pressure expression.

171

Unlike the one-dimensional case, the magnitude of the ice viscosities, k_1 and k_2, did not affect the time to approach the steady state significantly. At low viscosities, such as $k_1 = 10^3$ Ns/m^2, $k_2 = 10^2$ Ns/m^2, the model output exhibited some instability for the parameters used in this application. The effect of bulk viscosity, k_2, on ice drift and the ice area concentration was found to be insignificant, at least for the parameters used in the present study. The total elimination of the bulk viscosity did not visibly affect the numerical results. As seen in the figures, the model output is sensitive to the ice pressure. At higher ice pressures ($k = 3$) the response of the ice field is not as rapid as at lower ice pressures ($k = 5$). The most significant difference between the one-dimensional case and the two-dimensional case is the slowness of ice field compaction in the latter. While for the one-dimensional case, an initially uniform ice field of $N(x, t = 0) = 0.5$ within a one-dimensional space of 100 km rapidly reaches an ice area concentration of $N = 1$ at the downwind boundary after about 30 hours with $V_{ax} = 10$ m/sec. The ice area concentration does not exceed 0.9 in the two-dimensional case, even after 100 hours, for the same wind stress and less pressure than was present in the one-dimensional case.

In general, the preliminary two-dimensional model output, as displayed in Figures 4.14 to 4.17, indicates the basic characteristic features expected from the analytical considerations. However, the inefficiency of the explicit numerical scheme which required a time step of the order of one minute, and the uncertainties regarding the pressure expression and the magnitude of the ice viscosities, prevent the practical application of the numerical model at its present stage of development.

= 10 cm/sec

Ice Drift

Ice Area Concentration

Figure 4.14 Two-Dimensional Ice Area Concentration and Ice Velocity
Fields at t = 24 hrs. [k = 3 in Ice Pressure Equations
(4.50) and (4.52)].

Figure 4.15   Two-Dimensional Ice Area Concentration and Ice Velocity
Fields at t = 100 hrs. [k = 3 in Ice Pressure Equations
(4.50) and (4.52)].

174

→ = 10 cm/sec

y(km)

90
80
70
60
50
40
30
20
10
0

0 10 20 30 40 50 60 70

Ice Drift   x(km)
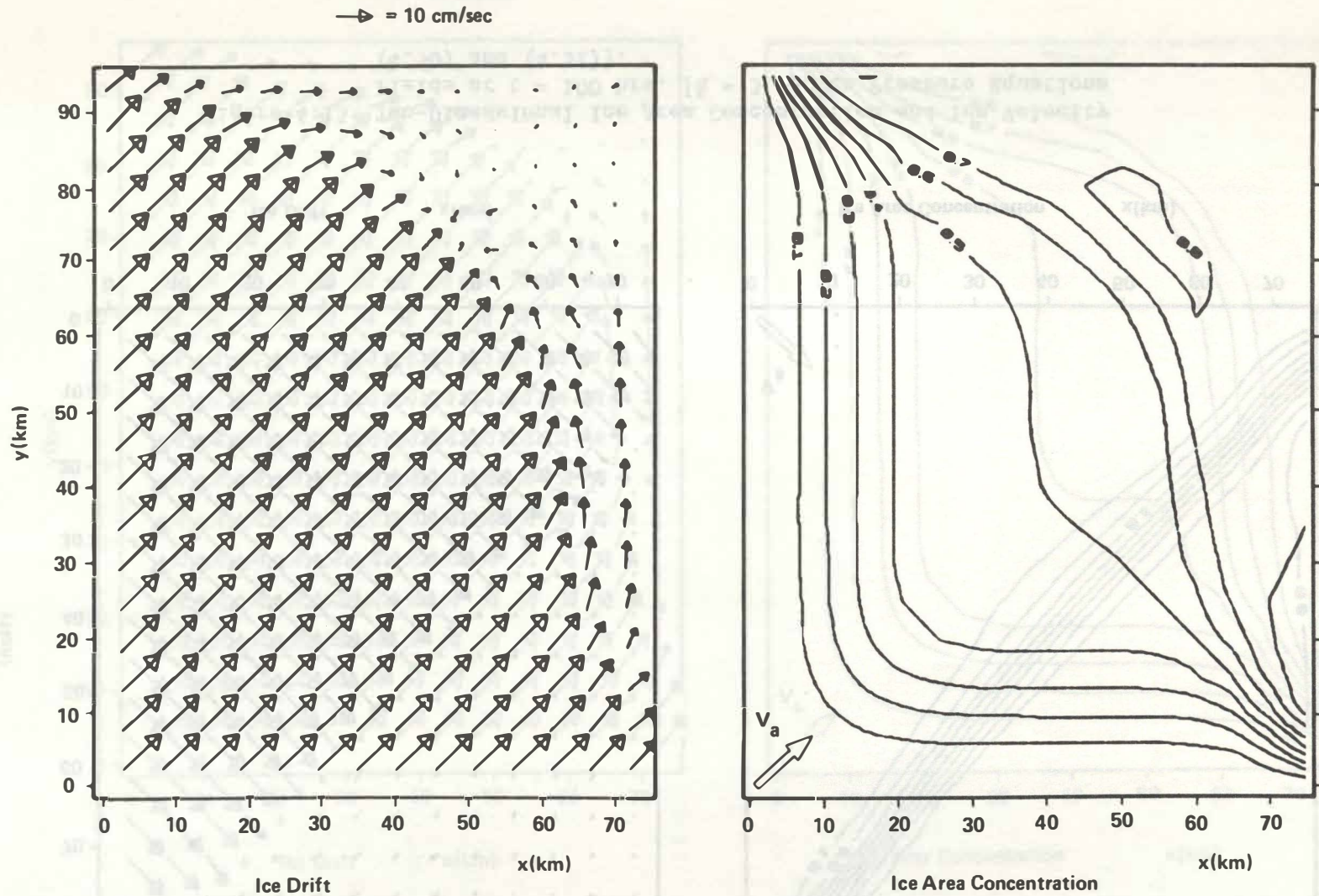
Ice Area Concentration   x(km)

V_a

Figure 4.16   Two-Dimensional Ice Area Concentration and Ice Velocity
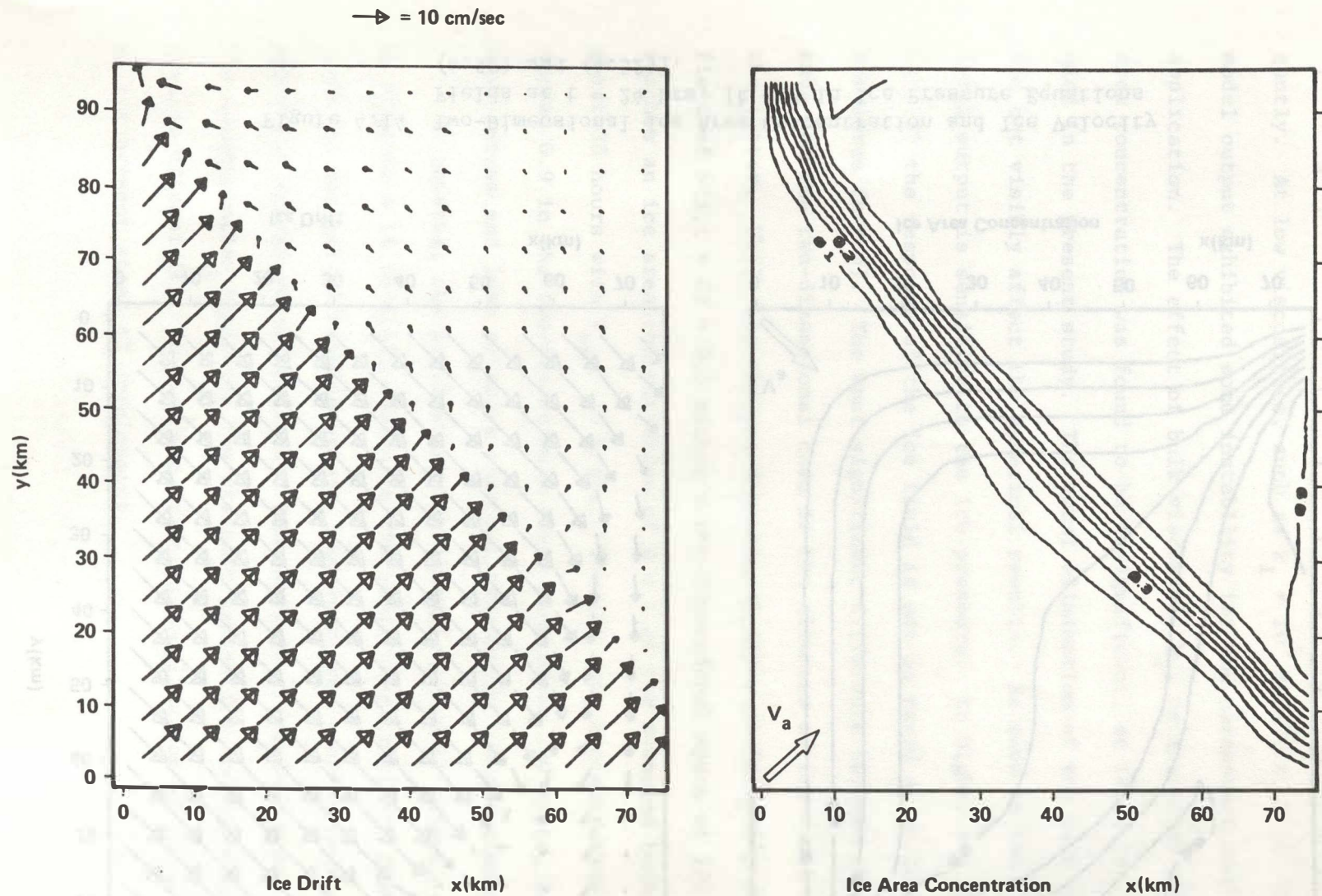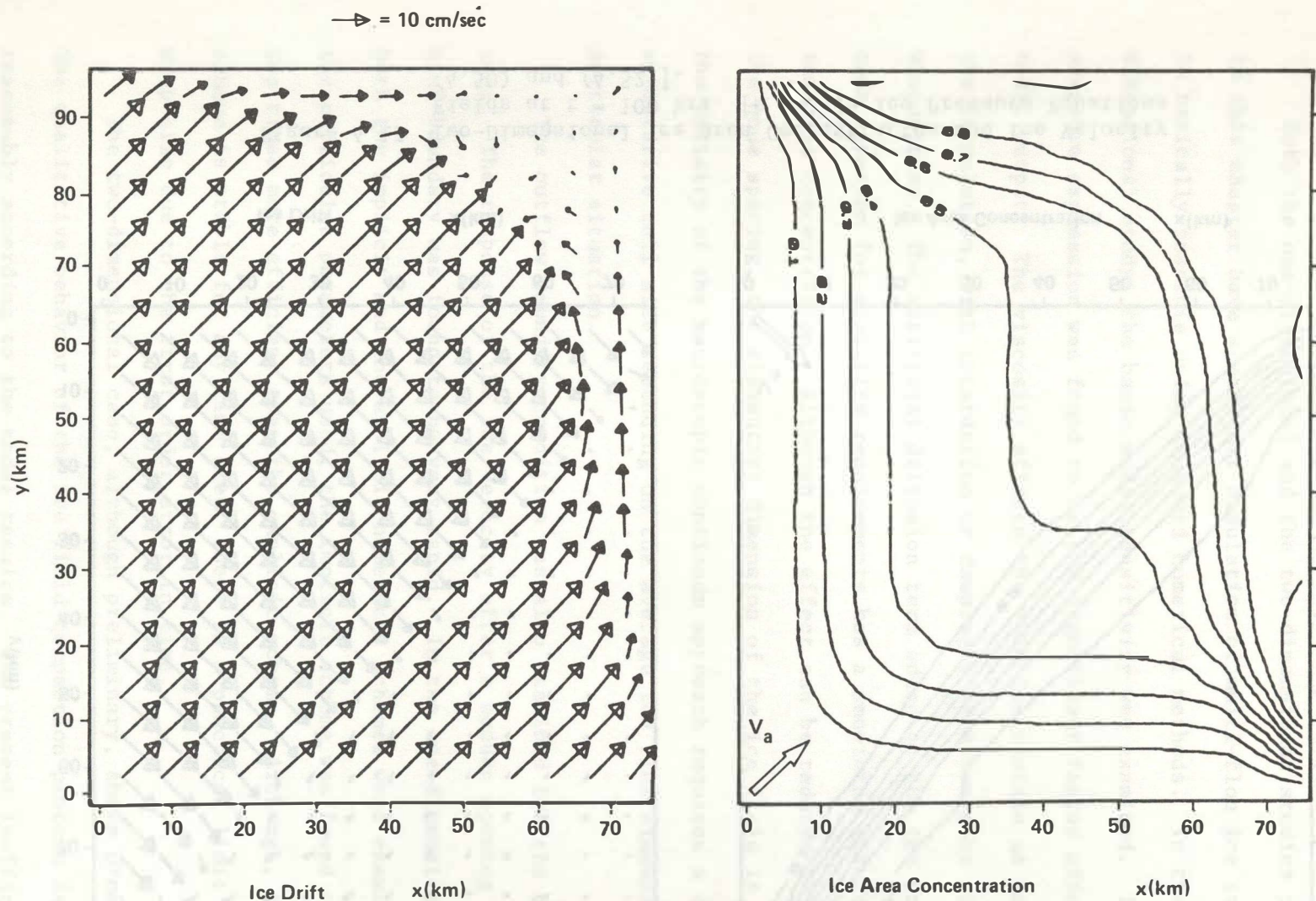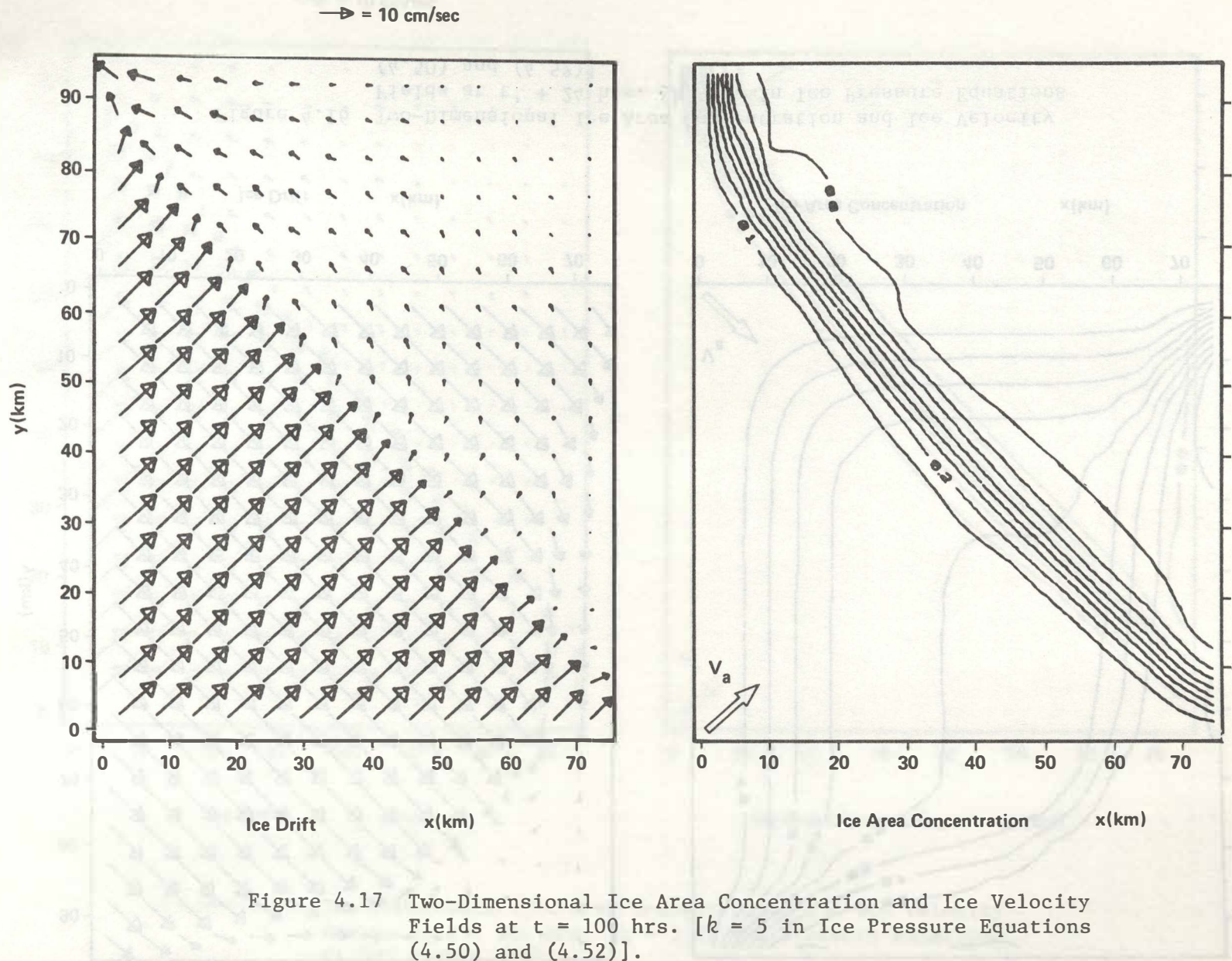Fields at t' + 24 hrs. [k = 5, in Ice Pressure Equations
(4.50) and (4.52)].

175

Figure 4.17 Two-Dimensional Ice Area Concentration and Ice Velocity
Fields at t = 100 hrs. [k = 5 in Ice Pressure Equations
(4.50) and (4.52)].

4.6 Summary of Numerical Study

Both the one-dimensional and the two-dimensional studies presented in this chapter have shown that simulation of multi-floe ice transport is basically possible using standard numerical methods. In the one-dimensional study, the basic model sensitivity was examined. The ice pressure expression was found to be the significant factor affecting the model output. The viscosity affects the velocity profile as expected from the formulation, with retardation or damping of ice movement at higher viscosities. The artificial diffusion term added to the ice area conservation equation for stability requirements has a smoothing effect on the ice area concentration. Although the effect can be reduced by decreasing the node spacing, the elementary dimension of the ice field is limited since the validity of the macroscopic continuum approach requires a certain representative cell size depending on the average ice floe dimensions in a particular situation.

The outflow boundary condition was also examined for the one-dimensional case. The response of the ice velocity after a sudden opening of the downwind boundary was found to be very rapid. In the one-dimensional case, both the implicit and the explicit numerical schemes were examined. For the particular parameters used, the implicit scheme was found to be about ten times more efficient than the explicit scheme. Although, the implicit scheme is stable for any time step, there is a practical limit on the time step size due to the first order error in time.

The two-dimensional case, although preliminary, shows promising results. The qualitative behavior of the ice field compaction process is simulated reasonably according to the model results. The present inefficiency of the numerical scheme can be improved by using the fully implicit scheme or a

177

combination of the explicit and implicit schemes. The most serious limitation of the present numerical model is the inadequacy of the pressure expression. For the closed boundaries without ice mass flux, the present expression seems to be sufficient. However, with open boundaries and non-zero ice mass flux, the present form does not provide realistic values for the internal ice pressure distribution.

In summary, the numerical model study presented in this chapter shows possibility for practical application. Extensive field and laboratory experiments, as well as further model refinements, are needed before the model can serve as a practical tool for ice transport predictions in the Great Lakes.

V. DATA AVAILABILITY AND ICE SURVEILLANCE TECHNIQUES

5.1 Introduction

The Great Lakes-St. Lawrence Seaway System has, historically, been closed to navigation from mid-December until early April because of the adversities imposed by weather and ice. However, winter navigation on the Great Lakes has, increasingly, become a desirable objective (Survey Study...., 1979). In response to this desire, the Great Lakes-St. Lawrence Seaway Navigation Season Extension Program was established in 1970.

This navigation season extension program relies, primarily, on the near real-time collection and dissemination of ice information. This aspect of the program has been the responsibility of the U.S. Coast Guard, which established the Ice Navigation Center in Cleveland, Ohio, in 1970, specifically for this purpose. The ice information has been received from several sources including the U.S. Lake Survey, the U.S. Coast Guard, Ice Forecasting Central in Ottawa, Canada, the Seaway Development Corp. (U.S.), and the Canadian Seaway Authority. Various techniques for observing and recording the ice information have been incorporated and include aerial reconnaissance, shore and ship based observations, radar imagery, and satellite imagery. This information is analyzed and transmitted in both verbal and chart form to shipping companies, Coast Guard icebreakers, and freighters already underway.

In 1970 the Canadian Ministry of Transport began its own navigation season extension studies of Lake Erie, the St. Lawrence River, and the Detroit-St. Clair reach of the Great Lakes . This task is now being done by the St. Lawrence Seaway Authority (1976-78). (Can. Marine Transp. Admin.,

1970-76). This effort has been primarily an ice information collection program and has not been used operationally. The majority of ice information has been obtained from ship and shore observations and aerial reconnaissance made by the Canadian Coast Guard and the Canadian Seaway Authority. Of the recommendations resulting from these navigation season extension studies, one has been that more information be obtained "....on the effects of wind and other phenomena, relative to build-up, orientation and movement of major ridges and rafted ice fields." Another recommendation has urged that shipping tracks be located in the Lake Erie ice field so as to avoid, whenever possible, areas of high ice pressure and ridged and rafted ice.

Although the objective of developing a simulation model that predicts ice movement and ice deformation (including estimates of the location of severe ice pressure and ridging) is presently being pursued; replacement of existing ice information collection-dissemination programs is not likely in the near future. Simulation models can augment existing programs and provide a framework for deducing the cause and effect relationships that control the dynamic evolution of the ice cover. In this section, ice information requirements for continued development, calibration, and verification of ice dynamics models are discussed along with the kinds of information historically and presently available, data collection techniques, and the adequacy of collected data relative to the development of ice transport models.

5.2 Ice Information Requirements

Development and calibration of a Great Lakes ice dynamics model requires definition of the ice mass and its position as a function of time. The frequency of ice data collection is as important as an accurate spatial

definition of the ice mass. Estimating the ice mass, at any instant in time, depends on information related to its areal and thickness distributions. Characteristics such as ice concentration, lead patterns, ice type, and ice age help to estimate the areal distribution. The thickness distribution is more difficult to estimate.

Modeling the growth and dissipation of the ice mass requires climotological data, water temperature, and surface albedo information. Ice transport into the lakes from tributaries and between lakes by connecting waterways can be important at times.

Calibration of an equation of motion for the ice mass requires frequent information on ice position, wind speeds and direction, and underlying water currents. A determination of the top and bottom surface roughnesses of the ice is required to calculate representative wind and water stress coefficients. Wind and current data are required to calculate the forces and pressures that cause the ice to move and deform. Estimates of ice strain rates and internal ice stresses will be needed to evaluate the appropriateness of proposed constitutive laws for lake ice. In view of the extensive data requirements associated with the development of ice dynamics models, it will be important to develop an "ice data bank" that can be accessed by various users depending upon their needs. Also, for the same reason, it is likely that well-designed laboratory experiments will supply information that would be difficult and costly to acquire in the field.

5.3 Visual Observations

Visual observations of ice have been recorded since the American Revolution, which brought about a military necessity for extending the Great Lakes navigation season (Snider, 1974). Most of the accounts have been shore and ship based and pertain to the harbors, inter-connecting waterways, and shipping lanes. Prior to 1841, observations were very sporadic and only locations having unusual ice conditions were reported. In that year, the U. S. Lake Survey, under the direction of the U. S. Army (transferred to NOAA in 1971) was created to gather information, including ice information, to improve the navigational safety of the Great Lakes. Until 1963, observations were still sporadic, but were usually recorded at least once a week during the later part of the ice season. These reports were used, primarily, to assist shipping interests in determining the opening of navigation and, once it was opened, to locate navigational hazards.

After World War II, Great Lakes ice observation was bolstered by aerial reconnaissance. The first documented aerial observation was in 1947, when ice conditions in the Lake St. Peter-Lake St. Louis reach of the St. Lawrence River were recorded. In 1953, the U. S. Lake Survey made aerial observations of the St. Clair and Detroit Rivers. The U. S. Coast Guard initiated an aerial reconnaissance program in 1958 for operational purposes (Rondy, 1969). The Canadian Ministry of Transport began ice reconnaissance flights over Lake Superior, Huron, Erie, and Ontario in 1960 (Heap, 1963).

In 1965, in order to better define the Great Lakes ice regime, the U.S. Lake Survey Center began a comprehensive ice observation program (Sleator, 1978). A paid ice observer network was established at strategic locations throughout the lakes. These shorebased observations have been

made on a weekly basis over the entire ice season. The data collection stations have been located at sites that generally have stable ice covers throughout the winter season (but at least 50 m off shore). During the 1969-70 ice season the number of observation stations was reduced from an original 90 to around 30 in order to make the program more cost effective. Ice thickness and stratigraphic structure were the principal observations recorded. The collected data are not representative of over-lake ice conditions and hence are of limited use in ice transport modeling. However, the relative severity of winter seasons can be estimated; the data can be used for ground truth in parallel with remote sensing programs; and the site specific nature of the data are useful for engineering purposes. Some additional ice thickness measurements have been reported for the Great Lakes during 1970-71 and 1971-72 (Bilello and Bates, 1975) at four different nearshore locations in Canada.

Stewart (1973) has reported ice thickness measurements for Lake Erie made during the 1971-72 winter season. The measurements were made along several lateral (U.S.-Canada) transects and along the longitudinal axis of the lake at different times during the winter season utilizing a heliocopter equipped with pontoons. His reported data are the most comprehensive ever recorded for a winter season in any one of the Great Lakes. The data are useful in assessing the spatial and temporal variability in ice thickness during a specific winter season.

The U.S. Lake Survey also initiated in 1965 an aerial reconnaissance program which averaged 10-15 flights per season over all of the Great Lakes. These aerial observations have been instrumental in characterizing the seasonal variation in the Great Lakes ice cover (Rondy, 1971).

Since the establishment of the Ice Navigation Center, additional visual observations have been made, on a daily basis, by a U.S. Coast Guard network scattered around the lakes. Commercial ships and Coast Guard icebreakers have reported ice conditions many times a day, while the Coast Guard has logged almost daily reconnaissance flights over some parts of the lakes (Boyce, 1974).

The Power Authority of the State of New York and Ontario Hydro of Canada, which both operate hydroelectric power generating stations on the Niagara River, conduct aerial surveys of ice conditions in eastern Lake Erie during the ice dissipation period. This information is needed to assess the potential for ice runs and jams that might form in the Niagara River leading to reductions in power production. This information also aids in decision-making relative to the removal of the Lake Erie-Niagara River ice boom that is operated by the power entities. The International Niagara Board of Control, in their annual reports, summarize ice conditions in eastern Lake Erie and the operation of the ice boom which was first installed in the 1964-65 winter season. A study of the effects that this ice boom may have on the ice regime of Lake Erie was conducted under the auspices of the International Niagara Board of Control (Rumer et al, 1975).

Direct visual observations and measurement of ice conditions in the Great Lakes, although limited in terms of areal coverage and frequency of observation, will continue to be necessary for establishing ground truth measurements for the remote sensing capability that is now developing in the Great Lakes. (Ramseier and Weaver, 1975; Suzuki, 1964; Ackley et al, 1976) These data, which tend to be site specific, will frequently be the only means of establishing cause and effect relationships for physical processes that occur at a scale too small to be resolved by other means.

5.4   Remote Sensing

The first remote sensing technique to be used over the Great Lakes was "visual" photography. Aerial photographs are instrumental in defining local ice problems affecting such activities as navigation and power generation. They are also used to assist in defining ice characteristics, such as age, concentration, and size of floes, and to aid in the establishment of ground truth for other types of remote sensing techniques. Because of weather limitations and for economical reasons, aerial photographs are not available on a regular basis nor do they cover wide areas. Alternative techniques for observing the large areal expanse of the Great Lakes include the remote sensing methods discussed below.

5.4.1 Side Looking Airborne Radar

Side looking airborne radar (SLAR) was developed in the 1950's and was first used to map sea ice in the early 1960's (Anderson, 1966). Since then, several investigations of the applicability of SLAR for monitoring floating ice have been conducted. SLAR images of sea ice were studied by Johnson and Farmer (1971), Ketchum and Tooma (1973), Gorbunov and Losev (1974), Dunbar (1975), Dunbar and Weeks (1975), Dunbar (1978), and Elachi and Brown (1975). Applications of SLAR to freshwater ice were investigated by Larrowe et al (1971), Anderson et al (1972), Gedney et al (1975), and Shertler et al (1975) and Bolsenga (1978). Campbell et al (1975a), Page and Ramseier (1975) and Campbell et al (1975b) present good summaries of the evolution of SLAR for remotely sensing floating ice.

It is now generally concluded that SLAR is useful in the identification of certain ice characteristics. These include: (1) distinguishing ice from water (in most cases); (2) delineating rafted and ridged ice and areas having small broken pieces of ice: (3) distinguishing ice from land; and (4) defining

size and shape of ice floes and their associated lead patterns. It has, also, been concluded that SLAR's all weather capability and large areal coverage make it superior to aerial photography.

The major limitation of using SLAR imagery to characterize either sea ice or freshwater ice deals with data interpretation. At present, interpretation is qualitative and subject to error. Rawson and Smith (1974) have demonstrated an ability to quantitatively correlate back-scattered radiation with ice types which, when calibrated, should reduce interpretation errors. Bolsenga (1978) has further studied the use of SLAR in defining ice characteristics. Other sources of error are caused by film processing and handling, aircraft flight path and altitude changes, and electronic malfunctions. A natural phenomenon that can produce some error is the presence of melt water on the ice, which causes very weak signal returns (Schertler, personal communication). However, the advantages of SLAR outweigh its limitations and this method should prove to be a very useful tool as interpretation of the imagery is improved.

Side Looking Airborne Radar is an active system that operates in the microwave range of the electromagnetic spectrum. Successive transmission of the microwave energy perpendicular (thus the term "Side Looking") to the aircraft flight path is the basis for obtaining images of the areal distribution of the ice field. Since the sytem uses wave lengths significantly longer than those in the optical range (10^4-10^5 times longer), it is capable of penetrating clouds, fog, rain, etc. This all weather, all night and day capability is the basis for increased frequency of observation.

Characterizing ice features with SLAR depends on the radiation backscatter, the range to the feature, and the receiver sensitivity. The radar senses variations in the radiation backscatter which in turn is related to

186

the radar frequency, surface roughness of the ice, dielectric properties of the ice, the angle of incidence, and the aspect angle. The various shades of gray in a SLAR image correspond to relative amounts of backscattered radiation within the antenna's field of view. Light-toned (white) areas indicate areas of high backscatter and are associated with highly deformed areas (ridges, etc.). Dark-toned areas, on the other hand, represent areas of low backscatter and are associated with open water or smooth ice.

The resolution of SLAR is affected by two factors: (1) the energy beam width, which governs the azimuthal (parallel to flight path) resolution; and (2) the energy pulse length, which governs the range (perpendicular to flight path) resolution. The range resolution is improved by shortening the pulse length and increasing the frequency, while the azimuthal resolution is improved either mechanically or electronically. Systems using mechanical techniques are referred to as non-coherent or real aperture, while those using electronic techniques are called coherent synthetic aperture (SAR) systems. The images produced by SLAR systems are similar, but not identical to aerial photographs.

NASA, one of the agencies involved in the Great Lakes-St. Lawrence Seaway Navigation Extension Program, in cooperation with the U.S. Coast Guard (1978-79), has implemented a SLAR data collection system over the Great Lakes since 1971. The system is a Motorola AN/APS-94C non-coherent radar that operates in the x-band at a frequency of 9.245 GHZ. This system is equipped to map both sides of the aircraft at once and has a range resolution of 8 m and an azimuth resolution that varies proportionally from 45 m at a range of 5 km to 450 meters at 50 km (Schertler et al, 1975). The images are presented on a slant range at a scale of 1;1,000,000 (Fig. 5.1).
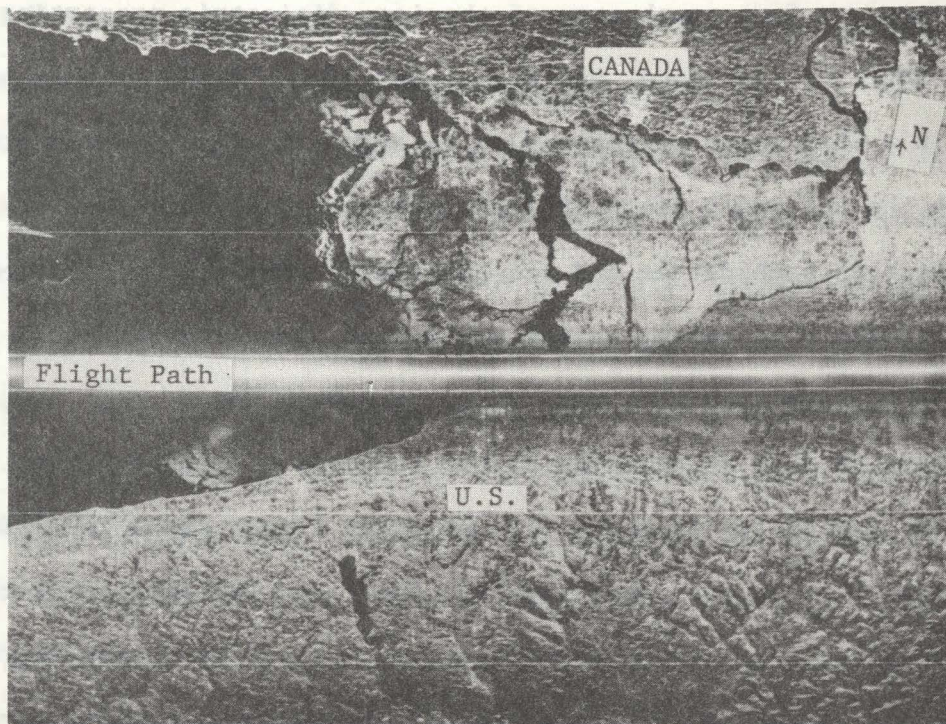
187

Figure 5.1 SLAR Image of Eastern Lake Erie.
(Scale: 1:1,000,000, Date: March 16, 1976)

SLAR flights by the Ice Navigation Center have generally been scheduled
to accommodate shipping interests on the Great Lakes. For example, during the
1975-76 ice season on Lake Erie, only the western basin was imaged during
the early ice season. During mid-winter five images of the entire lake were
recorded and later in the season, beginning in mid-March only the eastern
basin was imaged. The frequency of observations varied from 2-5 days and
depended, primarily, on the time of year. As far as SLAR images of the Great
Lakes are concerned, the Ice Navigation Center is the best available source.
Available SLAR data should prove to be useful in model calibration, even
though greater and more frequent coverage is desirable.

Pattern recognition and subsequent tracking of such patterns using SLAR imagery has been suggested as a method for estimating ice movement (Weeks, personal communication). The degree to which ice tracking can be accomplished using SLAR imagery will depend on the frequency of SLAR flights when tracking episodes are in progress, the quality of the image produced, and the satisfactory resolution of scale distortion that appears in the images. To illustrate the potential use of SLAR imagery for ice tracking purposes, three tracking episodes that occurred during the 1978-79 winter season are presented here.

Portions of the Lake Erie SLAR images obtained on March 7, 1979 and March 12, 1979 are shown in Figure 5.2. The circled ice floes are located south of Long Point, Canada. Line drawings of the selected ice floes are shown in Figure 5.4. During this same time period, several ice floes in the eastern basin have moved and rotated. The SLAR images for this region are shown in Figure 5.3 and the line drawings of the selected ice floes can be seen in Figure 5.3. It is interesting to note the relatively large displacement of the ice floes south of Long Point in contrast to the small displacement of the ice floes in the eastern basin. Apparently, the ice field was considerably more compacted in the eastern basin. It is also possible that the applied wind stress (magnitude and direction) was sufficiently different between these two locations so that this may also have been a factor.

An analysis of the wind record (see Figure 5.5) from the National Weather Service Meteorological Station at the Buffalo International Airport showed the winds to be somewhat variable from March 7, 8, 9, but on March 10, 11, and 12 a persistent and strong wind blew first from the southwest and then from the west. If this wind record is considered as representative of over lake winds on these days, then most of the ice movement probably occurred after March 9.
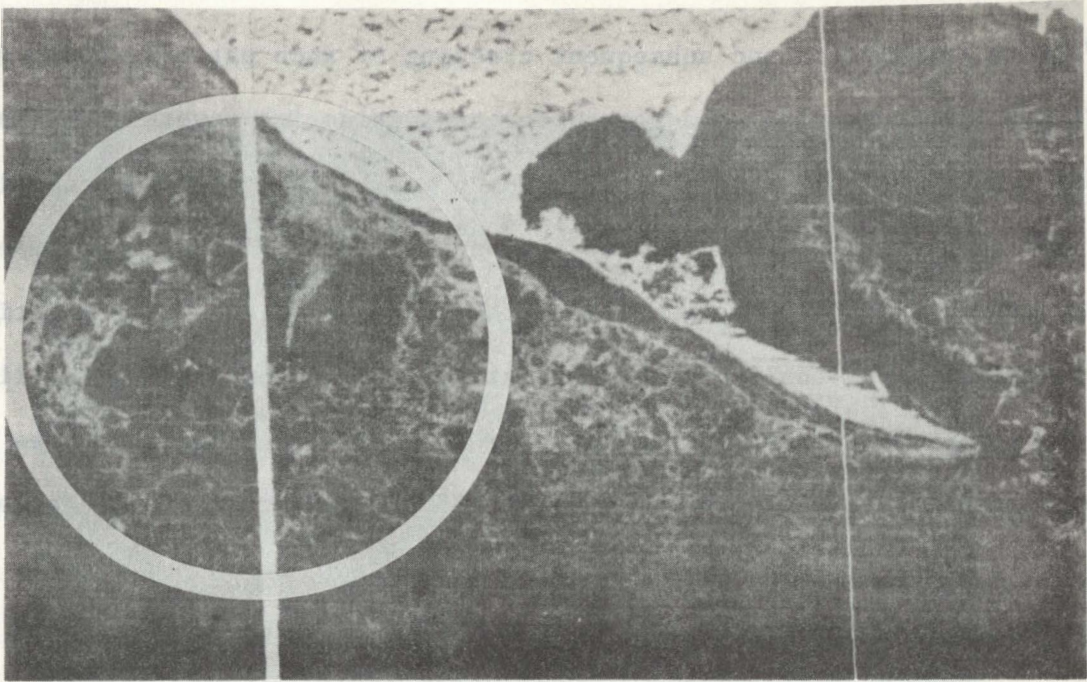
March 7, 1979
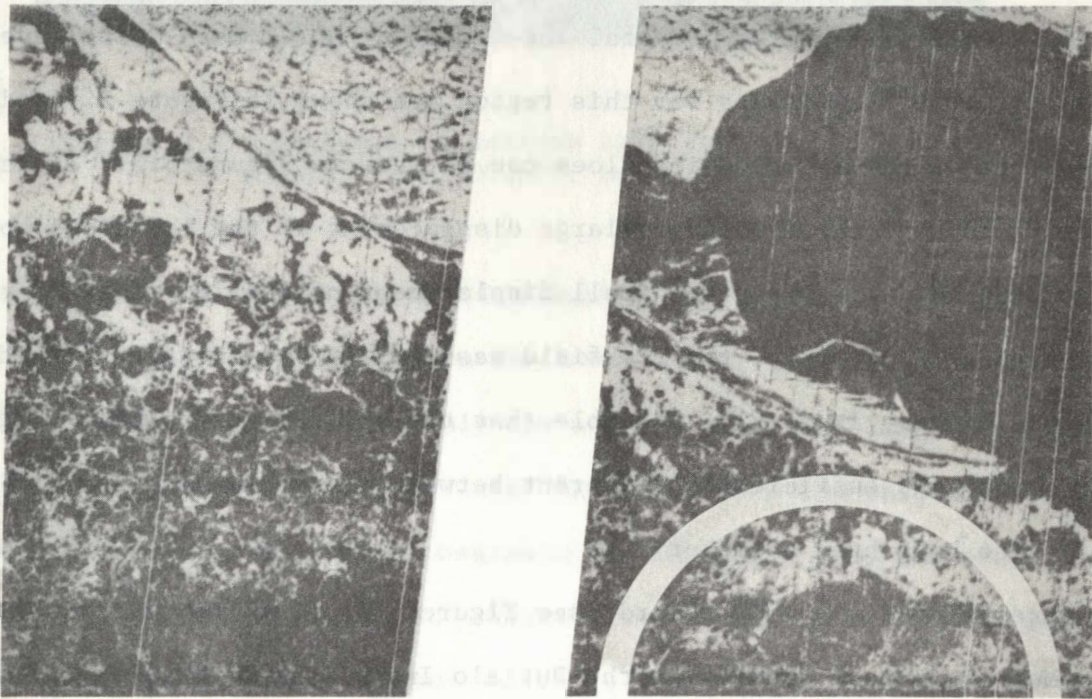
March 12, 1979

Figure 5.2 Lake Erie SLAR Images Showing Ice Field South
of Long Point, Canada on March 7 and March 12, 1979

190
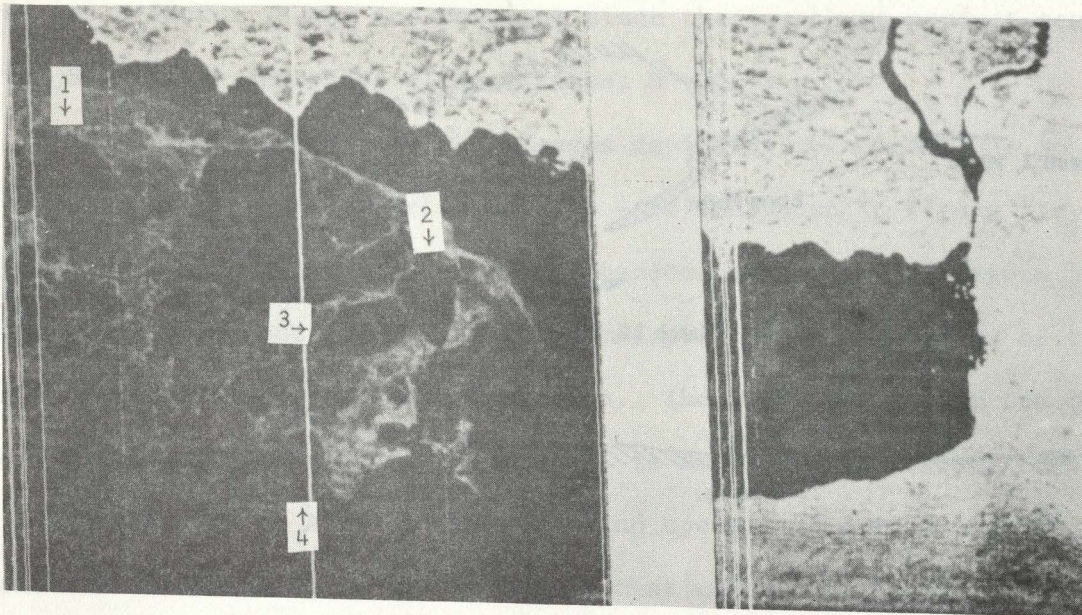
March 7, 1979
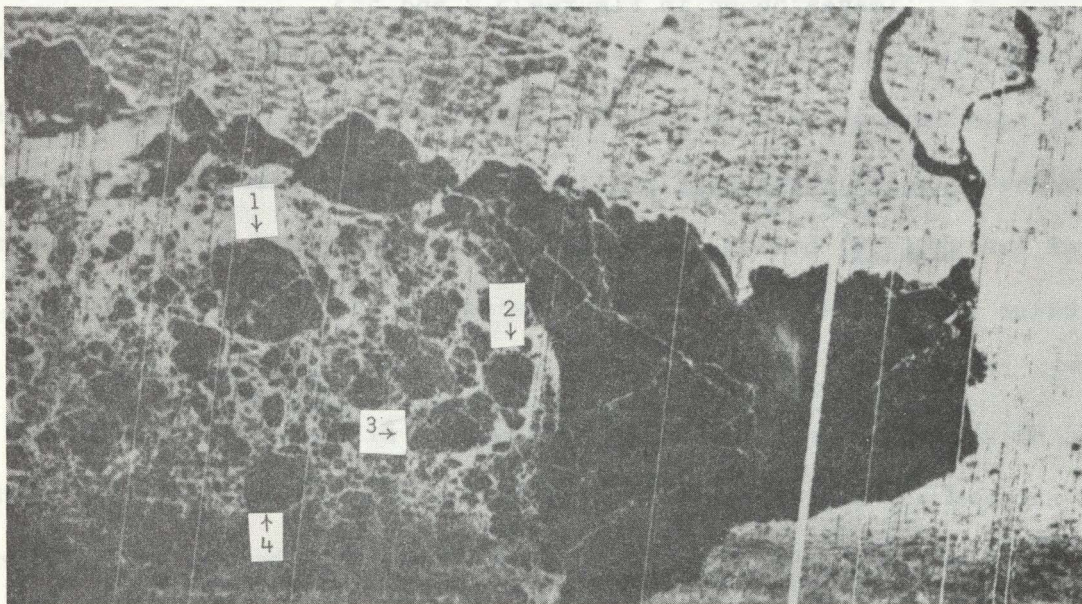
March 12, 1979

Figure 5.3   Lake Erie SLAR Images Showing Ice Field in
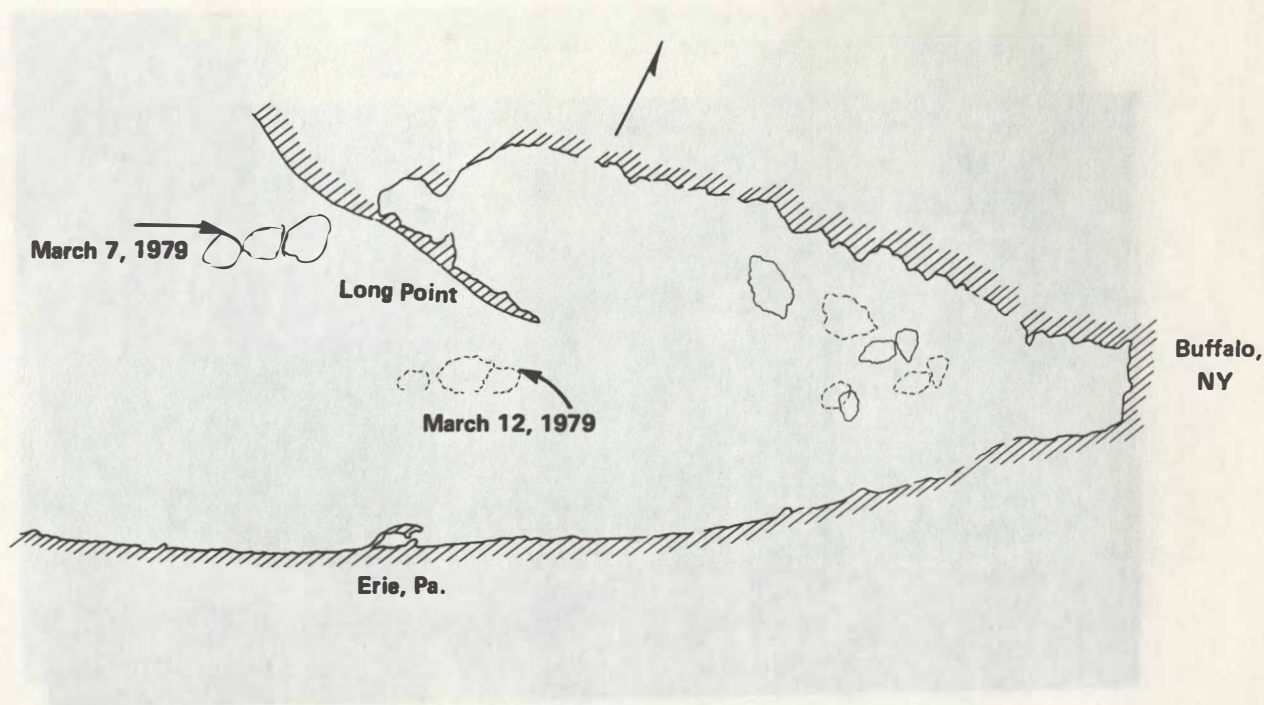Eastern Basin on March 7 and March 12, 1979

Figure 5.4 Line Drawing Replica of Selected Floes from SLAR
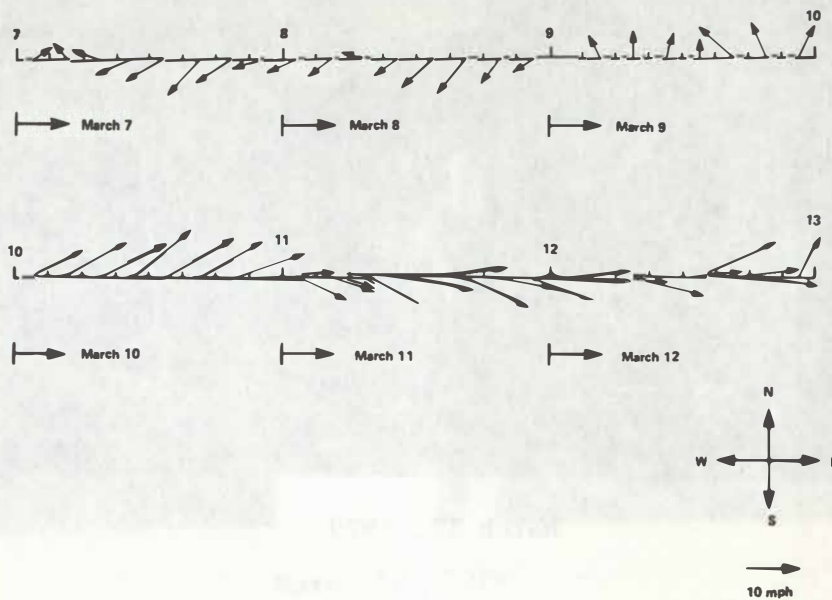Images Shown in Figures 5.2 and 5.3.

Figure 5.5 Wind Record from Buffalo, N.Y. National Weather
Service Station

The role of water currents is not known. It is likely that internal ice stress was a factor in the ice movement since the ice chart product accompanying the SLAR image indicated a compactness, N = 0.9.

Portions of the Lake Erie SLAR images depicting ice conditions in the eastern basin for the time period April 5 - 12 are shown in Figure 5.6. The interpretative line drawing for the same period can be seen in Figure 5.7. This particular episode illustrates the transport of an assemblage of rotting floes in an otherwise open water condition. The wind record from the Buffalo Airport for the time period, April 9 - 12, is shown in Figure 5.8. A strong west wind prevailed on April 6 (average wind speed = 26.3 mph) and was probably responsible for breaking up the ice field that existed on April 5, 1979.

A preliminary attempt was made to compute the trajectories of the two isolated ice floe assemblages from April 9 to April 12; however it became evident that the unknown water currents must have played a significant role in the force momentum balance equation. It was also discovered that the wind records obtained from the Buffalo Airport differed significantly from wind records obtained at Long Point for the same time period (Ecology and Environment, Inc., 1979). Thus, there was uncertainty in specifying the appropriate wind record to be used in the analysis.

The SLAR images shown in Figure 5.9 depict the ice conditions in the northern half of Lake Erie (including parts of the central and eastern basins) during the time period, January 27 to February 5, 1979. The daily averages for wind speed, wind direction and air temperature measured at the Buffalo airport are given in Table 5.1. The sequence shows the open water along the north shore created by winds having a strong component from the north followed by the formation of new ice as air temperatures dropped below freezing. The ice edge on January 27 has been compacted by January 29 due to a southward drift.
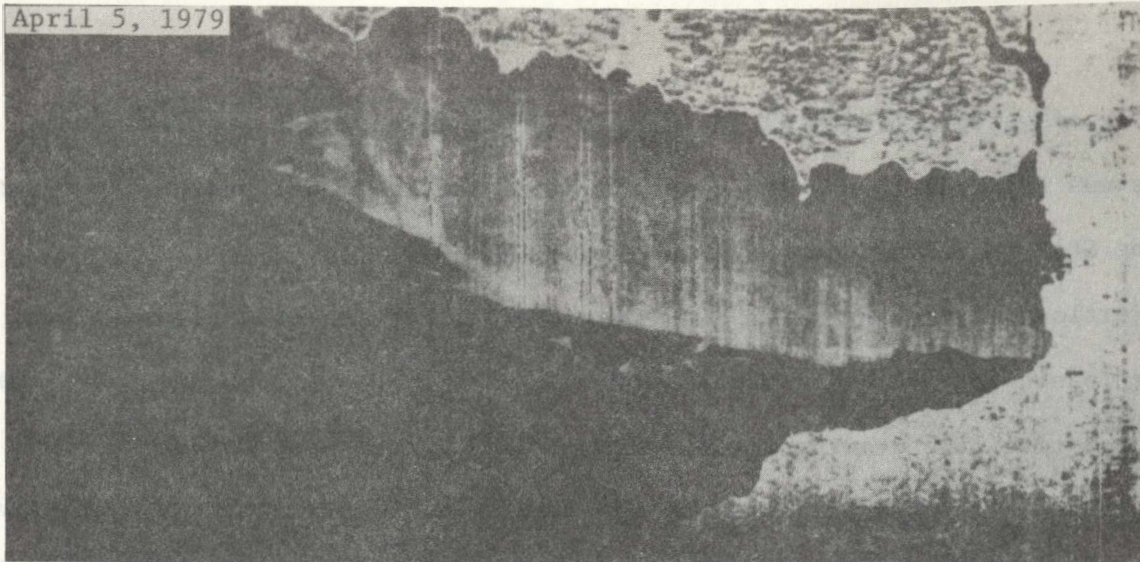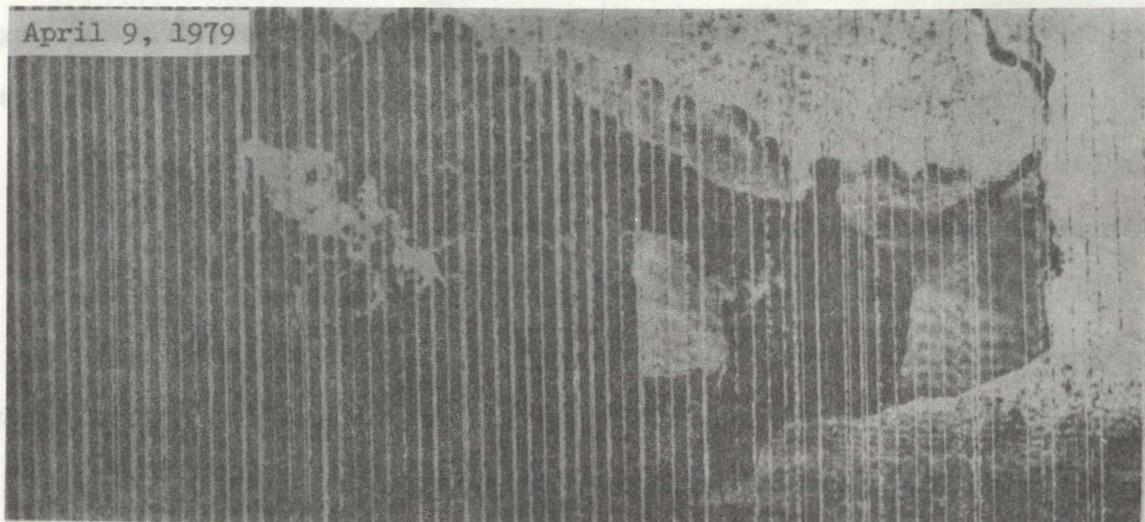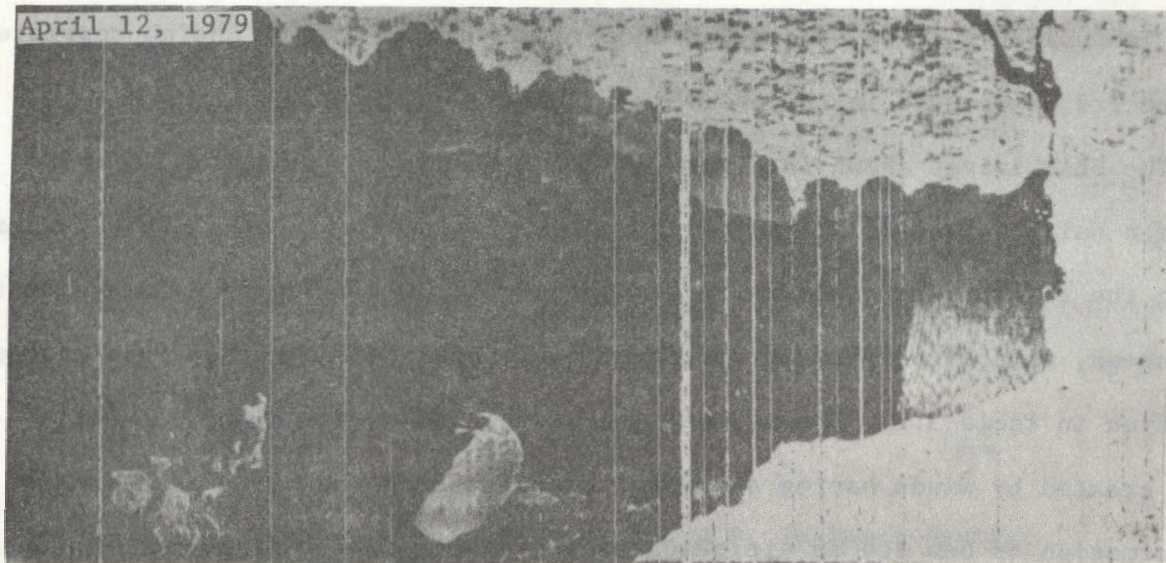
Figure 5.6   Lake Erie SLAR Images in Eastern Basin on April 5,7, and 12, 1979

194

Figure 5.7   Line Drawing Replica of Selected Floes from
             SLAR Images Shown in Figure 5.6
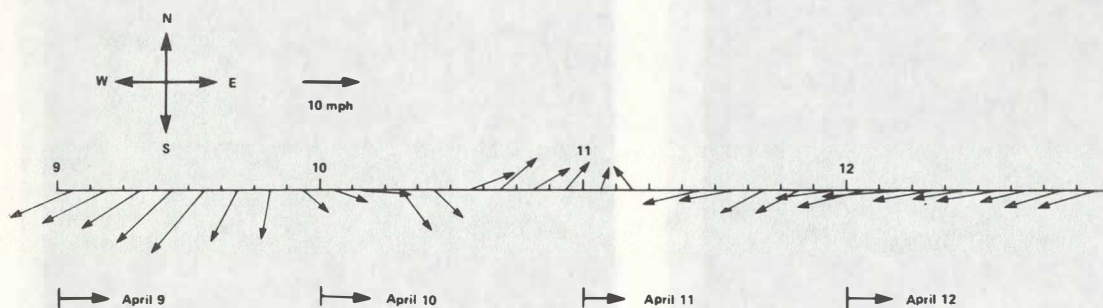
Figure 5.8   Wind Record from Buffalo, N.Y. National Weather
             Service Station (April 5 to 12, 1979)
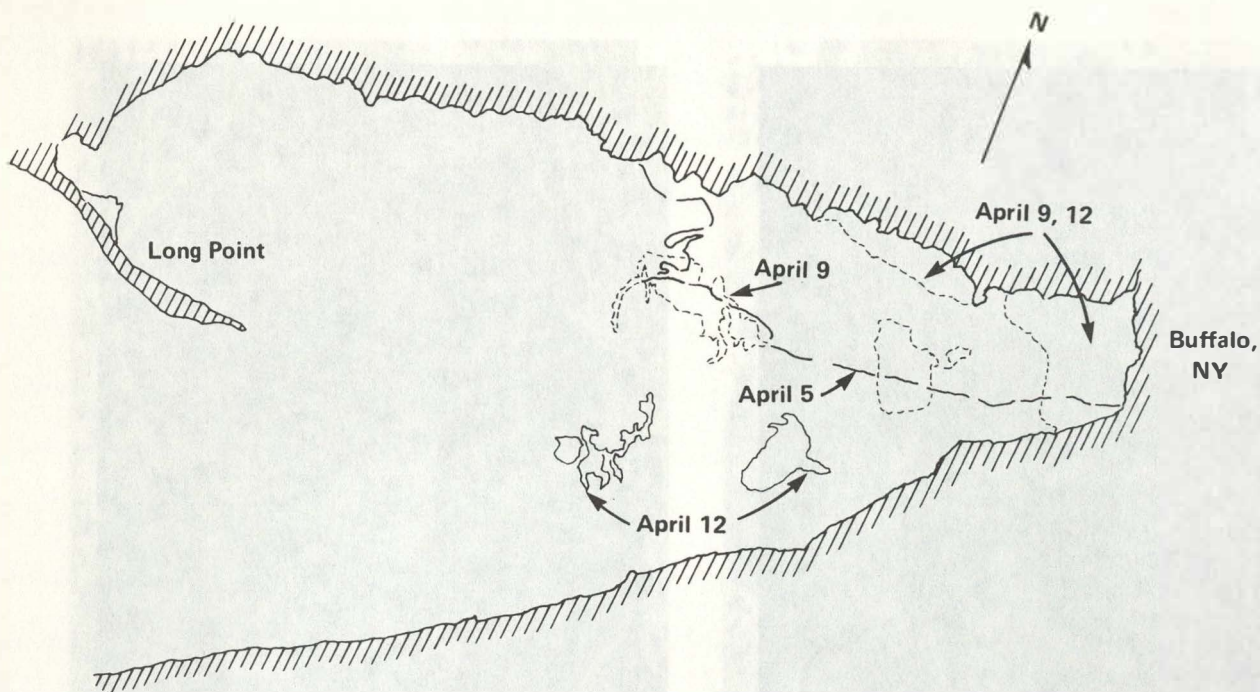
Jan. 27, 1979

Jan. 29, 1979

196
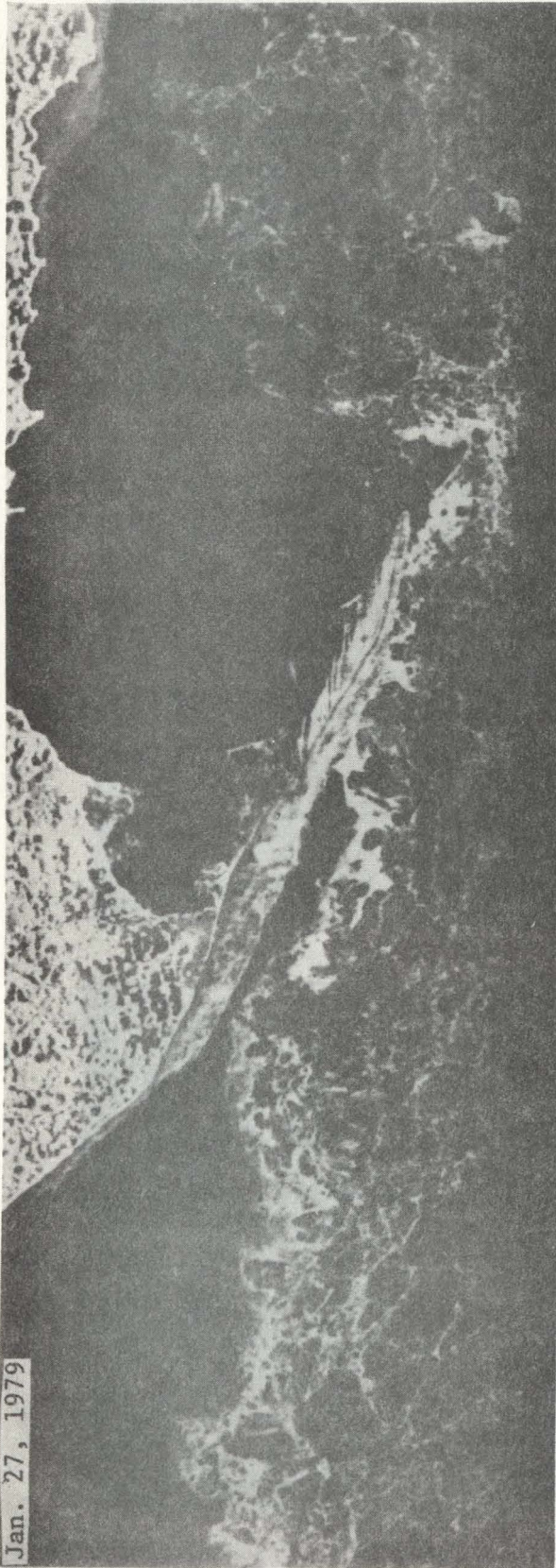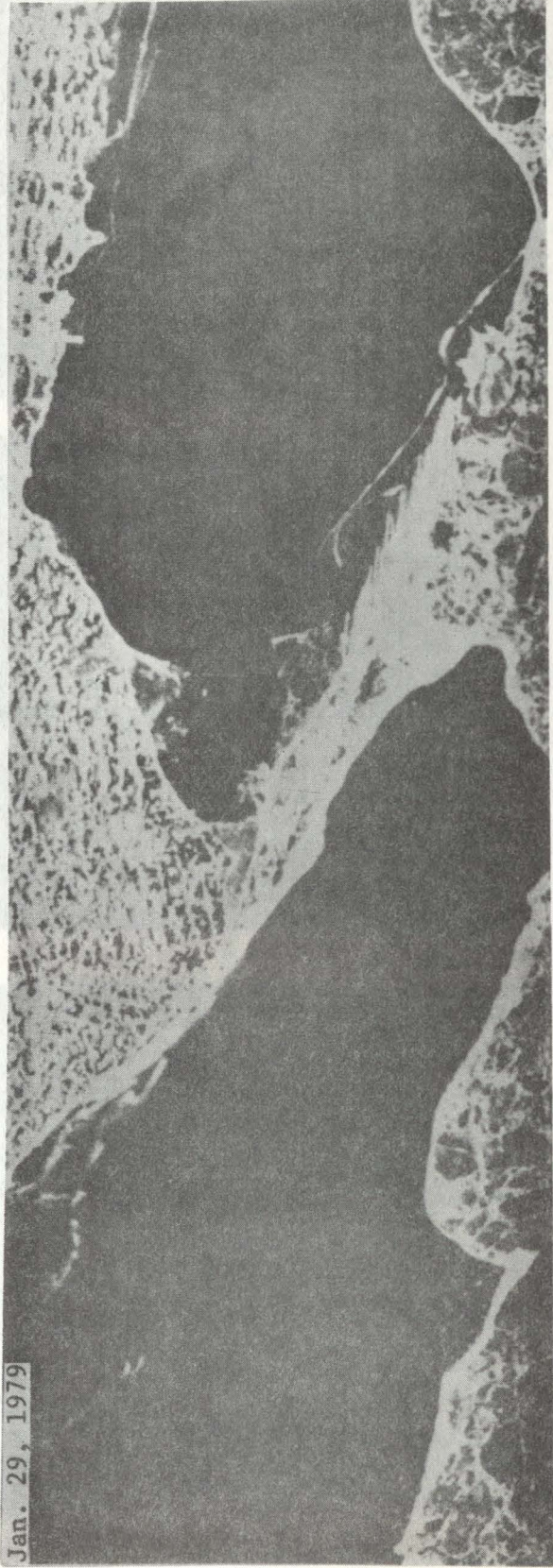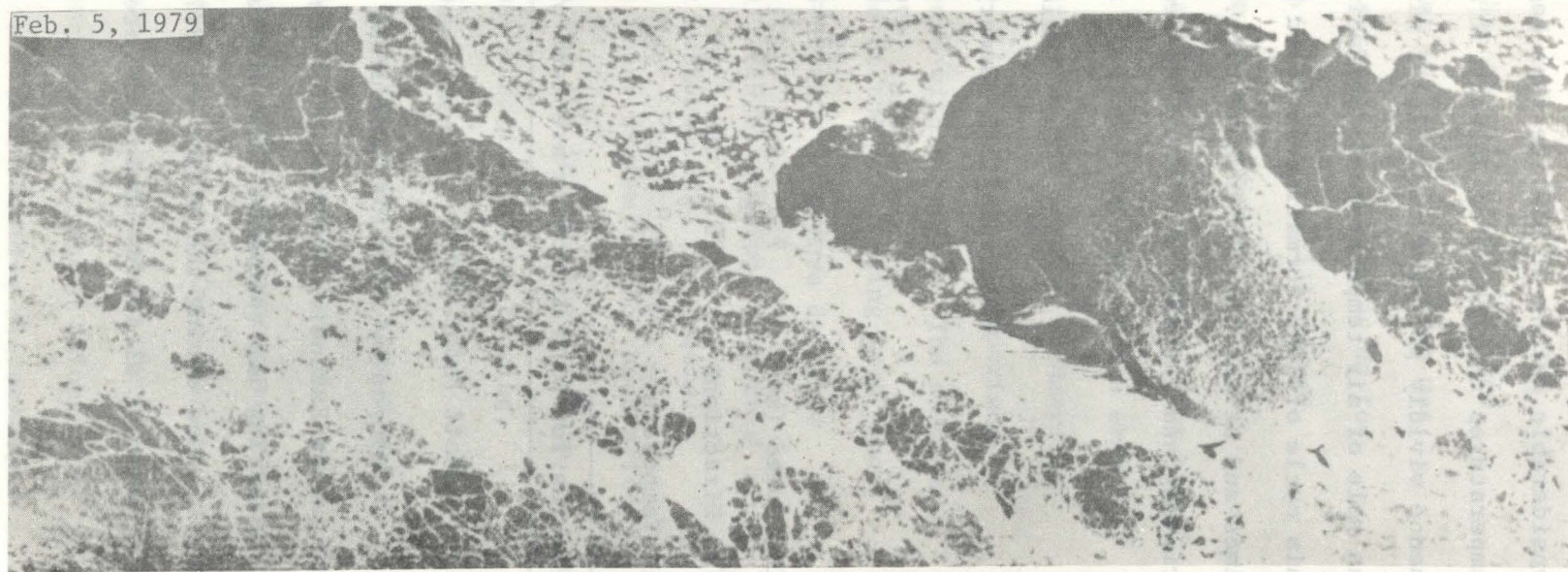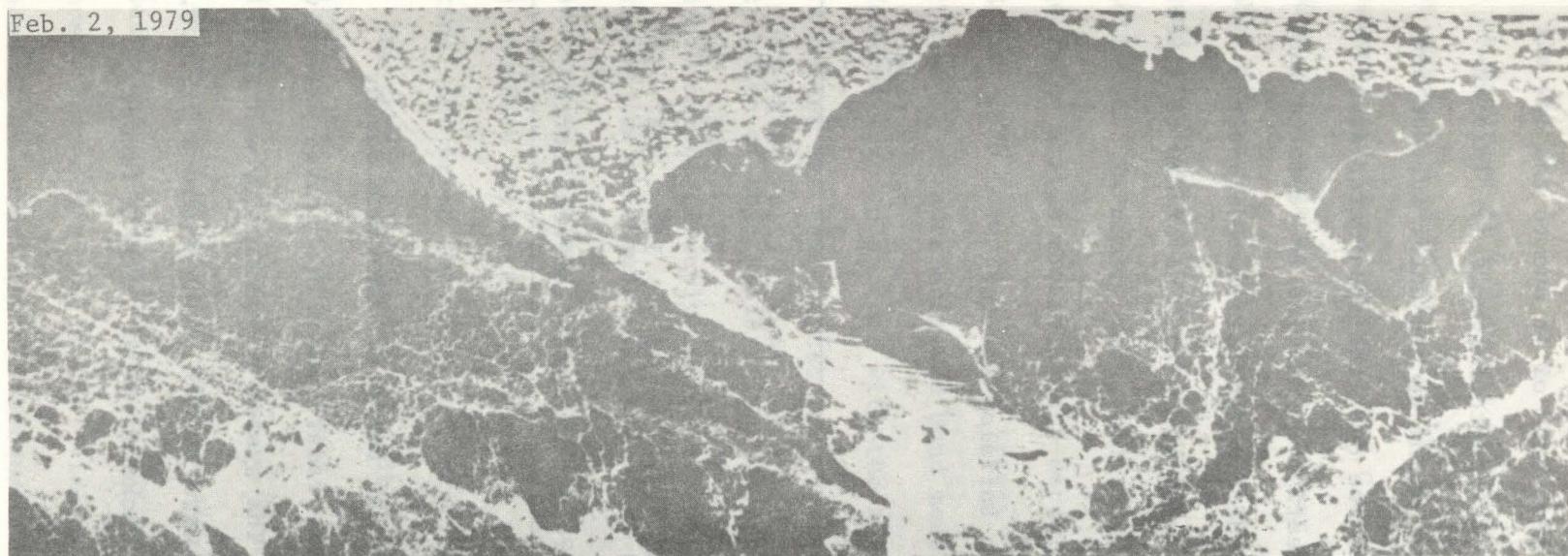
Figure 5.9 Lake Erie SLAR Images showing Central and Eastern Basins South of Canada
(Long Point is in center of image)

On February 5, the older compacted ice edge can still be seen along with the considerable extent of new ice that has formed north of it due to the low air temperatures that began on January 31 and extended to February 5. This sequence vividly portrays the role of wind in opening up new water surface and the role of air temperature in producing new ice over the open water area. This cycle of lead formation followed by creation of new ice is repeated many times and at many places in Lake Erie. The deformation of the ice cover (ridging and rafting) is strongly dependent upon these regions of new thin ice.

Table 5.1

Climatological Summary from Buffalo, New York

| | Jan. 1979 | | | | | Feb., 1979 | | | |
	27	28	29	30	31	1	2	3	4	5
Wind Speed (mph)	7.8	9.5	13.1	11.1	10.6	14.7	12.4	6.3	17.5	19.1
Wind Direction*	25	30	27	29	31	31	28	22	24	26
Air Temperature (^{O}F)	33°	32°	29°	26°	18°	16°	16°	14°	18°	8°

*Figures for wind direction are tens of degrees clockwise from true north

5.4.2 Short Pulse Radar

Developed by NASA for use during the Great Lakes-St. Lawrence Seaway Navigation Extension Program, the short pulse radar system has proved effective in measuring ice thickness from aircraft. The system's feasibility was first investigated during the winter of 1972-73, when it was flown aboard a U.S.C.G. helicopter at altitudes up to 100 meters. Vickers, et al (1973) report

that an accuracy of ± 2 cm was obtained in the case of an unbroken ice

layer thicker than 10 cm. For the next winter (1973-74) the system was

redesigned and flown aboard a U.S.C.G. C-47 aircraft at altitudes up to

2,300 m and speeds of 75 m/sec (Cooper et al, 1974). It still proved

capable of measuring thicknesses greater than 10 cm. However, lack of

"ground truth" prevented the accuracy and limitations of the system from being

established. To remedy this situation, NASA developed and operated a short

pulse radar system aboard an all-terrain vehicle on the Straits of Mackinac

in March, 1975 (Cooper, et al, 1975). This allowed accurate comparison

of the radar measurements and hand measurements with an auger. The maximum

difference was 9.8 percent with the magnitude of the error being less than

± 3.5 cm for ice thicknesses ranging from 29-60 cm. In a more detailed

description of this calibration, Cooper et al, (1976) conclude that this

accuracy can be directly applied to aircraft measurements. In general,

measuring ice thickness with the short pulse radar system has not been affected

by adverse weather and snow cover as long as the ice is relatively smooth.

Rain, surface meltwater, and surface roughness associated with ridging,

rafting, and brash ice, however, preclude measurement.

The short pulse system described above actually measures a time delay

that is converted to ice thickness. This time delay results from the single

frequency microwave radiation's (2.86 Hz; S-band) ability to penetrate snow

and ice but not water. At the ice-air or snow-ice interface (negligible

reflection occurs at air-snow interface) a partial reflection of the energy

occurs. This marks the initial time. The energy's propagation velocity is

reduced as it enters the ice because of the increased relative dielectric

constant, which for Great Lakes ice is approximately 3.1. At the ice-water
interface total reflection occurs and the time interval is recorded.
Modifying the time difference by a constant dependent on the dielectric
constant gives the ice thickness.

Results, to date, indicate that ice thinner than 10 cm cannot be measured
because the time delay becomes difficult to resolve. As long as the ice is
unbroken, thicker than 10 cm, and relatively smooth,accurate measurements can
be made. Rough ice, associated with ridges, etc., cannot be measured because
the surface reflections interfere with the ice-water reflections. Water on
the surface, as previously mentioned, negates measurement because the energy
is totally reflected before it reaches the ice.

Characterization of the ice thickness distribution needed for modelling
the ice dynamics of the Great Lakes seems possible using this technique.
Presently, thicknesses are almost always recorded along shipping routes
and are usually included in the SLAR image/Ice Product Area Charts supplied
by the Ice Navigation Center. A range of thicknesses pertaining to large
areal distributions is given in these charts, without regard to location.
At best, these could be used for estimating mid-lake thicknesses which would
otherwise not be available.

The advantage of this system is that it can cover large distances
expeditiously. With this capability, flight paths could be specified that
would, for the least possible expense, achieve an approximate definition
of the thickness distribution. The Great Lakes ice fields are almost always
broken, rafted, or ridged, in all or parts of its extent. Therefore,
estimates of thickness in these areas would be necessary. These estimates

could possibly be aided by correlating the radiation backscatter in the SLAR images with ice thickness. Difficulty would arise, however, when meltwater appears, either in the spring or during thaw periods.

5.4.3 Impulse Radar

Geophysical Survey Systems, Inc. (Hudson, New Hampshire) has developed an impulse radar system that can be considered the electromagnetic equivalent of marine subsurface profiling systems. The first application of this technique was reported by Campbell and Orange (1973) of GSSI, when both freshwater and sea ice thicknesses in the Canadian Arctic were measured to insure the safety of on-the-ice operations of oil companies and geophysical contractors. Another application of impulse radar is described by Dean (1977) in which the system was used to map accumulations of frazil and brash ice in the St. Lawrence River. The principle difference in these two applications was the location of the sensor relative to the ice surface. Campbell and Orange operated from an all-terrain vehicle traveling at 4-5 km/hr on the ice, while Dean operated from a helicopter a few meters above the ice surface at speeds of 75-110 km/hr.

The impulse radar system operates, basically, on the same principle as the short pulse radar. The time delay between interfaces is measured and then calibrated according to the dielectric constant of the ice, which is relatively constant for freshwater ice. Calibration can, also, be accomplished by direct measurement of ice thickness. The most significant difference is that the energy pulse from the impulse radar is broad banded (many frequencies) instead of the single frequency employed by the short pulse system. This characteristic enables penetration through water, such as surface melt or lenses between rafted ice floes. This is not possible with the short pulse system.

201

Campbell and Orange determined the system's accuracy to be on the order of 5-10 percent for freshwater ice. They also discovered that operation on freshwater ice presents fewer calibration and interpretation problems than on sea ice. The accuracy of Dean's system was comparable (7-15 percent). Some interpretation error is present in Dean's results, however, because the antenna employed was not designed for aerial use but for on-ice use (same type used by Campbell and Orange). Aerial operation introduced significant reflection noise into the data. Campbell and Orange recorded thicknesses much greater (on the order of meters) than those usually encountered in the Great Lakes. Dean's measurements ranged up to 20 feet, including the frazil accumulation, with surface ice ranging from 1-2 feet.

Presently, ice thickness measurements, using the impulse radar technique, are not routinely available for Great Lakes ice. The system's capability to penetrate water could prove useful during the dissipation season, when melt water may inhibit the use of the short pulse system. Thickness measurements of rafted, ridged, or brash ice areas also become feasible. The major drawback to the system, as it is presently designed, is its limited areal capability. This problem may be remedied if the system can be designed specifically for use aboard an aircraft.

5.4.4 Laser Instrumentation

Quantitative characterization of sea ice roughness has been demonstrated by airborne laser profilers. A preliminary analysis (Ketchum, 1971) of Arctic sea ice profiles, obtained by the Naval Oceanographic Office in 1968, revealed that laser profilimetry could provide quantitative data related to temporal and spatial distributions of ice type (first year vs. multi-year), ice ridges, and leads. In a later study, Tooma and Tucker (1973), through a statistical

202

analysis of digitized data, compared laser and stereophotogrammatic sea ice profiles and found that ice roughness details are described very well by the laser (Figure 5.10).

In a power spectrum analysis of the same profiles as those presented by Ketchum (digitized form), Hibler and LeShack (1972) present a technique for differentiating first and multi-year ice based on spectral densities.

Laser Profile
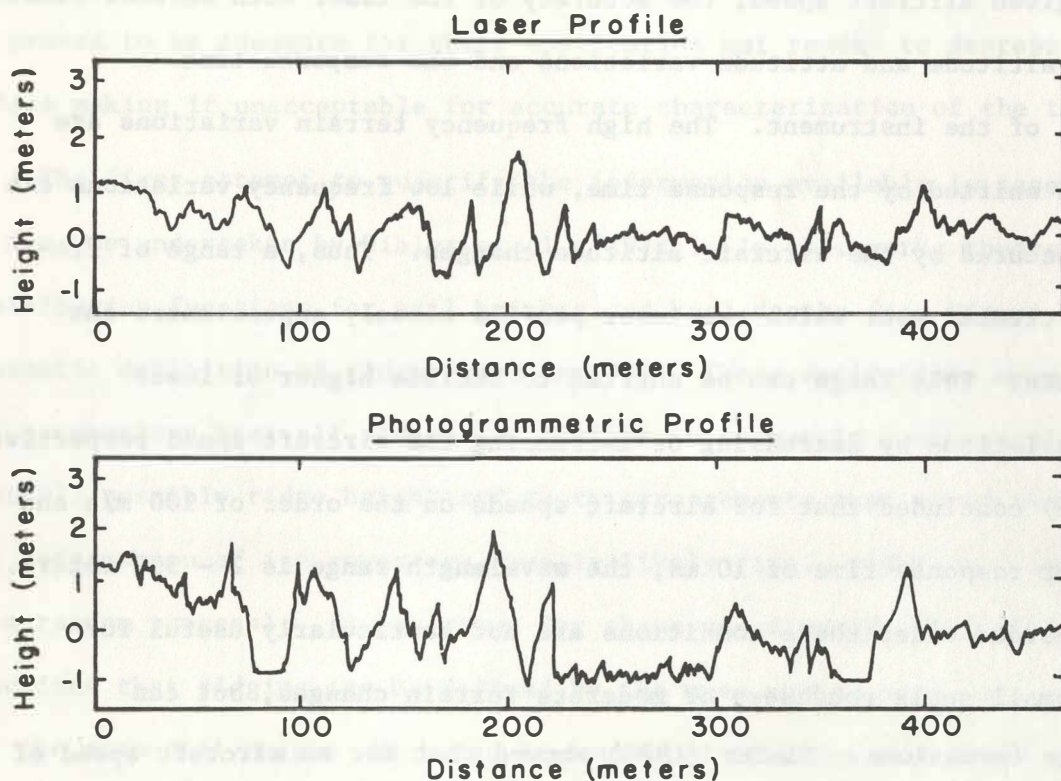

Photogrammetric Profile

Figure 5.10   Comparison of Computer Derived Laser and Photo
Profiles (after Tooma and Tucker, 1973)

This would not apply to the Great Lakes since they form annual ice covers. However, the spectral analysis approach was used by Banke and Smith (1973) to estimate wind stress over relatively unridged sea ice and could prove applicable to the Great Lakes.

To date, the profiler used to collect the majority of sea ice data has been a continuous wave laser altimeter (Geodilite 3A) manufactured by Spectra Physics, Mountain View, California. The instrument to ground distance is measured by the phase delay between the transmitted and reflected amplitude-modulated laser beam. The emitted beam is about 20 mm in diameter and has a divergence angle of less than 10^{-4} radians.

For a given aircraft speed, the accuracy of the laser data becomes limited by aircraft altitude and attitude variations and the response time (adjustable) of the instrument. The high frequency terrain variations are smoothed and shifted by the response time, while low frequency variations are partially obscured by the aircraft altitude changes. Thus, a range of frequencies is created over which the laser profile closely approximates the actual terrain. This range can be shifted to include higher or lower frequency variations by decreasing or increasing the aircraft speed respectively. Hibler (1975) concluded that for aircraft speeds on the order of 100 m/s and an instrument response time of 10 ms, the wavelength range is 2 - 300 meters. Profiles recorded under these conditions are not particularly useful for describing small scale roughness or moderate terrain changes, but can resolve ridge formations. Hibler (1975) showed that for an aircraft speed of 100 m/s, an optimum vertical accuracy of $\pm$ 10 cm resulted for an instrument response time of 10 ms and that shorter and longer response times decreased the accuracy.

Although others exist, two methods have been employed to reduce the error imposed by variations in aircraft altitude. Altitude variations in the profiles analysed by Ketchum (1971) were resolved to within 0.15 m by simultaneously detecting vertical atmospheric pressure changes with a

differential pressure transducer. It was pointed out by Hibler (1975), however, that horizontal pressure variations can decrease the resolution of this technique an additional 0.16 m, thus reducing the acceptability of the results. To eliminate the errors inherent in this technique, Hibler (1972) developed a three-step digital filtering procedure to remove altitude variations (Fig. 5.11). In their power spectrum analysis, Hibler and LeShack (1972) removed altitude variations using a standard high pass filtering procedure. It proved to be adequate for their application but tended to depress high ridges making it unacceptable for accurate characterization of the terrain.

The first attempt to quantify the information available in laser profiles of ice was undertaken by Hibler et al, (1972). In this work, theoretical distribution functions for sail heights and keel depths (see Figure 5.12) for schematic definition of ridge) were derived. These derivations were based on the assumptions that all ridges are similar in geometric cross section and that all possible ridge height and depth arrangements that yield the same net deformation of ice cover are equally likely (i.e., ridging is assumed to be a random process). It was shown for these one-dimensional distribution functions that ridging can be defined by the mean number of ridges per unit length and the mean sail height which can be extracted directly from laser profiles.

Based on a comparison of laser and sonar profiles of Arctic sea ice, Hibler (1975) showed that the keel depth, d, is related to the sail height, h, by d = 6.58 (h + 0.17 m). Weeks (1976) discusses this sail height/keel depth ratio and reports cored ridges give an average ratio of 1/5.

205
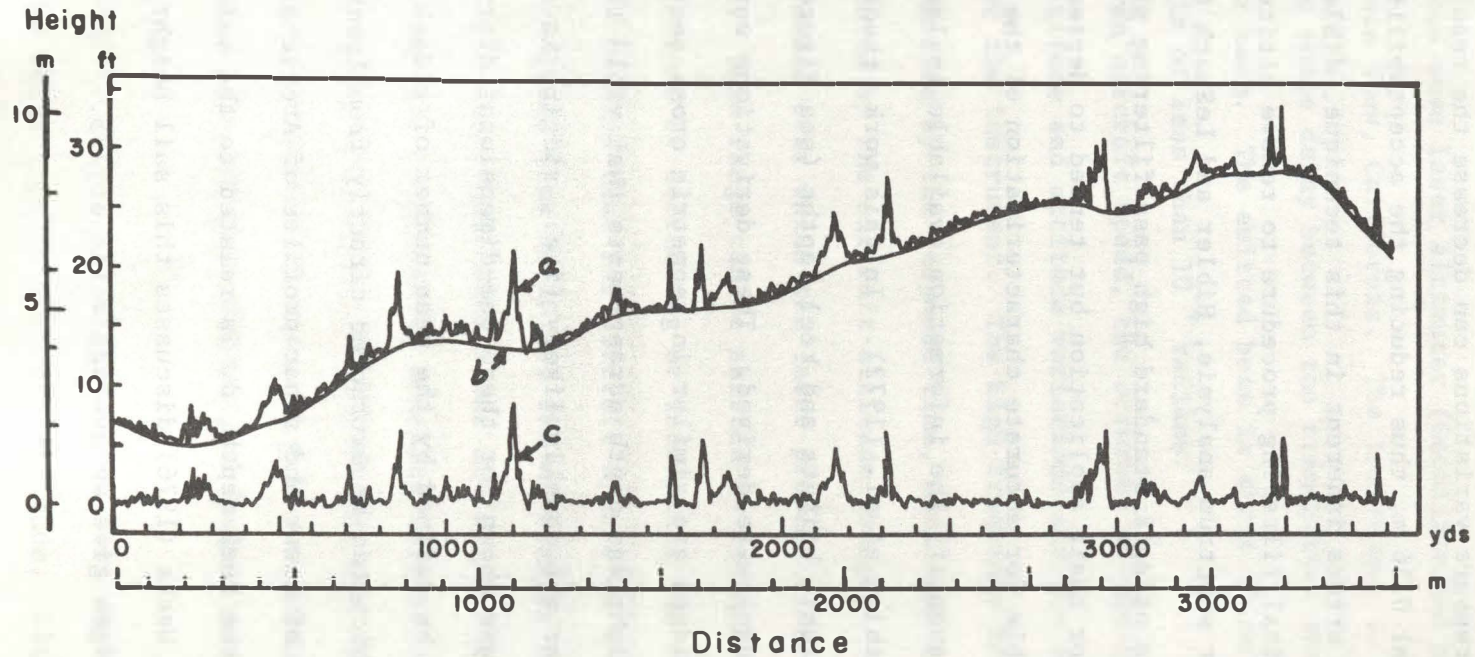
Figure 5.11 Results of Applying the Three Step Filtering Process. Curve a is the Unfiltered Profile, Curve b is the Estimated Aircraft Motion Obtained by the Three Step Filtering Process, and Curve c is the Resulting Ice Profile, When Curve b is Subtracted From Curve a (after Hibler, 1972).
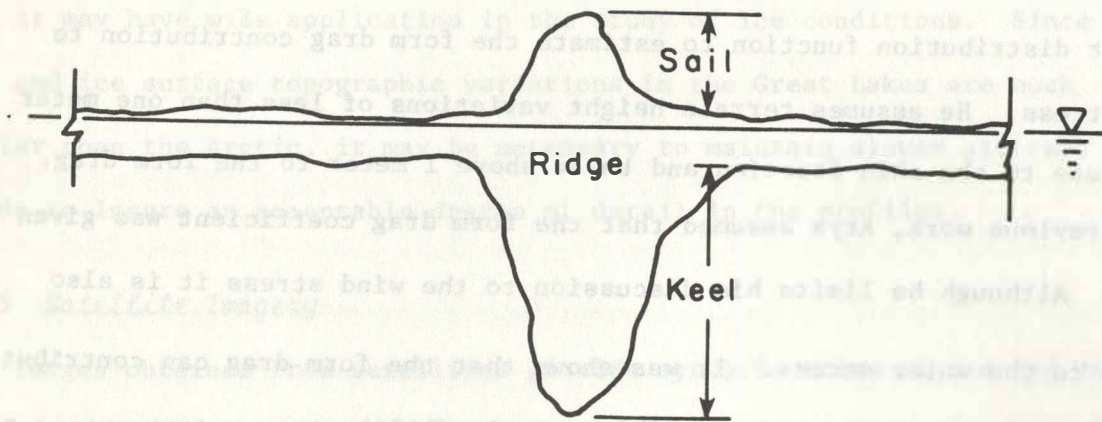
Figure 5.12 Schematic Representation of Ridge Cross Section

In an effort to predict maximum sail heights (thus keel depths) Wadhams (1976) suggests that the assumption of geometric similarity between ridges is not entirely valid. The effect being that shallower (those with gentler slopes) ridges in a certain height range are lost to lower height classes and steeper ridges to higher classes. Based on this assumption, more high ridges will be observed than predicted by the random distribution model. In an analysis of laser profiles obtained over the Beaufort Sea in 1974, Wadhams found this to be the case.

In a two-dimensional treatment of ridge spacing distribution derived by Hibler et al (1972), Mock et al (1972) confirm its usefulness and validity. In general, the average number of ridges per unit length varies with direction, but a mean value can be estimated from a series of randomly oriented traverses of a laser profile, aerial photographs, or SLAR images. This mean value is then shown to be related to the ridge density (total length of ridges per unit area)

207

Arya (1973) combines the concept of ridging density and Hibler et al.'s (1972) sail height distribution function to estimate the form drag contribution to the wind stress. He assumes terrain height variations of less than one meter to contribute to the skin friction and those above 1 meter to the form drag. Based on previous work, Arya assumed that the form drag coefficient was given by $C_D \approx 0.4$. Although he limits his discussion to the wind stress it is also applicable to the water stress. It was shown that the form drag can contribute significantly to the total stress. Hibler et al, (1974), in a modification of earlier work (Hibler et al, 1972), defines a ridging intensity parameter in which the number of ridges per unit length is dependent upon the specification of a minimum ridge height. Thus, the ridging intensity would be found to decrease as the cut-off ridge height was allowed to increase. The application of this concept gave comparable results to the earlier work on ridge spacing distribution.

Banke and Smith (1973) used a spectral density approach to estimate wind stress over relatively unridged ice. By integrating the power spectrum obtained from the laser profile data, they were able to relate a so-called "spectral roughness" to the wind stress coefficient. Hibler (1975) further showed that the ridging intensity parameter could be related to this so-called spectral roughness. This use of profilimetry data could lead to a rapid and accurate method for estimating wind stress coefficients.

Weeks et al, (1977) used a laser ranging system to study the motion of pack ice in the vicinity of Prudhoe Bay. The system had a maximum range of 12 km with a nominal accuracy of $\pm$ 5 mm. This high resolution enabled the detection of relatively small movements of fast ice.

The capability of laser profilimetry and laser ranging for rapid and accurate measurement of ice surface roughness and ice displacement suggests that it may have wide application in the study of ice conditions. Since the area and ice surface topographic variations in the Great Lakes are much smaller than the Arctic, it may be necessary to maintain slower aircraft speeds to insure an acceptable degree of detail in the profiles.

5.4.5 *Satellite Imagery*

Images obtained from satellites provide synoptic views of ice and snow covered waterbodies at varying frequencies of coverage and resolution. Sensors mounted on the orbital platforms record both reflected radiation in the visible wavelength range and emitted radiation in the thermal infrared wavelength range. Visible and infrared images are now routinely used in the monitoring of ice and snow conditions in the polar regions (McClain, 1978).

The National Environmental Satellite Service, operates the environmental satellite systems of the National Oceanic and Atmospheric Administration. Two different types of satellite systems are presently in operation. The polar orbiters (NOAA 2,3,4,5, Tiros N, and NOAA-A) range from 12 to 14 orbits per day at altitudes of 1500 to 800 km. Fortuna and Hambrick (1974) have described the basic characteristics of the NOAA polar satellite system although the specific details have changed with each new satellite that is launched. The Geostationary Operational Environmental Satellite (GOES) orbiters (SMS-1, SMS-2, GOES-1,2,3) hover over the equator at desired longitudes and at altitudes of 36,000 km (Bristor, 1975; Nelson, 1975). The resolution of both of these satellite systems is 1 km. Visible images are restricted by clouds and darkness while the infrared images are restricted only by clouds. The cover jacket to this report shows a visible image of the Great Lakes region obtained from NOAA-4 satellite on March 24, 1977.

The National Aeronautic and Space Administration operates a satellite
system (Landsat series) with a resolution of .08 km, that provides the most
detailed images of ice cover conditions. However, its narrow swath width and
15 to 18 day period between return visits render it secondary to the NOAA
satellite systems which provide coverage at least daily.

The polar orbiters provide reasonably undistorted views of the Great Lakes.
The geostationary orbiters provide images of the Great Lakes which appear quite
distorted. McMillan and Forsyth (1975), Wartha (1977), and Quinn et al,(1978)
have utilized visible and infrared images from the NOAA satellite systems in
reporting the ice conditions in the Great Lakes. In general, the images from
these satellites enable estimates of the extent of the ice cover at different
times during the ice season. The presence of clouds frequently obscures por-
tions of the images and hinders the accurate mapping of the ice cover. The
images do not lend themselves readily for use in determining ice displacement
or rate of ice movement. However, snow covered ice and open water can be dis-
tinguished. During the later stages of the ice dissipation season, the
images provide fairly good records of areal extent of ice cover (on cloud free
days) in the eastern basin of Lake Erie.

Considerable effort has been given to the use of satellite images in the
study of Arctic ice drift (Nye, 1975; Weeks and Campbell, 1975; Muench and
Ahlnas, 1976; Markham, 1977; Neralla et al, 1977; Kane et al, 1975; Hibler et al,
1975; Sodhi, 1977; McClain, 1978). The full extent of the findings and the
description of the most successful techniques for analysis are not available.

5.5 Summary

Modern electronic surveillance equipment is enabling better estimates of
ice coverage, thickness, and movement. There are still questions involving
frequency of observation, resolution, calibration using ground truth measurements,

reliability, error estimates and equipment limitations. For the purpose of calibrating ice dynamics models, the most promising techniques appear to be SLAR and the impulse radar system for measuring ice thickness. More effort will be needed in providing ground truth for calibration of the remotely sensed data. Well-planned and well-executed studies of ice conditions in the field will be important for resolving ice behavior processes at a smaller scale than can be observed using remote sensing devices.

Use has been made of small scale physical models to study ice behavior and ice forces. Such models have generally been site specific. Michel (1978) and Kivisild and Iyer (1978) have discussed the requirements for similitude between model and prototype, scaling problems, the materials that can be used for simulating ice, and the operation of actual models. The use of real ice in undistorted models is generally recommended, but this requires an unusually large refrigerated space (such as that available at the Ice Engineering Facility, Cold Regions Research and Engineering Laboratory, Corps of Engineers, U.S. Army, Hanover, New Hampshire). Nevertheless, even when concessions are made (i.e., model distortion and simulated ice), well planned and well-executed scale models can provide important information. Scale models can assist in the analysis of ice phenomena and ice problems when the prototype situation is complex and the solution to the governing equations is either not possible or, if obtained, leaves a high level of uncertainty because of the assumptions made.

Thus, the observation of ice behavior and the collection of data occurs over a wide range of scales; from the synoptic views obtained with satellite sensors, to direct observation in the field either on or adjacent to the ice, and in the laboratory using small scale models that simulate, approximately, the real world.

VI. SUMMARY

Ice transport in the Great Lakes is governed by wind action, water
currents, lake surface tilt, coriolis force due to the earth's rotation, and
internal ice stresses. Governing equations for the transport of a multi-floe
ice field can be written in differential form if the conditions for the
continuum approximation are satisfied. These conditions are stringent and
the ice transport process will not likely be represented by the derived
equations at all times and at all places during the ice season. It is not
necessary to invoke the continuum approximation when the ice field can be
treated as a single ice flow or assemblage of floes behaving as a rigid body.
In this latter case, the internal ice stress is not a factor and the governing
equation is considerably simpler than those for the multi-floe ice field.

Although most of the forces affecting ice movement have been long
recognized, models employing the continuum approximation have only been
developed recently. Furthermore, the equations associated with these models
have been solved through the use of numerical methods and high speed electronic
computers.

These advances, as significant as they are, are limited by the inability
to adequately represent the internal ice stress. Calibration and verification
of the mathematical models, formulated to simulate the complex process of
ice transport and ice deformation, are hampered by inadequate information on
actual ice cover conditions and behavior. None of the proposed constitutive
laws for pack ice have been adequately tested for application to Great Lakes ice.

The transferability of constitutive laws developed for the "perennial"
Arctic pack ice to an "annual" lake ice cover needs to be carefully investi-
gated. The uncertainty in the internal ice stress representation is compounded
by the uncertainty of its relative importance in the overall force-momentum
balance.

The above uncertainties will be reduced as more ice information becomes
available, from the trial and error experiences of applying mathematical
models to specific ice transport situations, and by improvements in our con-
ceptualization of the ice transport process. Related to these are some
important aspects that need continued study. They include the validity of
the continuum approximation, the representation of internal ice stress,
and the development of a suitable equation relating ice pressure to the state
of the ice cover. This latter question is especially important, particularly
in determining the force balance on an ice field that has come to rest
(static equilibrium) due to constraining boundaries.

Although thermodynamic effects on ice transport have been considered
(conceptually), this report has not dealt with them in any detail. Only the
physical aspects of the force-momentum balance and conservation of ice mass
were emphasized. The mass conservation equation, which allows for ice thick-
ness changes due to ice accretion or ice melt, is the link between the
thermodynamics and ice transport. This same equation also accounts for ice
thickness changes due to ice deformation. However, the mechanics of ridge
formation and ice rafting were not dealt with explicity. The special
problem of pressure ridges and grounded shore ice has not been adequately
dealt with. Such concentrations of ice pose one of the most severe situations

in terms of ice navigation. These additional processes remain to be treated
in the continued development of a complete ice dynamics model.

The coupling of ice dynamics models with both atmospheric and hydrodynamic
flows also remains to be done. At this stage, the wind and water currents
are treated as specified model input. Coupling ice dynamics models with
atmospheric and hydrodynamic flows is possible, conceptually; but the time,
effort, and cost involved may inhibit any serious effort to do this in a
generalized fashion. The development of this aspect is likely to occur when
specific problems develop in the Great Lakes.

The ice mass is one of the most important characteristics to be con-
sidered when modeling the response of an ice cover to applied stresses.
The ice mass distribution in a two dimensional sense, is determined from the
two relatively independent distributions of ice area and ice thickness. With-
out some reasonable conception of these distributions, any attempt to model
the dynamics of an ice cover may not be realistic. The use of side looking
airborne radar and the impulse radar system appears to be the most promising
approach for obtaining this information in the Great Lakes.

Application of the one dimensional and two dimensional simulation
models for ice transport, when judged to be adequate, requires input data
on wind and water currents. The former can be estimated from the network of
meteorological stations in the Great Lakes Basin. It may be necessary to
modify the wind data, in certain instances, to account for the differences
between overland and overlake wind characteristics. The water currents are
less likely to be known. Several approaches are available for estimating
water currents. These include direct measurement, hydraulic models, and

215

mathematical simulation. Under some conditions the water currents are small enough to be neglected in the overall force balance.

In the Arctic Ocean the concept of a steady-state ice drift has some validity based on observation and analysis. In contrast, ice movement in the Great Lakes results from highly variable weather patterns, is constrained by lake boundaries, and is much more influenced by the thermodynamic factors of ice accretion and ice melt. Ice transport calculations for specific wind episodes or for a series of episodes, in which the wind stress is time dependent, are most likely to provide only short-term forecasts. Specific episodes are estimated to have durations of one to three days. Estimates of stress coefficients can be made using data available from sea ice measurements. However, little information is available on the surface roughness of the Great Lakes ice cover. Although highly susceptible to deformation, the surface relief of Great Lakes ice is not as pronounced as that of the Arctic ice pack.

This report, although extensive, leaves many unanswered questions. An appreciation of the complexities and uncertainties of describing what little is known of the behavior of ice covers on a geophysical scale has been expressed in this report. This is not to deter continued development of ice dynamics models. Rather, it is hoped that this appreciation will aid in the judicious selection of the best avenues of approach to the development of Great Lakes ice forecasting models.

WIND STRESS AND WATER STRESS ON LAKE ICE

by

Jin Wu and Ernest Tang
University of Delaware

A.1 INTRODUCTION

Ice formation in the open water causes several important problems including navigation difficulties and damage to structures by large floating ice masses. The situation is especially serious for Lake Erie which has a comparatively narrow width and shallow depth. Consequently, the capacity for heat storage is small and ice can be formed to cover a significant part of the water surface, up to 100 percent at times (Richards, 1963; Assel, 1974). In order to solve these problems, it is desirable to have a thorough understanding of ice formation and its movement. The latter is governed by the forces acting on both upper and lower surfaces of the ice floes.

Theories on the motion of ice floes have been proposed at many different levels of complexity. In general, the stress at the air-ice interface $\vec{\tau}_a$, the stress at the ice-water interface $\vec{\tau}_w$, the Coriolis force $\vec{C}$, the gravitational force due to the tilt of the water surface $\vec{G}$ and the divergence of the internal ice stress $\vec{R}$ govern the movement. It is well known that the wind provides the main driving force on ice floes. The stress at the ice-water interface is another dominant force and usually retards the motion. Therefore, the stresses at the interfaces should be examined carefully.

Several experimental programs in the field have been carried out to relate the wind and water stress to wind or water speed and ice surface topography. The findings of these experiments are described here, and the data are futher analyzed in order to better estimate the wind and water stress acting on ice floes. The location of these field experiments are shown in Figure A.1.
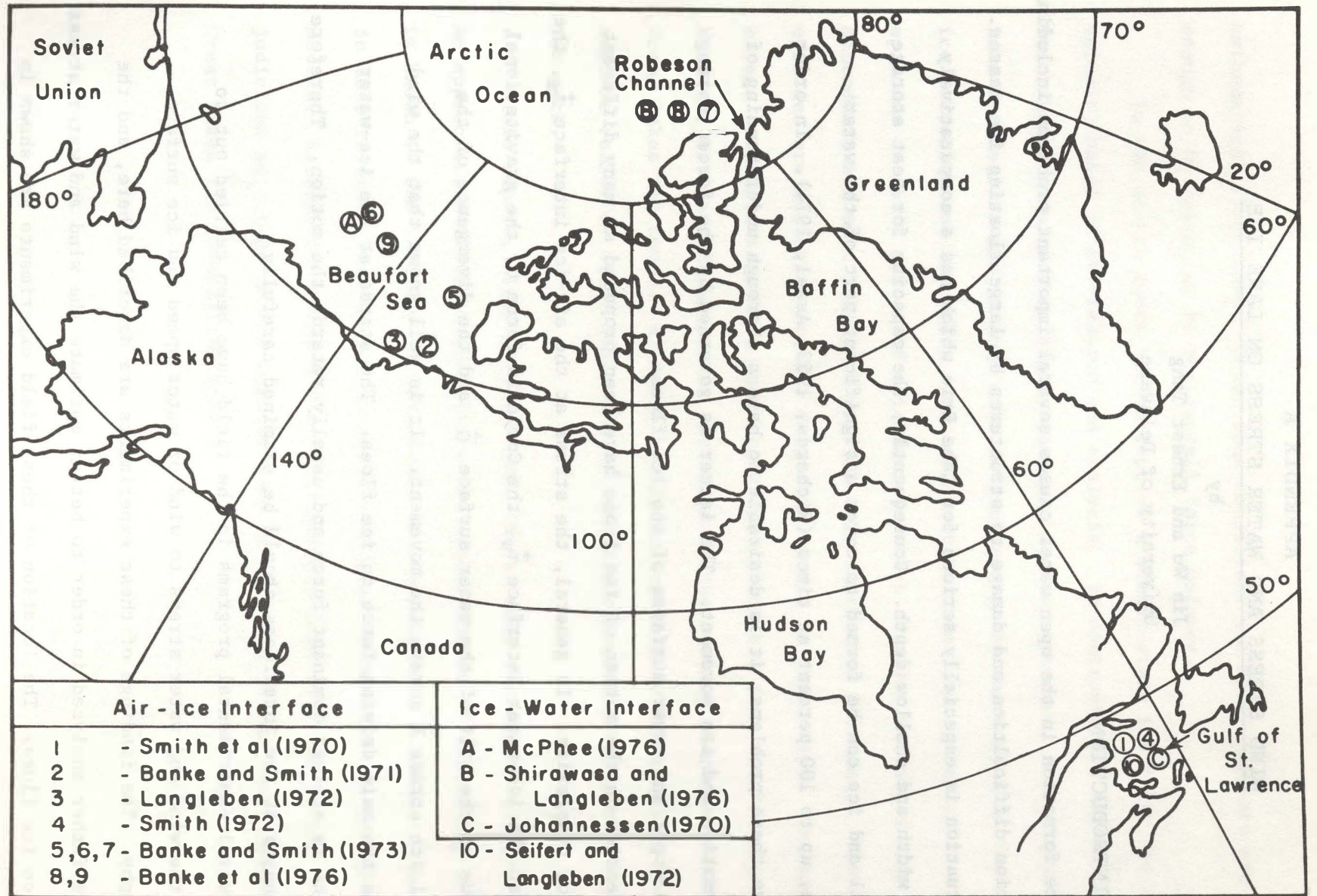
Figure A.1 Location of Field Experiments on Ice Movement.

A.2 LITERATURE REVIEW

The equation for ice motion can be written in terms of a unit surface area as

$$M_i \frac{D\vec{V}_i}{Dt} = \vec{\tau}_a + \vec{\tau}_w + \vec{C} + \vec{G} + \vec{R} \quad \ldots \ldots \ldots \ldots \ldots \ldots \ldots \ldots \ldots \quad (A.1)$$

where M_i is the ice mass and $\frac{D\vec{V}_i}{Dt}$ is the acceleration of the ice mass which is usually neglected. For simplicity, some of the forces may be reasonably neglected depending on the situation considered. The gradient force is often not a significant factor in the Great Lakes. The Coriolis force is well defined and in a simple form, $\vec{C} = M_i f(\vec{k} \times \vec{V}_i)$, where $f = 2\Omega \sin\phi$, Ω is the angular velocity of the earth, ϕ is the latitude, $\vec{V}_i$ is the velocity of the ice, and $\vec{k}$ is the upward normal direction from the horizontal plane. The wind and water drag on the ice may be separated into surface drag on relatively uniform terrain and form drag on isolated ridges.

A.2.1 ROUGHNESS PARAMETERS FOR THE AIR-ICE INTERFACE

The wind boundary layer developed along the upper surface of sea ice was surveyed by Untersteiner and Badgley (1965) at the United States Drifting Station Alpha. The observation was conducted at two sites located 2 km apart on an ice floe 2-4 meters thick. The surface was reported to be generally uniform and covered with snow or meltwater ponds. The nearest leads and prominent ridges were more than 500 meters away from the measurement sites. The wind velocity was measured by three-cup anemometers at 20, 40, 80, and 160 cm above the surface. They used the logarithmic profile method to determine roughness length z_o. The logarithmic profile for wind speed near a boundary is given by

219

$$\frac{\dot{V}_a(z)}{U_{*a}} = \frac{1}{\kappa} \ln\left(\frac{z}{z_o}\right) \quad \ldots \quad (A.2)$$

where $V_a(z)$ is the wind velocity measured at an elevation z from the air-ice

interface, U_{*a} is the wind friction velocity, and κ is the von Karman constant

which is usually considered to be 0.4. The physical situation is depicted in

Fig. A.2.

The data for z_o obtained by them were scattered, and the seasonal change

of z_o was obscured. There was a slight decrease of z_o with increasing wind

velocity. This variation of z_o was explained to be a consequence of change

of wind direction, since the snow surface was characteristically corrugated,

and a little change in wind direction would change the effective roughness

significantly. The average value of z_o was reported to be 0.02 cm.

Their results were further analyzed by Wu (1972). The drag coefficient,

at the air-ice interface, C_a, was calculated from the roughness length by the

relation

$$C_a(z) = \frac{\tau_a}{\rho_a[V_a(z)]^2} = \left[\frac{\kappa}{\ln(z/z_o)}\right]^2 \quad \ldots \quad (A.3)$$

where τ_a is the friction stress along the ice surface, ρ_a is the density of

the air. The velocity, $V_a(z)$, is measured at a height z above the ice surface.

The drag coefficient, $C_a(10)$, which is calculated based on the wind velocity

at 10 m above the surface, appeared to decrease with the increasing wind speed

when the velocity was lower than 3 m/sec and to reach a constant value of

1.6×10^{-3} at higher wind speeds. This observation was explained to result

from the snow cover acting similar to a sand bed. The air-ice interface might,

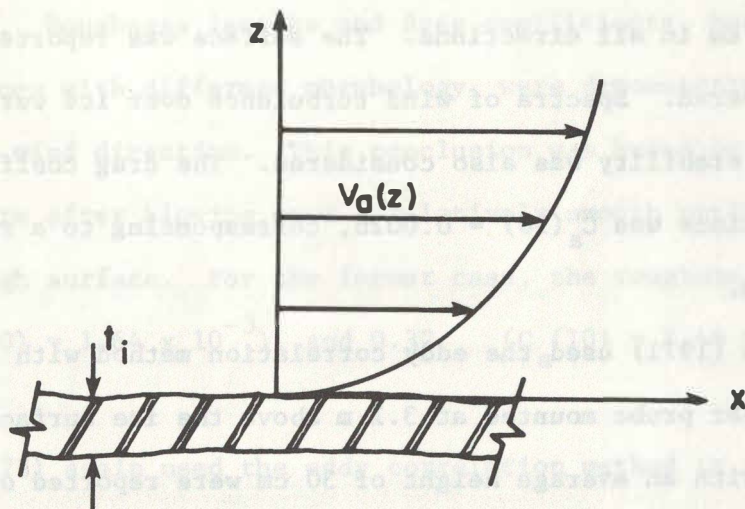therefore, be categorized as a loose boundary when snow covered.

Figure A.2 Diagrammatic Sketch of Air Flow Above an Ice Surface

Smith et al. (1970) used an eddy correlation method to measure the wind stress acting on the upper surface in the Gulf of St. Lawrence. The Reynolds stress, $\tau_z = \overline{u_x{}^* \, u_z^*}$, is measured at a height z above the surface. Here u_x^* and $u_z{}^*$ are the turbulent velocity fluctuations in the mean wind direction and in the vertically upward direction respectively. The bar denotes a time average. The drag coefficient and roughness length can be calculated from Equation (A.3) if τ_z is equal to τ_a.

An ultrasonic anemometer was mounted at 3.8 m above the ice floe that extended at least 5 km in all directions. The surface was reported to be uniform and snow covered. Spectra of wind turbulence over ice were examined and the atmospheric stability was also considered. The drag coefficient under neutral conditions was $C_a(10) = 0.0026$, corresponding to a roughness length, $z_o = 0.35$ cm.

Banke and Smith (1971) used the eddy correlation method with the anemometer-thermometer probe mounted at 3.1 m above the ice surface. Randomly distributed ridges with an average height of 30 cm were reported on the surface. The mean drag coefficient was 0.0026 ± 0.00023, corresponding to a roughness length of 0.33 cm. The drag coefficient appeared to decrease with increasing stability.

Seifert and Langleben (1972) analyzed the logarithmic profile at two sites on a floe measuring about 7.5 x 3.5 km^2 with nearly a 12 cm cover of slush snow. No evidence of ridges was found. The value of z_o for the first site was 0.084 cm, corresponding to $C_a(10) = 1.7 \times 10^{-3}$. For the second site, which was visibly rougher, z_o was 0.34 cm and $C_a(10)$ was 2.2×10^{-3}. Attempts to correlate roughness lengths and drag coefficients with wind speeds were unsuccessful. The roughness length was reduced within hours after the

initiation of precipitation, or on occasions when the air temperature just above the surface rose and remained above the freezing point for a period of more than several hours.

Langleben (1972) studied the roughness parameters of sea ice using the logarithmic wind profile. The ice cover was completely consolidated, flat, and unbroken, with a snow cover approaching 5 cm in thickness. The surface was flat for 1.5 km to the east with an adjacent heavily rafted floe approximately 5 m to the west of the site. The results were categorized by wind direction. Roughness lengths and drag coefficients, measured at a site between ice floes with different morphology, were demonstrated to differ in magnitude with wind direction. This conclusion was based on whether the wind reached the site after blowing over a relatively smooth surface or over a relatively rough surface. For the former case, the roughness length was 0.051 cm ($C_a(10) = 1.64 \times 10^{-3}$), and 0.32 ($C_a(10) = 2.48 \times 10^{-3}$) for the latter case.

Smith (1972) again used the eddy correlation method to measure the wind stress. The ice floe studied had a uniform surface extending for many kilometers in all directions. The drag coefficient was reported to be 0.00142 ± 0.0003.

Banke and Smith (1972) reported three other experiments measured by the eddy correlation method in the Beaufort Sea, the Arctic Ocean, and Robeson Channel. In the Beaufort Sea, $C_a(10)$ was reported to be 1.57×10^{-3}, and for one site with a visibly smoother surface, $C_a(10) = 1.13 \times 10^{-3}$. The terrains at the camps in the Arctic Ocean were reported to be generally flat, so the drag coefficient, $C_a(10) = 1.85 \times 10^{-3}$, was considered to be characteristic of an ice surface without pressure ridges. In Robeson Channel, about 20 percent

223

of the area was covered by irregular shaped melt ponds of fresh water each surrounded by a vertical wall about 0.2 - 0.5 m in height. $C_a(10)$ was found to be 2.1 x 10^{-3} at this site. The surface profiles and slopes of snow were surveyed. Surveyed lines were run upwind from the anemometer with the aim of correlating the roughness parameters with the root mean square (rms) elevation E or slope S of the snow cover (refer to Fig.A.3). Banke and Smith fitted two regression lines of $C_a(10)$ with E(cm) and S(m/m), i.e.,

$$10^3 C_a(10) = 1.2 + 0.026 \, E \quad \ldots \ldots \ldots \ldots \ldots \ldots \quad (A.4)$$

$$10^3 C_a(10) = 1.3 + 6.0 \, S \quad \ldots \ldots \ldots \ldots \ldots \ldots \quad (A.5)$$

Small ridges less than 1 meter high, occurring in the profile surveyed, were reported to be included in the measured drag coefficient by the regression equation (A.4). Larger ridges required special consideration.

Banke et al. (1976) published the results of experiments at Robenson Channel (1974) and Beaufort Sea (1975). A thrust anemometer and a microbead thermistor were mounted at a height of 1013 cm above the ice to measure the boundary layer turbulence at Robenson Channel site. The surface consisted of wet, slushy snow and numerous small, freshwater melt pools. The mean drag coefficient was 1.68 x 10^{-3}, which was less than the value 2.1 x 10^{-3} observed by Banke and Smith (1973) at the same site. The height of snow was also less. At Beaufort Sea, with a 10 m mast located at two sites on relatively flat ice, the drag coefficient was 1.27 x 10^{-3}, and on hummocked ice, the drag coefficient was 1.53 x 10^{-3}.

Surveys of surface elevation were made upwind from the anemometer tower during each experiment. Spectra of the surface elevation for the profiles
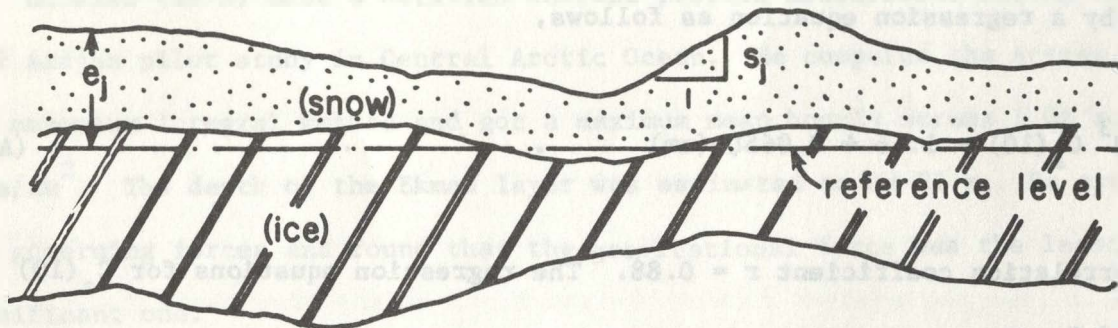
$$E = \left[\frac{1}{N} \sum_{j=1}^{N} e_j^2 \right]^{\frac{1}{2}} \qquad S = \left[\frac{1}{N} \sum_{j=1}^{N} s_j^2 \right]^{\frac{1}{2}}$$

Figure A.3   Ice Profile With Snow Cover (N=number of observations).

were made. The wavelengths shorter than 13 m, corresponding to the arbitrarily chosen wave number $k_o = 0.5$ rad/m, were considered to contribute to wind drag. The spectral roughness ω was defined to be the root mean square (rms) elevation at wavelengths shorter than 13 m and was calculated by integrating the power spectrum, $\phi(k)$, of surface elevation

$$\omega^2 = \int_{k_o}^{\infty} \phi(k)dk \quad \ldots \ldots \ldots \ldots \ldots \ldots \ldots \ldots \ldots \quad (A.6)$$

The data of Smith (1972), Banke and Smith (1973), and Banke et al. (1976) were fitted by a regression equation as follows,

$$10^3 C_a(10) = 1.16 + 0.065\zeta \text{ (cm)} \quad \ldots \ldots \ldots \ldots \ldots \ldots \ldots \quad (A.7)$$

with correlation coefficient $r = 0.88$. The regression equations for $C_a(10)$ on E and S were

$$10^3 C_a(10) = 1.16 + 0.032 \text{ E (cm)}, \quad r = 0.83 \quad \ldots \ldots \ldots \ldots \ldots \ldots \quad (A.8)$$

$$10^3 C_a(10) = 1.21 + 0.65 \text{ S (m/m)}, \quad r = 0.82 \quad \ldots \ldots \ldots \ldots \ldots \ldots \quad (A.9)$$

A.2.2 ROUGHNESS PARAMETERS FOR THE ICE-WATER INTERFACE

Untersteiner and Badgley (1965) measured the velocity profile below the bottom of the sea ice and obtained a value of $z_o = 2.0$ cm, corresponding to a drag coefficient $C_w(4)$ (based on the water velocity at 4 m below the ice) = 5.5×10^{-3}. The drag coefficient, $C_w(4)$, was found to be practically independent of water velocity.

Hunkins (1966) applied the Ekman layer theory to some observations taken

226

below the ice floe at Station Alpha. He found that the observations fitted the theory best if the boundary layer thickness was less than 2.0 meters. Hunkins' measurements gave a roughness length of about 1 cm.

Johannessen (1970) measured current profiles below ice floes in the Gulf of St. Lawrence and near the North Pole. He found that the roughness length of the lower surface had the same trend as observed for the upper surface condition. The roughness length z_o was 0.2 cm for smooth ice and 10 cm for rough ice. He suggested that the boundary layer thickness was about 0.6 - 1 m.

Hunkins (1975) made a detailed current profile measurement during the 1972 Aidjex pilot study in Central Arctic Ocean. He computed the stress by the momentum integral method and got a maximum mean hourly stress 1.66×10^{-3} dyne/cm^2. The depth of the Ekman layer was estimated to be 25 m. He evaluated the governing forces and found that the gravitational force was the least significant one.

McPhee and Smith (1976) reported the flow structure under pack ice during the 1972 Aidjex pilot studies. Local pressure gradient and advective acceleration due to topographic effects were included in their studies. The current friction velocity, U_{*_w}, was 1.0 ± 0.1 cm/s when the ice velocity relative to the ocean was 24 cm/s. Composite averages of nondimensional Reynold's stress and mean flow agreed well with mathematical models for a neutrally buoyant atmosphere. However, the lateral component departed from the predictions, indicating that the form drag associated with keel pressure was important. The maximum keel depth near the experimental sites was reported to be 5.3 m.

Shirasawa and Langleben (1976) used a three-component ultrasonic current meter to obtain measurements of current fluctuations in the frictional

227

boundary layer under an ice cover in Robeson Channel. The observations were obtained during a period when breakup of the ice cover was imminent. Summer melt had reduced the thickness of the flat first-year ice. The drag coefficient was computed as 3.25×10^{-3}.

A.2.3 RIDGE EFFECT

Arya (1973) tried to evaluate the form drag caused by ridges on the ice cover. The form drag per unit length, f_D, of a ridge oriented normal to the wind direction was calculated from

$$f_D = \frac{1}{2} \rho_a h \, C_D \, [V_a(z)]^2 \quad \ldots \quad (A.10)$$

where ρ_a is the density of air, h is the ridge sail height, $V_a(z)$ is the wind velocity of the undisturbed flow at height h, C_D is the drag coefficient of the ridge and was selected to be 0.4 based on laboratory results.

In his analysis, Ayra (1973) assumes pressure ridges to be randomly oriented and can be characterized by ridging density, R_D (total length of ridges per unit area). The total form drag, F_D, per unit area can be evaluated from

$$F_D = \frac{R_D}{\pi} \int_{h_o}^{\infty} f_D \times p(h) dh \quad \ldots \quad (A.11)$$

where p(h)dh is the probability that a given sail height is between h and h + dh. The error function type probability density function was suggested by Hibler et al. (1972) based on the assumption of random orientation of pressure ridges and geometric similarity of ridge shapes. The drag due to the small ice hummocks or ridges with height less than h_o is included in the effect of skin friction.

228

Arya (1975) developed a drag partition theory for determining the large-scale roughness on pack ice. This concept incorporates a roughness length measured at the ice surface, between ridges, to estimate the skin friction drag. This drag was considered to be less than the drag occurring over a surface without ridges, because of flow separation behind the ridges. The form drag, created by a roughness length related to the ridge distribution, is then added to the skin friction drag to obtain the total stress. Conceptually, the total stress is associated with an "equivalent roughness length", z_e.

Ayra (1975) described the ridge characteristics with two parameters, a roughness concentration parameter, R_c, and $<h>/z_o$, where z_o is the local roughness length of the ice surface. Typically, z_e is estimated to be between 0.1 and 4 cm. The roughness concentration parameter is given by:

$$R_c = \frac{2}{\pi} \; <h>R_D \qquad \text{. . . . .} \qquad \text{(A.12)}$$

where $<h>$ is the mean ridge height, and R_D is the ridging density. This relationship was developed by Ayra (1973). Arya (1975) indicated that when R_c is smaller than 0.0001, no form drag has to be considered.

Lettau (1969) provided an empirical formula for z_e, i.e.,

$$z_e = 0.5<h>R_c \qquad \text{. . . . .} \qquad \text{(A.13)}$$

The values of z_e calculated by this formula are comparable to that calculated by Arya's (1975) method for R_c larger than 0.02.

Banke and Smith (1973) determined the form drag acting on pressure ridges using an equivalent drag coefficient, $C_d(10)$. This coefficient was estimated by

$$C_d(10) = 0.3 <h> N_r \qquad \text{.........................} \qquad \text{(A.14)}$$

where N_r is the number of ridges per unit length. The total wind stress is then calculated by an effective drag coefficient $[C_a(10) + C_d(10)]$. The effective roughness length can be calculated from the drag coefficient by use of equation(A.3). The same procedure can be followed for the stress at the ice-water interface.

Brown (1974 used the momentum integral method to study the data of 1972 AIDJEX tethered balloon experiment. It was reported that the effects of form drag due to ridges might be included in this method. His result, $C_a(10) = 2.8 \times 10^{-3}$, is 50 percent larger than the value that would be measured using the eddy correlation method or logarithmic profile method. The difference could be due to the effect of the form drag due to pressure ridges or the method used.

Banke et al. (1976) determined the form drag on ice ridges by measuring the air pressure drop, Δp, from the upwind to the downwind side at several levels up and down the ridge. Analysis of the data gave the following relation for the equivalent form drag coefficient.

$$C_d(10) = \frac{1}{2} C_D <h> N_r \qquad \text{.........................} \qquad \text{(A.15)}$$

The form drag coefficient, C_D was related to the ridge angle α (refer to Fig. A.4), by the regression line

$$C_D = 0.012 + 0.012\alpha \qquad \text{.........................} \qquad \text{(A.16)}$$
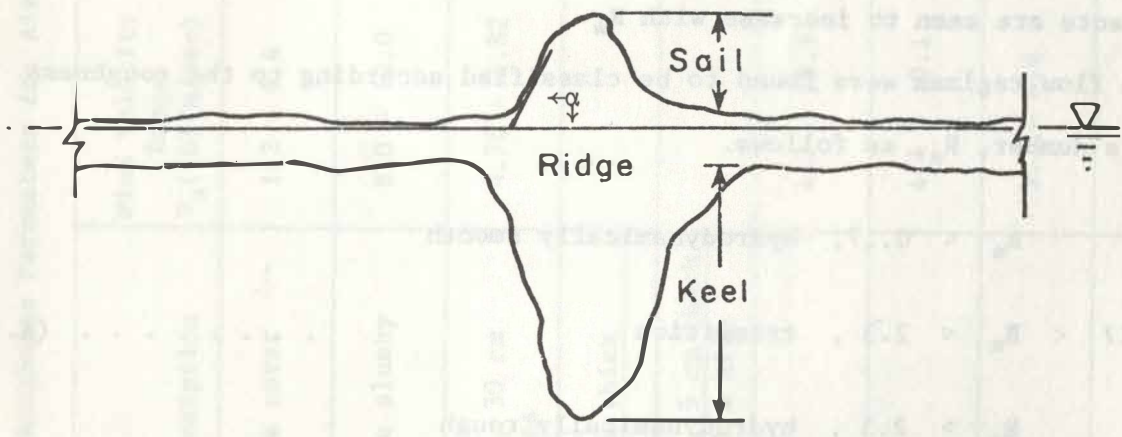
where α is in degrees.

Figure A.4 Schematic Representation of Ridge Cross Section.

A.3 DISCUSSION

Although the drag coefficient is dependent on the surface roughness condition and atmospheric stability, its dependence on wind or current velocity is yet unknown. Lower values of the drag coefficient were observed in highly stable stratification during most of the experiments reviewed. Only those data obtained under near neutral conditions are summarized in Table A.I and Table A.II. The rougher surface condition corresponds to higher values of the drag coefficient. The roughness Reynold's number, $R_* = U_* z_0/\nu$ is used as a measure of the surface condition. From Fig. A.5 and Fig. A.6, the drag coefficients are seen to increase with R_*.

The flow regimes were found to be classified according to the roughness Reynold's number, R_*, as follows.

$$R_* < 0.17, \quad \text{hydrodynamically smooth}$$

$$0.17 < R_* < 2.3, \quad \text{transition} \qquad \cdots \cdots \cdots \text{(A.17)}$$

$$R_* > 2.3, \quad \text{hydrodynamically rough}$$

The values of 0.17 and 2.3 are 1/30 of the values proposed by Schlichting (1968). The reason is that in the logarithmic equation (10) presented, a constant term ($\cong 8.75$) has been combined into the logarithmic term such that the computed values of z_0 in this study are about 30 times as large as Schlichting value and have to be modified accordingly. The data are classified by the criteria given in equation (A.15) and further analyzed.

A.3.1 STRESS AT THE AIR-ICE INTERFACE

All data are plotted in Fig. A.7 and divided into three parts. A regression

TABLE A.I

Summary of Roughness Parameters for Air-Ice Interface

No. of Data Set	Investigator	Surface Description	Wind Velocity Range $V_a(10)$(m/sec)	Drag Coefficient $C_a(10) \times 10^3$	Roughness Length z_o(cm)	Roughness Reynold's Number $R_* = \dfrac{U_* z_0}{\nu}$
1	Untersteiner and Badgley (1965)	Uniform with snow cover	1.2 – 8.4	0.85 – 2.53 1.4	0.0011 – 0.35 0.02	0.0011 – 24.19 3.445
2	Smith et al. (1970)	Snow covered, ice slushy	8.0 – 10.0	2.2 – 2.8 2.6	0.198 ~ 0.594 0.39	57.1 – 212.2 132.63
3	Banke and Smith (1971)	Broken level ice, 30 cm high over 25% area	4.76 – 4.82	2.27 – 2.87 2.6	0.226 – 0.571 0.39	39.9 – 128.4 78.75
	Seifert and Langleben (1972)	Snow cover, 12 cm thick		1.7	0.061	
		Visibly rough		2.2	0.20	
	Langleben (1972)	Light snow cover, 5 cm thick		1.64	0.051	
		Heavily rafted, 1 m high		2.48	0.32	
4	Smith (1972)	Snow covered	4.2 – 18.9	1.01 – 2.3 1.4	0.00342–0.2386 0.02	0.292 – 71.3 8.46
5		Snow covered	4.4 – 10.1	0.95 – 2.19 1.7	0.0023–0.194 0.061	0.54 – 58.67 15.122
6	Banke and Smith (1973)	Old glazed snow	3.7 – 6.4	1.01 – 1.24 1.13	0.00342–0.0116 0.0067	0.353 – 2.02 0.99
7		Snow covered	3.0 – 11.2	1.11 – 2.38 1.82	0.0061–0.2749 0.085	0.53 – 97.99 26.92

Summary of Roughness Parameters for Air-Ice Interface

No. of Data Set	Investigator	Surface Description	Wind Velocity Range $V_a(10)$(m/sec)	Drag Coefficient $C_a(10) \times 10^3$	Roughness Length z_0(cm)	Roughness Reynold's Number $R_* = \dfrac{U_* z_0}{\nu}$
8	Banke and Smith (1973)	Melt ponds surrounded by vertical wall 0.2 - 0.5 meters high	3.3 - 14.6	1.56 - 2.61 2.08	0.03997-0.3978 0.155	10.5 - 145.44 60.488
9	Brown (1974)	Ridge effect included	1.5 - 4.2	0.2 - 4.3 2.8	$.52 \times 10^{-9}$-2.243 0.52	1.87×10^{-8}-282.8 82.539
10		Flat ice	3.75 - 9.41	0.91 - 1.48 1.27	0.00174-0.0305 0.0133	0.15 - 8.5 3.88
11	Banke et al. (1976)	Hummocked ice	4.73 - 12.01	0.85 - 2.47 1.53	0.0011 - 0.32 0.036	0.1 - 122.27 16.99
12		With wet slushy snow	7.0 - 14.5	1.02 - 2.49 1.68	0.0036-0.33 0.058	1.35 - 95.04 26.58

TABLE A.II

Summary of Roughness Parameters for Ice-Water Interface

[1] No. of Data Set	Investigator	Roughness Length z_0(cm)	Drag Coefficient $C_w(1.0) \times 10^3$	Remark	Boundary Layer Thickness (m)	Roughness Reynold's Number $U*z_0/\nu$
6	Untersteiner and Badgley (1965)	0.0369 – 3.811 2.0	3.35 – 14.23 10.49	Old pack ice		218–335.38 162.86
1	Johannessen (1970)	0.999 – 6.098 3.2	7.54 – 20.45 13.5	Upper surface quite rough	0.6 – 1.0	86.7 – 1114.35 523.68
2		8.1 – 10.08 9.4	25.3 – 30.8 29.38	Very rough		573 – 1525 910.35
3		1.499 – 4.698 3.0	9.03 – 17.11 12.92	Rough		47.6 – 239 117.4
4		0.023 – 1.400 0.7	2.28 – 8.78 5.62	Smooth		10.702–92.87 33.18
	McPhee (1976)	0.4	3.4	Max. keel ridge 5.3 m	about 1.0	22.222
	Hunkins (1966)	1.0	5.95		about 1.0 ~ 2.0	
5	Shirasawa and Langleben (1976)	0.0004354 0.52×10^{-10}–2.206	0.2 – 11.0 3.25			1.3×10^{-9}–52.7 2.653

[1] The numbers serve as symbols plotted in the figures.

DRAG COEFFICIENT, $C_a(10)$

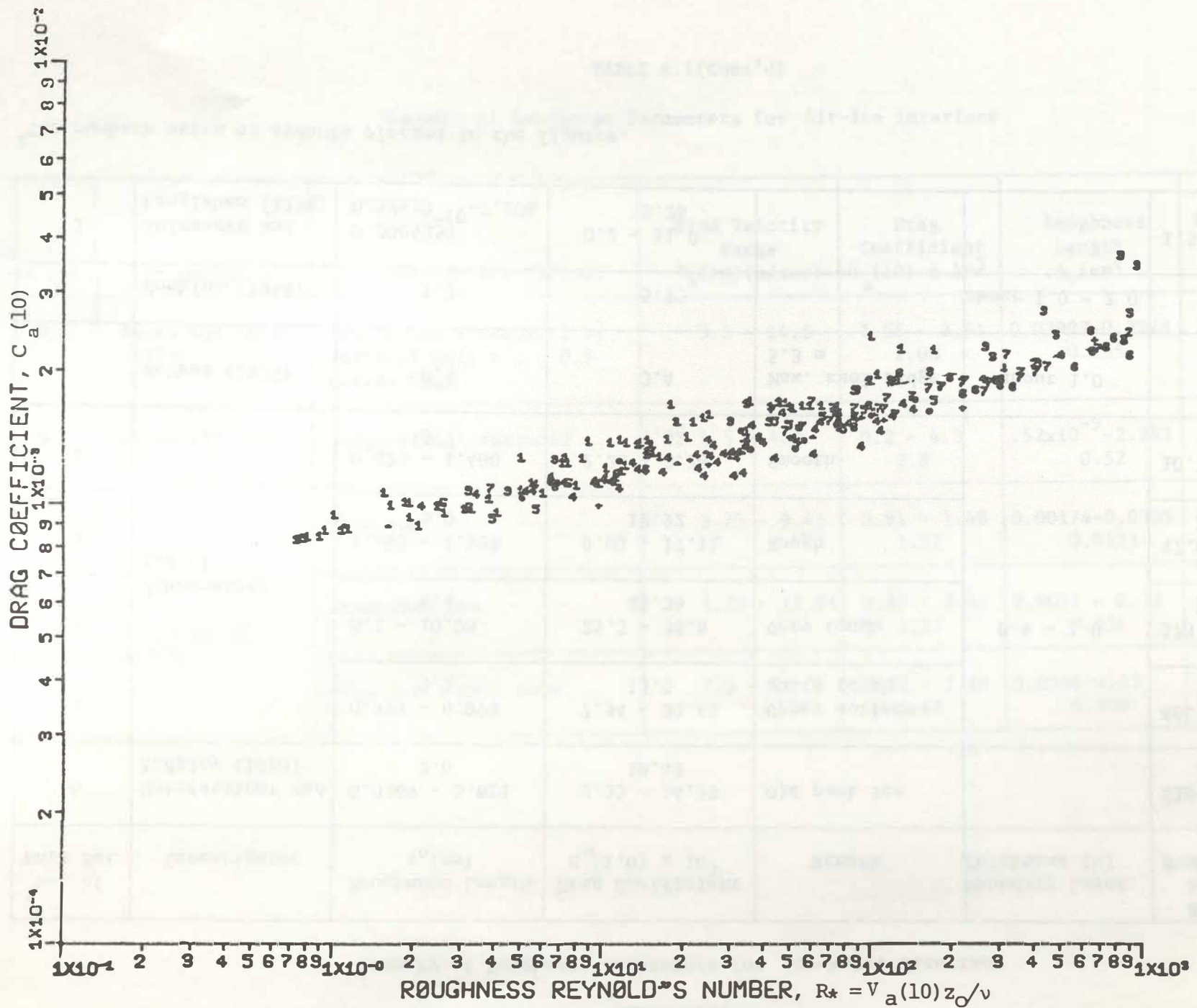ROUGHNESS REYNOLD'S NUMBER, $R_* = V_a(10)z_0/\nu$

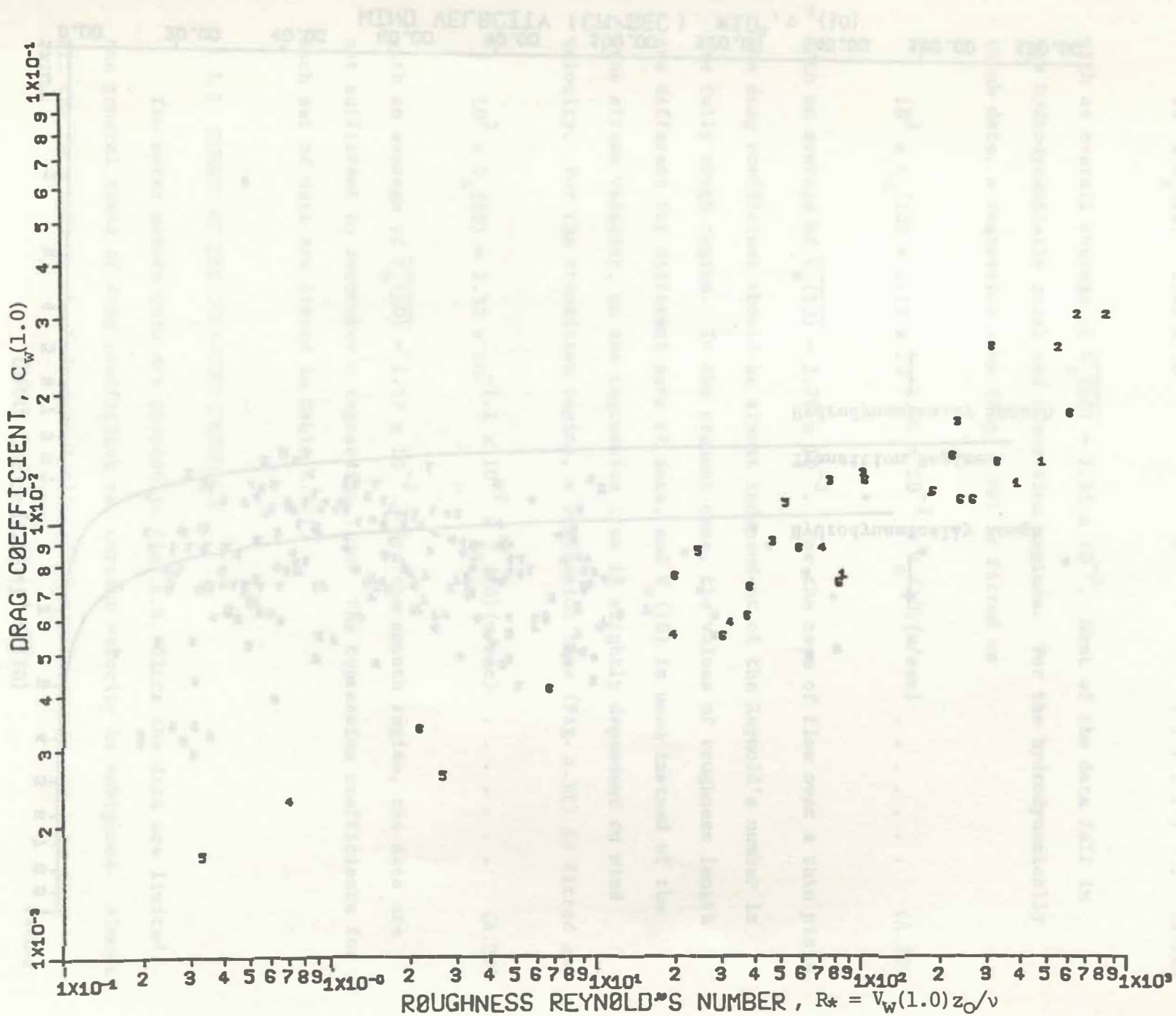Figure A.5 Wind Stress Coefficient on Ice vs. Roughness Reynold's Number (See Table A.I for key to symbols.)

Figure A.6 Water Stress Coefficient on Ice vs. Roughness Reynold's Number   (See Table A.I for key to symbols.)
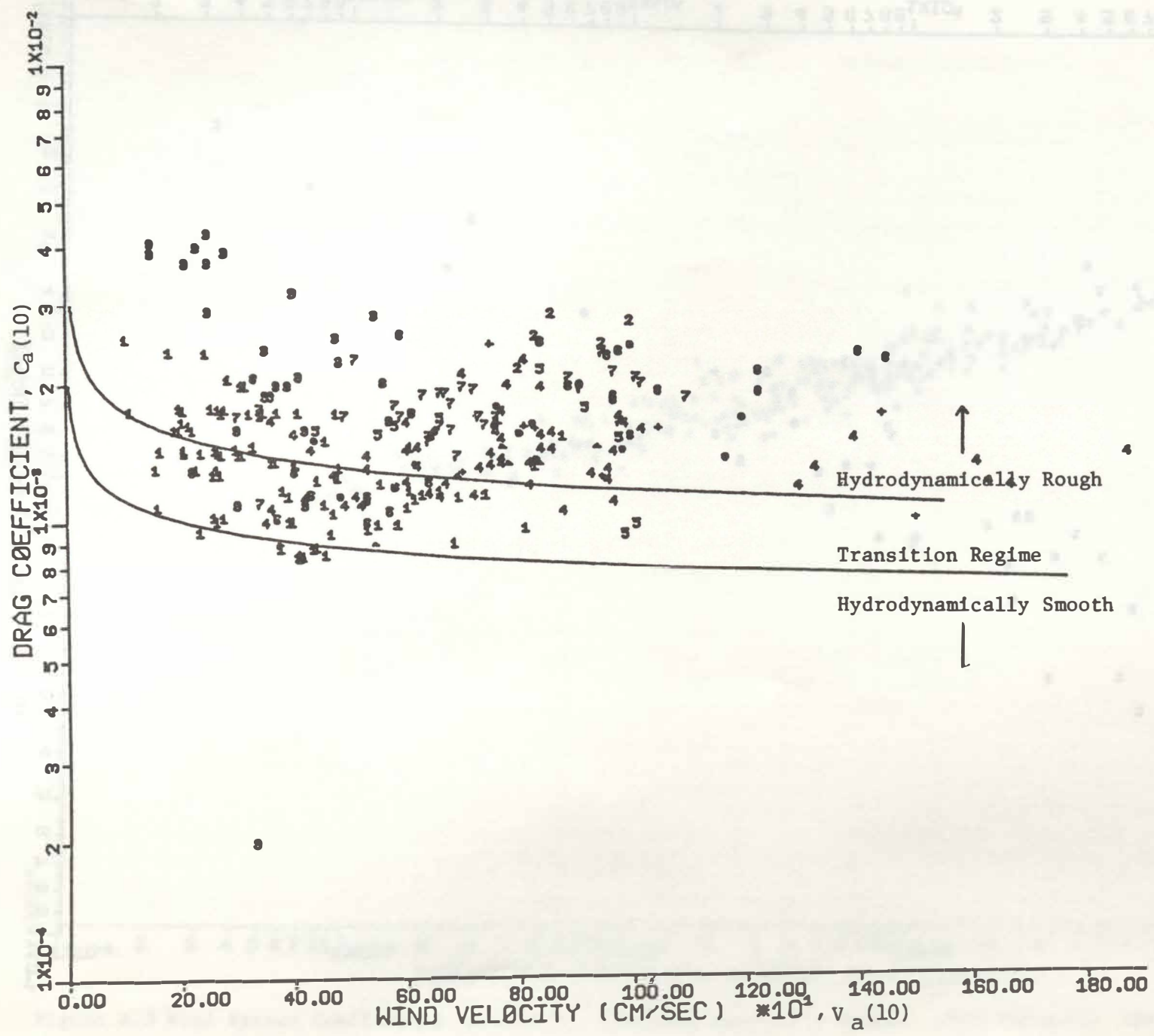
FigureA.7 Wind Stress Coefficient on Ice vs. Wind Velocity (See Table A.II for key to symbols.)

238

line (Fig. A.9) relating the drag coefficient to wind speed is fitted as

$$10^3 \times C_a(10) = 1.49 \times 10^{1.9 \times 10^{-3} \times V_a(10)(m/sec)} \qquad \cdots \cdots \cdots \cdots \qquad (A.18)$$

with an overall average of $\overline{C_a(10)} = 1.65 \times 10^{-3}$. Most of the data fall in the hydrodynamically rough and transition regimes. For the hydrodynamically rough data, a regression line (Fig. A.10) is fitted as

$$10^3 \times C_a(10) = 2.12 \times 10^{-1.01 \times 10^{-2} \times V_a(10)(m/sec)} \qquad \cdots \cdots \cdots \qquad (A.19)$$

with an average of $\overline{C_a(10)} = 1.79 \times 10^{-3}$. For the case of flow over a thin plate, the drag coefficient should be almost independent of the Reynold's number in the fully rough regime. In the present case, the values of roughness length are different for different sets of data, and $V_a(10)$ is used instead of the free stream velocity, so the regression line is slightly dependent on wind velocity. For the transition regime, a regression line (Fig. A.11) is fitted as

$$10^3 \times C_a(10) = 1.32 \times 10^{-1.1 \times 10^{-2} \times V_a(10)(m/sec)} \qquad \cdots \cdots \cdots \qquad (A.20)$$

with an average of $\overline{C_a(10)} = 1.17 \times 10^{-3}$. For the smooth regime, the data are not sufficient to determine a regression line. The regression coefficients for each set of data are listed in Table A.III.

A.3.2 STRESS AT THE ICE-WATER INTERFACE

The water stress data are plotted in Fig. A.8. Since the data are limited, the general trend of drag coefficient vs. current velocity is ambiguous. Almost all the data fall in the hydrodynamically rough regime except for some data
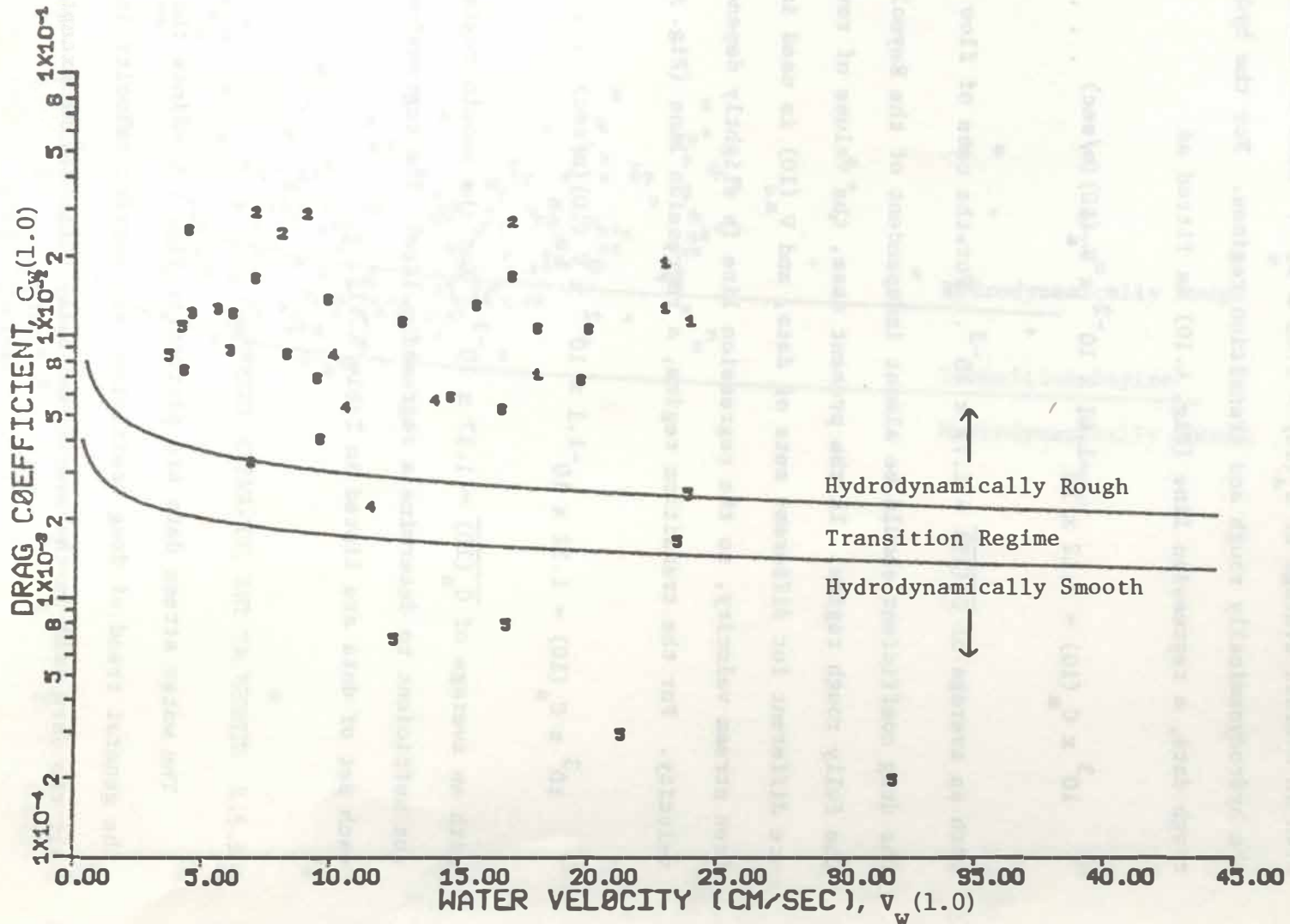
239

Figure A.8 Water Stress Coefficient on Ice vs. Water Velocity (See Table A.I for key to symbols.)

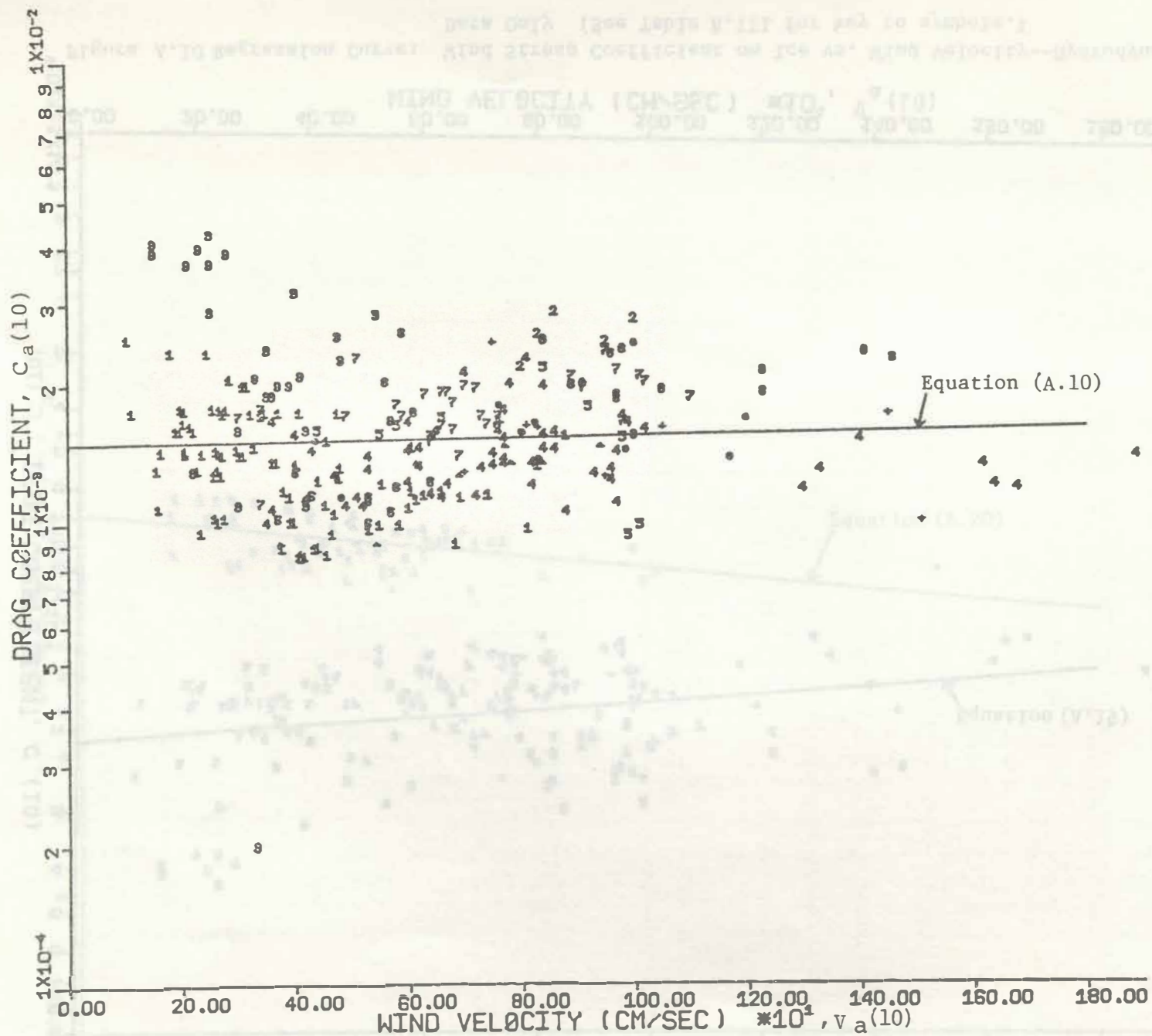Figure A.9 Regression Curve: Wind Stress Coefficient on Ice vs. Wind Velocity (See Table A.II for key to symbols.)
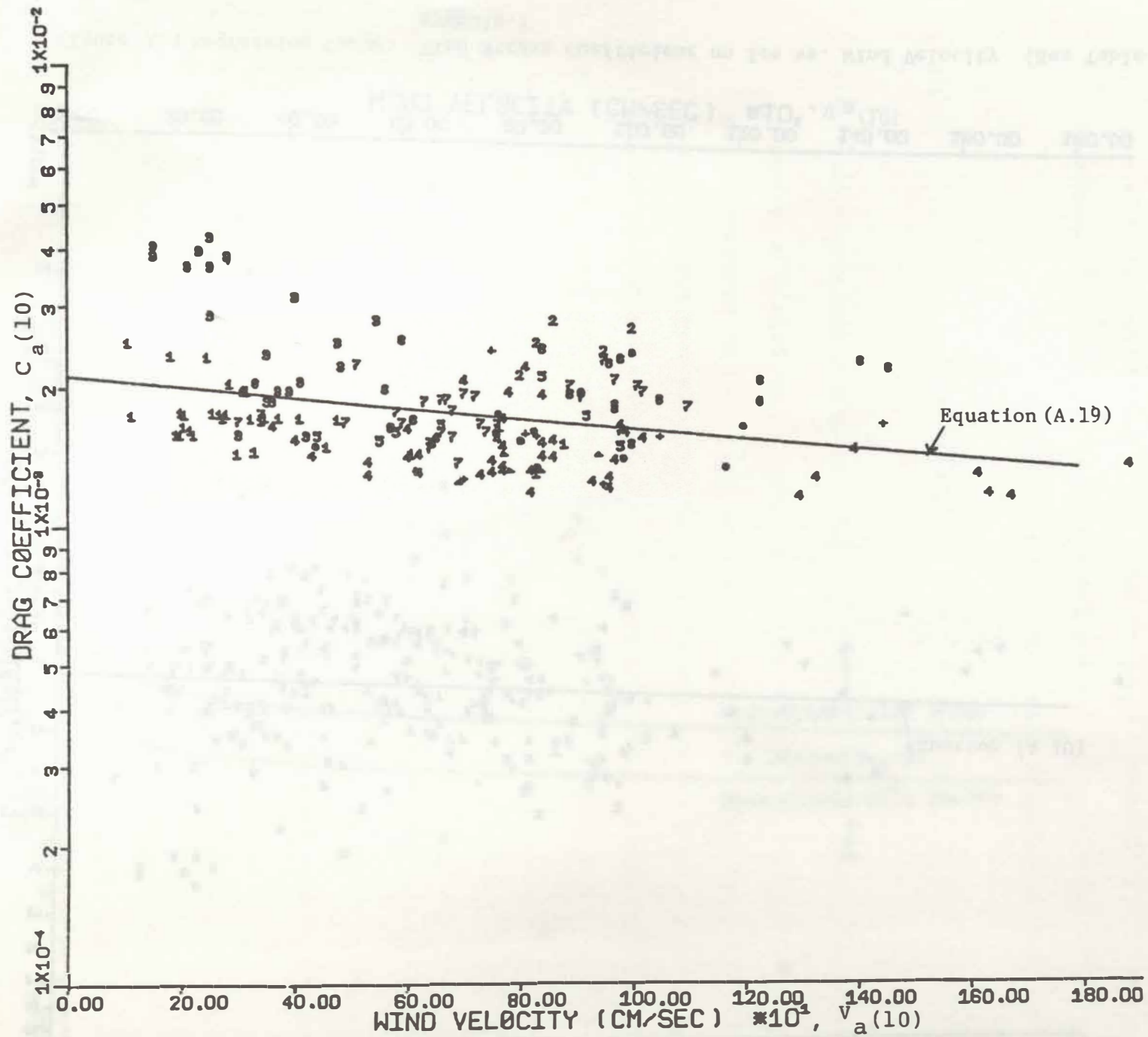
Figure A.10 Regression Curve: Wind Stress Coefficient on Ice vs. Wind Velocity—Hydrodynamically Rough
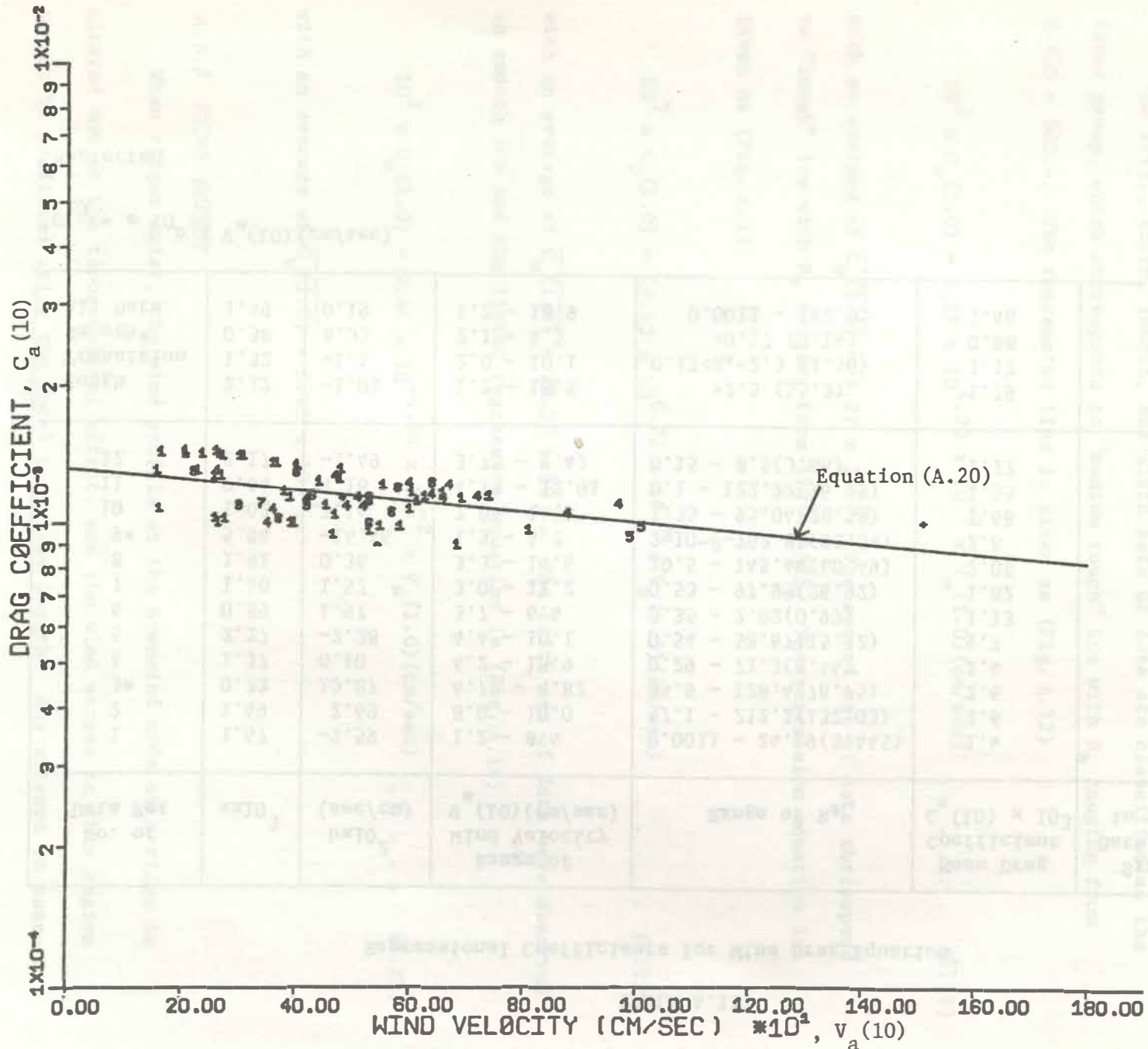Data Only (See Table A.III for key to symbols.)

Figure A.11 Regression Curve: Wind Stress Coefficient Ice vs. Wind Velocity--Transition Regime Data
Only (See Table A.III for key to symbols.)

TABLE A.III

Regressional Coefficients for Wind Drag Equation[1]

No. of Data Set	$a \times 10^3$	$b \times 10^2$ (sec/cm)	Range of Wind Velocity $V_a(10)$ (cm/sec)	Range of R_*	Mean Drag Coefficient $C_a(10) \times 10^3$	Symbol of Data Plotted in Figures
1	1.67	-2.59	1.2 - 8.4	0.0011 - 24.19(3.445)	1.4	1
2	1.49	2.69	8.0 - 10.0	57.1 - 212.2(132.03)	2.6	2
3*	0.73	10.87	4.76 - 4.82	39.9 - 128.4(78.75)	2.6	3
4	1.37	0.10	4.2 - 18.9	0.29 - 71.3(8.46)	1.4	4
5	2.27	-2.28	4.4 - 10.1	0.54 - 58.67(15.12)	1.7	5
6	0.89	1.97	3.7 - 6.4	0.35 - 2.02(0.99)	1.13	6
7	1.40	1.57	3.0 - 11.2	0.53 - 97.99(26.92)	1.82	7
8	1.91	0.36	3.3 - 14.6	10.5 - 145.44(60.49)	2.08	8
9*	5.94	-14.46	1.5 - 4.2	2×10^{-8}-282.85(82.54)	2.8	9
10	1.02	2.14	7.0 - 14.5	1.35 - 95.04(26.58)	1.68	
11	0.64	4.16	4.13 - 12.01	0.1 - 122.27(16.99)	1.53	+
12	2.17	-1.49	3.75 - 9.41	0.15 - 8.5(3.86)	1.27	Δ
Rough	2.12	-1.01	1.2 - 18.9	>2.3 (55.3)	1.79	
Transition	1.32	-1.1	2.0 - 10.1	$0.17 < R_* < 2.3$ (1.56)	1.17	
Smooth*	0.38	8.05	2.1 - 4.5	<0.17 (0.14)	0.88	
All Data	1.49	0.19	1.2 - 18.9	0.0011 - 282.85	1.46	

[1] $C_{10} = a \, 10^b \times V_a(10)$ (cm/sec)

*Neglected

reported by Shirasawa and Langleben (1976) which were reported as smooth first year ice. The data have been classified into three groups by inspecting the trend in Fig. A.8 and the range of roughness Reynold's numbers. Each group was fitted with one regression line. The results are listed in Table A.IV.

The first, third, fourth, and sixth sets of data are classified as the first group, which corresponds to "medium rough" ice with R_* ranging from 0.415 – 505.4. The regression line is given as (Fig. A.12)

$$10^3 \times C_w(1.0) = 8.19 \times 10^{4.23 \times 10^{-3} \times V_w(1.0)} \text{(cm/sec)} \quad \ldots \ldots \quad \text{(A.21)}$$

with an average of $\overline{C_w(1.0)} = 9.27 \times 10^{-3}$. The second set of data correspond to "rough" ice with R_* ranging from 573 – 1525. The regression equation is given as (Fig. A.13)

$$10^3 \times C_w(1.0) = 28.12 \times 10^{6.71 \times 10^{-4} \times V_w(1.0)} \text{(cm/sec)} \quad \ldots \ldots \quad \text{(A.22)}$$

with an average of $\overline{C_w(1.0)} = 29.35 \times 10^{-3}$. The fifth set of data were observed on smooth ice and the fitted regression equation is (Fig. A.14)

$$10^3 \times C_w(1.0) = 9.44 \times 10^{-4.84 \times 10^{-2} \times V_w(1.0)} \text{(cm/sec)} \quad \ldots \ldots \quad \text{(A.23)}$$

with an average of $\overline{C_w(1.0)} = 3.25 \times 10^{-3}$.

A.3.3 RIDGE EFFECT

When ridges exist, the wind profile at the downwind side of a ridge is altered due to the topographical effect, and the wind stress in this region cannot be predicted using the local roughness length. Any attempt to measure

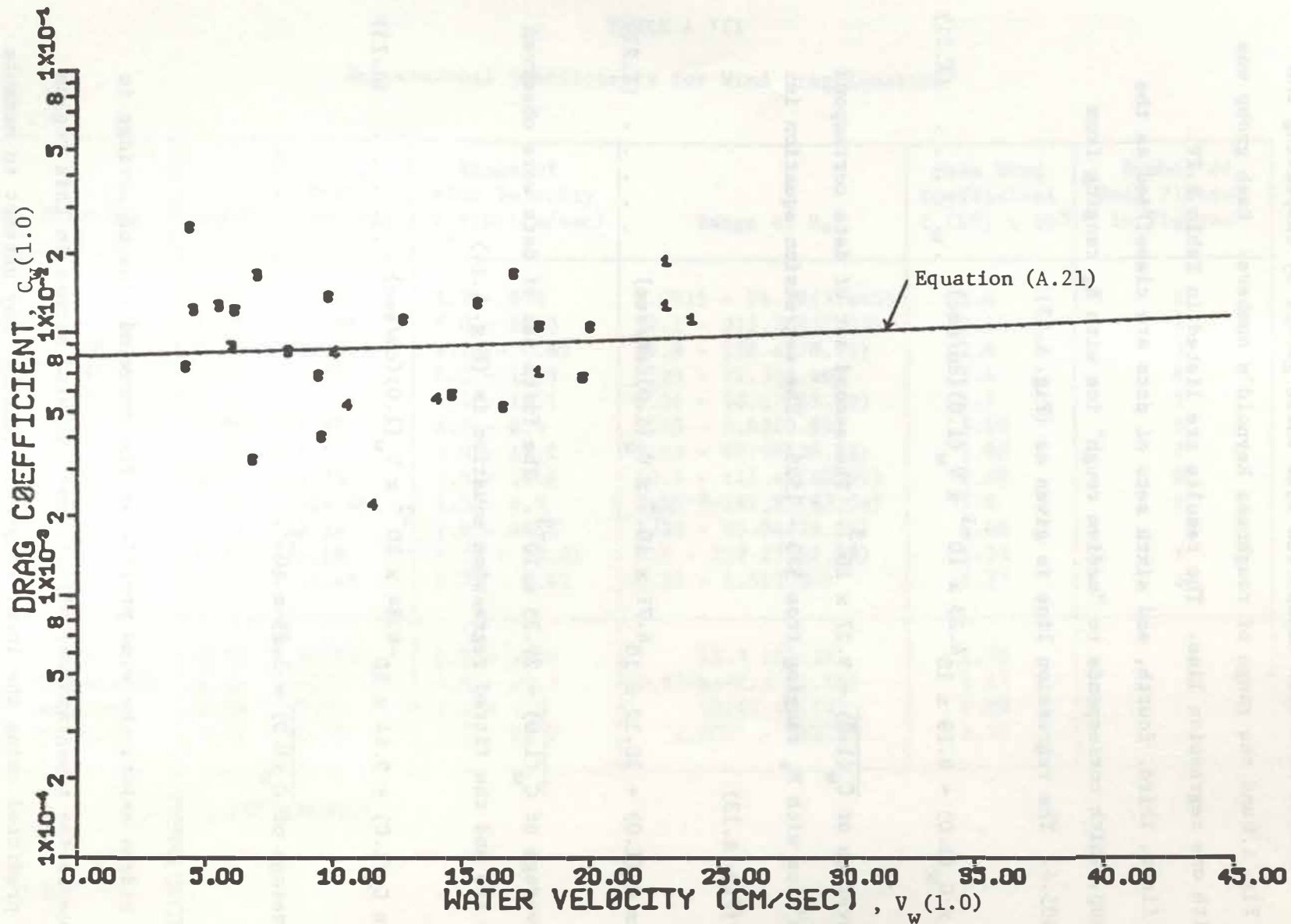Figure A.12 Regression Curve: Water Stress Coefficient of Ice vs. Water Velocity--"Medium Rough" Ice
(See Table A.IV for key to symbols.)
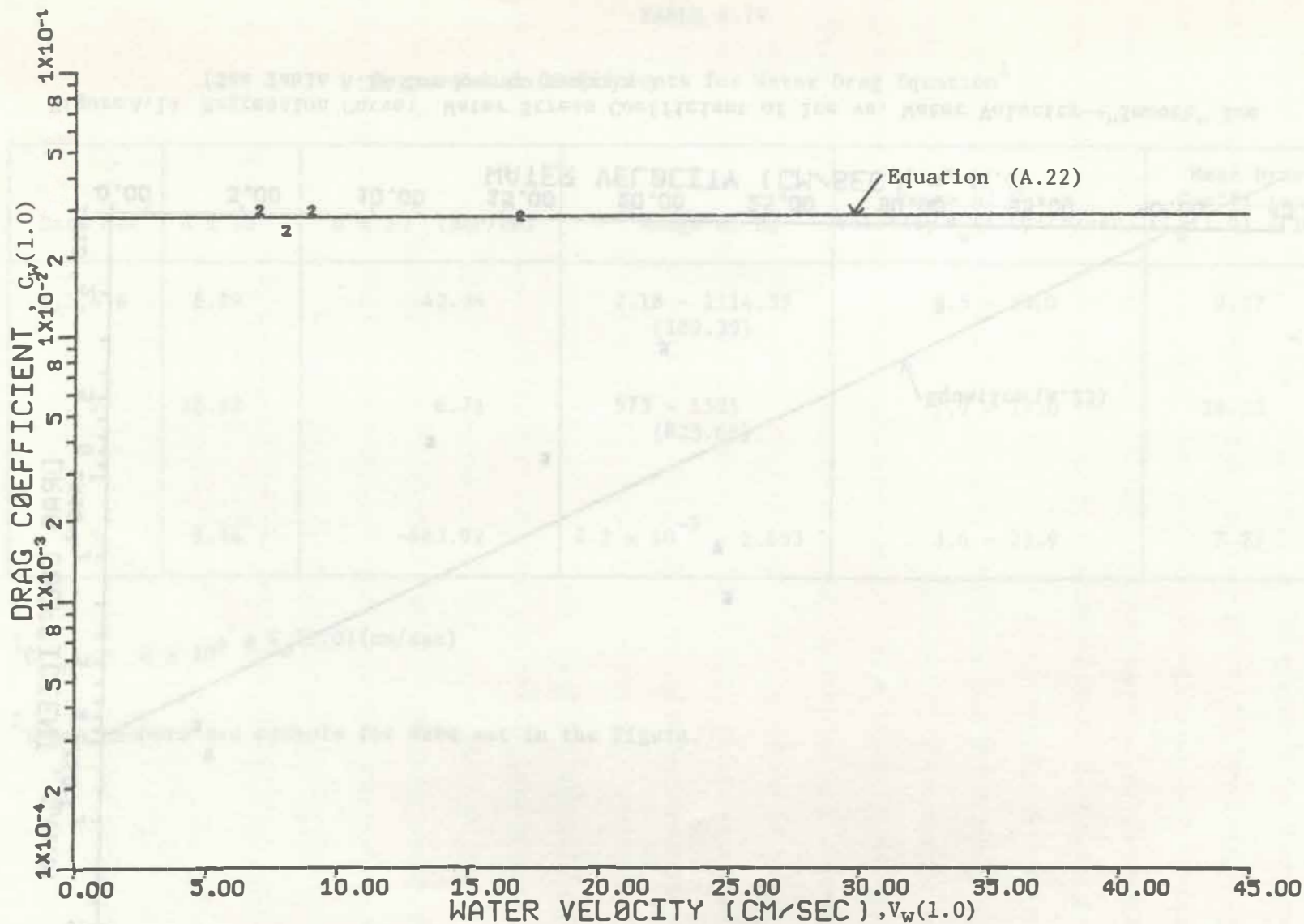
Figure A.13 Regression Curve: Water Stress Coefficient of Ice vs. Water Velocity--"Rough" Ice
(See Table A.IV for key to symbols.)
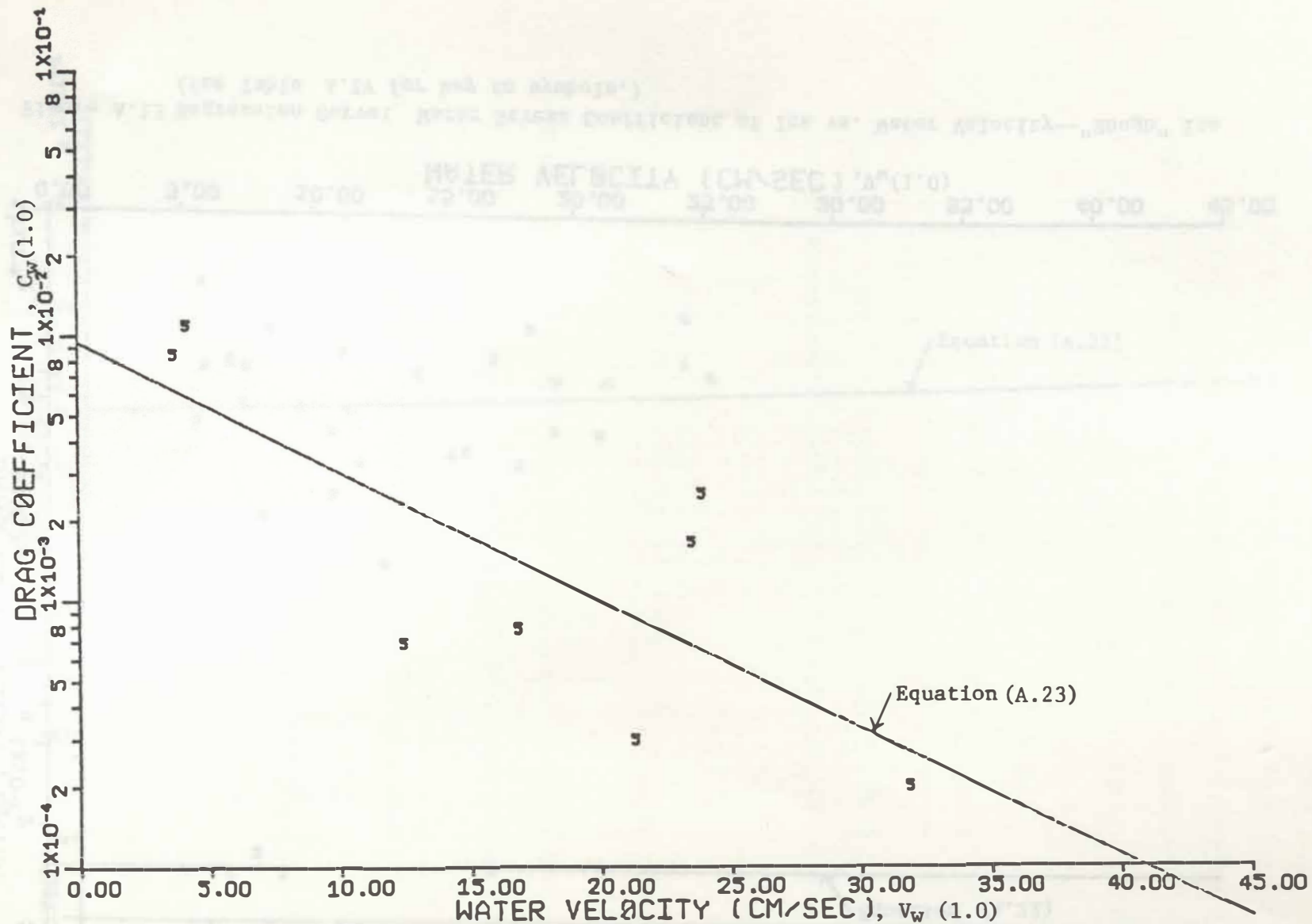
Figure A.14 Regression Curve: Water Stress Coefficient of Ice vs. Water Velocity—"Smooth" Ice
(See Table A.IV for key to symbols.)

TABLE A. IV

Regressional Coefficients for Water Drag Equation[1]

Data Set[2]	$a \times 10^3$	$b \times 10^4$ (sec/cm)	Range of R_*	Range of Water Velocity $V_w(1.0)$(cm/sec)	Mean Drag Coefficient $\bar{C}_w(1.0) \times 10^3$
1,3,4,6	8.19	42.34	2.18 – 1114.35 (189.39)	3.5 – 24.0	9.27
2	28.12	6.71	573 – 1525 (823.68)	7.9 – 17.0	29.35
5	9.44	−483.92	1.2×10^{-9} – 2.653	3.6 – 23.9	3.25

[1] $C_{1.0} = a \times 10^b \times V_w(1.0)$ (cm/sec)

[2] These numbers are symbols for data set in the Figure.

roughness length near a ridge will result in large errors. For example, in Langleben's (1972) experiment, computed values of the roughness height at a site near heavily rafted ice had large variations.

From Arya's (1975) result, the "equivalent roughness length," z_e, can be calculated if the roughness concentration parameter, R_c, and the roughness length for flat ice, z_o, are known. Arya gave an estimated value of z_e to be between 0.1 and 4 cm, corresponding to $C_a(10)$ between 1.89×10^{-3} and 5.25×10^{-3}. The effective drag coefficient, $[C_a(10) + C_d(10)]$, can also be estimated by Banke and Smith's (1973) simple theory and an "equivalent roughness length can be calculated.

Banke et al. (1976) made field measurements of form drag. The form drag coefficient, C_D, is related to the angle of the ridge (see Equation A.16). The form drag can be estimated with knowledge of the shape of the ridges and the ridging density. Banke et al. (1976) estimated $\overline{C_D} = 0.28$ as the average value for old, snow covered ridges.

A.4 APPLICATION TO LAKE ICE

Due to the limited data for roughness parameters measured on lake ice, the results on sea ice have been used to predict the drag coefficient for lake ice. The surface of polar ice is formed through natural metamorphic processes, which is different from the seasonal formation of lake ice (Hobbs, 1974). Therefore, lake ice is generally smoother than polar ice, and the drag coefficients measured on very rough sea ice are not considered.

A.4.1 AIR-ICE INTERFACE

Some measurements on smooth lake ice gave the following values: $z_o = 0.01$ cm ($C_a(10) = 1.21 \times 10^{-3}$) (Panofsky and Townsend, 1964), with $R_* = 0.96$. and $z_o = 0.015$ cm ($C_a(10) = 1.3 \times 10^{-3}$) (Lettau, 1969). These values are about the same

as the drag coefficient of sea ice when the flow condition is in the transition regime. Since lake ice is expected to become rougher with time due to the accumulation of snow and with the broken pieces accompanying the formation of pressure ridges, these values obtained on lake ice can only serve as an estimate of the lower limit of the drag coefficient at the air-ice interface of lake ice. Equations (A.7),(A.8) or (A.9) could be used to obtain reasonable estimates of the drag coefficient if surface profiles of lake ice were available.

As the lake ice roughens, the mean value of $C_a(10)$ for the hydrodynami- cally rough regime is estimated to be $\overline{C_a(10)} = 1.79 \times 10^{-3}$ and should serve as the upper limit for lake ice. The extreme value of the drag coefficient obtained on sea ice is neglected since lake ice is expected to be smoother. For unridged lake ice, $C_a(10)$ is estimated to be between 1.3×10^{-3} and 1.79×10^{-3}, with an average value of 1.55×10^{-3} ($z_o \cong 0.039$ cm).

To estimate the ridge effects, the ridge distribution should be known. A set of data, <h> = 1.0 m and R_c= 0.001, is selected as the ridge parameters for lake ice. These data are somewhat arbitrarily chosen by inspecting the photographs of the ice condition in Lake Erie and comparing with the data for ridges in the Arctic Region (Arya, 1975). Using Equation (A.13) and the data $R_c = 0.001$, $C_a(10) = 0.3 \times 10^{-3}$, the effective drag coefficient $[C_a(10) + C_d(10)]$ will be 1.85×10^{-3} (using $C_a(10) = 1.55 \times 10^{-3}$). In this case, the ridges contribute 16 percent of the total drag. By Banke's method (1976), using a ridge angle of 38°, the form drag coefficient is given by Equation (A.16) as $C_D = 0.468$. From Equation (A.15) $C_d(10) = 0.23 \times 10^{-3}$, and the ridges are found to contribute about 13 percent of the total drag (i.e. $C_a(10) + C_d(10) = 2.25 \times 10^{-3}$). From Arya's estimation (1975), for ice with <h> = 1.0 m, $R_c = 0.001$ and $z_o = 0.039$ cm, about 15 percent of the total stress is contributed by ridges. For the present, a value of $C_a(10) = 1.8 \times 10^{-3}$ is selected as representative for ridged ice surfaces.

McPhee and Smith's (1976) results show that by proper coordinate trans-
formation, the planetary boundary layer (including an inner surface layer and
an outer Ekman layer) of water under ice floe in the Arctic Ocean resembles
that of the atmosphere. The water depth of Lake Erie is much shallower than
that of the Arctic Ocean, so the water flow is influenced by both irregular
bottom topography and ice cover. The existence of similar planetary boundary
layer conditions is doubtful. Therefore, the outer boundary layer will not
be considered and the water stress is given by

$$\tau_w = \rho_w C_w(z)[V_w(z)]^2 = \rho_w \left[\kappa / [\ln(\frac{h_w + z_o}{z_o})] \right] [V_w(z)]^2 \quad \ldots \ldots \quad (A.24)$$

where h_w is the thickness of the inner surface boundary layer, V_w is the
velocity of the water relative to the ice at a distance h_w below the ice-water
interface, and C_w is the drag coefficient specified at depth h_w. The problem
will be the estimation of h_w, z_o, and V_w.

In general, the velocity of an ice floe is not negligible compared with
that of the water flow, so the relative velocity needs to be used to estimate
the water stress. The velocity of the water current may change due to the
existence of ice cover. A method of calculating the water currents in a
partially ice covered lake has been given by Sheng and Lick (1973). The
boundary layer depth, h_w can be assumed to be one meter by examining previous
experimental data (Table A.II).

Isostatic equilibrium requires the underside ridges to be 4.5 to 5.0
times larger than those above. This was proved to be generally true by the
observations of Kozo et al. (1973). Considering the fact that the height of
upper surface ridges sometimes exceeds 4 meters, it can be concluded that the

form drag on the ridge keels will be the dominating force acting on the bottom of ice floe (Arya, 1973). The isostatic equilibrium may not be established for first year ice cover, so the ridge keels could be smaller. Cooper et al. (1976) mentioned that the lower surface of lake ice might be flat and smooth according to their observation. Under this assumption, there is no form drag on lake ice. Ridge keel depths for lake ice are not available. However, estimates of the underside ridge effect can be made using the data for sea ice listed in Table A.II.

For the medium rough condition listed in Table A.IV, corresponding to R_* ranging from 2.18 to 1114, the drag coefficients take on values between 2.28×10^{-3} to 17.11×10^{-3} with a mean value of 9.27×10^{-3}. These data seem suitable to serve as the lower limit, upper limit and mean value for the water drag coefficient for lake ice.

Campbell (1965) used z_o = 2.65 cm ($C_w(1.0) = 12.14 \times 10^{-3}$) as an upper limit in his ice drift model. Ingram et al. (1969) estimate z_o to be 0.6 cm for new ice ($C_w(1.0) = 6.1 \times 10^{-3}$), and z_o = 2.0 cm ($C_w(1.0) = 10.45 \times 10^{-3}$) for thick ice. These values might be larger if ridges occurred. The estimation that $C_w(1.0)$ ranges between 2.28×10^{-3} to 17.11×10^{-3} seems to agree with these previous studies.

A.5 CONCLUSIONS

Recommended drag coefficients for upper and lower lake ice surface are listed in Table A.V; however, it should be pointed out that the value of $C_a(10)$ = 1.8×10^{-3} (z_o = 0.08 cm) for ridged ice is based on rather inconclusive information. This value could be improved if more reliable data were available. Observation of upper and lower surface pressure ridge distribution

253

TABLE A.V

Recommended Drag Coefficient

		Air-Ice Interface $(C_a(10) \times 10^3)$	Ice-Water Interface $(C_w(1.0) \times 10^3)$
Before Ridges Occur	Lower Limit	1.3	2.28
	Upper Limit	1.79	17.11
	Mean	1.55	9.27
After Ridges Occur		1.8	

is needed to estimate the form drag of ridges and further improve the estimate of wind and water stress acting on ice floes. According to our estimation listed in Table A.V the ridge effect is not an important factor in calculating wind stress.

The buoyancy effect was observed to be an important factor affecting the wind stress. By using the geostrophic drag method, this effect can be taken into consideration and some empirical results have been published (Arya, 1975a; Arya and Wyngaard, 1975; Bussinger et al., 1971; Fiedler and Panofsky, 1972). However, to use these empirical results, a detailed temperature profile and heat flux data are needed to calculate the stability parameters. Therefore, we only considered the case of neutral stability. To better estimate the wind and water stress, the buoyancy effect needs to be further considered.

BIBLIOGRAPHY

Ackermann, N. L. and A. Arbhabhirama, (1964), "Viscous and Boundary
Effects on Virtual Mass," Journ. Engg. Mech. Div., ASCE, Vol. 90,
No. EM4, pp. 123-130.

Ackley, S.F., W.D. Hibler, F.K. Kugzruk, A. Kovacs, and W.F. Weeks,(1976),
"Thickness and Roughness Variations of Arctic Multiyear Sea Ice,"
CRREL Report 76-18, Corps of Engineers, U.S. Army, Hanover, N.H.

Ames, W.F.,(1969), Numerical Methods for Partial Differential Equations,
Barnes and Noble, Inc., New York, N. Y.

Anderson, V.H.,(1966), "High Altitude Side Looking Airborne Radar Images
of Sea Ice in the Arctic," Proc. 4th Symp. Remote Sensing of the
Environment, Inst. Sci. and Tech., Univ. of Michigan.

Anderson, V.H., R. B. Arend, and M.J. Lynch, (1972), "Interpretation of
Winter Ice Conditions from SLAR Imagery," NTIS: AD-A016 295/8GI, 93p.

Arya, S.P.S., (1973), "Contribution of Form Drag on Pressure Ridges to
the Wind Stress on Arctic Ice," J. Geophys. Res., Vol. 78, pp. 7092-
7099.

Arya, S.P.S., (1975a), "Geostrophic Drag and Heat Transfer Relations for
the Atmospheric Boundary Layer," Quart. Journ. Roy. Met. Soc., Vol.
101, pp. 147-161.

Arya, S.P.S., (1975b), "A Drag Partition Theory for Determining the Large
Scale Roughness Parameter and Wind Stress on the Arctic Pack Ice,"
J. Geophys. Res., Vol. 80, pp. 3447-3454.

Arya, S.P.S. and J.C. Wyngaard, (1975), "Wind Profiles and the Geostrophic
Drag Law for the Convective Boundary Layer," J. Atmosph. Sci., Vol. 32,
pp. 767-778.

Assel, R.A., (1974), "Great Lake Ice Cover, Winter 1973-74," NOAA Technical
Report ERL 325-GLERL 1.

Banke, E.G. and S.D. Smith, (1971), "Wind Stress Over Ice and Over Water in
the Beaufort Sea," J. Geophys. Res., Vol. 76, pp. 7369-7374.

Banke, E.G. and S.D. Smith, (1973), "Wind Stress on Arctic Sea Ice," J. Geo-
phys. Res., Vo. 78, pp. 7871-7873.

Banke, E.G. and S.D. Smith, (1976), "Recent Measurements of Wind Stress on
Arctic Sea Ice," J. Fish. Res. Board Canada, Vol. 33, pp. 2307-2317.

Batchelor, G.K., (1967), <u>An Introduction to Fluid Dynamics,</u> Cambridge
    University Press, London.

Batten, E.S., (1976), "Sea-Ice Conditions in the Norwegian, Barents, and
    White Seas," R-1921-ARPA, Rand Corporation, Santa Monica, California.

Bear, J., (1972), <u>Dynamics of Fluids in Porous Media,</u> American Elsevier,
    N. Y.

Bilello, M.A. and R. E. Bates, (1975), "Ice Thickness Observations, North
    American Arctic and Subarctic 1970-71, 1971-72," Special Report 43,
    Part VII, CRREL, Corps of Engineers, U.S. Army, Hanover, N. H.

Bloomquist, A., C. Pilo, and T. Thompson, (1976), "SEA ICE-75, Summary
    Report," Winter Navigation Research Board, Swedish Admin. of Shipping
    and Navigation, Finnish Board of Navigation, Research Report 16:9,
    Norrkoping.

Bolsenga, S.J.,(1968), "River Ice Jams-A Literature Review," U.S. Lake
    Survey Research Report 5-5, U.S. Army Corps of Engineers, Detroit,
    Michigan, 568 p.

Bolsenga, S.J., (1978), "On the Use of Multispectral Radar to Define
    Certain Characteristics of Great Lake Ice," NOAA Tech. Memo. ERL
    GLERL-17, Great Lakes Environmental Research Lab., Ann Arbor, Mich.

Bristor, C.L., (1975), "Central Processing and Analysis of Geostationary
    Satellite Data," NOAA Tech. Memo. NESS 64, National Environmental
    Satellite Service, NOAA, Wash. D. C.

Brown, R.A., (1973), "On the Atmospheric Boundary Layer:Theory and Methods,"
    AIDJEX Bulletin No. 20, (NTIS: PB 222 057), pp. 1-141.

Brown, R.A., (1976), "The Resistance Law," AIDJEX Bulletin No. 31, pp. 21-31.

Brown, R.A., (1977), "Planetary Boundary Layer Modeling for AIDJEX," A Symp.
    on Sea Ice Processes and Models, Univ. of Wash., Seattle, Wash., pp.
    153-163.

Bussinger, J.A., J.C. Wyngaard, and E.F. Bradley, (1971), "Flux-Profile
    Relations in the Atmospheric Surface Layer," <u>J. Atmosph. Sci.,</u> Vol. 28,
    pp. 181-189.

Bye, J.A.T., (1967), "The Wave-Drift Current," <u>J. Mar. Res.,</u> Vol. 25, pp.
    95-102.

Campbell, W.J., (1965), "The Wind-Driven Circulation of Ice and Water in a
    Polar Ocean," <u>J. Geophys. Res.,</u> Vol. 70, pp. 3279-3301.

Campbell, W.J. and L.A. Rasmussen, (1971),"A Numerical Model for Sea Ice
    Dynamics Incorporating Three Alternative Ice Constitutive Laws," Sea
    Ice, Proc. Internat. Conf., Reykjavik, Iceland, pp. 176-189.

Campbell, W. J. and K. S. Orange, (1974), "A Continuous Profile of Sea Ice and Freshwater Ice Thicknesses by Impulse Radar," Polar Record, Vol. 17, No. 106, pp. 31-41.

Campbell, W.J., W.F. Weeks, R.O. Ramseier, and P. Gloersen, (1975a), "Geophysical Studies of Floating Ice by Remote Sensing," J. Glaciol., Vol. 15, No. 73, pp. 305-328.

Campbell, W.J., R.O. Ramseier, W.F. Weeks, and P. Gloersen, (1975b), "An Integrated Approach to the Remote Sensing of Floating Ice," Proc. 3rd Canadian Symp. Remote Sensing, pp. 39-72.

Canada, Ministry of Transport, Canadian Marine Transportation Admin., (1970-76), "Winter Navigation Studies: Lake,Erie, Detroit River, Lake St. Clair, St. Clair River: Winters 1970-71 to 1975-76", Six Volumes.

Charnock, H.,(1955), "Wind Stress on Water Surface," Quart. J. Roy. Met. Soc., Vol. 81, p. 639.

Coon, M.D., (1974), "Mechanical Behavior of Compacted Arctic Ice Floes," J. of Petrol. Tech., Vol. 26, pp. 466-470.

Coon, M.D., (1977), "A Review of AIDJEX Modeling," A Symp. on Sea Ice Processes and Models, Univ. of Wash., Seattle, Wash., pp. 40-56.

Coon, M.D., G.A. Maykut, R.S. Pritchard, D.A. Rothrock, and A.S. Thorndike, (1974), "Modeling the Pack Ice as an Elastic Plastic Material," AIDJEX Bulletin No. 24, pp. 1-103.

Cooper, D.W., J.E. Heighway, D.F. Shook, R.J. Jirberg, and R.S. Vickers, (1974), "Remote Profiling of Lake Ice Thickness Using a Short Pulse Radar System aboard a C-47 Aircraft," NASA Tech. Memo. NASA-TM-X 71588, 4 p.

Cooper, D.W., R. A. Mueller, and R. J. Schertler, (1976), "Measurement of Lake Ice Thickness with a Short Pulse Radar System," NASA Tech. Memo. NASA TN-D 8189, 24 p.

Cooper, D.W., R.A. Mueller, and R.J. Schertler, (1975), "Remote Profiling of Lake Ice using an S-Band Short Pulse Radar Aboard an all Terrain Vehicle," NASA Tech. Memo. NASA TM-X-71808, 18 p.

Dean, A.M., (1977), "Remote Sensing of Accumulated Frazil and Brash Ice in the St. Lawrence River," CRREL Report 77-8, Corps of Engineers, U.S. Army, Hanover, N.H., 43 p.

Doronin, Y.P., (1970), "On a Method of Calculating the Compactness and Drift of Ice Floes," AIDJEX Bulletin No. 3, pp. 22-39.

Dunbar, M., (1975),"Interpretation of SLAR Imagery of Ice in Nares Strait and the Arctic Ocean," Defense Res. Establishment Ottawa, DREO Report No. 712, 42 p.

Dunbar, M., (1978), "Interpretation of Ice Imagery from Original and Modified Versions of a Real-Aperture SLAR," Defense Res. Establishment Ottawa, DREO Report No. 770, 36 p.

Dunbar, M. and W.F. Weeks, (1975), "Interpretation of Young Ice Forms in the Gulf of St. Lawrence Using Side Looking Airborne Radar and Infrared Imagery," CRREL Research Report No. 337, Corps of Engineers, U. S. Army, Hanover, N. H., 46 p.

Dym, C.L. and I. H. Shames, (1973), Solid Mechanics: A Variational Approach., McGraw-Hill Book Co., New York, N. Y.

Eddy, E.D., (1949), "Stability in Numerical Solution of Initial Value Problems in Partial Differential Equations," NOLM 10232, Naval Ordnance Lab., White Oak, Silver Springs, Md.

Ekman, V.W., (1905), "On the Influence of the Earth's Rotation on Ocean Currents," Arkiv. Mat. Astron. Fysik., Vol. 2, No. 11, Sweden, pp. 1-53.

Elachi, C. and W. E. Brown, Jr., (1975), "Imaging and Sounding of Ice Fields with Airborne Coherent Radars," J. Geophys. Res., Vol. 80, No. 8, pp. 1113-1119.

Evans, R.J. and D. A. Rothrock, (1975), "Stress Fields in Pack Ice," Proc. 3rd Internat. Symp. Ice Problems, Hanover, N.H., pp. 527-540.

Ficke, E.R. and J.F. Ficke, (1977), "Ice on Rivers and Lakes," USGS Water Resources Investigations 77-95, Reston, VA, 179 p.

Fiedler, F. and H.A. Panofsky, (1972), "The Geostrophic Drag Coefficient and the Effective Roughness Length," Quart. J. Roy. Met. Soc., Vol. 98.

Fortuna, J.J. and L. N. Hambrick, (1974), "The Operation of the NOAA Polar Satellite System," NOAA Tech. Memo. NESS-60, Office of Systems Integration, Wash. D.C.

Garrison, C.J., (1974), "Dynamic Response of Floating Bodies," Offchore Tech. Conf., Preprint #OTC 2067, 6th Annual Offshore Tech. Conf., Houston, TX, pp. 365-373.

Gedney, R.T. and W. Lick,(1970), "Numerical Calculations of the Steady State Wind Driven Currents in Lake Erie," Proc. 13th Conf. Great Lakes Res. IAGLR, pp. 829-838.

Gedney, R.T., R. J. Schertler, R.A. Mueller, R.J. Jirberg, and H. Mark, (1975), "An Operational All-Weather Great Lakes Ice Information System," NASA Tech. Memo. NASA TM-X-71812, 11 p.

Glen, J. W., (1970), "Thoughts on a Viscous Model for Sea Ice," AIDJEX Bulletin No. 2, pp. 18-27.

Gorbunov, Y.A. and S.M. Losev, (1975), "Side Looking Radar Imagery Assembly 'TOROS' for Studying Ice Drift," NASA Tech. Memo. NASA TTF 16664, 16 p.

"Guide to Great Lakes Ice Navigation," (1978-79), U.S. 9th Coast Guard District, Ice Navigation Center, Cleveland, Ohio.

"Guide to World Inventory of Sea, Lake and River Ice," (1972), UNESCO Technical Papers in Hydrology No. 9, Paris.

Hagman, B.B., (1976), "An Analysis of Great Lakes Ice Cover from Satellite Imagery," NOAA Tech. Memo. ERL GLERL-9, Great Lakes Environmental Research Lab., NOAA, Ann Arbor, Mich.

Hamblin, P.F. and F.C. Elder, (1973), "A Preliminary Investigation of the Wind Stress Field over Lake Ontario," Proc. 16th Conf. Great Lakes Res., IAGLR, pp. 723-734.

Heap, J.A., (1963), "Some Characteristics of the Winter Ice Cover of Lake Michigan, 1962-63," Pub. No. 10, Great Lakes Res. Div., Univ. of Mich., pp. 216-218.

Hendrickson, J.A., L. M. Webb, and R.J. Quigley, (1962), "Study of Natural Forces Acting on Floating Ice Fields," Report to U.S. Naval Civil Engineering Lab., Port Hueneme, CA.

H.G. Acres Limited, (1971), "Review of Current Ice Technology and Evaluation of Research Priorities," Report to the Inland Waters Branch, Dept. of the Environment, Report Series No. 17, Ottawa, Canada.

Hibler, W.D., (1972), "Removal of Aircraft Altitude Variation from Laser Profiles of the Arctic Ice Pack," J. Geophys. Res., Vol. 77, pp. 7190-7195.

Hibler, W.D., (1974), "Differential Sea Ice Drift II: Comparison of Mesoscale Strain Measurements to Linear Drift Theory Predictions," J. Glaciol., Vol. 13, No. 69, pp. 457-471.

Hibler, W.D., (1975), "Characterization of Cold-Regions Terrain Using Airborne Laser Profilimetry," J. Glaciol., Vol. 15, No. 73, pp. 329-347.

Hibler, W.D., (1977a),"A Viscous Sea Ice Law as a Stochastic Average of Plasticity," CRREL Manuscript submitted to J. Geophys. Res., Corps of Engineers, U.S. Army, Hanover, N. H.

Hibler, W.D., (1977b), "Modeling Pack Ice as a Viscous-Plastic Continuum: Some Preliminary Results," A Symp. on Sea Ice Processes and Models, Univ. of Wash., Seattle, Wash., pp. 46-55.

Hibler, W.D. and L.A. LeSchack, (1972), "Power Spectrum Analysis of Under-Sea and Surface Sea Ice Profiles," J. Glaciol., Vol. 11, No. 63, pp. 345-356.

Hibler, W.D., W.F. Weeks, and S.J. Mock, (1972), "Statistical Aspects of Sea Ice Ridge Distributions," J. Geophys. Res., Vol. 77. No. 30, pp. 5954-5970.

Hibler, W.D., S. J. Mock, and W. B. Tucker, (1974), "Classification and Variation of Sea Ice Ridging in the Western Arctic Basin," J. Geophys. Res., Vol. 79, No. 18, pp. 2735-2743.

Hibler, W.D., W.B. Tucker, and W.F. Weeks, (1975), "Measurement of Sea Ice Drift Far from Shore Using Landsat and Aerial Photographic Imagery," Proc. 3rd Internat. Symp. Ice Problems, Hanover, N.H., pp. 541-554.

Hibler, W.D. and W.B. Tucker, (1976),"Seasonal Variations in Apparent Sea Ice Viscosity on the Geophysical Scale," Tech. Note, Corps of Engineers, U.S. Army, Hanover, N.H., 16 p.

Hibler, W.D. and W.B. Tucker, (1977),"An Examination of the Viscous Wind-Driven Circulation of the Arctic Ice Cover over a Two Year Period," AIDJEX Bulletin No. 37, pp. 95-134.

Hirt, C.W.,(1968),"Heuristic Stability Theory for Finite-Difference Equations," J. Computational Physics, Vol. 2, pp. 339-355.

Hobbs, P.V., (1974), Ice Physics, Oxford Univ. Press, London, p. 473.

Hunkins, K., (1966),"Ekman Drift in the Arctic Ocean," Deep Sea Res., Vol. 19, pp. 607-620.

Hunkins, K., (1974), "An Estimate of Internal Wave Drag on Pack Ice," AIDJEX Bulletin No. 26, pp. 141-152.

Hunkins, K., (1975), "The Oceanic Boundary and Stress Beneath a Drifting Ice Floe," J. Geophys. Res., Vol. 80, pp. 3425-3433.

Hunt, J.N., (1952), "Viscous Damping of Waves over an Inclined Bed in a Channel of Finite Width," La Houille Blanche, No. 7, pp. 836-842.

Ingram, R.G., O.M. Johannessen, and E.R. Pounder,(1969), "Pilot Study of Ice Drift in the Gulf of St. Lawrence," J. Geophys. Res., Vol. 74, pp. 5453-5457.

Ippen, A.T. (Ed.), (1966), Estuary and Coastline Hydrodynamics, McGraw-Hill Book Co., New York, N. Y.

Johannessen, O.M., (1970), "Note on Some Vertical Profiles below Ice Floes in the Gulf of St. Lawrence near the North Pole," J. Geophys. Res., Vol. 75, pp. 2857-2862.

Johnson, J.D. and L. D. Farmer, (1971), "Use of Side Looking Airborne Radar for Sea Ice Identification," J. Geophys. Res., Vol. 75, No. 9, pp. 2138-2155.

Kane, D.L., R. F. Carlson, and R.D. Seifert, (1975), "Alaskan Arctic
    Coast Ice and Snow Dynamics as Viewed by the NOAA Satellites,"
    Proc. 3rd Internat. Symp. Ice Problems, Hanover, N.H., pp. 567-575.

Karwowski, J.,(1962),"Influence of Waves on the Movement of Ice Floes
    and Icebergs," Bulletin de L'Academe Polonaise des Sciences, Serie
    des sciences techniques, Vol. X, No. 7, pp. 27-30.

Ketchum, R.D., (1971), "Airborne Laser Profiling of the Arctic Pack Ice,"
    Remote Sensing of Environment, Vol. 2, No. 1, pp. 41-52.

Ketchum, R.D. and S.G. Tooma, (1973), "Analysis and Interpretation of
    Airborne Multifrequency Side Looking Radar Sea Ice Imagery," J.
    Geophys. Res., Vol. 78, No. 3, pp. 520-538.

Keulegan, G., (1951), "Wind Tides in Small Closed Channels," National
    Bureau of Standards, Res. Paper No. 2207, Wash. D. C.

Kinsman, B.,(1965), Wind Waves, Prentice-Hall, Inc., Englewood Cliffs, N.J.

Kivilsild, H.R. and S.H. Iyer, (1978),"Mathematical and Physical Modeling
    of Ice," Proc. Symp. Ice Problems, IAHR, Lulea, Sweden, Part 1,
    pp. 379-392.

Kozo, T.L. and O.I. Diachok, (1973), "Spatial Variability of Topside and
    Bottomside Ice Roughness and its Relevance to Underside Acoustic
    Reflection Loss," AIDJEX Bulletin No. 19, pp. 113-122.

Krutskih, B.A., Z.M. Gudkovic, and A.L. Sokolov, (1976), Ice Forecasting
    Techniques for the Arctic Seas, published for the Office of Polar
    Programs and the National Science Foundation, Wash. D.C. by Amerind
    Publishing Co., Pvt. Ltd., New Delhi.

Langleben, M.P., (1972), "A Study of the Roughness Parameters of Sea Ice
    from Wind Profiles," J. Geophys. Res., Vol. 77, pp. 5935-5944.

Larrowe, B.T., R.B. Innes, R.A. Rendleman, and L.J. Porcello, (1971),
    "Fine Resolution Radar Investigation of Great Lakes Ice Cover,"
    Final Report, Willow Run Lab., Univ. of Mich., Ann Arbor, MI, 179 p.

Lax, P.D. and R. D. Richtmyer, (1956), "Survey of the Stability of Linear
    Finite Difference Equations," Communications on Pure and Applied
    Mathematics, Vol. 9, pp. 267-293.

Lettau, H.H., (1969), "Note on Aerodynamic Roughness Parameter Estimation
    on the Basis of Roughness Element Description," J. Applied Met., Vol. 8,
    pp. 828-832.

Lick, W.J., (1976), "Numerical Models of Lake Currents", Environmental Res.
    Lab., EPA, Duluth, Minn., EPA-600/3-76-020, 152 p.

Lilly, D.K., "On the Computational Stability of Numerical Solutions of Time Dependent Non-linear Geophysical Fluid Dynamics Problems," Monthly Weather Review, Vol. 93, No. 1, pp. 11-26.

Ling, C.H., (1976), "On the Calculation of Surface Shear Stress Using the Profile Method," J. Geophys. Res., Vol. 81, No. 15, pp. 2581-2582.

Ling, C.H. and W.J. Campbell, (1976), "Antisymmetric Stress for Sea Ice," AIDJEX Bulletin No. 33, pp. 77-84.

Ling, C.H. and N. Untersteiner, (1974), "On the Calculation of the Roughness Parameter of Sea Ice," J. Geophys. Res., Vol. 79, No. 27, pp. 4112-4114.

Longuet-Higgins, M.S., (1953), "Mass Transport in Water Waves," Phil. Trans. Roy. Soc. (A), Vol. 245, pp. 535-581.

Longuet-Higgins, M.S., (1977), "The Mean Forces Exerted by Waves on Floating or Submerged Bodies with Applications to Sand Bars and Wave Power Machines," Proc. Roy. Soc. London,(A), Vol. 352, pp. 463-480.

Markham, W.E., (1977), "Ice Movement in Canadian Coastal Waters," Manuscript Report Series No. 43, Symp. on Modeling of Transport Mechanisms in Oceans and Lakes," Marine Sciences Directorate, Dept. Fisheries and the Environment, Ottawa, Canada.

Marshall, E.W., (1966), "Air Photo Interpretation of Great Lakes Ice Features," Special Report No. 25, Great Lakes Res. Div., Univ. of Mich., Ann Arbor, MI.

Maykut, G.A. and A.S. Thorndike,(1973),"An Approach to Coupling the Dynamics and Thermodynamics of Arctic Sea Ice," AIDJEX Bulletin No. 21, pp. 23-29.

McClain, E.P., (1978), "The Use of Infrared and Visible Imagery for Sea Ice Monitoring," National Environmental Satellite Service, NOAA, Wash. D.C., Prepared for WMO Workshop on Remote Sensing of Sea Ice, Wash. D. C., 16-20 Oct.

McMillan, M. and D. Forsyth, (1976), "Satellite Images of Lake Erie Ice: January - March, 1975," NOAA Tech. Memo. NESS-80, Wash. D.C.

McPhee, M.G., (1975),"Ice-Ocean Momentum Transfer for the AIDJEX Ice Model," AIDJEX Bulletin No. 29, pp. 93-111.

McPhee, M.G. and J.D. Smith, (1976), "Measurements of the Turbulent Boundary Layer under Pack Ice," J. Phys. Oceanog., Vol. 6, pp. 696-711.

Mei, C.C., Liu, P.L. and T.G. Carter, (1972), "Mass Transport Velocity in Water Waves," M.I.T., Dept. of Civil Engg. , Ralph M. Parsons Lab. Report No. 146.

Michel, B., (1971), "Winter Regime of Rivers and Lakes," Monograph 111-Bla, Cold Regions Research and Engineering Lab., Corps of Engineers, U.S. Army, Hanover, N.H.

Michel, B., (1978), Ice Mechanics, Les Presses de L'Universite Laval, Quebec, Canada.

Mock, S.J., A.D. Hartwell, and W.D. Hibler, (1972), "Spatial Aspects of Pressure Ridge Statistics," J. Geophys. Res., Vol. 77, No. 30, pp. 5945-5953.

Muench, R.D. and K. Ahlnas,(1976), "Ice Movement and Distribution in the Bering Sea from March to June 1974," J. Geophys. Res., Vol. 81, No. 24, pp. 4467-4476.

Nelson, M.L., (1975), "Data Collection System Geostationary Operational Environmental Satellite: Preliminary Report," NOAA Tech. Memo. NESS 67, National Environmental Satellite Service, NOAA, Wash. D.C.

Neralla, V.R., S. Venkatesh, and M.B. Danard, (1977), "Ice Motion in the Beaufort Sea,"Symp. on Modeling of Transport Mechanisms in Oceans and Lakes, Manuscript Report Series No. 43, Marine Sciences Directorate, Dept. of Fisheries and the Environment, Ottawa, Canada, pp. 259-277.

Noh, W.F. and M.H. Protter, (1963),"Difference Methods and the Equations of Hydrodynamics," J. Math. Mech., Vol. 12, No. 2, pp. 149-191.

Norton, D., (1976), personal communication, Great Lakes Environmental Research Lab., NOAA, Ann Arbor, MI.

Nye, J.F., (1975), "Suggested Procedure for Observing Ice Displacement, Strain, and Thickness Distribution during the AIDJEX Main Experiment," AIDJEX Bulletin No. 28, Univ. Wash,, Seattle, Wash., pp. 127-140.

Nye, J.F. and D.R. Thomas, (1974), "The Use of Satellite Photography to Give the Movement and Deformation of Sea Ice," AIDJEX Bulletin Nθ. 27, pp. 1-21.

O'Brien, G.G., M.A. Hyman, and S. Kaplan, (1950), "A Study of the Numerical Solution of Partial Differential Equations," J. Math. Mech., Vol. 29, pp. 223-251.

Onstott, R. G., G.J. Dome, R.A. Hand, J. Hague, H. Pope, and R.K. Moore, (1977), "Backscatter Properties of Sea Ice with Radar," RSL Tech. Memo. 331-1, Univ. of Kansas Space Technology Center, Lawrence, Kans.

Page, D.F. and R.O. Ramseirer, (1975), "Application of Radar Techniques to Ice and Snow Studies," J. Glaciol., Vol. 15, No. 73, pp. 171-191.

Pai, S.I.,and H. Li, (1976), "A Note on the Dynamics of Pack Ice in the Arctic Ocean and its Surrounding Seas," AIDJEX Bulletin No. 28, pp. 167-172.

Panofsky, H.A. and A.A. Townsend, (1964), "Change of Terrain Roughness and the Wind Profiles," Quart. J. Roy. Met. Soc., Vol. 90, pp. 147-161.

Parkinson, C.L.,(1978), "A Numerical Simulation of the Annual Cycle of Sea Ice in the Arctic and Antarctic," National Center for Atmospheric Research, Boulder, Colo., NTIS PB-279-789, U.S. Dept. Commerce, Springfield, VA, 190 p.

Parmerter, R.R. and M.D. Coon, (1972), "A Model of Pressure Ridge Formation in Sea Ice," J. Geophys. Res., Vol. 77, pp. 6563-6575.

Plate, E.J., (1970), "Water Surface Velocities Induced by Wind Shear," J. Engg. Mech. Div., ASCE, Vol. 96, pp. 295-312.

Phillips, N.A., (1959), "An Example of Non-linear Computational Instability," Atmosphere and Sea in Motion, Rossby Memorial Vol. (Bolin, B., Ed.), Rockefeller Institute Press, New York, N. Y.

Phillips, D.W. and J.A.W. McCulloch, (1972), "The Climate of the Great Lakes Basin," Climatologic Studies No. 20, Atmospheric Environment Service, Environment Canada, Toronto.

Pritchard, R.S., (1975), "An Elastic-Plastic Constitutive Law for Sea Ice," J. Appl. Mech., pp. 379-384.

Quinn, R., R.A. Assel, D. Boyce, G.A. Leshkevich, C.R. Snider, and D. Weisnet, (1978), "Summary of Great Lakes Weather and Ice Conditions, Winter 1976-77," NOAA Tech. Memo. ERL GLERL-20, Great Lakes Environmental Research Lab., NOAA, Ann Arbor, MI.

Ramseier, R.O. and R.J. Weaver, (1975), "Floating Ice Thickness and Structure Determination: Heated Wire Technique," Bulletin No. 88, Inland Waters Directorate, Water Resources Branch, Environment Canada, Ottawa.

Reed, R.J. and W. J. Campbell, (1962), "The Equilibrium Drift of Ice Station Alpha," J. Geophys. Res., Vol. 67, pp. 281-297.

Resio, D.T. and C.L. Vincent, (1976), "Design Wave Information for the Great Lakes: Report 1, Lake Erie," Tech. Report H-76-1, U.S. Army Corps of Engineer Waterways Experiment Station, Vicksburg, Miss.

Resio, D.T. and C.L. Vincent, (1976), "Estimation of Winds over the Great Lakes," Misc. Paper H-76-12, U.S. Army Corps of Engineer Waterways Experiment Station, Vicksburg, Miss.

Richards, T.L., (1963), "Meteorological Factors Affecting Ice Cover on the Great Lakes," Proc. 6th Conf. Great Lakes Res., IAGLR, pp. 204-218.

Richards, T.L., H. Dragert, and D.R. McIntyre, (1966), "Influence of Atmospheric Stability and Over-Water Fetch on Winds over the Lower Great Lakes," Monthly Weather Review, Vol. 94, No. 1, pp. 448-453.

Richtmyer, R.D. and K.W. Morten, (1967), Difference Methods for Initial Value Problems, Interscience Publishers, New York, N. Y. 2nd. Ed.

Rigby, F., (1974), "Theoretical Calculations of Internal Wave Drag on Sea Ice," AIDJEX Bulletin No. 26, pp. 129-140.

Roache, P.J., (1972a), Computational Fluid Dynamics, Hermosa Publishers, Albuquerque, N.M.

Roache, P.J., (1972b), "On Artificial Viscosity,", J. Computational Physics, Vol. 10, No. 2,

Rondy, D.R., (1969), "Great Lakes Ice Cover Winter 1962-63 and 1963-64," U.S. Lake Survey, Basic Data Report 5-5, Detroit, MI, 47 p.

Rondy, D.R., (1971), "Great Lakes Ice Atlas," NOAA Tech. Memo. NOAA TM NOS LSCR 1, 48 p.

Rothrock, D.A.,(1975a), "The Mechanical Behavior of Pack Ice," Annual Review of Earth and Planetary Sciences, Vol. 3, pp. 317-342.

Rothrock, D.A.,(1975b), "The Steady Drift of an Incompressible Arctic Ice Cover," J. Geophys. Res., Vol. 80, No. 3, pp. 387-397.

Rothrock, D.A.,(1975c), "The Energetics of the Plastic Deformation of Pack Ice by Ridging," University of Washington, Seattle, Wash., 30 p.

Rumer, R., C.H. Atkinson, and S.T. Lavender, (1975), "Effects of Lake Erie-Niagara River Ice Boom on the Ice Regime of Lake Erie," Proc. 3rd Internat. Symp. on Ice Problems, Hanover, N.H., pp. 289-300.

Rumer, R. and P.M. Yu, (1978), "Modelling Ice Dissipation in Eastern Lake Erie," J. Great Lakes Res., Vol. 4, No. 2, pp. 194-200.

Russel, R.C.H. and J.D.C. Osorio, (1959), "An Experimental Investigation of Drift Profiles in a Closed Channel," Proc. 6th Conf. Coastal Engg., Council on Wave Res., Cal., pp. 171-193.

Schertler, R.J., Mueller, R.A., R.J. Jirberg, D.W. Cooper, T. Chase, J.E. Heighway, A.D. Holmes, R.T. Gedney, and H. Mark, (1975), "Great Lakes All-Weather Ice Information System," Proc. 10th Internat. Symp. on Remote Sensing of Environment, Vol. II, pp. 1377-1404.

Schertler, R.J.,(1976), personal communication, NASA, Cleveland, Ohio.

Schlichting, H., (1968), Boundary Layer Theory, McGraw-Hill Book Co., New York, N. Y.

Seifert, W.J. and M.P. Langleben, (1972), "Air Drag Coefficient and
    Roughness Length of a Cover of Sea Ice," J. Geophys. Res., Vol. 77,
    pp. 2708-2713.

Sendel, U. and W.H. Graf, (1974), "Transmission of Regular Waves past
    Floating Plates," Proc. 14th Coastal Engg. Conf., Copenhagen, Denmark,
    pp. 1924-1936.

Shemdin, O.H., (1972), "Wind-Generated Current and Phase Speed of Wind
    Waves," J. Phys. Oceanog., Vol. 2, pp. 411-419.

Sheng, Y.P. and W.J. Lick, (1973), "The Wind-Driven Currents in a Partially
    Ice Covered Lake," Proc. 16th Conf. Great Lakes Res., pp. 1001-1008.

Shirasawa, K. and M.P. Langleben, (1976), "Water Drag on Arctic Sea Ice,"
    J. Geophys. Res., Vol. 81, pp. 6451-6454.

"Shore Protection Manual," (1975), 3 vols., Coastal Engineering Research
    Center, U.S. Army Corps of Engineers, Ft. Belvoir, VA.

Shulyakovskii, L.G. (Ed.), (1966), Manual of Forecasting Ice-Information
    for Rivers and Inland Lakes, Translated from Russian by the Israel
    Program for Scientific Translations, Jerusalem.

Simons, T.J., (1976), "Continuous Dynamical Computations of Water Trans-
    ports in Lake Erie for 1970," J. Fish. Res. Board Canada,Vol.33, No. 3,
    pp. 371-384.

Sleath, J.F.A., (1973),"Mass Transport in a Water Wave of Very Small Ampli-
    tude," J. Hyd. Res., Vol. 11, No. 4, pp. 369-383.

Sleator, F.E., (1978), "Ice Thickness and Stratigraphy at Nearshore Loca-
    tions on the Great Lakes," NOAA Data Report ERL GLERL-1-2, NOAA,
    Ann Arbor, MI.

Smith, G.D., (1965), Numerical Solutions of Partial Differential Equations,
    Oxford Univ. Press, London.

Smith, S.D., (1972), "Wind Stress and Turbulence over a Flat Ice Floe,"
    J. Geophys. Res., Vol. 77, pp. 3886-3901.

Smith, S.D., E. G. Banke, and O.M. Johannessen, (1970), "Wind Stress and
    Turbulence over Ice in the Gulf of St. Lawrence," J. Geophys. Res.,
    Vol. 75, pp. 2803-2812.

Snider, C.R., (1974), "Great Lakes Ice Forecasting," NOAA Tech. Memo. NWS
    OWD 1, 106 p.

Sodhi, D.S., (1977), "Ice Arching and the Drift of Pack Ice through Restricted
    Channels," CRREL Report 77-18, Corps of Engineers, U.S. Army, Hanover,
    N.H.

Sodhi, D.S. and W.D. Hibler, (1977), "A Finite Element Formulation of a Sea Ice Drift Model," A Symp. on Sea Ice Processes and Models, Univ. Wash., Seattle, Wash., Vol. II, pp. 67-76.

Stelson, T.E. and F. T. Mavis, (1957), "Virtual Mass and Acceleration in Fluids," Trans. ASCE, Vol. 122, pp. 518-530.

Stewart, K.M., (1973), "Winter Conditions in Lake Erie with Reference to Ice, Isotherms, and Aspects of Circulation, and Comparison to Lakes Winnebago and Mille Lacs," Proc. 16th Conf. Great Lakes Res., pp. 845-857.

St. Lawrence Seaway Authority, (1976-78), "Navigation Season Extension Studies; St. Lawrence River and Great Lakes: Winters 1976-77 and 1977-78", 2 vols.

Stokes, G.G., (1847), "On the Theory of Oscillatory Waves," Trans. Cambridge Phil. Soc., Vol. 8.

"Survey Study, Great Lakes and St. Lawrence Seaway Navigation Season Extension," (1979), U.S. Army Engineers, Detroit District, MI.

Suzuki, Y., (1964), "On the Measurement of the Wind Drag of an Ice Floe," Low Temp. Sci., Series A, Vol. 22, pp. 155-170.

Thoman, D. and A. A. Szewczyk, (1966), "Time Dependent Viscous Flow over a Circular Cylinder," Phys. of Fluids, Supplement II, pp. 76-87.

Thommen, H.U., (1966), "Numerical Integration of the Navier-Stokes Equations," Zeitschrift fur Angegandte Mathematik und Physik, Vol. 17, pp. 369-384.

Thorndike, A.S., D.A. Rothrock, G.A. Maykut, and R. Colony, (1975), "The Thickness Distribution of Sea Ice," J. Geophys. Res., Vol. 80, No. 33, pp. 4501-4513.

Tooma, S.J. and W.B. Tucker, (1973),"Statistical Comparison of Airborne Laser and Sterophotogrammetric Sea Ice Profiles," Remote Sensing of Environment, Vol.2, No. 4, pp. 261-272.

Udin, I. and A. Omstedt, (1976), "SEA ICE-75, Dynamical Report," Winter Navigation Research Board, Swedish Admin. Shipping and Navigation, Finnish Board of Navigation, Research Report 16:8, Norrkoping.

Untersteiner, N., (1977), "AIDJEX Review," A Symp. on Sea Ice Processes and Models, Univ. Wash., Seattle, Wash., Vol. I, pp. 2-9.

Untersteiner, N. and E.I. Badgley, (1965), "The Roughness Parameters of Sea Ice," J. Geophys. Res., Vol. 70, pp. 4573-4577.

Vickers, R.S., J.E. Heighway, and R.T. Gedney, (1974), "Airborne Profiling of Ice Thickness using a Short Pulse Radar," Advanced Concepts and Techniques in the Study of Snow and Ice Resources, Nat. Acad. Sci., Wash. D. C. , pp. 422-442.

Wadhams, P., (1976), "Sea Ice Topography in the Beaufort Sea and its Effect on Oil Containment," AIDJEX Bulletin No. 33, pp. 1-52.

Wake, A. and R. Rumer, (1979), "Modeling Ice Regime of Lake Erie," Journ. Hyd. Div., ASCE, Vol. 105, No. HY7, pp. 827-844.

Wartha, J., (1977), "Lake Erie Ice: Winter 1975-76," NOAA Tech.Memo. NESS 90, National Satellite Service, Wash. D.C.

Weeks, W. F., (1976), "Sea Ice Properties and Geometry," AIDJEX Bulletin No. 34, pp. 137-171.

Weeks, W. F. and W. J. Campbell, (1975), "The Remote Sensing Plan for the AIDJEX Main Experiment," AIDJEX Bulletin No. 29, pp. 21-46.

Weeks, W. F., A. Kovacs, S.J. Mock, W. B. Tucker, W.D. Hibler, and A.J. Gow, (1977), "Studies of the Movement of Coastal Sea Ice Near Prudhoe Bay, Alaska," manuscript submitted to the J. Glaciol., CRREL, Corps of Engineers, U.S. Army, Hanover, N. H.

Weeks, W. F. and M. Mellor, (1978), "Some Elements of Iceberg Technology," CRREL Report No. 78-2, Corps of Engineers, U.S. Army, Hanover, N. H.

Wendler, G. and K.O.L.F. Jayaweera, (1974), "A Technique to Obtain Ice Movement," J. Geophys. Res., Vol. 79, No. 24, pp. 3478-3479.

Wiesnet, D.R., D.F. McGinnis, and D.G. Forsyth, (1974), "Selected Satellite Data on Snow and Ice in the Great Lakes Basin 1972-73 (IFYGL)," Proc. 17th Conf. Great Lakes Res., IAGLR, pp. 334-347.

Williams, G.P., (1965),"Correlating Freeze-up and Break-up with Weather Conditions," Canadian Geotechnical Journal, Vol. 11, No. 4, pp. 313-326.

World Meteorological Organization, (1975), "Hydrological Forecasting Practices," Operational Hydrology Report No. 6, (WMO-No. 425), Geneva, Switzerland.

Wu, J., (1968), "Laboratory Studies of Wind Wave Interactions," J. Fluid Mech. Vol. 34, Part 1, pp. 91-112.

Wu, J., (1972), "A Note on Surface Roughness and Resistance Coefficient of Sea Ice," J. Geophys. Res., Vol. 77, pp. 3272-3277.

Wu, J., (1975), "Wind-induced Drift Currents," J. Fluid Mech., Vol. 68, Part 1, pp. 49-70.

Yuan, S.W., (1967), Foundations of Fluid Mechanics, Prentice-Hall, Inc., Englewood Cliffs, N. J.

Zubov, N.N., (1943), Arctic Ice, translation by the U.S. Navy Oceanographic Office.

NOTATION

Notation is defined according to Chapter in which introduced.

Chapter II

A_i = ice surface area

A_T = total surface area (ice area plus open water)

A_{T_o} = limiting size of representative elemental area

C = empirical coefficient used in ice pressure equation

$\vec{C}$ = Coriolis force

C_a = wind stress coefficient

C_w = water stress coefficient

C_1 = $(\rho_a/\rho_i)\, C_a$

C_2 = $(\rho_w/\rho_i)\, C_w$

E_a = rate of ice area change due to thermodynamic processes

E_m = rate of ice mass change due to thermodynamic processes

f = Coriolis parameter ($= 2\Omega \sin \phi$)

$\vec{F}_a$ = wind stress force on ice

F_a = $|\vec{V}_a|/\sqrt{gL}$

$\vec{F}_w$ = water stress force on ice

$\vec{G}$ = gravitational force on ice

$g(t_i)$ = ice thickness distribution function

H = mean water level height

i = subscript denoting ice quantity

k = subscript, index notation ($= x,y$)

k_1 = ice shear viscosity

k_2 = ice bulk viscosity

$'$ = prime denotes dimensionless quantity

271

L = characteristic length

M_i = ice mass per unit surface area

N = ice area concentration

p = ice pressure (also water pressure in equations (2.7), (2.8) only)

P_c = ultimate crushing strength of ice

p^* = empirical ice strength constant

$\vec{q}$ = fluid velocity vector (= $\vec{i}u_f + \vec{j}v_f$)

$\vec{R}$ = ice internal resisting force

R_a = rate of ice area change due to mechanical redistribution of ice mass

R_1 = $|\vec{V}_a|\rho_i L/k_1$

R_2 = $|\vec{V}_a|\rho_i L/k_2$

R_o = $\vec{V}_a/(fL)$

t = time

t_i = ice thickness

u,v = average ice drift velocity components

$\vec{V}_i$ = ice drift velocity vector

$\vec{V}_w$ = water velocity vector

$\vec{V}_a$ = air velocity vector

x,y = coordinate directions in horizontal plane

ρ_a = air density

ρ_i = ice density

ρ_w = water density

μ = fluid viscosity in equations (2.7), (2.8), (2.9)

α = rate of ice thickness change due to thermo dynamic processes, eq. (2.22)

ψ = mechanical changes in ice thickness, eq. (2.22)

τ_a = wind shear on ice surface

τ_w = water shear on ice surface

σ = ice stress (subscripts denote whether normal or tangential)

$\bar{\sigma}$ = mean normal ice stress, eq. (2.13)

Ω = earth's angular velocity

ϕ = geographic latitude

Chapter III

a = water wave amplitude

a_i = incident water wave amplitude

a_r = reflected water wave amplitude

a_t = transmitted water wave amplitude

A = ice surface area, also coefficient in equations (3.16) and (3.17)

$\vec{A}_r$ = acceleration reaction

C = wave celerity

$\bar{C}_D$ = drag coefficient

C_m = virtual mass coefficient for ice floe

C_g = water wave group velocity

D_g = drag on guides

f_a = natural frequency of vibration of ice floe in air

f_w = natural frequency of vibration of ice floe in water

F_g = gravitational force on ice floe

F_T = $|\vec{v}_{i_T}|/\sqrt{g\ell}$

$\vec{F}_v$ = wave force on ice floe

h = water depth

H = wave height

K_1, K_2, K_3 = coefficients, see equation (3.14)

k = $2\pi/L_w$

ℓ = horizontal dimension of ice floe

273

$\vec{M}$ = wave momentum

$\vec{M}_F$ = wave momentum flux

m_i = mass of single ice floe

S_i = specific gravity of ice

$t_{.98}$ = time for ice floe to reach 98% of terminal velocity

T = wave period

U_o = water surface drift velocity

$\bar{u}$ = mass transport velocity

U_{*_w} = $\sqrt{\tau_a/\rho_w}$

V_{i_T} = terminal ice floe velocity

z = depth beneath water surface

z_{o_w} = roughness height of air-water interface

α = angle water surface makes with horizontal

ξ = water particle displacement in x-direction

κ = von Karman constant ($\simeq 0.4$)

η_w = water wave displacement from mean water level

σ = $2\pi/T$

ϕ_w = velocity potential for wave motion

ψ_w = stream function for wave motion

Chapter IV

c = Courant numer (= $\hat{u}\,\Delta t/\Delta x$)

i = subscript denoting node spacing

k = superscript in ice pressure modifier, eq. (4.52)

k_3 = $k_1 + k_2$ (combined ice viscosity)

k,ℓ = subscript denoting index notation (= x,y)

n = superscript denoting temporal index

R_c = $\hat{u}\Delta x/\alpha$

R_3 = $(|\vec{V}_a|\rho_i L)/k_3$

S = linear space dimension

T = boundary forces on ice

U = velocity

$\hat{u}$ = representative ice velocity

α = ice momentum transfer coefficient

α_e, α_a = artificial diffusion coefficients

β = sum of body forces on ice

Δt = time step in computations

Δx = node spacing

δ = prefix denoting incremental variation in a quantity

$\dot{\varepsilon}$ = strain rate field

Φ = ice area flux

ν = direction cosine index notation

ψ = flux divergence

ξ = any convected quantity